

Design and Construction of a Solar Pond and Desalination System for Coupling with Irrigation

by

Claudio Mascialino

Submitted for the Degree of Doctor of Philosophy

**Chemical & Process Engineering Department
Faculty of Engineering and Physical Sciences**



University of Surrey

January 2022

Supervisors:

Prof. Rex Thorpe

Prof. Mohammed Sanduk

Acknowledgements

This thesis is dedicated to my late father, Dr Emilio Mascialino, the source of inspiration to whom we owe so much. His dedication to mathematics and physics has never left our home since I was a child.

I am very grateful to Professor Rex Thorpe. With great patience he has taught me how the scientific approach should be applied in any research and carefully corrected my written errors and my poor “Italianised” English expressions.

I would like to express my deep and highest gratitude to my sincere friend Professor Adel Sharif for all his encouragement, positivity, support and understanding, notwithstanding his personal guidance during the course of this thesis. I also would like to extend my thanks to AquaMa Ltd and the Water Research Centre at the Ministry of Agriculture and Fisheries within the Sultanate of Oman for supporting this research and providing the necessary facilities to carry out the experimental work.

Special thanks and appreciation to my mother and brothers. Their prayers, the bond, the constant encouragement, support and love made it possible.

I am grateful to my wife Vivien, my daughter Amanda and my son Matteo for their endless support and encouragement.

To all those mentioned above and those who like me, I would say that it would have been impossible for me to finish this work without your encouragement and support.

Claudio Mascialino, November 2021, Brescia, Italy

Table of Contents

Acknowledgements	2
Abstract	7
Aim and Objectives:	8
1. Desalination Technologies	9
1.1 Introduction to Desalination Technologies.....	10
1.2 Water Desalination Technologies.....	15
1.2.1 Thermal Desalination.....	21
1.2.2 Membrane Desalination	24
1.3 Renewable Energy Desalination Technologies.....	37
1.3.1 Direct Solar Thermal Desalination Systems.....	38
1.3.2 Indirect Solar Thermal Desalination Systems	47
2. Solar Pond Combined with Thermal Desalination.....	49
2.1 Introduction to Solar Ponds	50
2.2 Solar Pond History	51
2.3 Solar Pond Types	53
2.3.1 Non-Convective Solar Pond	53
2.3.2 Convective Solar Pond	57
2.4 Historical Background of Desalination Coupled to Solar Ponds.....	58
2.4.2 Solar Pond Coupled with Multi-Effect Multi-Stage (MEMS) - El Paso	59
2.4.3 Solar Pond coupled with MSF – Atlantis.....	62

2.4.4	Solar Pond coupled with MED	63
2.4.5	Solar Pond coupled with MSF – Tripoli (Lybia)	64
2.4.6	Conclusions on the Best Desalination Processes Coupled with SGSP and some Economics	65
3.	Simulations of the Performance of Solar Collectors (Solar Pond and Flat Plate Collector) coupled with Membrane Distillation	68
3.1	Introduction	69
3.2	Process Unit Descriptions.....	69
3.2.1	Solar Pond.....	70
3.2.2	Air Gap Membrane Distillation	72
3.3	Modelling of the Units	74
3.3.1	Solar Radiation Model	74
3.3.2	Solar Pond Model	75
3.3.3	AGMD Model	81
3.4	The Proposed System Combinations	85
3.4.1	Solar Pond/PV Assisted AGMD (SGSP/PV/AGMD).....	86
3.4.2	Solar FPC/PV Assisted AGMD (FPC/PV/AGMD)	87
3.5	Simulations.....	88
3.5.1	Environmental Operating Conditions	88
3.5.2	Solar Pond Results	89
3.5.3	AGMD results.....	91
3.5.4	The Data Comparison for the Proposed Models SGSP+AGMD vs. FPC+AGMD	92

3.6	Conclusions.....	98
4.	Solar Pond Construction/Failure	100
4.1	Introduction	101
4.2	Solar Pond Design, Construction, Operation and Data Collection	103
4.2.1	Solar Pond Design Challenges.....	103
4.3	Solar Pond Construction Challenges & Conclusions	125
5.	Experimental Design and Results from Seawater Irrigation and Seawater Distillation techniques	130
5.1	Introduction	131
5.2	Previous Works.....	133
5.3	Design of the Experiment of SWI and SWD.....	148
5.4.	Novelties of the Experiments	153
5.5	Experimental Design of SWI & SWD	155
5.5.1	Experimental Design of SWI	156
5.5.2	Experimental Design of SWD	198
6.	Modelling of the Experiment and Comparison with Experimental Results for SWI and SWD.....	219
6.1	Introduction	220
6.2	SWI and SWD System Models	220
6.2.1	Flat Plate Solar Collector (Air & Water)	221
6.2.2	SWI with membrane model.....	225
6.2.3	SWD without Membrane Model (Still Cover Type)	230

6.2.4	The Developed Software Models	232
6.2.5	Meteorological data of selected Omani locations.....	234
6.2.6	Data Results.....	236
6.3	Comparison between Experimental Results and Modelling.....	243
6.4	Conclusions.....	245
7.	Cost Estimation and Economic Analyses	247
7.1	Introduction to Cost Analyses	248
7.2	Cost Estimation and Economic Analyses.....	249
8.	Conclusions and Recommendations for Future Work.....	255
8.1	Conclusions and Novelties	256
8.2	Analysing the Commercial Viability of Large Commercial Units	257
8.3	Recommendations for Future Works	259
	References	261
	Appendix I - Abbreviations and Symbols	281
	Appendix II – Nomenclature.....	284
	Appendix III - Mathematical Models (Matlab)	290

Abstract

Most of countries in the world, especially those near the tropics of Capricorn and Cancer, are struggling to address water and food security. The increase in population and consequent demand for food and water resources combined with ever-diminishing natural resources are driving these countries to find sustainable and long-lasting technologies to address these problems and provide for the survival of their peoples. Fresh-water access and consequently water desalination in many cases will be a key element for their future development, independence and stability, especially if derived from sustainable resources.

Desalination technologies available today are mostly designed and engineered for large-scale applications associated with cities and industry. The use of these technologies for small-scale distributed fresh-water production especially linked to irrigation of crops is most of the time economically and technically unfeasible. Thus small-scale desalination technology is needed in very poor countries, arid regions and remote locations where access to energy and technology is limited and consequently it is very important to develop technologies or even better techniques that can be easily arranged with simple local products (possibly already used for the daily life needs of the population) managed by unskilled people and requiring a low amount of energy that should preferably be obtained from Renewable Energy Sources (RES).

To improve agricultural production in arid regions and remote locations, it is not only important to choose an efficient and reliable desalination technology but also to combine it with the right crop cultivation technique, choosing the best soil mixture and the suitable crops/plants that can grow within these limitations. Thanks to the support of the Ministry of Agriculture and Fisheries of Oman (MoAF) and the cooperation of a private company Aquama Ltd, the opportunity to build and test a suitable Solar Pond in Oman was offered together with novel irrigation and distillation techniques for crop and date palm growing. A direct seawater enhanced evaporation subsurface irrigation technique (SWI) and a direct seawater distillation technique (SWD) have been developed and some experimental work has been performed to validate the findings. The Solar Pond is demonstrated to have major limitations in its applications due to the extreme difficulties in its construction and maintenance in such an adverse climate. Thus, it is advisable to replace it with other simple, more reliable technologies such as flat solar panels or heat pipes. However, both SWI and SWD have shown potential for future applications in this context and the results obtained in terms of water production have been satisfactory.

The SWI and SWD systems have been modelled and the good agreement with the experimental results offers another important tool to predict the systems' behaviour at full scales and in differing local conditions and underpins the derivation of costs.

The predicted low capital and operational expenditure, combined with the acceptable productivity of the systems, demonstrates their potential compared with other experimented solutions and highlights the promising conditions for continuing the experimental research.

Aim and Objectives:

The aim of this study was to find sustainable, affordable, accessible and secure sources of fresh-water especially linked to irrigation, using seawater and renewable energies and scouting new technologies for small-scale distributed fresh-water for growing high-value crops and trees that could be applied in arid countries.

To satisfy this aim, several objectives have been addressed:

- Investigation of a low capital, sustainable, novel seawater desalination technique that is to be coupled with irrigation and implemented in arid regions.
- Model the systems and understand the governing parameters (geometry, flow rate, temperature, productivity).
- Prove in the field and take to a near-market product the innovative seawater/impure water Irrigation Techniques.
- Analyse the system scale-up and commercial exploitation in Oman and the region once the technology has been proven in the field.

1. Desalination Technologies

1.1 Introduction to Desalination Technologies

Fresh-water is essential to life and necessary for all human activities. Mankind has always been dependent on rivers, lakes and underground reservoirs for fresh-water requirements in domestic life, agriculture and industry.

However, rapid industrial growth and the worldwide population explosion have resulted in a large escalation of demand for fresh-water for both household needs and for crop irrigation. In terms of total global water consumption, about 70% is used by agriculture, 20% by industry and only 10% for domestic needs (Figure 01.01).

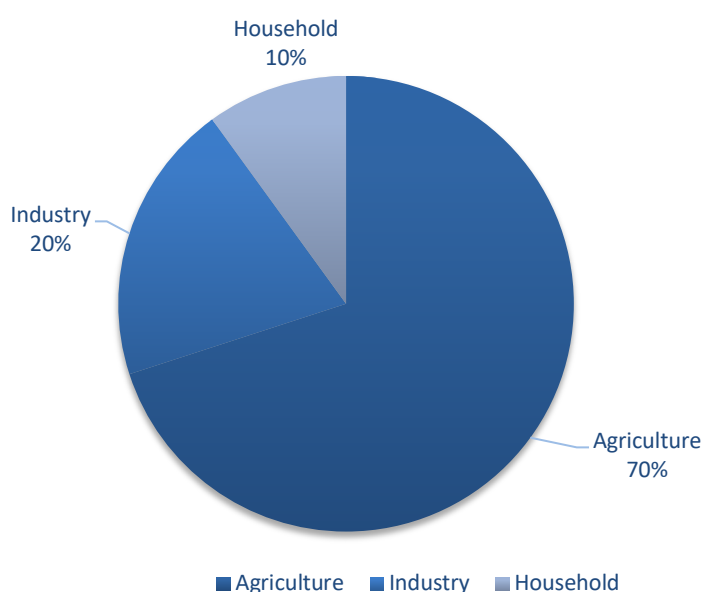


Figure 01.01 – Water Consumption Worldwide per sector. Data source: UNEP, UD, FAO (2012).

The demand for fresh-water is increasing annually by 64 billion cubic meters (Figure 01.02), driven primarily by the following factors:

- . Population growth of approximately 80 million people each year.
- . Changes in lifestyles and eating habits in recent years are requiring more water consumption per capita.
- . Accelerating energy demand with corresponding implications for water usage.

These changes will increase total fresh-water demand by 2030 to approximately 6,900 billion cubic metres (Water Resource Group, 2011).

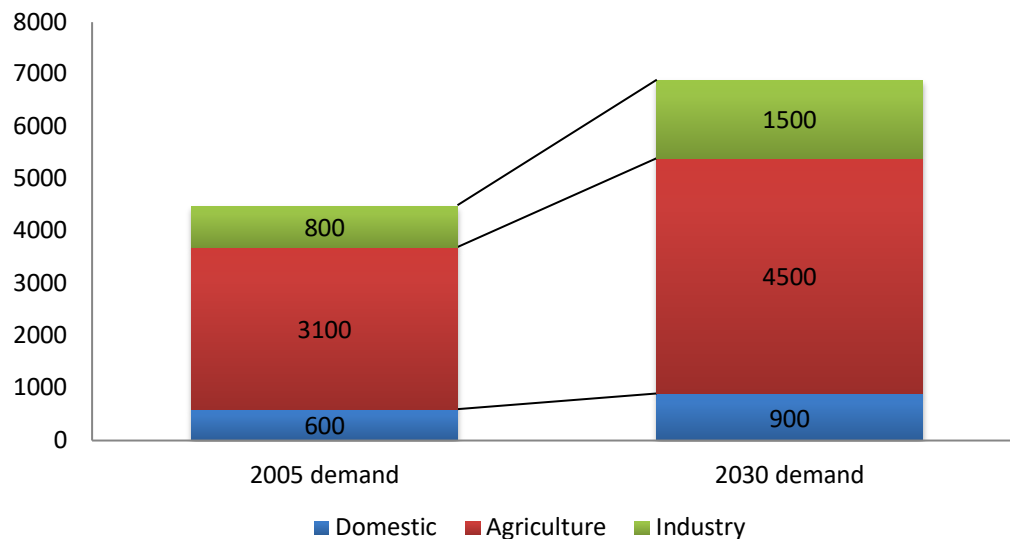


Figure 01.02 – Fresh-water Demand Worldwide (Forecast 2030) in billion cubic meters. Data source: Water Resource Group (2011).

Natural resources of fresh-water are not sufficient to sustain this rapid growth in demand and the pollution of rivers and lakes by industrial waste and the large amounts of sewage discharged are making the situation even worse. Water is one of the most abundant resources on earth (Kalogirou 2005), covering approximately 75 % of the planet's surface, yet almost 97.5% of the earth's water is saltwater and only 2.5% (about 36 million km³) is fresh-water contained in ice caps, groundwater, lakes, and rivers. These supply most human and animal needs. Nearly 70% of this 2.5% of the world's fresh-water is frozen in the form of glaciers, permanent snow cover, ice and permafrost. Thirty per cent of all fresh-water is found underground, most of it in deep, hard-to-reach aquifers, while lakes and rivers together comprise a little over 0.25% of all our fresh-water reserves, and lakes contain most of this (Gleick 1993) (Figure 01.03).

Where is Earth's Water?

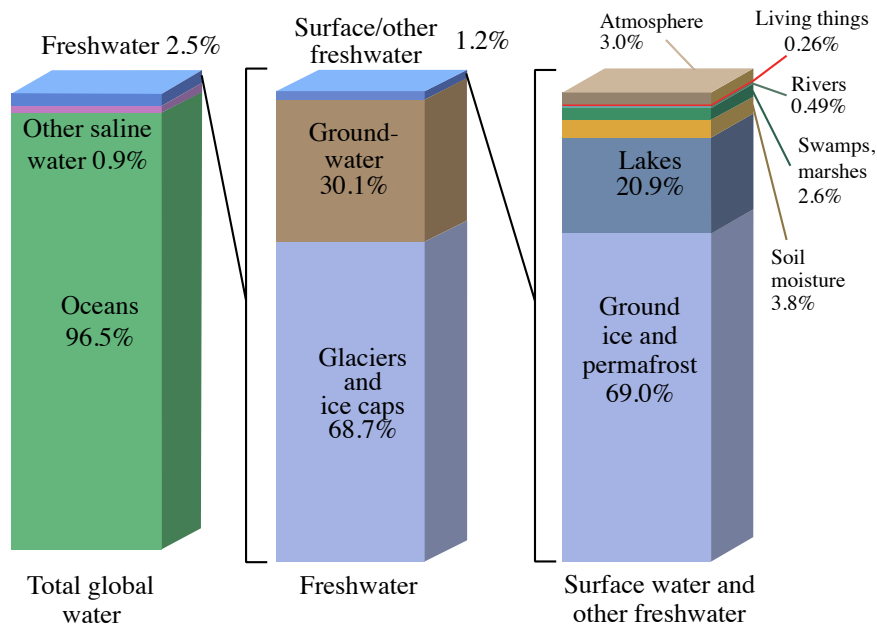


Figure 01.03 – Water Resources. Credit: U.S. Geological Survey, Water Science School. Data source: (Gleick, 1993).

The only way to sustain this demand is to make use of our saltwater reserves, and the only nearly inexhaustible sources of water are the oceans. Their main drawback is their high salinity and, therefore, it would be attractive to tackle the water shortage problem through the desalination of this water. The permissible limit of salinity in water (World Health Organization, 2008) is 500 ppm and, in special cases, 1,000 ppm. However, most of the water available on earth has a salinity of up to 10,000 ppm, while seawater normally has a salinity in the range of 35,000-45,000 ppm in the form of TDS (total dissolved salts). We also have to consider the uneven distribution of fresh-water. For example, Canada has 10% of the world's surface fresh-water, yet less than 1% of its population. The lack of potable water poses a big problem in arid regions of the world where fresh-water is becoming very scarce and expensive. The areas with the most severe water shortages are the warm, arid countries of the Middle East and Africa (MENA region). These areas are also characterised by increased groundwater salinity and infrequent rainfall. Desalination is their only choice, yet it involves a recurrent energy expense which few of the arid areas of the world can afford. Irrigated agriculture for food production drives global water demand, reaching figures of over 85% across arid and semiarid regions (Entezar et al. 2019). Moreover, global climate change prospects predict that available water resources will diminish further under arid and semiarid climates, exacerbating water scarcity problems in the near future in many parts of the world (Betts et al. 2018). This complex scenario is putting pressure on agriculture in many regions unable to meet current or future demand

for irrigation relying solely on conventional water sources. It has thus become necessary to explore new agricultural water supply options as food demand and water scarcity intensify.

Large commercial desalination plants using fossil fuel are already in operation in several oil-rich countries to supplement the traditional sources of water supply. However, people in many other areas of the world have neither the money nor the oil resources to develop such facilities on a similar scale. The dramatic increase in desalinated water supply will create a series of problems, the most significant of which are those relating to energy consumption and environmental pollution caused by using fossil fuels. It has been estimated by Kalogirou (2005) that the production of 1,000 m³/day of fresh-water requires 10,000 tons of oil per year.

Problems relevant to the use of fossil fuels could be resolved, in part, by considering the possible utilisation of renewable resources such as solar, biomass, wind, or geothermal energy. It often happens that those geographical areas where water is most needed are well served by renewable energy sources (RES). Thus, the obvious solution is to combine these RES with a desalination plant to provide water supply, as required. In fact, most developing countries with vast areas without access to an electric grid appear to be well suited to renewable energies. Such sources, available even in remote and isolated areas, could be exploited to power low to medium scale desalination plants and subsequently integrated for agricultural production. The World Health Organisation (2008) estimates that over a billion people lack access to purified water for drinking and irrigation and most of these people live in rural areas where the low population density and remote locations make it very difficult to install traditional clean water solutions.

Recently, considerable attention has been given to the use of renewable energy for desalination, especially in remote areas and on islands, owing to high costs, inaccessibility, and environmental considerations pertaining to fossil fuels. It should however be noted that, despite the aforementioned favourable characteristics, the contribution of RES to energy demand worldwide, though increasing, is still marginal: solar, wind and geothermal sources account for little more than 1% of global energy production (Qiblawey et al. 2015).

Improvements to thermal desalination technologies and the advent of low-cost, integrated designs for solar-thermal collection and storage can reduce the cost of desalination while also enabling smaller and more portable systems to be developed. Today's desalination operations need to be grid-connected, limiting their applications to those areas with access to electricity, while solar-thermal energy, which concentrates sunlight and converts it into heat, has the potential to expand access to desalination by enabling smaller systems that do not need to be grid-connected. Markets that are particularly attractive for solar desalination technologies include municipal water production,

agriculture, industrial processes, and water purification produced by energy development, including oil and gas extraction.

We should also consider the economics of the different desalination technologies available. In fact, projects that address challenges for large-scale plants which process high-volume, low-salinity water, like seawater for a municipal utility, are expected to target a levelised cost of water (LCOW) of \$0.50 per cubic metre. In contrast, projects that address challenges for small-scale plants that process low-volume, high-salinity water for agricultural use target a LCOW of \$1.50 per cubic metre (IRENA, 2013).

Owing to the diffuse nature of solar energy, the main problems with the use of solar thermal energy in large-scale desalination plants are their relatively low productivity rate, low thermal efficiency and considerable land area required (Figure 01.04). However, since solar desalination plants are characterised by freely available energy and insignificant operation costs, this technology is suitable for small-scale production, especially in remote arid areas and on islands where the supply of conventional energy sources is otherwise scarce.

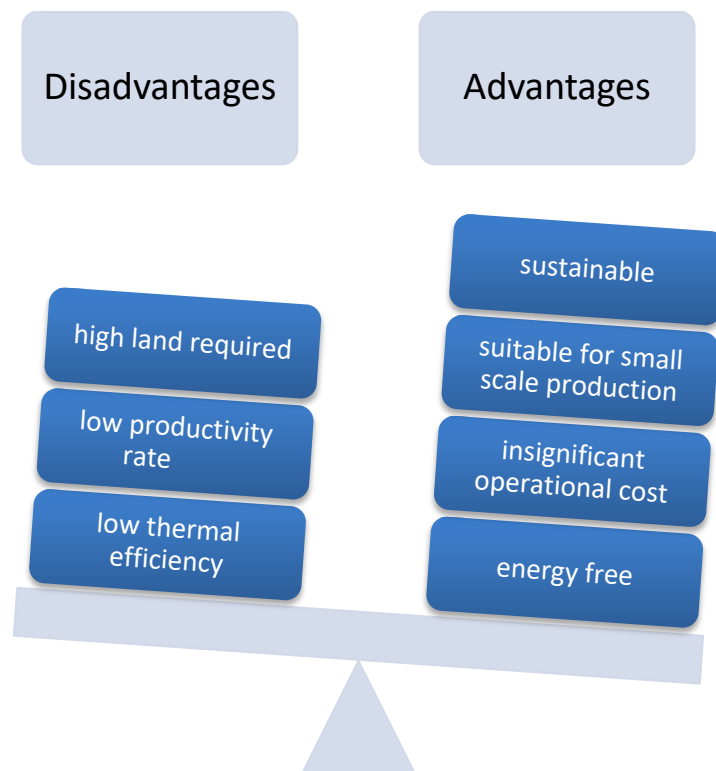


Figure 01.04 – Solar thermal energy vs traditional technologies.

Aside from cost implications, there are environmental concerns associated with the burning of fossil fuels, so that the coupling of renewable energy sources, especially solar thermal with desalination

processes, is seen to offer a sustainable route for increasing the supplies of potable water, both for drinking and agricultural use. Although solar energy-powered desalination systems cannot compete with conventional techniques in terms of the cost of water produced, they are applicable in certain areas and are likely to become feasible solutions in the near future.

1.2 Water Desalination Technologies

Desalination is a water-treatment process that separates salts from saline water to produce potable water, or water that is low in total dissolved solids (TDS). It is one of mankind's earliest forms of water treatment and remains a popular solution to this day.

In nature, solar desalination produces rain when solar radiation is absorbed by the sea causing water to evaporate. The evaporated water rises above the surface and is moved by the wind. Once this vapour cools to its dew point, condensation occurs and the fresh-water is precipitated as rain. This fundamental process is responsible for the water cycle, or hydrologic cycle, and this same principle is used in all industrial distillation systems using alternative means of heating and cooling.

Desalination uses a large amount of energy (in the form of heat or electricity) to remove a portion of pure water from a saltwater source after the saltwater (feed water) has been fed into the process. The result is one output stream of pure water (fresh-water) and another of wastewater of high salinity (saline brine) (Figure 01.05).

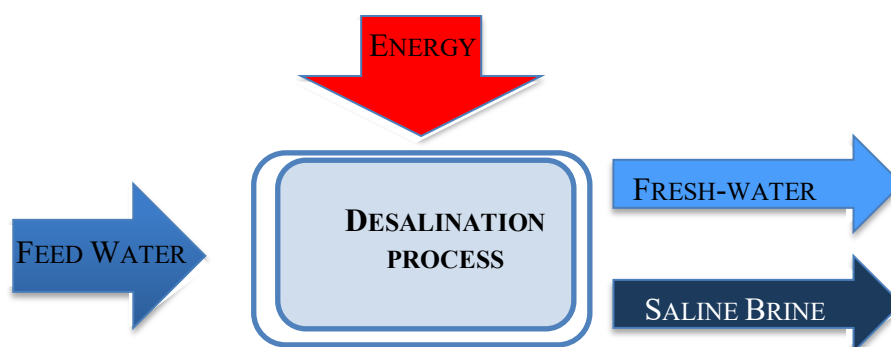


Figure 01.05 - Desalination process.

There are basically two families of industrial desalination technologies used throughout the world today. These include thermal technologies and phase change or membrane technologies (use of semi-permeable membranes to separate the solvent and solute).

The basics of these technologies are as follows:

- a) Thermal Processes—where salted water is heated to boiling point, salts, minerals, and pollutants are too heavy to be included in the steam and therefore remain in the base water while the steam is cooled and condensed. The thermal energy required may be obtained from a conventional fossil fuel source, nuclear energy or else from a non-conventional solar energy source or geothermal power.

The main thermal desalination processes are:

Multi-Stage Flash (MSF) distillation

Multiple-Effect Distillation (MED)

Vapour Compression (VC), which can be Thermal (TVC) or Mechanical (MVC)

The MSF process is based on the generation of vapour from seawater or brine due to a sudden pressure reduction when seawater enters an evacuated chamber. This process is repeated stage by stage for successive decreases in pressure and temperature requiring an external steam supply, normally at a temperature of around 100 °C. The maximum temperature is limited by the salt concentration to avoid scaling and this limits the performance of the process.

In MED, vapours are generated due to the absorption of thermal energy by the seawater. The steam generated during one stage or effect can heat the salt solution in the next stage as the next stage is at a lower temperature and pressure. MED plants normally use an external steam supply at a temperature of about 70°C. The performance of the MED and MSF processes is proportional to the number of stages or effects.

For TVC and MVC, after the initial vapour is generated from the saline solution, this vapour is thermally or mechanically compressed to generate additional production.

- b) Membrane or single-phase processes—where salt separation occurs without phase transition—involve lower energy consumption.

The main membrane processes are:

Reverse Osmosis (RO)

Electro-Dialysis (ED)

Forward Osmosis (FO)

Membrane Distillation (MD)

RO and FO require electricity or shaft power to drive the pump that increases the pressure of the saline solution to the level required. The required pressure depends on the salt concentration of the resource of saline solution and it is generally around 70 bar for RO seawater desalination and up to 10 bar for FO. ED also requires electricity for water ionisation, which is cleaned by using suitable membranes located at the two oppositely charged electrodes. All these technologies efficiently

desalinate brackish water, yet only RO and FO effectively compete with distillation processes in seawater desalination.

Other processes include solar still distillation, humidification, de-humidification and freezing. Thus, not only distillation processes that involve phase change are exploited, but also freezing and humidification/dehumidification processes. The conversion of saline into fresh-water via freezing has always existed in nature and has been known to man for thousands of years. In desalination of water by freezing, fresh-water is removed and leaves behind concentrated brine. This is followed by a separation process related to the solid-liquid phase change phenomenon. When the temperature of saline water is reduced to its freezing point, which is a function of salinity, ice crystals of pure water are formed within the salt solution and these ice crystals can be mechanically separated from the concentrated solution, washed and melted to obtain pure water. Therefore, the primary energy input for this method is that of powering the refrigeration system (Tleiman 1980).

The humidification/dehumidification method also uses a refrigeration system although the principle of operation is different. The humidification/dehumidification process is based on the fact that air can be mixed with large quantities of water vapour and that the vapour carrying capacity of air increases with temperature (Parekh et al. 2003). In this process, seawater is added into an air stream to increase its humidity, then this humid air is directed to a cooling coil on the surface on which water vapour contained in the air condenses and is collected as fresh-water. These processes, however, exhibit some technical problems which effectively limit their mass industrial development. While they can offer an economical solution for low scale water production, they will be analysed in depth in the following chapters because they can provide promising solutions if coupled with new irrigation techniques.

Three other membrane processes which are not considered desalination processes, yet are relevant include microfiltration (MF), ultrafiltration (UF), and nanofiltration (NF). The ion-exchange process (IE) itself is also not regarded as a desalination process but is generally used to improve water quality for some specific applications.

All processes require the chemical pre-treatment of raw seawater to avoid scaling, foaming, corrosion, biological growth and fouling in addition to a chemical post-treatment. The most important technologies are summarised in the chart below (Figure 01.06).

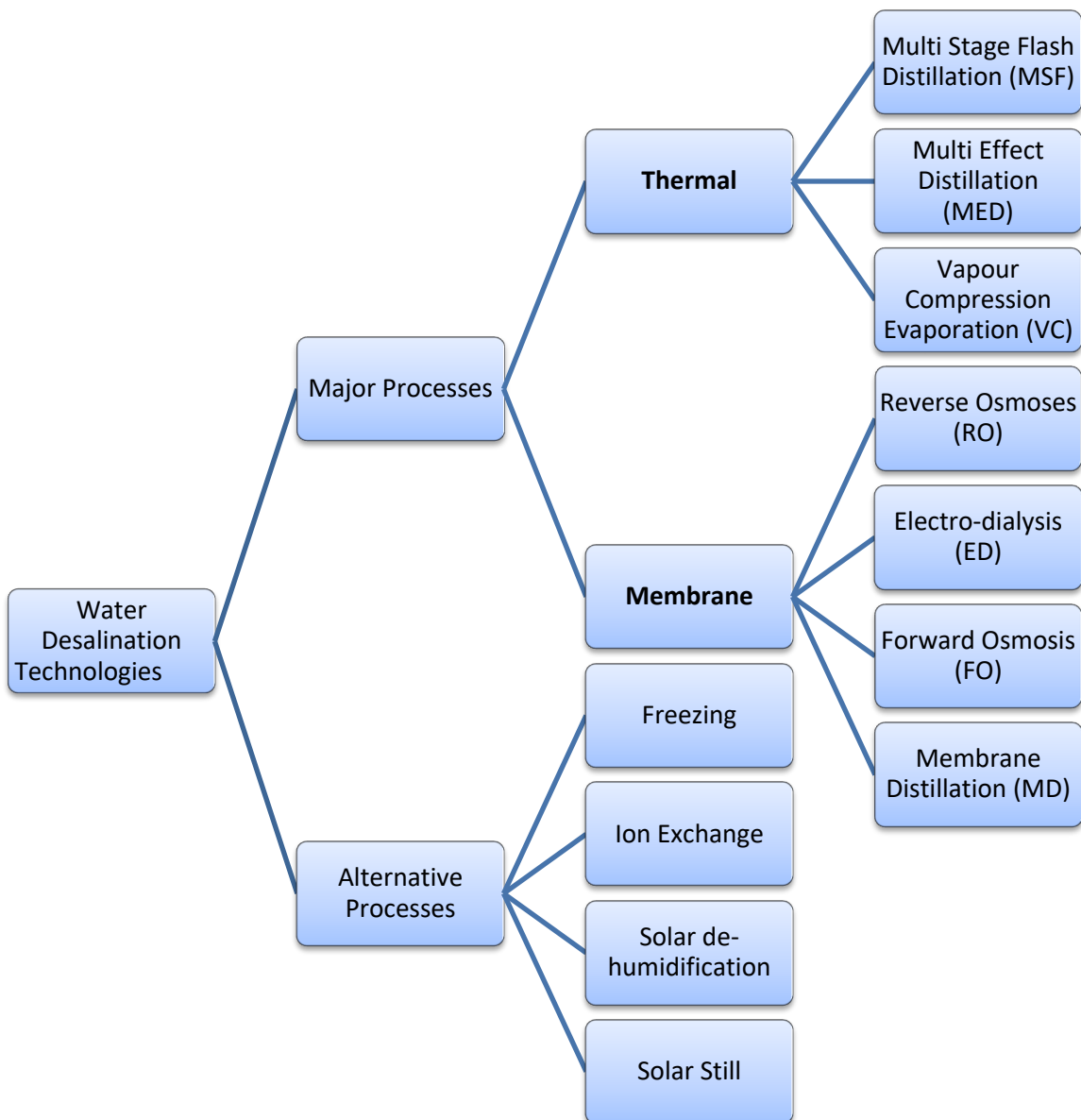


Figure 01.06 – Desalination technologies.

The two most widely used desalination technologies are MSF and RO systems. As the latest technology, RO has become dominant in the desalination industry. In 1999, about 78% of global production capacity comprised MSF plants while RO accounted for a modest 10%. However, by 2015, RO accounted for 65% of worldwide capacity, whereas MSF contributed around 21%. Although MED is less common than RO or MSF, it still accounts for a significant percentage of global desalination capacity (7%), while ED is only used on a limited basis (3%) (Figure 01.07).

Membrane desalination has grown rapidly since 2003 and, despite expectations of decline, thermal desalination also continues to grow (Figure 01.08).

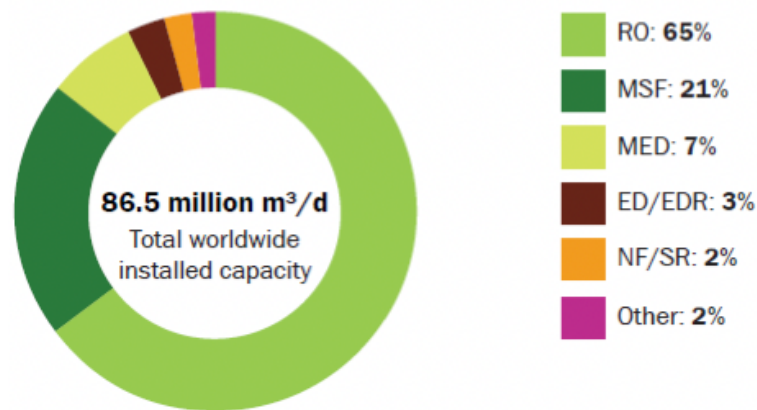


Figure 01.07 – Desalination technologies per process in 2015. Credit: Water Resource Group (2015).

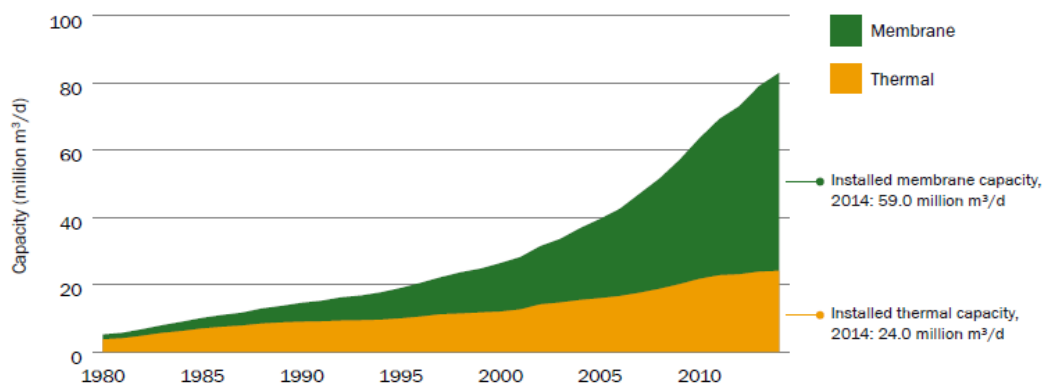


Figure 01.08 – Proportion of thermal and membrane technologies installed 1980 – 2014 (GWI, 2015). Credit: GWIWaterData.com, Media Analytics Ltd.

The cost of water desalination varies depending on access to a suitable water source, its salinity and quality, the specific desalination process, power costs, concentrate disposal method, project delivery method and the distance to the point of use. According to Water Resource Group (2011), power consumption for the 3 most widely used technologies may account for 30% to 60% of the operating costs. Thus, slight variations in power rates can directly impact the cost of treated water (Figure 01.09).

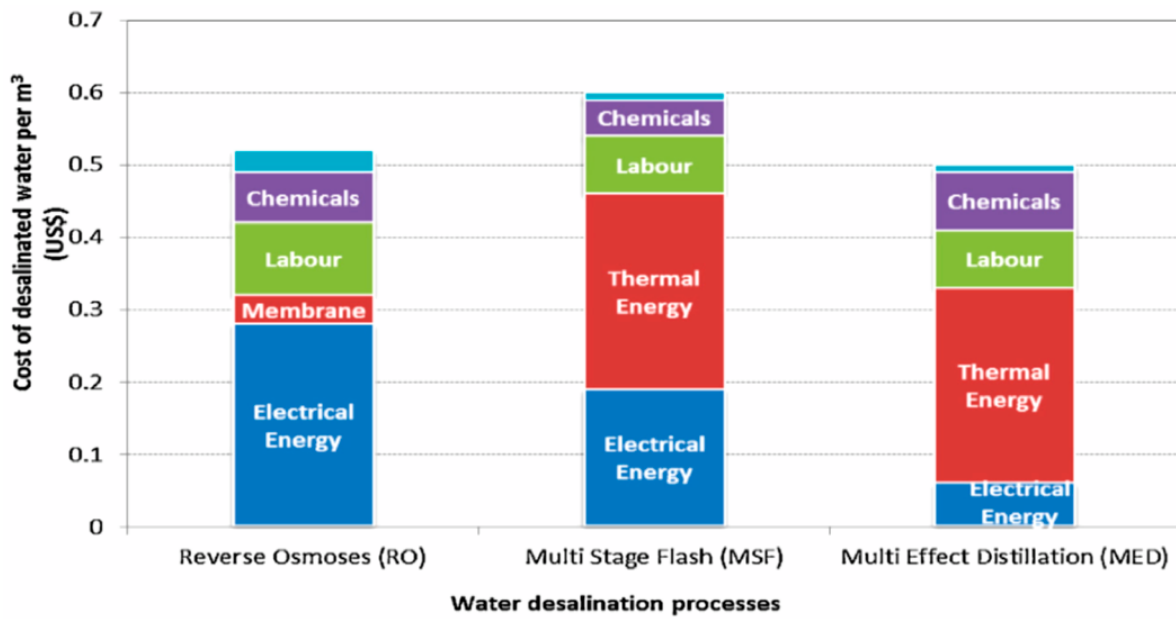


Figure 01.09 – Cost analysis of large-scale commercial plants for thermal and RO desalination processes. Credit: Water Resource Group (2011).

1.2.1 Thermal Desalination

Thermal desalination is based on the principles of evaporation and condensation whereupon water is heated until it reaches its saturation temperature, beyond which point evaporation occurs. The salt is left behind, whilst vapour is taken away and condensed in another heat exchanger to produce fresh-water.

1.2.1.1 Multi-Stage Flash distillation (MSF)

In MSF, a seawater feed is pressurised and heated to the plant's maximum allowable temperature at which point the heated liquid is discharged into a chamber maintained at slightly below the saturation vapour pressure of the water. A fraction of its water content flashes into steam and the flashed steam is then stripped of suspended brine droplets as it passes through a mist eliminator and condenses on the exterior surface of the heat-transfer tubing. The condensed liquid drips into trays as hot fresh-water product. Figure 01.10 provides a diagram of a typical MSF unit.

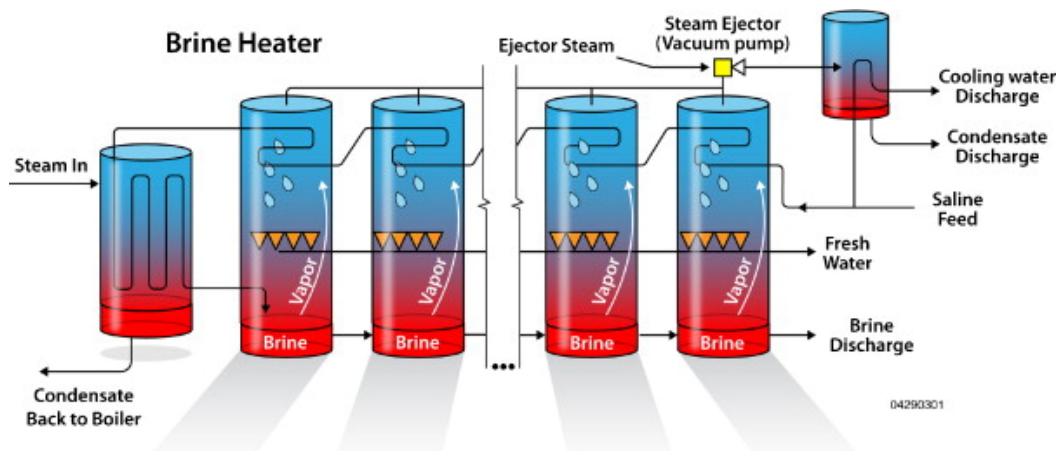


Figure 01.10 – Diagram of typical MSF unit (Al-Karaghoul et al. 2019). Reproduced with permission of the rights holder Elsevier Ltd.

1.2.1.2 Multi-Effect Distillation (MED)

MED units operate on the principle of reducing the ambient pressure at each successive stage of the process, allowing the feedwater to undergo multiple boiling cycles without having to supply additional heat after the first stage. In this unit, steam and/or vapour from a boiler or some other available heat source (such as renewable sources or waste energy) is fed into a series of tubes where it condenses and heats the surface of the tubes and acts as a heat-transfer surface to evaporate saline on the other side. The evaporated saline - now free of a percentage of its salinity and slightly cooler - is fed into the next, lower-pressure stage where it condenses into fresh-water product while giving up its heat to evaporate a portion of the remaining seawater feed. The energy used for evaporation of the saline is the heat of condensation of the steam in the tube. Figure 01.11 illustrates a MED unit.

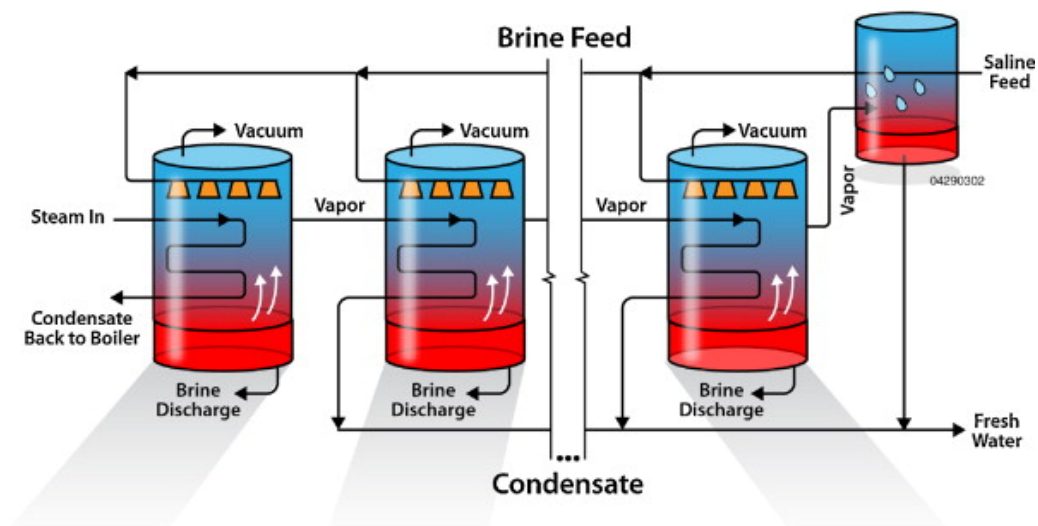


Figure 01.11 – Diagram of typical MED unit (Al-Karaghoul et al. 2019). Reproduced with permission of the rights holder Elsevier Ltd.

1.2.1.3 Vapour-Compression Distillation

The VC distillation process is generally used for small and medium-scale seawater desalination units. The heat for evaporating the water comes from the compression of vapour rather than from the direct exchange of heat from steam produced in a boiler. Two primary methods are used to condense the vapour sufficiently to produce enough heat to evaporate incoming seawater, namely a mechanical compressor (MVC) or a steam jet (TVC). The mechanical compressor is usually electrically driven, allowing the sole use of electrical power to produce water via distillation (Figure 01.12) while, in the steam jet-type of VC unit, also called a thermal compressor, a Venturi orifice at the steam jet creates and extracts water vapour from the main vessel by creating a lower ambient pressure. The steam jet compresses the extracted water vapour and condenses it onto the tube walls to provide the thermal energy (heat of condensation) to evaporate the seawater being applied on the other side of the tube walls. The vessels of MVC units typically range in capacity to as much as 3,000 m³/day, whereas TVC units may range in size to 20,000 m³/day. They are often used for resort and industrial applications.

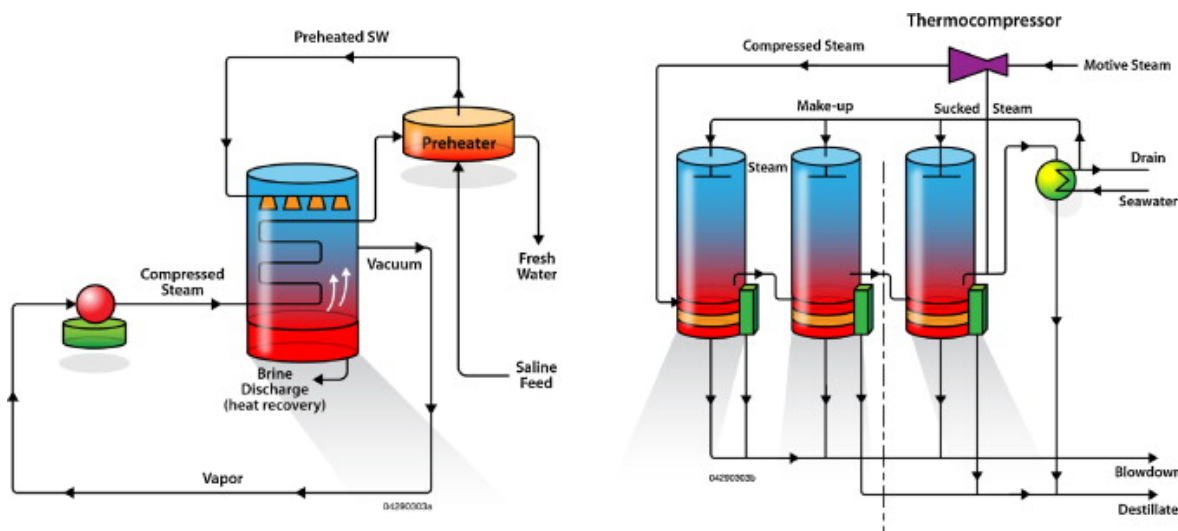


Figure 01.12 – Diagram of typical VC unit (Al-Karaghoul et al. 2019). Reproduced with permission of the rights holder Elsevier Ltd.

1.2.2 Membrane Desalination

Membranes and filters can selectively permit or prohibit the passage of certain ions, and desalination technologies have been designed around these capabilities. Membranes play an important role in separating salts in the natural processes of dialysis and osmosis and these natural principles have been adapted in two commercially important desalination processes, specifically electrodialysis (ED) and reverse osmosis (RO). Although they have typically been used to desalinate brackish water, versions are increasingly being applied to seawater and these two approaches now account for more than two-thirds of all desalination capacity. A growing number of desalination systems are also adding filtration units before the membranes to remove contaminants that may adversely affect long-term filter operation. These filtration systems include microfiltration and nanofiltration. Another emerging desalination process that represents a challenge for the future is forward osmosis (FO), wherein the salt separation is achieved via the natural osmotic pressure differential.

1.2.2.1 Reverse Osmosis (RO)

Reverse osmosis is a form of pressurised filtration in which the filter is a semi-permeable membrane that allows water, but not salt, to pass through (Figure 01.13). A typical RO system consists of four major subsystems, namely a pre-treatment system, high-pressure pump, membrane module and post-treatment system.

Feedwater pre-treatment is a critical factor in operating an RO system as the membranes are sensitive to fouling so the pre-treatment commonly includes sterilising feed water, filtering, and adding chemicals to prevent scaling and biofouling. The high-pressure pump, operating at pressures ranging from 17 to 27 bar for brackish water and 55 to 82 bar for seawater, force the pre-treated feedwater to flow across the membrane surface. Part of the feed water—the product or permeated water—passes through the membrane, which removes most of the dissolved solids, while the remainder, together with the rejected salts, emerges from the membrane modules at high pressure as a concentrated reject stream (brine).

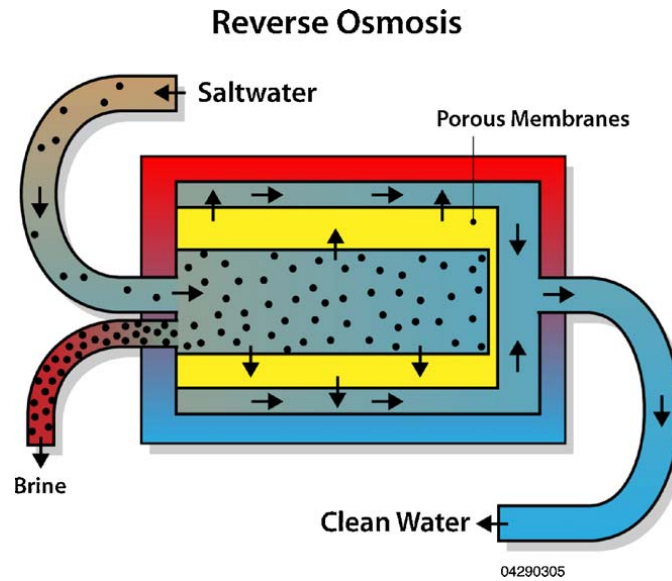


Figure 01.13 – Diagram of RO desalination (Al-Karaghoul et al. 2019). Reproduced with permission of the rights holder Elsevier Ltd.

The energy efficiency of seawater RO depends heavily on recovering the rejected brine pressure energy. In large plants, this is done using a turbine, commonly a Pelton-wheel turbine, recovering as much as 20% to 40% of the consumed energy. The RO membrane is semi-permeable, offering a high degree of water permeability yet an impenetrable barrier to salts. It has a large surface area to enable maximum flow rates and is extremely thin so that it offers minimal resistance to water flow while being sufficiently sturdy to withstand the pressure of the feed stream. RO membranes are normally made of polymers, based either on cellulose acetates (cellulose di-acetate, cellulose triacetate, or combinations of the two) or polyamide and, for desalination, they are commonly found in spiral-wound (SW) (Figure 01.14), hollow fibre (HF) (Figure 01.15), or other configurations. Tubular and plate-frame designs are sometimes used in the food and dairy industries.

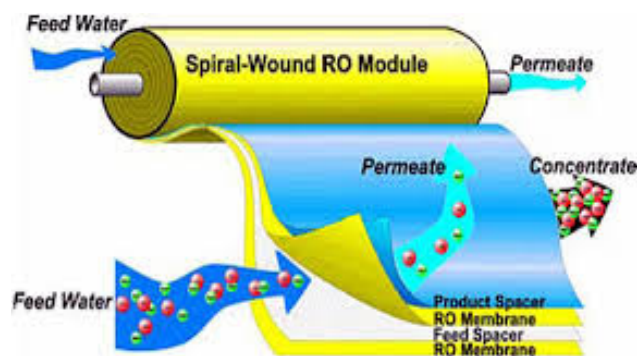


Figure 01.14 – Spiral-Wound (SW) membranes (Al-Karaghoul et al. 2019). Reproduced with permission of the rights holder Elsevier Ltd.

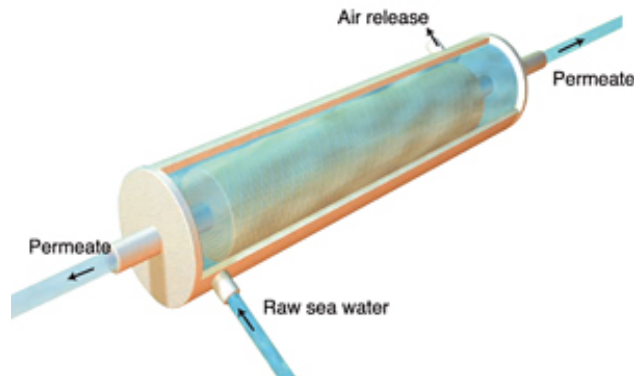


Figure 01.15 – Hollow-Fibre (HF) membranes (Al-Karaghoul et al. 2019). Reproduced with permission of the rights holder Elsevier Ltd.

A typical industrial SW membrane is about 100–150 cm long and 20–30 cm in diameter, while an HF membrane is made of millions of fibres folded to produce bundles about 120 cm long and 10–20 cm in diameter. SW and HF membranes are used to desalt both seawater and brackish water, the decision of which to use is based on factors such as cost, feed-water quality, and product-water capacity. The main membrane manufacturers have based in the United States and Japan.

The post-treatment system consists of sterilization, stabilization and mineral enrichment of the product water, because the RO unit operates at ambient temperature, corrosion and scaling problems are diminished compared to distillation processes, however, effective pre-treatment of the feed water is required to minimize fouling, scaling, and membrane degradation and in general, the selection of proper pre-treatment and proper membrane maintenance is critical for the efficiency and shelf-life of the system.

1.2.2.2 Electrodialysis (ED)

Electrodialysis is an electrochemical separation process that uses electrical currents to move salt ions selectively through a membrane, leaving fresh-water behind. It is a low-cost method for desalinating brackish water with a salinity of up to 12,000 ppm TDS. In fact, due to the dependence of the amount of energy consumed upon the feedwater salt concentration, the ED process is not economically attractive for desalinating seawater with higher salinities.

An ED unit consists of the following basic components: pre-treatment system, membrane stack, low-pressure circulation pump, power supply for direct current (rectifier or PV system), and post-treatment system (Figure 01.16).

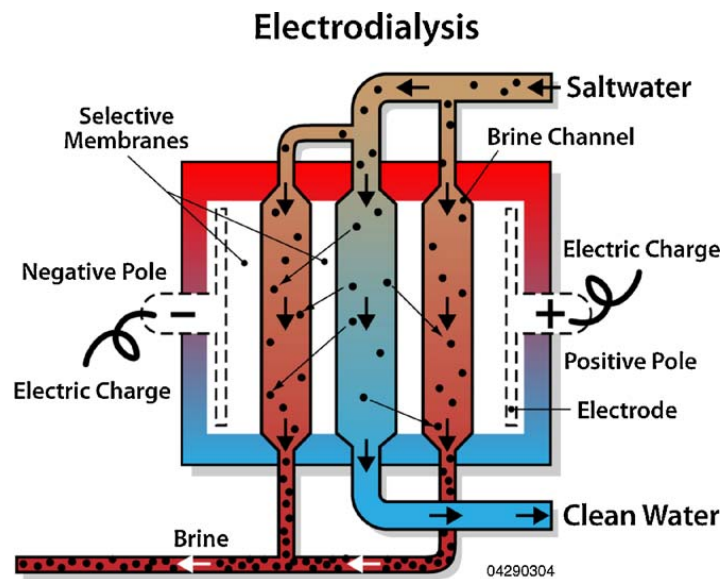


Figure 01.16 – Ion Exchange Electro Dialysis unit ED part.1 (Al-Karaghoul et al. 2019). Reproduced with permission of the rights holder Elsevier Ltd.

The principle of ED operation is that electrodes (which are generally expensive as they are constructed from niobium or titanium with a platinum coating) are connected to an external source of direct current (such as a battery or PV source) and immersed in a container of saline or brackish water. Once the electrical current is applied and conducted through the solution, the ions migrate to the electrode with the opposite charge, with positively charged ions migrating to the cathode and negatively charged ions migrating to the anode. The salinity of the water is reduced as water passes through ion-selective membranes positioned between the two electrodes. These membranes consist of sheet polymers that have been subjected to a special treatment in which micro-sized cracks or crevices are produced within the plastic film surface to permit the transport of ions, while ion-exchange sites which are incorporated into the membrane's polymer matrix promote membrane selectivity. Anion-permeable membranes allow anions to pass through to the positively charged electrode while rejecting cations and, conversely, cation permeable membranes permit cations to pass through to the negatively charged electrode while rejecting anions (Figure 01.17).

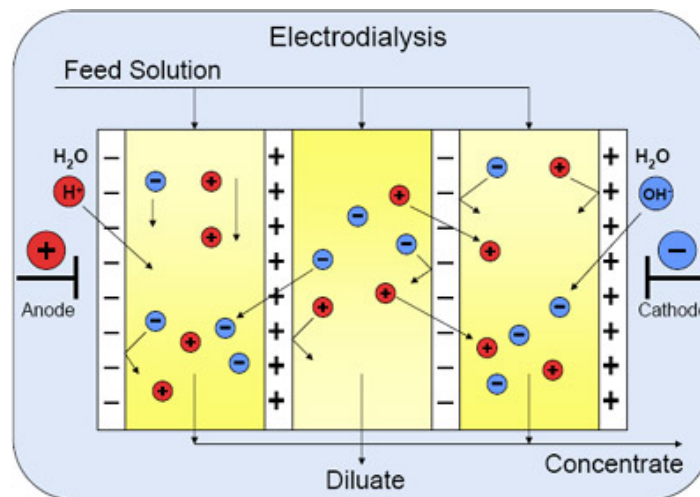


Figure 01.17 – Ion Exchange Electro Dialysis unit ED part.2 (Al-Karaghouli et al. 2019). Reproduced with permission of the rights holder Elsevier Ltd.

A spacer sheet is placed between each pair of membranes to permit water to flow along the face of the membrane and to induce a degree of turbulence. One spacer provides a channel that carries feedwater (and product water), whereas the adjacent spacer carries brine. Through this arrangement, both concentrated and diluted solutions are created within the spaces between the alternating membranes and both feedwater and brine pass simultaneously in parallel paths through all the cells, thus providing a continuous flow.

Commercial ED plants contain many cell pairs, usually several hundred, and such cells can either be stacked horizontally or vertically although, in practice, several membrane pairs are used between a single pair of electrodes, thereby forming an ED stack.

1.2.2.3 Forward Osmosis (FO)

Forward osmosis (FO), also known as manipulated osmosis or engineered osmosis, is one of the emerging membrane technologies, as it can desalinate seawater or brackish water with a lower energy cost than traditional processes. The novelty of this process lies in utilising the natural osmotic process for desalination rather than the hydraulic pressure, as in RO (Figure 01.18).

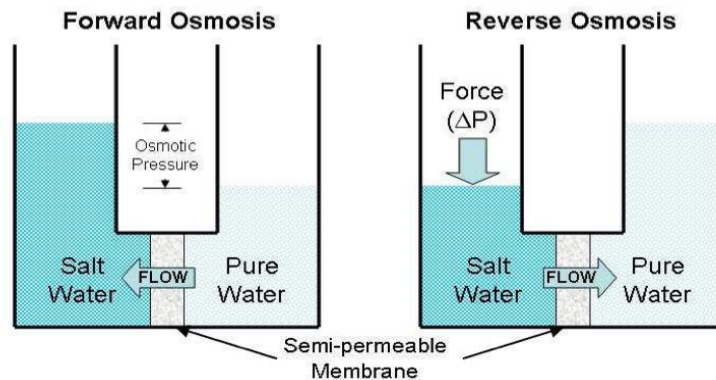


Figure 01.18 – Schematic representations of the osmosis phenomena in reverse and forward osmosis (Zhao et al. 2012). Reproduced with permission of the rights holder Elsevier B.V.

When saline feedwater and the highly concentrated solute (referred to as the draw solution (DS) or osmotic agent, draw agent, etc.) are separated by a semi-permeable membrane, water moves from the saline (lower solute concentration) to the concentrated DS (with a higher solute concentration) due to osmotic gradient, while retaining solutes on both sides of the membrane. Hence, the driving force in the FO process is created naturally by the difference in osmotic gradient arising between the feed stream and the DS (Figure 01.19). This process offers many advantages such as a lower energy cost and significantly lower membrane fouling potential and, consequently, there has been a growing interest in studying the FO process, particularly in relation to desalination applications. Although there are currently some commercial applications of FO, several challenges still need to be overcome to achieve an effective large-scale standalone FO process. One of these key challenges is in developing a suitable DS that can generate a high osmotic pressure to produce high water flux while being easy to concentrate and recover at a lower energy cost. Therefore, the selection and development of a suitable DS presents one of the significant challenges to achieving the commercialisation of the FO process, especially as regards desalination for drinking water production. Even if the number of research publications on FO has recently increased, most efforts have been focused on the development of new membranes and process performance. However,

relatively few are dedicated to the improvement of DS, even though the performance of the FO process is highly dependent on the selection of an appropriate DS.

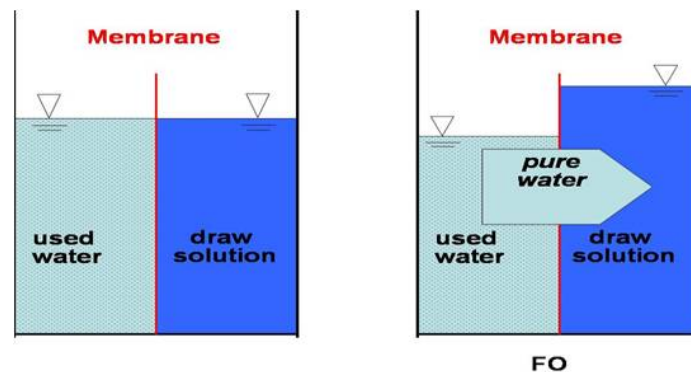


Figure 01.19 - Schematic representation of the forward osmosis process (Zhao et al. 2012). Reproduced with permission of the rights holder Elsevier B.V.

The concept of FO, aside from water desalination, has been studied for many applications including treatment of industrial wastewaters, liquids from the food industry, membrane bioreactors, the concentration of anaerobic digester effluent and the dilution of fertilisers. Extensive research has also been conducted into evaluating the use of FO in reclaiming wastewater for potable reuse.

The use of forward osmosis (FO) is of growing interest to the water desalination sector due to its potential energy savings. However, its industrial implementation is still limited by its actual performance limitations in terms of water permeation and reverse salt diffusion due to its membrane properties.

The FO desalination process operates with some advantages when compared to RO desalination (Zhao et al. 2012):

- Low hydraulic pressure leads to low fouling, low energy requirement, and reduced cleaning.
- High osmotic pressure leads to increased water flux and high rates of recovery (over 75%).
- High rejection leads to a high-quality product and fewer contaminants.
- No need for chemical pre-treatment.
- Less brine discharge.
- No membrane compaction.

In summary, FO represents a potentially lower-cost technology, yet the lack of high-performance membranes that minimise fouling, concentration polarisation and reverse diffusion – as well as the necessity for a simple separable draw solution – have limited the wider adoption of this process.

Novel membrane materials and different draw solutions have been tested and research is continuing to find the best combination to improve overall process performance.

Membranes

The desired FO membrane should have mechanical and performance stability, a high density in the active layer for high salt rejection, resistance to a wide range of pH, high water flux, and low concentration polarisation.

In the very early stages, various types of materials, including animal bladders, collodion (nitrocellulose), rubber and porcelain, were tested for FO applications. Most of the studies on FO had used RO membranes and, since the 1960s, many efforts have been dedicated to finding the optimal material following the initial development of the Loeb–Sourirajan membrane. An overview of development in recent years is presented in Table 01.01.

YEAR	MEMBRANES	MATERIALS	PREPARATION METHODS
2005	CAPSULE WALL MEMBRANE	CELLULOSE ACETATE OR ETHYL CELLULOSE	DIP-COATING, PHASE INVERSION
2007	HOLLOW FIBRE NF	POLYBENZIMIDAZOLE (PBI)	DRY-JET WET PHASE INVERSION
2008	FLAT SHEET CELLULOSE ACETATE MEMBRANE	CELLULOSE ACETATE	PHASE INVERSION AND THEN ANNEALING AT 80-95°C
2009	DUAL-LAYER HOLLOW FIBRE NF	PBI- PES/PVP	DRY-JET WET PHASE INVERSION (I.E. COEXTRUSION TECHNOLOGY)
2010	HOLLOW FIBRE	PES SUBSTRATES, POLYAMIDE ACTIVE LAYER	DRY-JET WET SPINNING AND INTERFACIAL POLYMERIZATION (IP)
2010	HOLLOW FIBER NF	CELLULOSE ACETATE	DRY-JET WET SPINNING
2010	FLAT SHEET DOUBLE-SKINNED	CELLULOSE ACETATE	PHASE INVERSION AND THEN ANNEALING AT 85 °C
2010	FLAT SHEET TFC MEMBRANE	POLYSULFIDE (PSF) SUPPORT, POLYAMIDE ACTIVE LAYER	PHASE INVERSION AND IP
2010	DOUBLE DENSE-LAYER MEMBRANE	CELLULOSE ACETATE	PHASE INVERSION
2011	MODIFIED RO	PSF SUPPORT MODIFIED BY POLYDOPAMINE	CHEMICAL COATING
2011	FLAT SHEET COMPOSITE	CELLULOSE ACETATE CAST ON A NYLON FABRIC	PHASE INVERSION
2011	FLAT SHEET COMPOSITE	PAN SUBSTRATE, MULTIPLE PAH/PSS POLYELECTROLYTE LAYERS	LAYER-BY-LAYER ASSEMBLY
2011	POSITIVELY CHARGED HOLLOW FIBRE	PAI SUBSTRATE TREATED BY PEI	CHEMICAL MODIFICATION

2011	POSITIVELY CHARGED FLAT SHEET	PAI SUBSTRATE TREATED BY PEI	CHEMICAL MODIFICATION
2011	FLAT SHEET TFC POLYAMIDE	PES/SPS SUBSTRATE, POLYAMIDE ACTIVE LAYER	PHASE INVERSION AND IP
2011	FLAT SHEET TFC POLYAMIDE	PES/SULFONATED POLYMER SUBSTRATE, POLYAMIDE ACTIVE LAYER	PHASE INVERSION AND IP
2011	FLAT SHEET TFC	PSF SUPPORT, POLYAMIDE ACTIVE LAYER	PHASE INVERSION AND IP
2011	NANOPOROUS PES	PES CAST ON PET FABRIC	PHASE INVERSION
2011	CELLULOSE ESTER MEMBRANE	CELLULOSE ESTER	PHASE INVERSION
2011	FLAT SHEET TFC POLYAMIDE	PES NANOFIBRE SUPPORT, POLYAMIDE ACTIVE LAYER	ELECTROSPINNING AND IP
2011	FLAT SHEET TFC POLYAMIDE	PSF NANOFIBRE SUPPORT, POLYAMIDE ACTIVE LAYER	ELECTROSPINNING AND IP

Table 01.01 - Recent developments in FO membrane technology.

According to their fabrication methods, these recently developed membranes can be classified into three categories, specifically phase inversion-formed cellulosic membranes, thin-film composite (TFC) membranes and chemically modified membranes. In FO applications for desalination, the active layer of the membrane faces the feed solution, while the porous layer faces the draw solution because the feed solution has a higher fouling tendency. The main challenge with FO membrane technology is in overcoming the internal concentration polarisation (ICP). This phenomenon is similar to that of the external concentration polarisation (ECP), except for the fact that it takes place within the porous layer and higher crossflow and higher temperatures can minimise it.

As regards the membrane module, different configurations can be used. Flat sheet membranes in plate-and-frame configurations are studied at the laboratory scale, whereas tubular or hollow fibre membranes are used in larger-scale applications. Spiral-wound membrane elements cannot usually be operated in FO applications because the draw solution cannot be forced to flow inside the envelope formed by the membranes.

Plate-and-frame is the simplest flat sheet configuration available, but the lack of adequate membrane support limits operation to low pressures and the low packing density leads to a larger systemic footprint and, consequently, a higher capital cost. The use of tubular elements (like hollow fibre) for FO applications is more practical as the tubular membrane is self-supported, the packing density is relatively high, and liquids flow freely on both sides of the membrane. The main difference between tubular membranes and hollow fibre is the larger internal diameters of the membranes which modify

the flow regime from laminar to turbulent. Thus, in ICP, fouling and scaling are reduced. The use of backwash may present a better solution to clean the membranes and remove any deposited particles, and this could be done by simply replacing the draw solution with pure water or reducing the concentration of the draw solute (DS) to generate a net water flux in the opposite direction. Similar results can be obtained by increasing the salt concentration on the feed side or by fluctuating the operating pressure.

Draw solution

The availability of a suitable draw solution is crucial for advancing FO technology, as an appropriate draw solution not only promotes the efficiency of the FO process but also lowers the costs of the subsequent steps in recovering and replenishing the draw solute. Further, to ensure minimal toxicity and low cost, an ideal draw solution needs to fulfil the following requirements:

Firstly, it should be able to generate high osmotic pressure. As the osmotic pressure difference between the draw solution and feed solution across the membrane is the driving force for the FO process, the osmotic pressure of a draw solution must be higher than that of the feed solution. Therefore, to achieve a high osmotic pressure, a good solubility of the DS in water is required, so suitable DS should have a high number of solute moles (N) or molarity (M) (Qingchun et al. 2013).

Secondly, the reverse flux or back-diffusion of the DS must be minimal.

As most FO membranes are not ideally semipermeable, the DS is likely to diffuse from the draw solution into the feed solution's permeate flux.

Thirdly, easy regeneration of the diluted draw solution is desirable.

After an FO process, regeneration of the draw solution is required to separate the solute and reuse it. There are a few applications (like fertigation) in which the diluted DS is used as is for other applications.

Many efforts have been devoted to discovering a suitable DS (Chung et al. 2012) and an optimal way to recover them from the diluted solution. Since the first draw solution for seawater desalination was initially introduced by Neff (1964) with a mixture of ammonia and carbon dioxide gases the field has evolved. An overview of development in this field over recent years is presented in Table 01.02.

YEAR	RESEARCHER (S)	DRAW SOLUTE (S)	METHOD OF RECOVERY	DRAWBACKS
1964	NEFF	AMMONIA AND CARBON DIOXIDE (NH ₄ HCO ₃)		ENERGY-INTENSIVE
1965	BATCHELDER	VOLATILE SOLUTES (E.G. SO ₂)	HEATING OR AIR STRIPPING	ENERGY-INTENSIVE AND TOXIC
1965	GLEW	MIXTURE OF H ₂ O AND ANOTHER GAS (SO ₂) OR LIQUID (ALIPHATIC ALCOHOLS)	DISTILLATION	ENERGY-INTENSIVE
1970	HOUGH	ORGANIC ACID AND INORGANIC SALTS	METHOD OF RECOVERY	COMPLICATED PROCEDURES, MANY CORROSIVE CHEMICAL INVOLVED
1972	FRANK	AL ₂ SO ₄	HEATING	TOXIC BY-PRODUCTS
1975	KRAVATH AND DAVIS	GLUCOSE	NONE	NOT PURE WATER
1976	KESSLER AND MOODY	GLUCOSE AND FRUCTOSE	NONE	NOT PURE WATER
1989	STACHE	FRUCTOSE	NONE	NOT PURE WATER
1992	Yaeli	GLUCOSE	LOW PRESSURE RO	ENERGY-INTENSIVE
1997	LOEB ET AL.	MgCl ₂	NONE	NOT PURE WATER
2002	McGINNIS	KNO ₃ & SO ₂	SO ₂ WAS RECYCLED THROUGH STANDARD MEANS	ENERGY-INTENSIVE, TOXIC
2005-2007	McCutcheon et al.	NH ₃ & CO ₂ (NH ₄ HCO ₃) OR NH ₄ OH (NH ₄ HCO ₃)	MODERATE HEATING (AT 60°C)	HIGH REVERSE DRAW SOLUTE FLUX INSUFFICIENT REMOVAL OF AMMONIA
2007	ADHAM ET AL.	MAGNETIC NANOPARTICLES	CAPTURED BY A CANISTER SEPARATOR	POOR PERFORMANCE, AGGLOMERATION
2007	ADHAM ET AL.	DENDRIMERS	ADJUSTING pH OR UF	NOT FEASIBLE
2007	ADHAM ET AL.	ALBUMIN	DENATURED AND SOLIDIFIED BY HEATING	NOT FEASIBLE
2008	McCORMICK ET AL.	SALT, ETHANOL	PERVAPORATION-BASED SEPARATIONS	HIGH REVERSE DRAW SOLUTE FLUX AND LOW WATER FLUX
2010	YEN ET AL.	2-METHYLIMIDAZOLE BASED SOLUTES	MEMBRANE DISTILLATION (MD)	MATERIALS COSTLY
2010-2011	LING ET AL.	MAGNETIC NANOPARTICLES	RECYCLED BY EXTERNAL MAGNETIC FIELD	AGGLOMERATION
2011	LI ET AL.	STIMULI-RESPONSIVE POLYMER HYDROGELS	DESWELLING OF THE POLYMER HYDROGELS	ENERGY-INTENSIVE, POOR WATER FLUX
2011	LING & CHUNG	HYDROPHILIC NANOPARTICLES	UF	POOR WATER FLUX

2011	PHUNTSHO ET AL.	FERTILIZERS	NONE	ONLY APPLICABLE IN AGRICULTURE
2011	IYER AND LINDA	FATTY ACID-POLYETHYLENE GLYCOL	THERMAL METHOD	POOR WATER FLUX
2012	SU ET AL.	SUCROSE	NF	RELATIVELY LOW WATER FLUX
2012	GE ET AL.	POLYELECTROLYTES	UF	RELATIVELY HIGH VISCOSITY
2012	NOH ET AL.	THERMO-SENSITIVE SOLUTE (DERIVATIVES OF ACYL-TAEA)	NOT STUDIED	POOR WATER FLUX
2012	YONG ET AL.	UREA, ETHYLENE GLYCOL AND GLUCOSE	NOT STUDIED	LOW WATER FLUX AND HIGH DRAW SOLUTE FLUX
2012	BOWDEN ET AL.	ORGANIC SALTS	RO	LOW WATER FLUX, ENERGY-INTENSIVE
2012	CARMIGNANI ET AL.	POLYGLYCOL COPOLYMERS	NF	HIGH VISCOSITY, SEVERE ICP
2012	STONE ET AL.	HEXAVALENT PHOSPHAZENE SALTS	NOT STUDIED	NOT ECONOMICAL AND PRACTICAL

Table 01.02 - Different draw solute used and tested in the recent years

The use of FO is growing as an alternative to the RO desalination process due to its advantages as compared to pressure-driven membrane processes. However, to scale up FO from research applications to industrial plants, significant improvements to both FO membrane performance and the DS must be achieved and a suitable process for reconcentrating the draw solution (such as column distillation, membrane distillation, heating or stripping) and obtaining the fresh-water product should be properly addressed.

1.2.2.4 Membrane Distillation (MD)

Membrane distillation (MD) is another emerging separation technology that has the potential to be used for seawater desalination. In an MD process, the feed and permeate streams flow across both sides of a hydrophobic microporous membrane and water vapour transports from the feed to the permeate side due to the vapour pressure gradient arising across the membrane (Figure 01.20).

The advantages of applying MD to desalination processes include the high purity of water product, the absence of any requirement for external hydraulic pressure and the applicability for highly concentrated salt solutions. Despite these advantages, there remain several challenges to be addressed

when targeting MD industrial applications. These include membrane pore wetting by water molecules, the relatively low mass flux and flux decay over time. Many efforts have been made in recent years to fabricate MD membranes with better performances, to design more reasonable membrane modules to facilitate heat and mass transfers, and to optimise the MD system to achieve higher energy efficiencies. Of all design considerations, fabricating an appropriate membrane remains the most crucial task, as the membrane is the critical component of the system (Zuo et al. 2013).

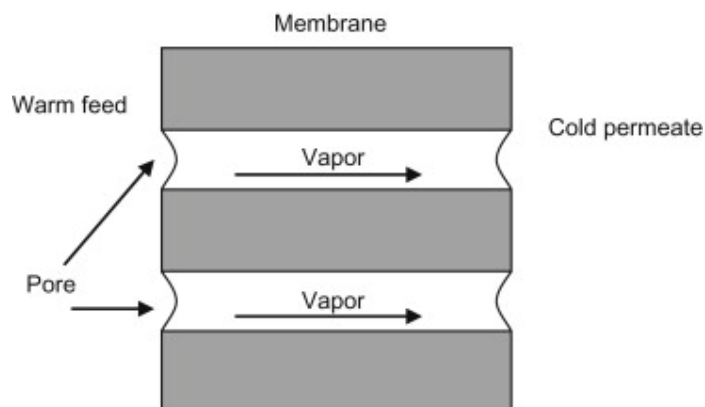


Figure 01.20 - Schematic representation of Membrane Distillation (Zuo et al. 2013). Reproduced with permission of the rights holder Elsevier B.V.

An essential requirement for membrane distillation is that the membrane material should be intrinsically hydrophobic to prevent pore wetting. Typical hydrophobic materials commonly used include polypropylene (PP), polytetrafluoroethylene (PTFE), and polyvinylidene fluoride (PVDF). However, currently, most of the membranes used for MD are microfiltration (MF) membranes that are not specifically designed for the MD process as their relatively large pores accelerate membrane wetting.

Membrane surface modifications can be applied to reduce the maximum membrane pore size, narrow its distribution and/or further enhance membrane hydrophobicity; nevertheless, this process should be performed with care as a highly hydrophobic membrane surface enhances membrane fouling. When a highly hydrophobic membrane surface is in contact with an aqueous media containing hydrophobic species such as oils that have a high affinity for such surfaces, this results in the blockage of the membrane pores and membrane wetting. In this case, hydrophilic modification seems to be more appropriate, not only reducing membrane pore size, but also protecting the membrane pore from fouling.

There are two major strategies for hydrophilic surface modification, namely surface coating and surface grafting. The common limitation of surface coating is the instability of the coating layer on

the membrane surface due to their relatively weak interaction. In contrast, surface grafting, which can be achieved by high energy plasma and ultraviolet (UV) irradiation or by chemical treatment, can induce covalent bonding between the membrane surface and the grafted molecules, thereby leading to a more stable modified layer on the membrane surface.

1.3 Renewable Energy Desalination Technologies

Since antiquity, humankind has used RES for desalination, yet a remarkably rapid development in their technology has been spurred in the wake of the petroleum crisis of 1973, especially during the last decade owing to rising environmental concerns.

Aside from the aforementioned arguments in support of the use of RES in addressing the emerging era of energy insufficiency, water scarcity is becoming an increasing problem in both arid and semiarid regions which are often remote. In those coastal areas and small islands where there is abundant solar radiation but no affordable conventional energy supply, RES often represents the best energy supply option for autonomous desalination systems (Mathioulakis et al. 2007).

Desalination systems, whether thermal or membrane processes, can be coupled with three primary renewable energy sources, namely wind, solar (photovoltaic or solar thermal) and geothermal energy. The decision as to which energy should be used is based on economic, environmental and safety considerations.

Due to its desirable environmental and safety advantages, it is widely believed that, where possible, solar energy, and especially solar thermal, should be utilised instead of energy derived from fossil fuels, even when the costs involved are slightly higher.

Solar energy can either be directly or indirectly harnessed for water desalination. Collection systems that use solar thermal energy to produce a distillate directly in the solar collector are termed direct solar thermal desalination systems, whereas those which combine solar energy collection with conventional desalination are called indirect desalination systems.

Within indirect desalination systems, solar energy is used either to generate the heat (solar thermal) required for desalination and/or to generate the electricity (photovoltaic) that is used to provide the necessary power to drive conventional desalination plants such as multi-effect (ME), multi-stage flash (MSF), or reverse osmosis (RO) systems (Figure 01.21).

Solar thermal desalination, both direct and indirect, offers the best potential for irrigation in remote arid regions due to the small-scale application required and its use of simple technology that can be sourced locally. The most suitable processes that can satisfy water requirements for irrigation in these

regions are mainly solar stills, particularly Solar Pond combined with MSF and MD and solar humidification-dehumidification processes.

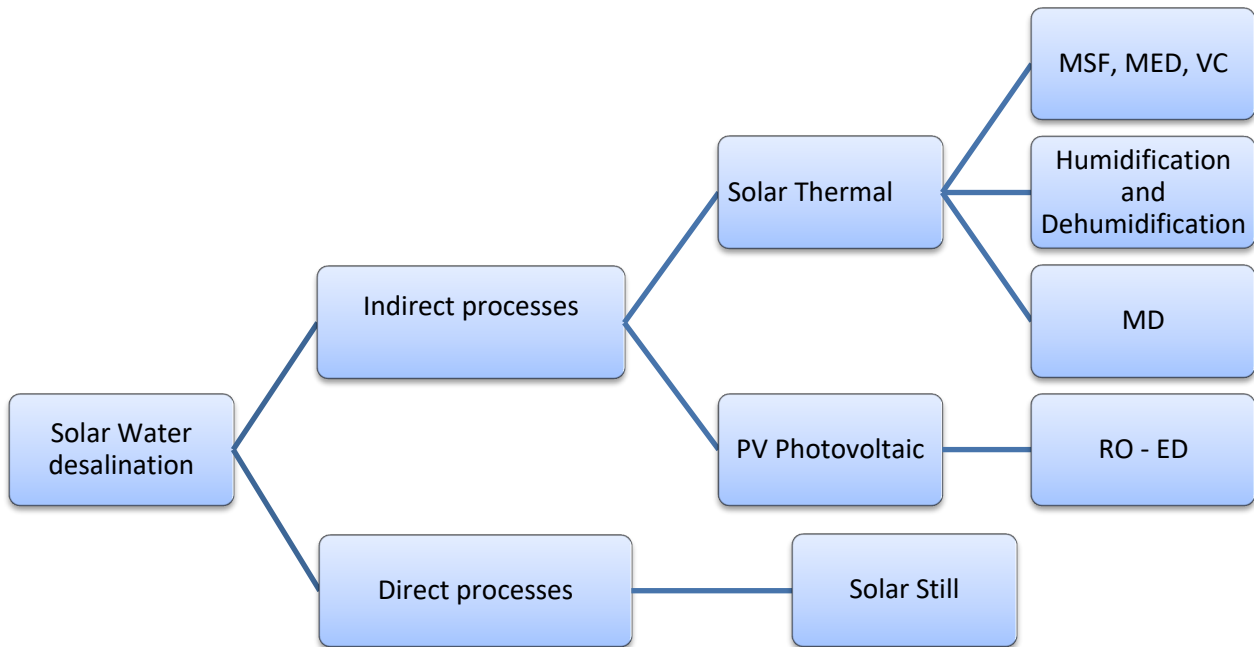


Figure 01.21 – Solar water desalination processes.

1.3.1 Direct Solar Thermal Desalination Systems

Direct solar thermal desalination systems are those in which the desalination process takes place in the same device as the fresh-water is produced. These are mainly suited to small production systems in those regions and applications where the fresh-water demand is less than 200 m³/day (Garzia-Rodriguez 2002).

A representative example of a direct desalination system is the conventional solar still. This uses solar thermal energy to create a greenhouse effect to evaporate salty water, although its low production rate is explained by the steam's low operating temperature and pressure.

A solar still consists of a basin, usually covered by a glass roof, in which a constant amount of seawater is enclosed (Figure 01.22). As the sun's rays pass through the glass roof they are absorbed by the blackened bottom of the basin and, as the water is heated, its vapour pressure is increased and when it reaches the cooler roof surface it is condensed on the underside and runs down into the troughs that conduct the distilled water to the storage reservoir (Kaviti et al. 2016). While the roof is translucent to the incoming sunlight, it is opaque to the infrared radiation emitted by the hot water

(the so-called greenhouse effect). Therefore, it contains all the vapour, prevents losses, and keeps the wind from reaching and cooling the salty water.

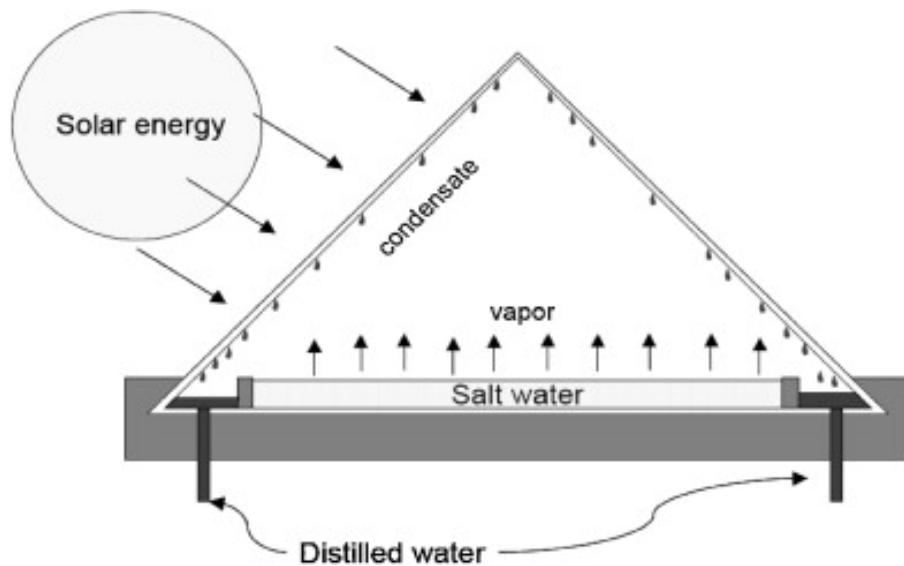


Figure 01.22 – Solar Still – an example of a solar water desalination process.

The amount of water that can be distilled is dependent on several factors, including geographical location, the sun's position, general meteorological conditions, solar still design and operational techniques.

Single-effect solar stills have an efficiency of about 30–40% (Mink et al., 1998). To evaporate 1 kg of water at a temperature of 30°C almost 2.4×10^6 J is required which, assuming insolation of 250 W/m²/day, this energy could be sufficient to evaporate a maximum of 9 l/m²/day, although in practice heat losses will occur and the average daily yield from a solar still is as little as 3–4 l/m²/day, as confirmed by Manchanda and Kumar (2015), who made an extensive study of many different configurations.

The primary disadvantage of solar stills is their very low yield, which implies that large areas of flat ground are required to achieve adequate production. However, they can be a viable solution where cheap desert land is available, possibly near the sea where the saline can be readily collected.

Solar stills remain the cheapest solution amongst all available desalination systems in use today as they are very easy to construct and operate. In fact, the cost of water produced by direct solar distillation systems depends only on the total capital investment needed to build the plant, given that the operational and maintenance costs are either limited, or negligible, because no external energy supply is required unless pumps are used to transfer the saltwater from the sea.

The production rate is proportional to the area of the solar still, which means that the cost per unit of

water produced is nearly the same, regardless of the size of the installation. This is in contrast with conditions for traditional fresh-water supplies, as well as for most other desalination methods, whereupon water costs diminish because the capital cost of equipment per unit of capacity decreases as the size increases.

Solar stills are often ideal for implementation in remote areas where fresh-water demand must be met economically using inexpensive construction materials. However, extensive work is still needed to cost-effectively improve existing designs.

One of the main weaknesses for this type of desalination plant is their low thermal efficiency and productivity, although these could be improved via various passive and active methods (Naim et al. 2003). For instance, in active solar stills, extra-thermal energy is fed into the basin of a passive solar still for faster evaporation. The external equipment may be in the form of a collector/concentrator panel, Solar Pond, or waste thermal energy device obtained from any chemical/industrial plant or conventional boiler. If such external equipment is not used, then the solar still is known as passive.

Passive solar distillation is an attractive process for saltwater desalination, in that the process can be self-operating, of simple construction and relatively maintenance-free (Fath 1998). However, these advantages of simple passive solar stills are offset by the low amounts of fresh-water produced and the need for regular flushing of accumulated salts (Malik et al. 1997). Modifications using passive methods include basin stills, wick stills, diffusion stills, stills integrated within a greenhouse, amid other configurations. Accordingly, these modifications will be briefly presented.

Basin type stills

The performance of a simple basin type passive still can be augmented by several techniques such as using single or double slope. The dual-slope still offers better performance than a single slope under hot climatic conditions (Malik et al. 1997).

The focus, when trying to improve the rate of condensation and consequently the operating performance in a basin type still, is to increase the temperature difference arising between the water in the basin and the glass cover. This can be achieved either by increasing the temperature of the water or decreasing the temperature of the covering glass.

Cooling water or saline can be fed into the gap of a double glass cover (Haddad et al. 2000) to reduce the temperature of the covering glass while adding a passive condenser within the shaded region of a single slope still, while injecting black dye into the seawater increases its temperature and consequently increases the distillate yield by up to 45% (Fath 1998).

Wick type stills

In a wick still, the feedwater flows slowly through a porous, radiation-absorbing pad (the wick). This presents several advantages over the basin type still. First, the wick can be tilted so that the feedwater offers a better angle to the sun, thereby reducing reflection and presenting a large effective area. Second, less feedwater is, at any given time, present in the still, and so the lower water level is heated more quickly and to a higher temperature.

Tanaka et al. (1981) have proven the superiority of the tilted wick type solar still and confirmed an increase in productivity by up to 20–50%. Sodha et al. (1981) designed a simple multiple wick solar still comprised of an aluminium frame, a glass cover and a water reservoir made of galvanised iron, claiming the design offered several advantages, including its low weight, low cost and significant output.

Diffusion type stills

Diffusion solar stills are comprised of two separate units, namely a hot storage tank which is generally coupled to a solar collector and a distillation unit that produces the distilled water. Such a still can have multiple distillation chambers (“effects”). Graeter et al. (2001) and Rheinlander and Graeter (2001) designed a four-effect still for the desalination of sea and brackish water and experimentally investigated its efficiency in a test facility under different modes and configurations of heat recovery (natural and forced convection). The theoretical distillate output from their distillation unit was 8.7 l/m²/day for an energy input of 2.0 kW/m²/day for an active cross-section of 1 m², representing 4 m² of evaporator and 4 m² of condenser surface area.

Solar still greenhouse combination

Several studies have recently focused on small-scale systems for solar desalination with capacities below 50 m³ day and potential applications in remote areas combined with a water-efficient greenhouse.

Greenhouses, in combination with solar stills, represent an interesting possibility for developing small-scale cultivation in those environs where only saline or brackish water is available (Malik et al. 1996). The seawater greenhouse combines a solar desalination system with an environment for cultivating crops in which transpiration is minimised while producing sufficient water for its use through a process of solar distillation.

Desalination is a highly energy-intensive process, making the fresh-water produced by fossil fuels an expensive resource, one which most of those populations living in arid regions cannot afford for

agricultural use. As such, water is primarily used in agriculture to grow high-value crops, especially in greenhouses, since the irrigation demand of a modern greenhouse is 60-90% of that required for open fields (Chaibi 2003; Radhwan 2005).

The short-term solution adopted by these regions has so far been to import food and water (El-Kady and El-Shibini 2001) instead of implementing small to medium scale solar thermal desalination plants which, it has been estimated, could meet more than 50% of their agricultural water needs (Chaibi 2011). This strategy, if combined with water-efficient irrigation methods such as drip or subsurface irrigation, could liberate yet further water to increase food security (Kuylensstierna et al. 2009).

Chaibi et al. (2004) designed and fabricated a roof-integrated water desalination system for greenhouses (Figure 1.23). In this design, the solar still consisted of a double-glazed part of the south-facing roof, in which the lower glass was only partly translucent, thereby absorbing a substantial amount of the solar irradiation while transmitting those wavelengths favourable for the photosynthesis of the underlying vegetation (the photosynthetic active radiation, or PAR, has the wavelength interval 380–710 nm).

The incident solar thermal radiation absorbed within the glass layer also reduced the ambient temperature within the greenhouse, leading to an improved climate for the crops and a reduced requirement for ventilation and associated reduction in water consumption by the crops.

During the day, saline was pumped from a reservoir to the rooftop of the greenhouse, from where it was distributed evenly to the evaporation surface in the still. The water vapour produced condensed on the top glazing, ran along the inner wall of the top cover and was collected in the fresh-water store. The residue of the feedwater was collected in a separate storage vessel. The returned feedwater was partly returned to the feedwater duct for another cycle in the still, while some of the residual saline was also mixed with the fresh-water prior to irrigation to bulk out the supply. The desalination roof was operated day and night, as excess heat could be stored in the saline.

The water produced used for irrigation in the greenhouse was mixed with some brackish water so as to be economical with the fresh-water supply. When mixing the fresh-water produced with the same amount of brackish water, the water production was sufficient to meet the water demands of low-canopy crops in a climate such as Tunisia (Chaibi and Jilar 2004).

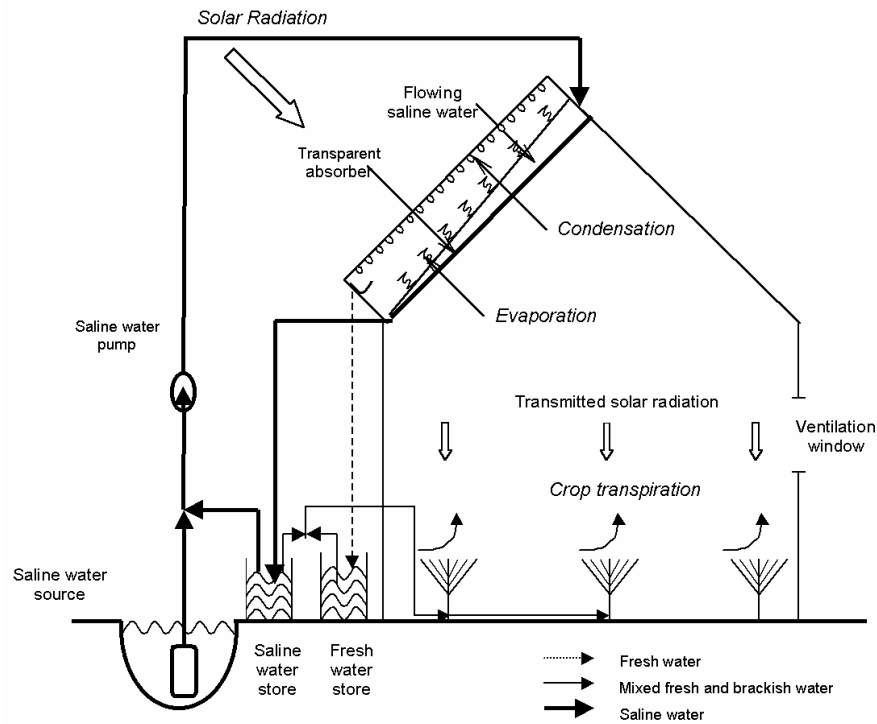


Figure 01.23 - Greenhouse with integrated solar still on the roof (Chaibi 2004). Reproduced with permission of the rights holder Elsevier Ltd.

Radhwan (2005) conducted a theoretical study of a stepped solar still with an inclined glass cover connected to a greenhouse in Saudi Arabia. The still consisted of five trays of saline water in an insulated basin (Figure 1.24). Air from the greenhouse entered the solar still from the bottom, flowed upwards over the trays to pick up heat and vapour and re-entered the greenhouse from the top of the still as vapour saturated air.

The estimated daily water yield from the still was about 4.9 kg/m^2 , of which 0.8 kg/m^2 was condensed on the glass cover, and 4.1 kg/m^2 entered the greenhouse as vapour. The air temperature leaving the solar still reached 42°C under the midday sun and the relative humidity of the circulating air increased along with the still and always left the still saturated. The results indicated that decreasing the airflow rate has an insignificant influence on still yield, while the greenhouse heat load is decreased.

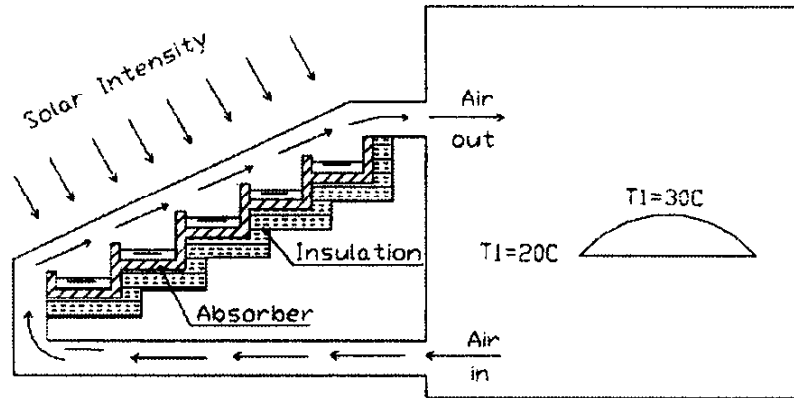


Figure 01.24 - Stepped solar still connected to a greenhouse for heating and humidifying air (Radhwan 2005). Reproduced with permission of the rights holder Elsevier B.V.

Other researchers have proposed different designs for a solar still greenhouse in combination with humidification-dehumidification processes. Davies and Paton (2004) confirmed the feasibility of designing a seawater greenhouse such that the amount of fresh-water produced exceeded any evapotranspiration.

Multiple-effect basin stills

Multiple-effect basin stills have two or more stages in which each stage essentially reuses the heat given off by the condensing vapour of the previous step to provide energy to vaporise the feedwater of the following stage typically placed above it. In this design, the condensing surface of the lower compartment is the floor of the upper compartment (Figure 1.25).

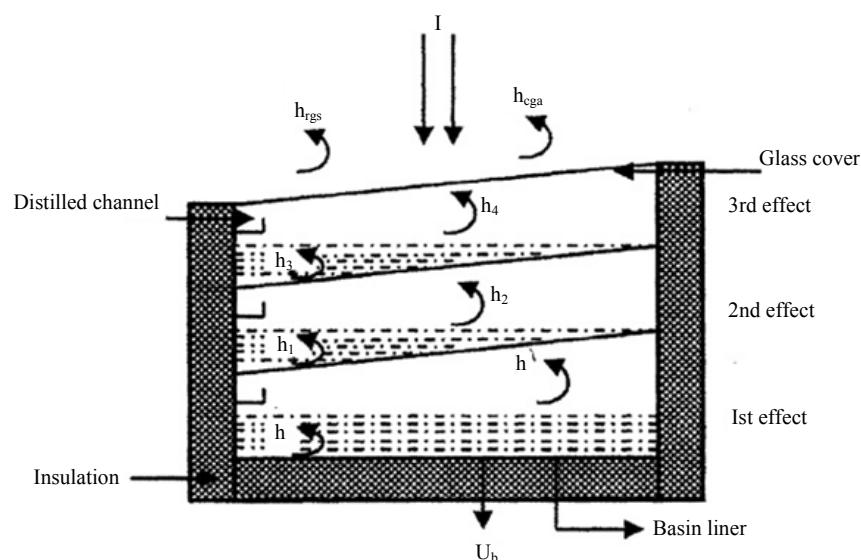


Figure 01.25 - Schematic of triple basin solar still (El-Sebaii 2005). Reproduced with permission of the rights holder Elsevier B.V.

Multiple-effect solar desalination systems are more efficient than single-effect systems due to the reuse of the latent heat of condensation, yet the increase in efficiency usually increases both capital and operating costs. Efficiency is greater than for a single basin still, typically being 35% or greater, but the cost and complexity are correspondingly higher.

Schwarzer et al. (2001) have presented numerical simulations and experimental results for a thermal desalination unit with a heat recovery system. The desalination unit is comprised of a solar collector and a multi-effect still made of six stages incorporating a water circulation system to avoid salt accumulation. The authors demonstrated that the production rate of the unit could reach 25 l/m²/day for a value of 4.8 kWh/m²/day of solar radiation.

Externally heated active solar stills

For active solar stills, the temperature of saline in the basin can be increased through additional external heating to achieve faster evaporation. The external heat source can be a:

- (1) Solar heater or Solar Pond;
- (2) Solar collector/concentrator;
- (3) Waste heat recovery system from any chemical/industrial plant or conventional boiler.

Circulation through the external heating source and the still could either be achieved through natural circulation (thermosyphon) or else by forced circulation using a pump and a heat exchanger.

Other types of active stills are hybrid or miscellaneous. Hybrid stills are a particular category of active stills in which the solar still is coupled to some other system such as solar dryer, solar photo-voltaic panels, or thermoelectric generators, while miscellaneous solar stills encompass unique designs such as a tubular solar still, a still with an external condenser, or a spherical/hemispherical solar still.

Katecar et al. (2021) made a techno-economic analysis of passive and active solar stills to investigate the most economic and productive design. From their study, it was observed that, for passive solar stills, stills with trays and internal mirrors (Abdullah et al., 2020) were found to be the most cost-effective design having a cost per litre (CPL) of \$0.0021 and a productivity of 4.80 l/m²/day, while the solar still with Fresnel lens (Johnson et al. 2019) was found to be the most productive at 9.22 l/m²/day.

For active solar stills, the double-slope/single-basin solar design with a flat plate collector (Sethi and Dwivedi 2013) was the most efficient with a CPL of \$0.0078, while a single-slope, single-basin still

connected to two solar dishes (Kabeel et al. 2019) was found to be the most productive at 13.63 l/m²/day.

Considering hybrid and miscellaneous solar stills, the low concentrating photovoltaic-thermal solar still (Xinxin et al. 2019) was the most economical design with a CPL = \$0.0013 and a productivity of 2.653 l/m²/day; while a spherical solar still with a parabolic reflector (Modi et al. 2020) was the most productive design at 8.25 l/m²/day.

Comparing all available solar still designs, the average water production rate was 4.67 l/m²/day with a CPL of \$0.0388, values that are in line with the tubular still with a parabolic concentrator sun tracking system, as presented by Elashmawy (2017), which had a productivity of 4.71 l/m²/day and a CPL of \$0.033.

1.3.2 Indirect Solar Thermal Desalination Systems

Indirect solar thermal desalination systems are those in which the desalination process is separated into two sub-systems, specifically a solar collector and a desalination unit (Figure 01.26). The solar collector can be a flat plate collector (FPC), an evacuated tube, solar still, Solar Pond or solar concentrator (SC), and it can be coupled with any thermal desalination process which uses the evaporation and condensation principle, including MSF, VOC, MED, MD and HD systems. The additional use of PV to supply the power needed to operate pumps and other process units can help to minimise the external energy demand of the thermal desalination system and make it standalone.

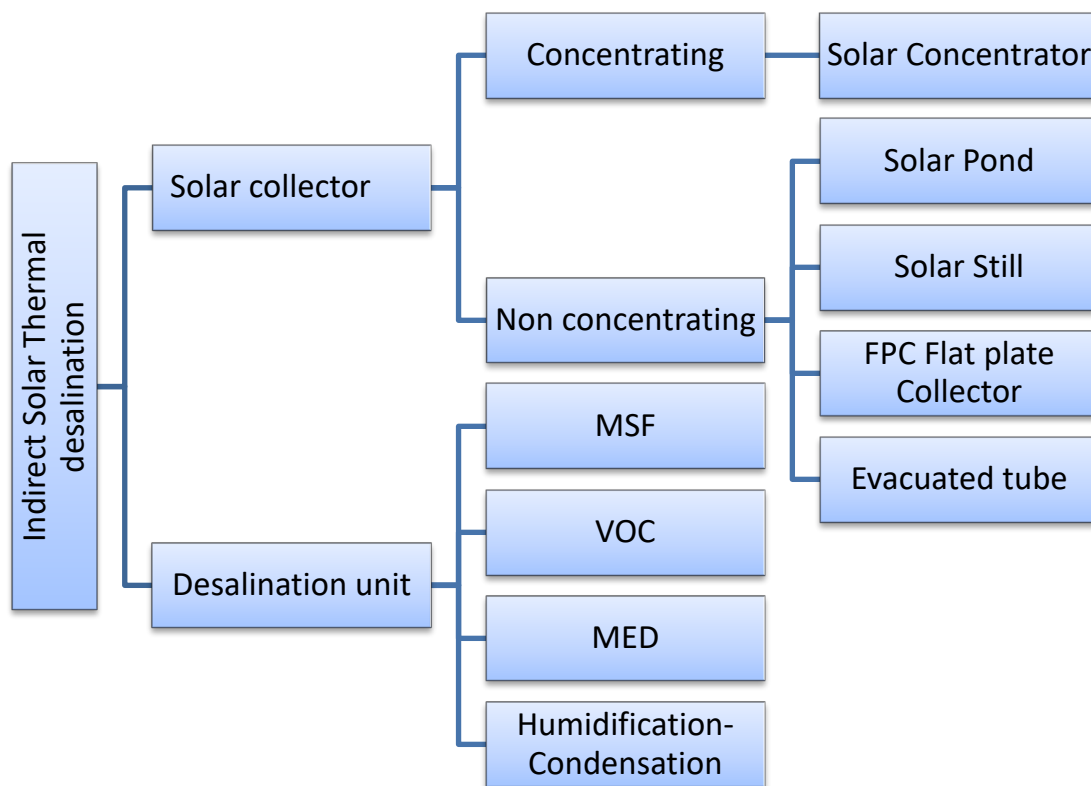


Figure 01.26 – Indirect solar thermal desalination systems.

The major component of any solar thermal desalination system is the solar collector. This absorbs the incoming solar radiation, converts it into heat, and transfers this heat to a fluid (usually air, water, or oil) flowing through the collector. This accumulated heat is then carried from the circulating fluid either directly to the following thermal desalination process, or to a thermal energy storage tank from which it can be drawn for use on demand.

There are two primary types of solar collector; non-concentrating or stationary and concentrating. A non-concentrating collector has the same area for intercepting and absorbing solar radiation, whereas

a concentrating solar collector, like a sun-tracking system, has concave reflecting surfaces to focus the sun's radiation onto a smaller receiving area, thereby increasing the radiation flux.

A solar still can be considered an indirect solar collector, wherein the stored heat is not used directly to produce and condensate the distillate in the unit, but rather as a humidifier to provide humid air to the following dehumidification processes.

Many different types of simple and small-scale indirect solar thermal desalination systems have been tested and used for agriculture in arid regions and are available today. Their efficiency is continuously improving and their capital costs are steadily being reduced, thereby offering a promising solution to tackle water shortages and supply agricultural needs in remote arid regions.

2. Solar Pond Combined with Thermal Desalination

2.1 Introduction to Solar Ponds

The Solar pond is a unique large-area solar collector that uses a body of still water to collect solar energy and stores it as thermal energy. From a practical standpoint, all ponds, lakes, oceans, and other expanses of water in nature collect solar energy and convert it into thermal energy, although their heat retention efficiency is low because the water near the surface is quickly cooled as the heat is rapidly dissipated to the environment. Water warmed by the sun at the lower depths of the pond expands and rises as it becomes less dense and, once it reaches the surface, the water loses its heat to the air (via natural convection) or evaporates, taking the heat with it.

The Solar pond converts solar radiation into thermal energy (heat), although most of it is subsequently lost due to convection and/or evaporation. Therefore, a water-pond system will be more effective in the collection and storage of solar energy if its thermal losses to the environment are reduced, either by suppressing the natural convection of water within the pond or by covering the pond surface with a partially transparent layer of insulation. Therefore, the term Solar pond is used for a water pool with reduced heat losses if it can collect solar energy, concentrate, and store it as heat to approximately 100°C (the boiling point of water restricts higher temperatures). The Solar pond thus involves simple technology and uses water as a working material for all three functions, namely collecting solar radiant energy and converting it into heat, storing this heat, and transporting thermal energy from the system (Figure 02.01).

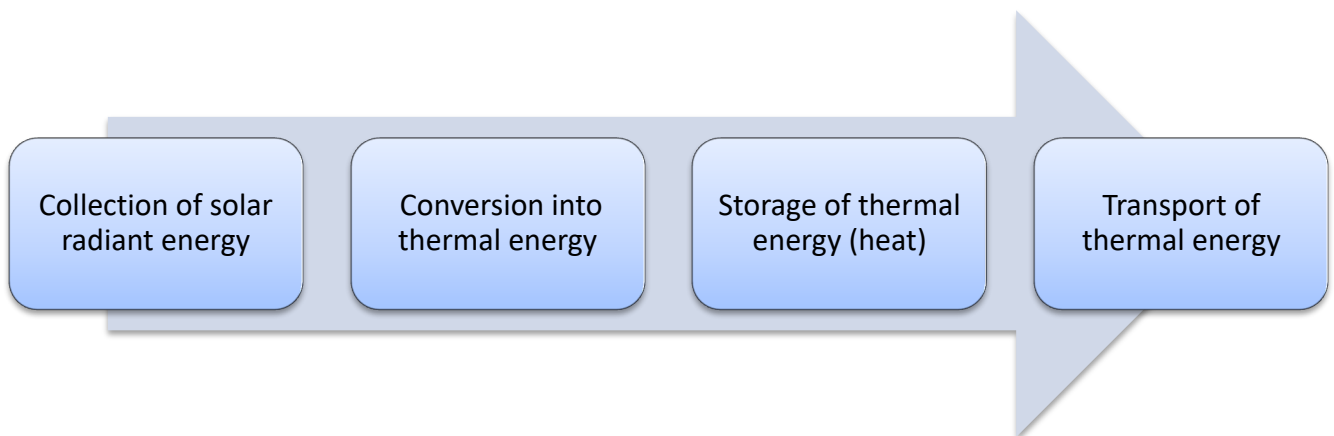


Figure 02.01 – Functions of a Solar pond.

A Solar pond is a relatively low-tech and less capital-intensive technology as compared with other solar technologies. However, it is space consuming and only works well in regions with high incident solar radiation (Figure 02.02).

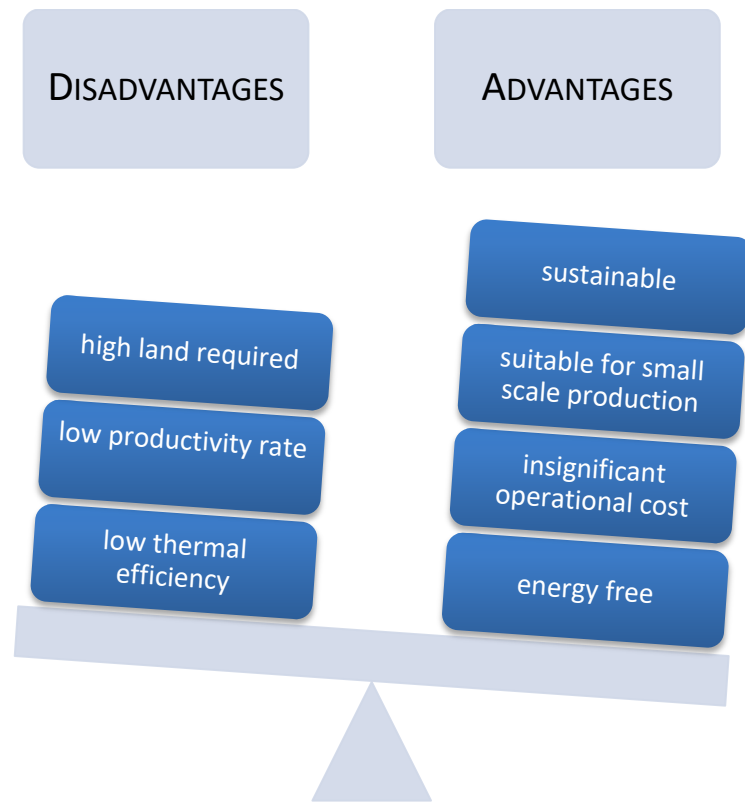


Figure 02.02 – Solar thermal energy vs Solar pond.

2.2 Solar Pond History

The first recorded use of solar energy for heating a pool was approximately 2,500 years ago when great Roman baths were heated by the sun. However, it was only just over a century ago, in 1902, that Von Kalecsinsky reported that the bottom of Madve lagoon in Transylvania in summer had a temperature of approximately 70°C at a depth of 1.32 m, even if the temperature during the summer season never exceeded 26°C (El-Sebaï et al. 2011). In this lake, salt concentration was observed to increase with depth, and the increase in salt concentration at greater depths actually prevents convection currents, thereby making the surface region of the lake a partially transparent insulator that traps solar heat in the depths of the lake. The conceptual design of the first artificial “sun pool” was first provided by Tabor and Bloch in 1958. Their proposed system was an artificial pond (approximately 1 m deep) with a black bottom and salt gradient, with a maximum salt concentration at the bottom which was obtained by filling the pond with progressively less dense layers of brine.

Although this report was followed by several studies in the same natural lake, there were no further attempts to construct similar Solar Ponds for the collection and utilisation of solar energy until later in the twentieth century (Dickinson et al. 1980).

After Tabor and Bloch's discoveries, Solar pond research began in Israel (Tabor 1966) and carried on until 1967. The main goal of this research was to produce electrical power, providing important results which are still used to this day. Given that the Solar Ponds used for electricity production were not cost-competitive with other contemporary conventional technologies owing to their very high construction costs (Tabor and Matz 1965), they were abandoned until 1975. In 1974, research into Solar Ponds as long-term heat storage systems began in the United States at Ohio University (Rabl and Nielsen 1975), soon followed by the University of New Mexico in 1975 (Zangrando and Bryant 1976).

Solar Ponds have been studied in many countries, including Chile, the former Soviet Union and India and, over the past few decades, many Solar Ponds have been established across the world. One of the most famous Solar Ponds is the El Paso Solar pond which was constructed in 1983 as a research development and demonstration project operated by the University of Texas. Soon after its construction, the El Paso salinity gradient Solar pond recorded a water temperature of about 90°C although this effectively destroyed the standing gradient layer as a result of heat rising to near boiling temperature. After this event, it was rebuilt and the system was improved to avoid such problems in future. Subsequent research focused on coupling Solar Ponds with thermal desalination techniques (Lu et al. 2001).

2.3 Solar Pond Types

There are two main categories of Solar pond (Figure 02.03):

- Non-convective ponds that reduce heat loss by preventing convection from occurring.
- Convective ponds that minimise heat loss by hindering evaporation with a cover over the pond's surface.

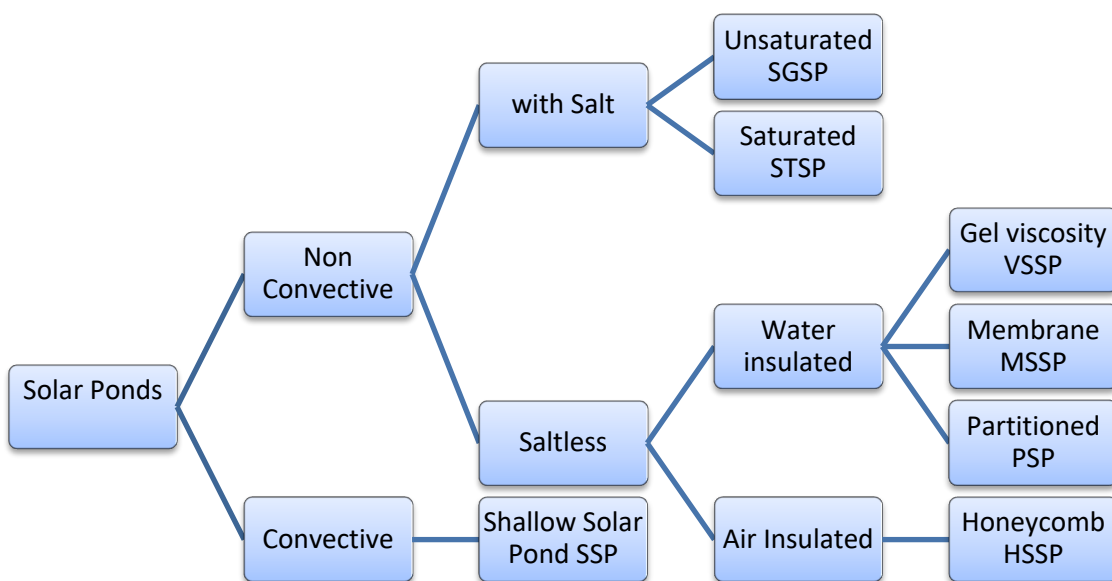


Figure 02.03 – Types of Solar pond.

2.3.1 Non-Convective Solar Pond

Non-convective Solar Ponds restrict heat loss to the environment by suppressing any natural convection arising between the upper layer of the pond and the atmosphere. Such natural convection can be reduced by using a salt gradient that may be unsaturated for a Salt Gradient Solar Pond (SGSP), saturated for Saturated Solar Ponds (STSP), or salt-less using a transparent insulation layer of water or air (salt-less). Salt-less non-convective Solar Ponds were conceived primarily to overcome the convection issues arising within a salt gradient, although there were other numerous problems encountered, including:

- Biological growth of algae and bacteria.
- Decrease of transparency due to dirt.
- High rates of evaporation.
- Possible soil contamination due to salt leaking.

We can mention within these various solutions the Membrane Stratified Solar Pond (MSSP), Viscosity Stabilised Solar Pond (VSSP), Partitioned Solar Pond (PSP), and Honeycomb Stabilised Solar Pond (HSSP). Salt gradient Solar Ponds have advantages for long-term energy storage while salt-less ponds are more suitable for short-term energy storage as the temperature rise of the pond is much faster.

2.3.1.1 Salt Gradient Solar Pond (SGSP)

The salt gradient of a Solar pond is typically 1 to 2 m deep, and the convection currents that normally develop due to the presence of hot water at the bottom and cold water at the top are prevented by the presence of a strong density gradient. This density gradient is obtained by using a high concentration of suitable salts such as NaCl or MgCl_2 at the bottom of the pond and a lower concentration at the top. The thermal conductivity of the salt solution decreases with salinity and thus acts as an insulating layer while, at the same time, the temperature profile increases (Figure 02.04).

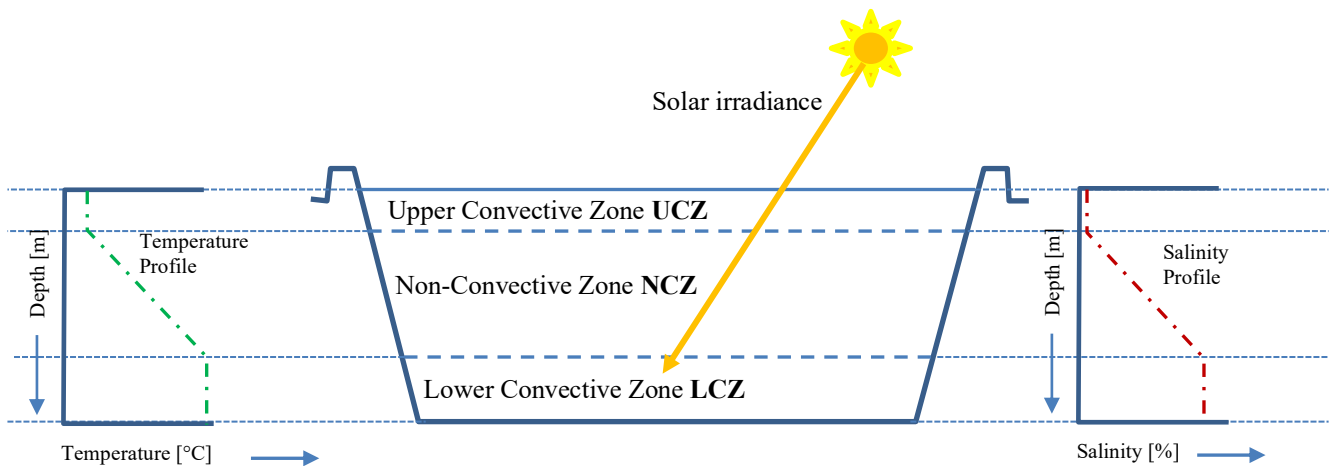


Figure 02.04 – Design of Non-Convective Solar pond (SGSP).

The salt gradient of a Solar pond is comprised of three layers:

The top surface layer is the upper convection zone (UCZ), a zone of constant temperature and salinity. The depth of this surface layer varies from 0.1 to 0.4 m and is formed due to upward salt transport, surface heating/cooling and wave action.

The second layer is the non-convective zone (NCZ) with a depth ranging from 0.6 to 1.0 m and this acts as the insulating layer of the pond. The density in the NCZ increases with the depth of the gradient layer in parallel with salinity and temperature (Kaushik et al. 1980). The thickness of the gradient layer depends on the desired temperature, solar transmission properties and thermal conductance of

water.

The bottom, or third layer, is the lower convective zone (**LCZ**), or storage layer. This is a heat storage layer of constant salinity and temperature. Its thickness depends on the temperature and the amount of thermal energy to be stored. Normally the energy is extracted from this layer.

2.3.1.2 Saturated Solar Pond (STSP)

The STSP is a special type of SGSP where the water is saturated at all levels. In an STSP the higher salinity is primarily intended to reduce the evaporative heat losses of the UCZ and also the overall salinity of the pond is increased to maintain its stability (Garg 1987).

The density gradient is obtained by using a high concentration of suitable salts such as KNO_3 whose solubility increase with temperature so that the near saturation of salt concentration is maintained at all depths. The temperature of the pond is higher in the lower region so that a larger amount of salt is progressively dissolved and forms a standing concentration gradient that increases toward the bottom of the pond. Such saturated ponds apparently have no diffusion problems and the gradients are self-sustaining. Thus, such stability makes the pond a maintenance-free solution.

2.3.1.3 Partitioned Solar Pond (PSP)

A PSP is a pond with two transparent partitions, one either on top (or just under) the water's surface and the other at a depth of 1 to 2 m. The surface insulation of the pond is provided by a non-convective layer of a transparent fluid such as ethanol or silicone oil in a Teflon film (Kaushik et al. 1980). A thin layer of water can be left above the top partition and this can create a decrease in reflective losses because the water has a lower index of refraction than plastics, such that reflective losses at a water-plastics boundary are small and yet, at the same time – especially in windy locations – it can induce evaporative cooling and increase reflectivity due to wave action. The lower partition separates the insulating layer from the convective layer and consequently improves the stability of the pond and facilitates heat extraction. Instabilities arising due to buoyancy can be avoided either by making the lower partition stiff (e.g. by using glass panes) or, if a flexible partition is used, in the form of a polyvinyl fluoride (PVF) film, by filling the convection zone with salt water (Garg 1987). To improve convection, heat is extracted from just below the partition, either by removing hot water or brine directly, or else by running fresh-water through a network of heat exchanging plastic pipes. The use of the PVF film may be preferable if brine is to be used in the convective zone.

2.3.1.4 Viscosity Stabilised Solar Pond (VSSP)

A viscosity stabilised Solar Pond is a pond in which the salt is replaced with another substance to reduce maintenance intervals and prevent environmental pollution in case of a leakage. Shaffer (1978) proposed a new type of Solar pond using a transparent polymer gel as a non-convecting layer. This polymer gel has low thermal conductivity and is used in a near solid-state so that it will not convect (Taga et al. 1990).

Materials suitable for VSSPs should have high transmittance for solar radiation, high efficiency for the chosen thickness and be capable of performing at temperatures up to 60°C. Polymers such as Arabic gum, locust bean gum, starch and gelatine are potentially useful materials. The viscosity stabilised Solar Pond appear to be promising though as yet not economically competitive with a SGSP (Garg 1987).

2.3.1.5 Membrane Stabilised Solar Pond (MSSP)

A MSSP is a type of salt-less Solar pond that comprises a body of liquid utilising closely spaced transparent membranes to suppress convection. The membrane space should be tiny and many high transparent films are required (Taga et al. 1990). Hull (1980) presented a concept in which closely spaced membranes are placed horizontally or vertically in the upper part of the pond fluid's reservoir to quench convective heat transfer.

The buoyancy effect on the partitions is balanced by the weight of water so that solar radiation is converted into sensible heat. Three types of membranes have thus far been studied for the MSSP, specifically horizontal sheets, vertical tubes, and vertical sheets (Rabl et al. 1975).

2.3.1.6 Honeycomb Stabilised Solar Pond (HSSP)

The HSSP is another method of suppressing naturally occurring convection currents using an air layer instead of water. Air-filled honeycomb panels are positioned on the top of the pond's surface to reduce the convection, achieving a 40-60% solar efficiency at temperatures ranging between 70°C to 90°C. Lin (1982) suggested a sealed air-filled two-tier honeycomb floating on the fresh-water body, whereas Ortabasi et al. (1983) proposed a honeycomb structure containing a thin layer of oil. Despite several investigations, all experiments using the HSSP have demonstrated poor functionality, a predisposition to collecting dirt and a premature loss of insulation.

2.3.2 Convective Solar Pond

Convective Solar Ponds are ponds where heat losses to the environment are reduced by covering the pond's surface. The cover is usually transparent and the pond is often of shallow depth. A typical example of such a system is the Shallow Solar Pond (SSP), comprising a water-filled plastic bag glazed at the top with a blackened, insulated bottom.

2.3.2.1 Shallow Solar Pond (SSP)

The SSP is a solar energy collector intended to supply large amounts of heat for industrial applications at a cost that is competitive with fossil fuels. It is used to convert solar energy into low-grade thermal energy. It has been a subject of intensive investigation for several years, especially by the solar energy group of the Lawrence Livermore Laboratory (USA). The term SSP was largely derived from the solar still, although the name implies that the depth of water is minimal, typically only a few centimetres, akin to a conventional solar still. A SSP is essentially a blackened tray holding some water which takes advantage of the evaporation of saltwater due to solar heating. In the SSP, the pond surface is covered using a plastic film so that the film is in contact with the top surface of the water, thereby preventing the cooling effect due to evaporation. It can heat a large quantity of water to an appreciable temperature and due to its simplicity of operation. As such, it holds promise of becoming one of the cheapest known methods for harnessing solar energy. A SSP is essentially a large water bag or pillow placed within an enclosure with clear upper glazing. Water at a depth of 4 to 15 cm is placed within the bag which is generally constructed from transparent upper plastic film and a black lower one (Figure 02.05). The solar energy collection efficiency is directly proportional to water depth, whereas the water temperature is inversely proportional to it. The water in the SSP is heated during the day, during which time solar energy is converted into thermal energy, while it is withdrawn from the SSP before sunset (or more precisely when the collection efficiency approaches zero) for utilisation or storage. In the SSP, the black bottom of the pond absorbs solar radiation and, as a result, the water gets heated, although not all the total solar energy absorbed by the entire system is converted into useful energy owing to several loss factors and some other mechanisms that reduce the total input of solar radiation such as, for instance, the absorptivity of the surface of the collector which is not unity or the failure of the overlying transparent sheet at the surface to allow all the radiation to pass through. There are also other losses arising due to conduction, convection, and radiation. Therefore it is important to use a suitable insulation material that reduces these losses, and normally one or two transparent sheets are used to cover the pond (Garg et al. 1982).

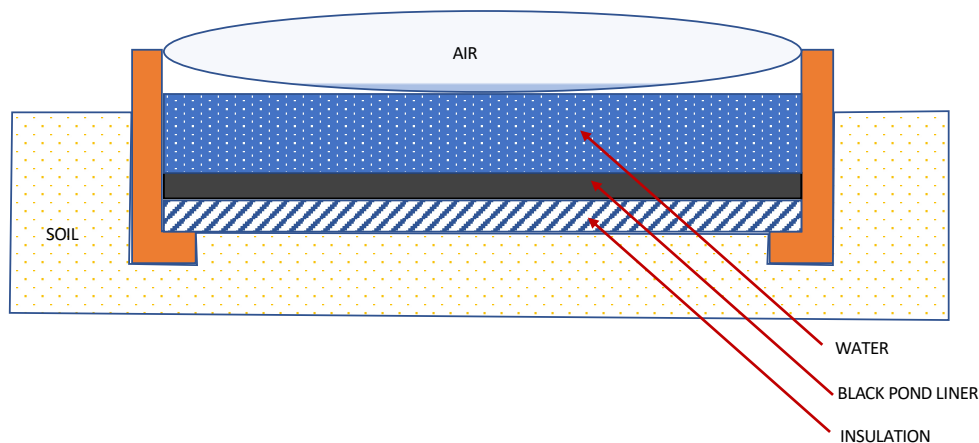


Figure 02.05 – Schematic of Shallow Solar Pond (SSP).

2.4 Historical Background of Desalination Coupled to Solar Ponds

One of the most promising solar energy technologies for producing potable water from seawater or brackish water is a SGSP combined with a thermal desalination unit. Solar Ponds combine solar energy collection with long-term storage and can provide reliable thermal energy across a temperature range from 50° to 90°C. Thus, they are ideal for combination with thermal desalination processes that require approximately 97% heat and 3% electricity (48 kWh heat and 1.3 kWh electricity per m³ of desalinated water; Mesa et al. 1997).

Such heat storage enables the Solar pond to power desalination during cloudy days and at night, ensuring stable and constant water production. Another advantage of using a Solar pond as a heat source is that they can utilise what is often considered a waste product, namely rejected brine, as the basis to construct new Solar Ponds. As such, a Solar pond can also be used as the second stage in a proposed zero-discharge desalination process (Farahbod et al. 2013).

Solar pond powered desalination has been studied since 1987 at the El Paso Solar Pond Project, El Paso, Texas (Lu et al. 2001). From 1987 to 1992, the research primarily focused on the technical feasibility of thermal desalination in combination with Solar Ponds but, since 1999, the research has focused on long-term reliability and the improvement of thermodynamic efficiency and economic viability. Over this period at El Paso a small multi-effect, MSF distillation (MEMS) unit and a MD unit have been tested.

A few other Solar Ponds have been built and tested although few are still active today. Worthy of mention are the large 25,000 m² Margherita di Savoia pond in Italy (Folchitto 1991); the Alexandria

Solar Pond in Egypt (Amer 1986); the 1,700 m² pond in Kuwait (Al-Homoud et al. 1989; Al-Marafie et al. 1991); the 2,000 m² pond situated at the University of Illinois (Newell et al. 1990); and the 6,000 m² pond in Bhuj in India (Kumar and Kishore 1999).

At the same time various desalination processes have been evaluated as suitable options for the Solar pond, including MSF, LT-MED, and Sea Water RO (SWRO), as shown by Kyathsandra (1988), Fisher et al. (1991), Glückstern (1991) and Hoffman (1992) in their comprehensive works. The limited activity in terms of Solar pond development is mainly because Solar Ponds have, to date, been studied as power-producing facilities relative to lower cost solutions employing gas and oil rather than as a heat source for water desalination. In the case of thermal desalination, Solar Ponds offer an advantage as lower temperatures are desired and the combination can be highly efficient.

2.4.2 Solar Pond Coupled with Multi-Effect Multi-Stage (MEMS) - El Paso

The El Paso Solar Pond was a research and development project operated by the University of Texas and funded by the US Bureau of Reclamation of the State of Texas; the pond had the specifications reported in Table 02.01.

El Paso Solar Pond	
Started in	1983
Surface area	3,000 m ²
Water depth	Total depth: 3.25 m - UCZ (0.7 m), NCZ (1.2 m), LCZ (1.35m)
Salt used	NaCl (LCZ near saturation 26%)
Start-up temperature increase	1° C /day in LCZ
Temperature daily fluctuation Day/Night	1-3°C in LCZ if no heat is extracted.
Extraction flow rate max	2.3 m ³ /min = 138 m ³ /hr

Table 02.01 – El Paso Solar Pond specifications. Data source: (Lu et al. 2001; 2002).

The operating temperature of the pond ranged from 70°C in winter to 90°C in early fall. The maximum temperature of the pond during the testing period from 1991-1993 was 93°C and, during the summer months, heat had been regularly extracted to prevent the water from reaching boiling so

as to maintain the stability of the gradient zone. The maximum ΔT (temperature difference between lower zone and surface zone) was measured at over 70°C in the summer months. Further, it has also been noted that the pond surface temperature was several degrees lower than the ambient temperature, with the opportunity of using this phenomenon as a cold source for the purposes of condensation. Experience has also been gained in how to:

- Build up the salinity gradient, partially filling the pond with saturated brine and injecting fresh-water in a step-by-step scanning modality through a diffuser immersed in the solution (scanning injection technology).
- Extract the heat from Solar pond by pumping the hot brine from an extraction diffuser placed at the maximum temperature of the LCZ to an external heat exchanger and returning it to a return diffuser placed at the bottom of the pond.

Thermal desalination technologies tested in the El Paso Solar pond were:

- a) MSF
- b) MEMS + VC (robust design –low-quality input energy)
- c) MEMS + MD
- d) Brine Concentration and Recovery System (BCRS)

A brief description of the results of the different desalination technologies, especially the most interesting ones, MEMS and MD, are summarised and reported below.

MEMS

The MEMS unit was tested for three effects, namely a four-stage flash distillation unit designed to produce high-quality distilled water from salt or brackish water at a rate of about 3.5 to 4 l/min with a water quality, or TDS < 2 mg/l. During the experiment, a model was built to predict the production rate (PD) [l/min] and performance ratio (PR). According to such model, the production rate was influenced mainly by the flash range (FR in °C); the concentration of rejected brine (COR in mg/l), and the circulation rate of 1° first effect/stage (CS1 in l/min) according to Equation (1).

$$PD = -0.964353 + 0.0688765 \cdot (FR) - 0.000002 \cdot (COR) + 0.02679032 \cdot (CS1) \quad (1)$$

While the PR was influenced by the FR, the temperature of the distillate and COR (in °C) were calculated from Equation (2).

$$PR = 6.81729121 - 0.0696854*(FR) - 0.12534092*(TOD) - 0.1545689*(TOR) \quad (2)$$

The unit can be effectively and economically operated at a first stage vapour temperature of between 60°C and 75°C with a very high concentration ratio and rejected brine near saturation. The temperature level is fundamental as it affects both PR increases (although PR decreases with increased temperature) and the increased temperature difference observed between the distillate and rejected brine (1st and 4th stages). The colder surface water of the Solar pond was used as a cooling mean for the desalination unit. In fact, having a lower cooling temperature will increase the FR and improve the PD and PR. The main problems for the long-term operation of the system were scaling and corrosion. Therefore, the units should preferably be fabricated from stainless steel or titanium (Caruso et al. 2001).

MD

A MD system was also tested at the El Paso Solar pond (Walton et al. 2004) to create and study a zero-discharge system, wherein MD was applied after nanofiltration and combined with flash distillation. MD differs from other membrane filtration technologies in that the driving force for desalination is the differential in vapour pressure of water rather than the total pressure of the system. The membranes for MD are hydrophobic, allowing water vapour to pass through but not liquid water. The minimum temperature differential (i.e. brine temperature – permeate temperature) required to drive MD is a function of brine temperature and salinity. The flux is more significant for a greater temperature drop and at higher source water salinities. The flux begins at the minimum temperature difference of 1°K, although practical production requires higher temperature differences. The advantages of MD are that:

- a) It produces high-quality distillate;
- b) Water can be distilled at relatively low temperatures (30°C to 100°C); and,
- c) The water does not require extensive pre-treatment to prevent membrane fouling as required in pressure-based membrane treatments.

The potential disadvantages are uncertain economic costs and relatively low production fluxes (~3–6 l/m²/h).

2.4.3 Solar Pond coupled with MSF – Atlantis

An SGSP coupled with a MSF called the Atlantis desalination system (Figure 02.06) was described by Szacsvey et al. (1999). In an MSF process, the pressure decreases during each stage by a predetermined amount according to the prevailing temperature. Unfortunately, when the MSF is coupled to a Solar pond, it cannot be operated at a constant temperature, leading to a change of pressure difference between stages. To avoid this pressure drop, Atlantis is designed with an inter-stage pressure self-regulating system (Autoflesh).

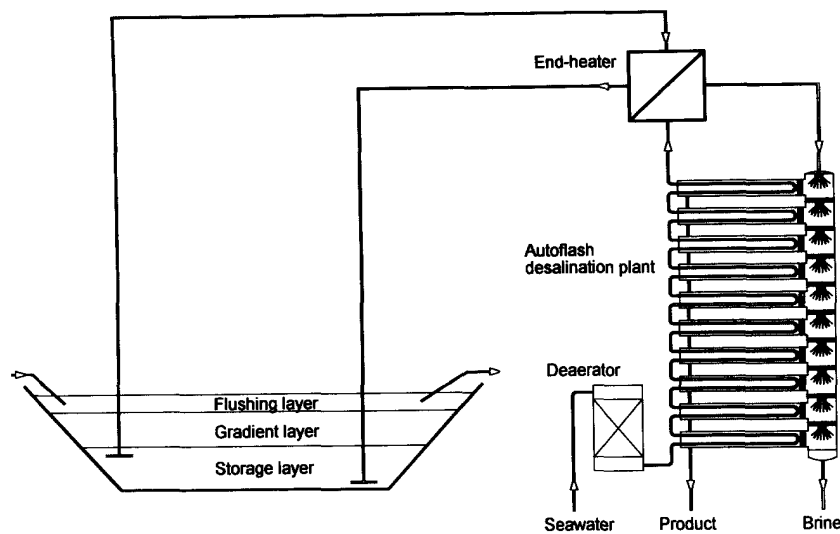


Figure 02.06 – Autoflesh desalination system powered by an SGSP (Szacsvey et al. 1999). Reproduced with permission of the rights holder Elsevier B.V.

For MSF desalination coupled to Solar pond, many stages are typically required (from 12 to 16) to optimise fresh-water production and reduce energy demand (approx. 70 kWh/m³). It is also possible to reduce the thermal energy demand by adding condenser stages, but this creates a sharp increase in capital costs of the plant.

The proposed system has been tested in the Atlantis Solar Pond in Switzerland, a small Solar pond which has been in operation for nine years and supplied enough data to build a simulation programme. Starting from the experimental Solar pond, both efficiency and costs have been estimated for different Solar pond sizes. A small size Solar pond with a water generation capacity of 15 m³/day has a predicted annual collection efficiency of 10.5% and an estimated cost for produced water of 5.48 USD/m³, while for larger systems of 300 m³/day, the efficiency may reach 12.5% and the estimated cost of produced water is 2.39 USD/m³ (Table 02.02). This compares to a real-world efficiency of a 250,000 m² pond in Israel which was 16%.

Pond type	Smaller pond – 2,500 m ²	Medium pond – 36,000 m ²
Solar Pond cost	25 USD/m ²	15 USD/m ²
Efficiency	10.5 %	12.5%
Water production	15 m ³ /day	300 m ³ /day
Water cost estimation	5.48 USD/m ³	2.39 USD/m ³

Table 02.02 – Cost of Solar pond according to size. Data source: (Szacsvey et al. 1999).

2.4.4 Solar Pond coupled with MED

Garmana and Munstasser (2008) studied the interaction between a Solar pond and a MED unit in a mathematical model as described in Figure 02.07.

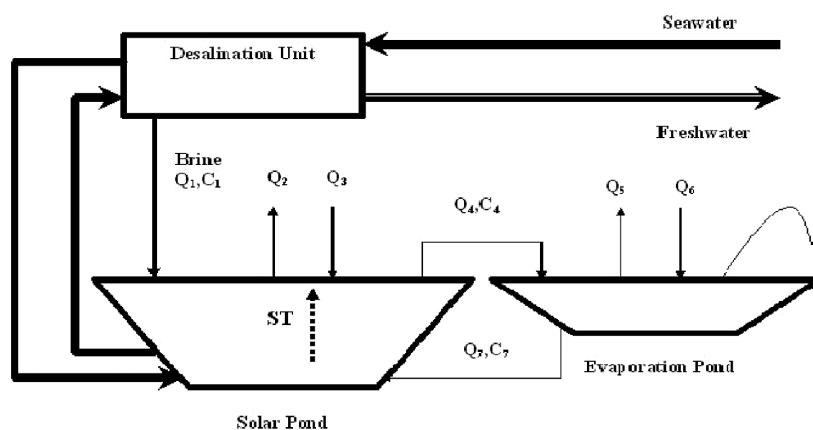


Figure 02.07 – MED desalination unit coupled with an SGSP and evaporation pond (Garmana and Munstasser 2008). Reproduced with permission of the rights holder Elsevier B.V.

The main subject of their work was to find the optimal dimension of the pond layers to store the maximum amount of energy necessary to feed the MED unit. The optimal thickness of the pond layers, according to their study, was as follows: UCZ 0.3 m, NCZ 1.1 m, LCZ 4 m.

They also found that the heat which can be transferred to the MED unit depends on the number of stages and the plant capacity (in m³/day) and that there was a linear relationship between the thermal load and the required surface area of the pond.

2.4.5 Solar Pond coupled with MSF – Tripoli (Lybia)

Agda (2009) created a simulation model describing the transient solar thermal behaviour and economic analysis of an SGSP combined with an MSF plant with a daily product water output of 1000 m³/day. The thermal simulation was achieved using a mathematical model based on stage-by-stage calculations considering both fluid properties and flow conditions, predicting such process variables as temperature and flash evaporation rates. The reference Solar pond was located in Tripoli, Libya, and had the following parameters: UCZ 0.2 m, NCZ 1.3 m, LCZ 1.0 m.

Agda (2009) noted that it is essential to run the MSF unit within a specific temperature range of LCZ to avoid thermal losses. In his case, this was 70 ±5°C. The temperature of LCZ depends on yearly and daily fluctuations and the heat extraction rate. Thus, the desalination system should be sized correctly and, for some part of the summer, heat will have to be wasted in order to allow the system to work across the desired temperature range (Figure 02.08).

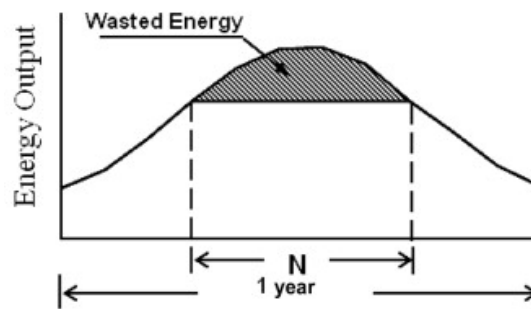


Figure 02.08 – Sketch of the thermal energy output of the Solar pond wasted to stay within the operational temperature range.

The sizing of the desalination unit was executed according to the energy supplied by the pond on a chosen peak day. All heat at temperatures exceeding this limit was wasted to maintain the thermal stability of the pond. The simulation considered equal temperature intervals between stages. It was also noted that the quantity of vapour generated decreases from the first stage to the penultimate stage. In contrast, in the final stage, vapour increases sharply due to the extra amount of moisture obtained by flashing the seawater feed. The evaporation rate is dependent on the LCZ temperature, with higher LCZ temperatures resulting in higher evaporation rates. Agda also tried to calculate the productivity and the cost of produced water, realising that one of the most important parameters to determine is the interest rate arising due to the high initial investment in the thermal unit. He confirmed that coupling Solar pond with a MED unit could allow the production of high-quality water of less than 25 ppm salinity and estimated the cost of produced water to be around 1.8-1.94 \$/m³ for a plant with a capacity of 1200-1500 m³/day.

Other studies on Solar Ponds coupled with desalination

Several other studies and simulations have been conducted to determine the best desalination technology that can be coupled to the Solar pond and those pond parameters that can influence the productivity of the desalination unit. Garmana and Munstasser (2008) created a mathematical model to predict the influence of the various pond parameters. They concluded that the main factor influencing the total thermal load is the size of the pond. Leblanc et al. (2007) developed a computer simulation to determine that the low temperature MSF process has the best performance and lowest greenhouse impact. Saleh et al. (2011) demonstrated the feasibility of a Solar pond located near the Dead Sea to supply enough heat end energy to run a large-scale MSF desalination plant without the need for any other supplementary sources of energy. The system is characterised by its high-performance efficiency (ability to use pond's heat); high capacity (how much water it can produce); and high water purity (TDSs contained in the product water).

2.4.6 Conclusions on the Best Desalination Processes Coupled with SGSP and some Economics

Comparing the different studies previously mentioned, it may be concluded that the best desalination processes, as driven by solar pond energy, are those using a low amount of auxiliary electric energy and low temperature heat sources such as MSF and LT-MED. Any additional energy required when it is not available onsite at a low cost can be produced by using a binary liquid power cycle such as ORC (Organic Rankine Cycle). In the study conducted by Fischer et al. (1988), where they compared MSF and LT-MED with SWRO, they finally concluded that LT-MED is not only a sound technical solution, but is also the most economically viable, able to compete with SWRO where cheap power is available. The product water produced by LT-MED, apart from being competitive (Table 02.03), has also very low TDS as compared to other technologies (Table 02.04). There could be the possibility of considering, as an alternative process, a combination LT-MED + SWRO. At the same time, the idea of running an SWRO with electricity produced by an SGSP is not economically sustainable. The scale factor strongly influences the water cost and is based on specific cost evaluations of desalination plants. It seems that combined plants of even 10,000 m³ per day are already economically viable.

A great deal of work and simulations have been carried out to understand the yields and the economic returns of the Solar pond for large-scale applications although, unfortunately, there are a few studies where the construction of a small size Solar pond coupled with desalination has been investigated, and there are even fewer available experiments of such an implementation.

The project's first aim in Oman has been to design a small modular Solar pond with an upper cover to reduce convection and evaporation and to use the stored heat accrued to supply a desalination unit based on a humidification-dehumidification system or a small MD system.

The focus has been to develop a Solar pond that could be industrialised at low cost and also guarantee low maintenance and a long shelf-life. Assuming, from the outset, that there would be difficulty in the management of the Solar pond, an assumption which was confirmed by the experimental trial, a mathematical simulation of the Solar pond and solar panel system coupled with a MD unit was needed. The results from this will be explained in the following chapter.

Size	10,000 m ³ per day fresh-water	
Global solar radiation	2,200 kWh/m ² per year	
Average conditions	SP thermal efficiency	18%
	ORC thermodynamic efficiency	6.2%
	ER Economy Ratio	10
	Electrical power consumption	2.5 kW
	Power cost per kWh	0.07 USD
SP area for thermal energy	593,496 m ²	
SP area for electrical energy	370,935 m ²	

Investments	
Desalination plant	14,000,000 USD
SP for heat production	9,500,000 USD
SP for energy production	8,000,000 USD

Cost of Fresh-water USD/m³ without amortisation				
	Without power production		With power production	
Cost of Energy	0.175			
Maintenance cost 4% of investment per year	0.258		0.345	
Chemicals and consumables	0.050		0.050	
TOTAL	0.483		0.395	
Cost of Fresh-water USD/m³ with amortisation and different interest rates				
	Without power production		With power production	
Interest rate	Fixed water costs	Total water costs	Fixed water costs	Total water costs
2%	0.328	0.811	0.440	0.835
4 %	0.412	0.895	0.552	0.947
6%	0.502	0.985	0.673	1.068
8%	0.605	1.088	0.811	1.206

Table 02.03 – Economic evaluation of SP desalination coupled with LT-MED. Data source: Fischer et al. (1988).

Permeate salinity	SWRO	500 ppm TDS
Permeate salinity	LT-MED	20 ppm TDS
Permeate salinity	MSF	50 ppm TDS

Table 02.04 – Permeate salinity for different desalination processes. Data source: Fischer et al. (1988).

3. Simulations of the Performance of Solar Collectors (Solar Pond and Flat Plate Collector) coupled with Membrane Distillation

3.1 Introduction

One viable option for powering irrigation in arid countries using solar energy is combining an energy storage system like a SP or solar panel with MD. The interest in using solar power MD for desalination is growing due to MD's attractive features. MD, as compared with MED, offers the advantage of being modular (despite being less efficient), and it is more feasible at smaller scales. Coupling a SP with MED does not make much sense, because MED pays a very high penalty when scaling down to small sizes. Thus, the SP required for combination with MED would be too large. MD can readily be implemented in any remote areas without any special skills or technology, yet concerns remain as to its efficiency, especially in combination with a SP. There has been a lot of research conducted on SP modelling, and models of SPs have been investigated by Yadav et al. (2004) and Sayer et al. (2016), as well as the doctoral thesis of Al-enezi (2012). Other literature on the subject was also taken into consideration (Tsilingiris 2007; Assari et al. 2015; Ganesh et al. 2016; Monjezi et al. 2016). Further, the combination of a SP with MD is not new, as Nakoa et al. (2015) previously modelled and experimented with a solar pond coupled with a Direct Contact MD (DCMD). The novelty of our simulation is the tentative use of a pond cover acting as an insulation layer, one which is transparent to radiation yet, at the same time, works as a medium to reduce conduction and evaporation to the ambient air. This last solution is studied to maintain the pond temperature overnight and increases the pond temperature faster during the day. The higher water temperature will benefit the productivity of the MD system. Mathematical equations have been revised with the introduction of pond cover insulation and a mathematical model was created in Matlab to run in accordance with the location parameters. The SP model, with and without cover, has been coupled with an air gap membrane distillation (AGMD). The predicted productivity has been compared with that of a FPC for water heating associated with AGMD, and the expected results of the two processes have been analysed and compared.

3.2 Process Unit Descriptions

The following model investigates the utilisation of an AGMD coupled to a SGSP, with and without cover, for sustainable fresh-water production and the reduction of any brine footprint upon the environment. A mathematical model for heat and mass flux in the AGMD module and a thermal model for SGSP are co-developed and coupled to evaluate the feasibility of fresh-water production and the predicted results are presented. The feed stream of 1.20% salinity deriving from the ground is heated through an external heat exchanger within the SGSP and then circulated through the AGMD

module before being injected into an evaporation pond. The productivity of the combination SGSP + AGMD is then compared with an FPC + AGMD.

3.2.1 Solar Pond

The SGSP is described as a large artificial body of water reservoir that collects and stores solar energy. It is about 1 to 3 metres deep and the bottom of the pond is usually painted black. The solar radiation incident on the pond's surface penetrates the liquid and is absorbed by the blackened base, increasing its temperature.

If the liquid is homogeneous, which means that there is no density gradient, convection currents will be set up and the heated fluid, being lighter, will travel towards the surface and dissipate its heat to the atmosphere. In a SP, these convection currents are prevented by having a salt concentration gradient. The solution's concentration and density are highest at the bottom and lowest at the surface of the pool. Typically, ponds are composed of three zones, as shown in Figure 03.01.

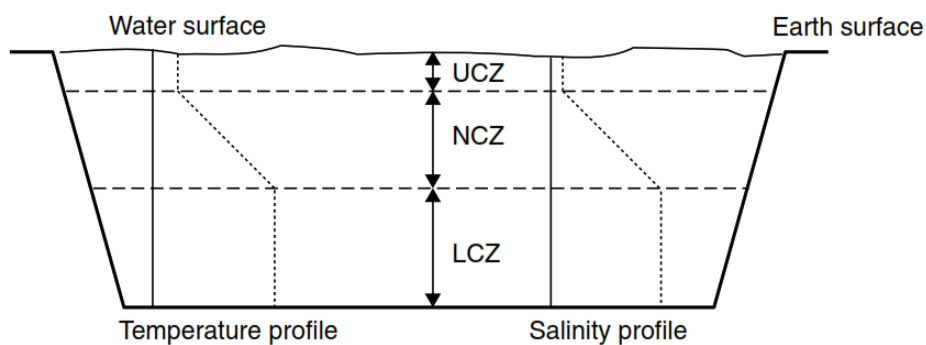


Figure 03.01 – Solar Pond gradient layers.

The first zone is the Upper Convective Zone, or UCZ, which is colder and remains close to the ambient temperature. It has a low salt concentration (almost that of fresh-water) and its depth varies from 0.1 to 0.4 m. The second zone is the NCZ, or insulation layer, which has a salt density increasing with depth. The thickness of NCZ ranges from 0.6 to 1.0 m.

Hot water in the NCZ cannot rise because of its high relative density (due to its salt content) and the fact that the supernatant water is lighter (i.e. of lower density). Similarly, water in the layer above cannot descend because the water below has a higher salt content and is, therefore, heavier, being of higher density. The lowest layer is the LCZ which has a constant high density and depth that ranges from 0.3 to 0.8 m. Convection motions from lower zones to higher ones of the pond are

hindered and heat transfer from the hotter third zone, LCZ or storage layer, to the cold UCZ can only occur through conduction.

Given the moderately low water conductivity, the NCZ layer acts as a transparent insulator, permitting solar radiation to be trapped within the hotter LCZ from which useful heat is withdrawn. The NCZ is much thicker and occupies more than half of the total depth of the pond. Both the salt concentration and temperature increase within this layer and its absolute thickness is dependent on the temperature and the amount of thermal energy that is to be stored. Some parts of this zone also serve a thermal storage function. Irrespective of this, the main storage area is in the lower zone LCZ, where the concentration and temperature are constant and its thickness varies according to the amount of heat stored.

The lowest zone traps heat energy for longer periods (which is the main advantage of Solar Ponds). As such, the energy can be stored, since the saltwater near the bottom heats up and expands. However, it cannot rise to the top because it is denser than the less salty water above. Hence a non-convective SP is best utilised for storing solar energy at a reasonable cost.

Extraction of thermal energy from the lower layers of the pond can be easily accomplished without disturbing the non-convecting salt gradient zone above. Hot water can be extracted from a Solar pond without disturbing the concentration gradient, for example by installing the water outlet at the same height as the water inlet (Goutham and Krishna 2016). Hot brine can be withdrawn and cold brine returned via a laminar flow. For small ponds, the heat exchanger is normally external. In the current model, the following assumptions are considered:

- Thermal losses to sides and ground are neglected.
- Solar radiation losses are considered.
- Solar radiation is time-variant and will vary according to the location and day throughout the year.
- Ambient temperature is time-variant.
- Design aspects (area, depth, width) will be fixed.
- The cover material will be considered in this study.
- Hot water is extracted and returned to the LCZ through an external heat exchanger.

In the present study, the transient analysis of an SGSP is carried out under the metrological conditions of Muskat, Oman. The study aims to select the maximum heat and temperature extracted from the

LCZ under a given set of operating conditions using a finite difference method, a numerical model of a SGSP (both with and without cover). A brief diagram of the configuration of the SGSP and the heat fluxes used to develop the mathematical model are reported in Figure 03.02, together with the connection between the SP and its external heat exchanger. Heat is transferred from the LCZ (hot stream) to the permeate stream (cold stream) that is heated and sent to the AGMD.

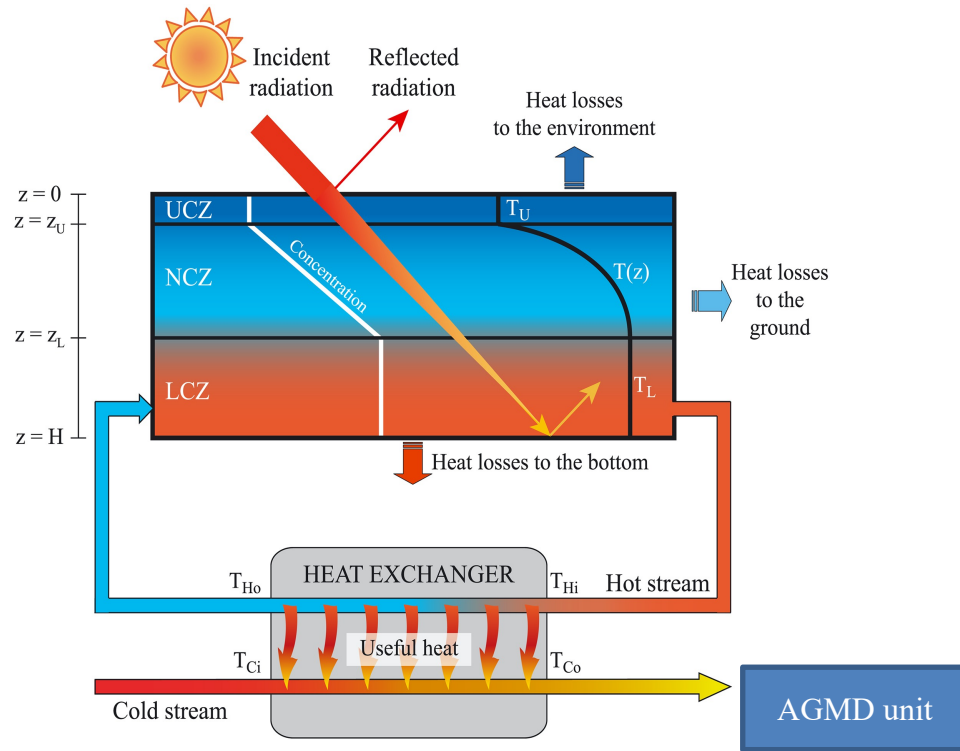


Figure 03.02 – Configuration of the SGSP and the heat fluxes used to develop the mathematical model (González et al. 2014). Reproduced with permission of the rights holder John Wiley and Sons.

3.2.2 Air Gap Membrane Distillation

Membrane distillation (MD) is a thermally driven separation process in which separation is enabled due to phase change. A hydrophobic membrane presents a barrier to the liquid phase, enabling the vapour phase to pass through the membrane's pores. The driving force of the process is given by a partial vapour pressure difference and this is commonly triggered by a temperature difference. In an AGMD, the evaporator channel resembles that featured in DCMMD, whereas the permeate gap lies between the membrane and cooled walling and is filled with air. The vapour passing through the membrane must additionally overcome this air gap before condensing onto the cooler surface. The

advantage of this method is the high thermal insulation towards the condenser channel, thereby minimising heat conduction losses.

For MD, the plant total productivity should be assigned as the primary input for the whole system; membrane type is also considered, which will affect the system design and permeability results. Membrane type, which would give the most striking operating results, will be selected; for that purpose, all input data were set the same for all types to ensure a fair comparison between each membrane type.

Table 03.01 illustrates the data comparison between all types of membrane addressed. The specific power consumption (SPC) in [kWh/m³] ranged between 1 and 2.6 kWh/m³, which is considered relatively low and remarkable as compared to RO (Solima et al. 2020). The membrane types C-PVDF, E-PH, E-CNT 0.5, E-CNT1, E-CNT2 and E-CNT3 were recorded as being lower among the remainder relating to the SPC [kWh/m³]. The PE type yielded the largest membrane area among the remainder by 10.7~11 m² followed by the PTEE type at 9.5~10 m².

The gain of ratio (GOR) parameter was in the range of 1.8 to 3.4 for all membranes analysed, with PE found to be the highest with a value of 3.7 and E-CNT2 type the lowest with a value of 1.85. Based on the presented characteristics, the membrane types E-PH/AQ7 and E-PH/AQ24 were selected for this study, as their permeate fluxes are in an acceptable range. Further, they would give remarkable results related to the hourly costs in [\$/h] (Zaragoza et al. 2014; Shahu and Thombre 2019).

The following assumptions have been made:

- AGMD has been considered for this analysis.
- The membrane area is for Aquastill's SW air gap MD module, 7.2 m² of membrane and channels 1.5 m long (AQ-7) and for a module comprising 24 m² of membrane and channels 5 m long (AQ -24).
- Process modelling is performed under steady-state conditions.

Parameter:	PTFE	PP	PVDF	PE	C- PVDF	E-PH AQ- 24	E- CNT0 .5	E- CNT1	E- CNT2	E- CNT3
Exergy destruction,[kW]	5.584	5.608	5.545	5.592	5.567	5.57	5.57	5.565	5.565	5.55
SPC, [kWh/m ³]	2.217	3.365	0.334	2.618	1.4	1.547	1.48	1.3	1.33	0.9
GOR	3.438	2.885	3.28	3.74	3.288	1.923	1.976	1.9	1.85	1.92
Permeate flux, [kg/m ² h]	2.205	2.847	2.36	1.944	2.355	5.503	5.23	5.616	6	5.52
Liquid entry pressure,[kPa]	274	416	41.36	323.6	172.3	191.2	183	160	164	110.5
Permeability coefficient	0.105	0.135	0.112	0.092	0.112	0.261	0.25	0.267	0.282	0.262
Area, [m ²]	9.448	7.318	8.818	10.72	8.847	3.786	4	3.71	3.5	3.77
No. of pores	25	608	321	608	25	82	302	630	631	28
Hourly costs, [\$ /h]	0.035	0.027	0.033	0.040	0.033	0.014	0.015	0.013	0.013	0.014
Productivity, [m ³ /day]=0.5-1500.			Product salinity, [ppm]=500			Inlet water temperature, [°C]=20-45				

Table 03.01 – Data results of the AGMD method based on different membrane types.

3.3 Modelling of the Units

3.3.1 Solar Radiation Model

The total, or global, amount of solar radiation passing through the atmosphere and reaching the earth's surface can be classified into two components, namely beam and diffuse radiation. Beam radiation is solar radiation propagating along the line adjoining the receiving surface and the sun and is also referred to as direct radiation. In contrast, diffuse radiation is solar radiation scattered by aerosols, dust particles and molecules and, as such, does not have a unique direction.

A solar radiation model for predicting average daily and hourly global radiation, beam radiation, and diffuse radiation has been created and is reported in Appendix III. The knowledge of local solar radiation is essential for the proper design of the SGSP and the evaluation of its thermal behaviour. The best database would be the long-term measured data at the site where the SGSP is installed. However, the limited availability of real radiation measuring networks informs the need for solar radiation models. Direct radiation is the most important parameter in designing and analysing systems

using solar thermal energy and such information can be determined based on readily measurable quantities. There are different solar radiation models already available in the literature to predict the beam component or sky component.

Precise radiation models require detailed information of atmospheric conditions, including the type, amount, and distribution of clouds (or other observations), atmospheric turbidity, water content, rain and wind. A more straightforward method for calculating the radiation beam was developed by Hottel (1976), which gives an estimate of direct irradiation only, while a model to determine both direct and diffuse radiation was developed by ASHRAE (1985) and this is now widely used by engineering communities.

The ASHRAE clear sky model predicts the average monthly hourly direct solar radiation via a simple equation containing two constants, A and B , while diffuse irradiation is given as a fraction C of the direct normal component. The constants A , B , C are tabulated via ASHRAE for each month of the year, giving 12 sets of these constants. The model was developed for a ‘basic atmosphere’ sample containing 200 dust particles per cm^3 and a specific value for the ozone concentration. Both models have been analysed, compared and implemented to determine the global solar radiation for the modelled SP located in Oman.

3.3.2 Solar Pond Model

Solar Ponds are composed of three zones that must be considered to define the energy transfers used in the model. A schematic of these three zones is represented in Figure 03.03. An energy balance between these zones and the environment is necessary to develop a complete model which can predict the thermal performance of the system.

- The UCZ temperature is obtained from solar radiation, convection, conduction, and superficial evaporation. The heat loss through the pond walls and heat transfer to NCZ must be considered, while radiative heat loss from the pond surface due to thermal or long-wave radiation (Kurt et al. 2000) is neglected.
- The NCZ is assumed to have a variable temperature. To define the vertical variation of salinity and temperature within the NCZ, the gradient zone is divided into different subzones wherein individual energy balances are calculated considering the contribution of solar radiation, heat losses through the walls, and heat transfers to and from the UCZ and LCZ.

- The LCZ is assumed to have a uniform temperature and solar radiation and heat losses through the walls and the ground of the pond are considered, along with heat transfers to the NCZ.

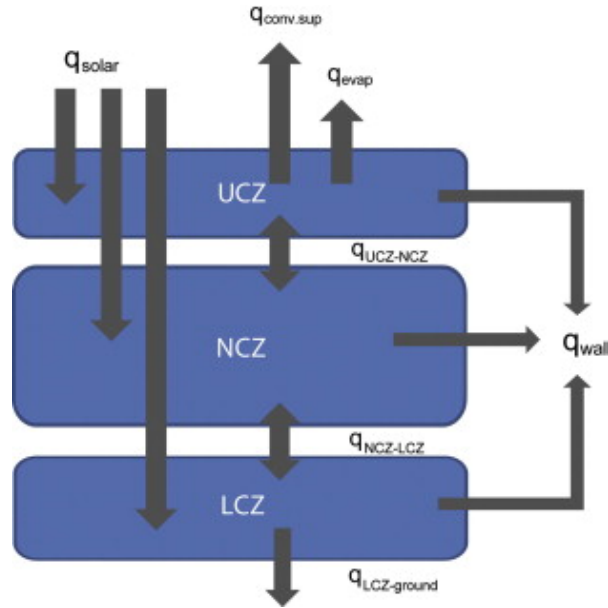


Figure 03.03 – Energy balance between layers zone of SGSP (Bernard et al. 2013). Reproduced with permission of the rights holder Elsevier Ltd.

The SGSP model may be derived from the following equation (1) as proposed by Chiasson et al. (2000) which can describe the rate of change in the average temperature of the SP, as follows:

$$MC_p \frac{dT}{dt} = Q_u \quad (1)$$

where:

M: Mass of Water

C_p : Heat capacity

T: Hourly Water Temperature

t: Operating Time

Q_u : The Useful Heat

we also know that

$$M = \rho V \quad (2)$$

where:

ρ : NaCl brine density

V: Volume of the pond

and,

$$Q_u = q_{in} - q_{out} \quad (3)$$

where:

q_{in} : Heat transfer entering the pond

q_{out} : Heat transfer exiting the pond

Equation (1) can be written as follows:

$$\frac{dT}{dt} = \frac{q_{in} - q_{out}}{\rho V C_p} \quad (4)$$

$q_{in} - q_{out}$ can be calculated according to the term:

$$q_{in} - q_{out} = q_{solar} - q_{evap} - q_{conv.sup} - q_{wall} - q_{ground} \quad (5)$$

A_p is the SP area in $[m^2]$:

$$A_p = L_p \times W_p$$

where,

L_p : length of the SP [m]

W_p : width of the SP [m]

T_{pm} , is the mean pond temperature $[^{\circ}C]$

$$T_{pm} = \frac{T_p + T_{amb}}{2}$$

where,

T_{amb} : ambient temperature $[^{\circ}C]$

T_p : pond temperature $[^{\circ}C]$

The calculation parameters for the transmission and reflection of the solar radiation can be calculated according to Duffie and Beckman (1991):

$$\rho_1 = \frac{\sin(\theta_r - \theta_t)^2}{\sin(\theta_r + \theta_t)^2} \quad \rho_2 = \frac{\tan(\theta_r - \theta_t)^2}{\tan(\theta_r + \theta_t)^2} \quad \rho = \rho_1 + \rho_2 \quad \tau = 1 - \rho.$$

where,

θ_t : incidence angle in [deg]

θ_r : is the angle of reflection [deg]

T_{amb} : ambient temperature [°C]

T_p : pond temperature [°C]

$$\theta_r = \frac{\text{asin}(\sin\theta_t)}{1.33}$$

I_{rw} is the flux reflected from the water surface, [W/m²] such that:

$$I_{rw} = (I_b \times \rho) + (I_d \times \rho)$$

where,

I_b : radiation beam [W/m²]

I_d : diffuse radiation [W/m²]

h_{ca} is the convective heat transfer between the cover and ambient [W/m²°K]. This is, in turn, based on wind speed, V_w , [m/s]:

if $V_w < 5$

$$h_{ca} = 2.8 + (3 \times V_w)$$

if $V_w \geq 5$

$$h_{ca} = 5.7 + (2.8 \times V_w)$$

I_{sw} is the flux entering the water, [W/m²]:

$$I_{sw} = I_g - I_{rw}$$

where,

I_g : global radiation [W/m²]

The transmission of solar radiation τ_a to the SP based on absorption has been proposed in the studies of Rabl and Nielsen (1975) and Bryant and Colbeck (1977) as reported below:

Rabl and Nielsen

$$\tau_a = (0.237 \times \exp(-0.023 \times D_{sp})) + (0.193 \times \exp(-0.45 \times D_{sp})) + (0.167 \times \exp(-3 \times D_{sp})) + (0.179 \times \exp(-35 \times D_{sp}))$$

Bryant and Colbeck

$$\tau_a = 0.36 - \left(0.08 \times \log \left(\frac{D_{sp}}{\cos \theta_r} \right) \right)$$

where,

D_{sp} : SP depth, [m].

$I_{s_{dsp}}$ is the solar flux at various depth, [W/m²]:

$$I_{s_{dsp}} = (I_b \times \tau_r \times \tau_a) + (I_d \times \tau_r \times \tau_a)$$

The pond calculation parameters are found to have the following values:

$$A1=0.237; A2=0.193; A3=0.167; A4=0.179;$$

$$K1=0.023; K2=0.45; K3=3; K4=35.$$

$$K11 = \frac{K1}{\cos \theta_r}$$

$$K22 = \frac{K2}{\cos \theta_r}$$

$$K33 = \frac{K3}{\cos \theta_r}$$

$$K44 = \frac{K4}{\cos \theta_r}$$

$$\begin{aligned}
x1 &= \left(\frac{A1}{K11} \right) \times \left(1 - \exp \left(-1 \times (D_{sp} \times K11) \right) \right) \\
x2 &= \left(\frac{A2}{K22} \right) \times \left(1 - \exp \left(-1 \times (D_{sp} \times K22) \right) \right) \\
x3 &= \left(\frac{A3}{K33} \right) \times \left(1 - \exp \left(-1 \times (D_{sp} \times K33) \right) \right) \\
x4 &= \left(\frac{A4}{K44} \right) \times \left(1 - \exp \left(-1 \times (D_{sp} \times K44) \right) \right) \\
Xp &= \left(\tau_r \times \frac{H_o \times 1e6}{24 \times 3600 \times kw(T_{pm})} \right) \times (x1 + x2 + x3 + x4),
\end{aligned}$$

where,

H_o : hourly global radiation [MJ/m²/day]

k_w : water thermal conductivity [W/m °C]

We can then calculate the total losses Ul [W/m²°C], pond temperature T_{p_new} [°C], and pond load Q_{load} , [kW] as follows:

$$\begin{aligned}
Ul &= \frac{1}{\frac{D_{sp}}{kw(T_{pm})} + \frac{1}{h_{ca}}} \\
T_{p_new} &= T_{amb} + \left(\frac{Is_{dsp}}{Ul} \right) - \left(\left(\left(\frac{Is_{dsp}}{Ul} \right) + T_{amb} - T_p \right) \times \left(\exp \left(\frac{-1 \times Ul \times OH}{\rho(T_{pm}) \times D_{sp} \times Cp(T_{pm})} \right) \right) \right) \\
Q_{load} &= \frac{A_p \times \left(kw(T_{pm}) \times \left(Xp - (T_{p_new} - T_{amb}) \right) \right)}{1000 \times D_{sp}}
\end{aligned}$$

The detailed model code for the SP with cover is presented in more detail in Appendix III.

3.3.3 AGMD Model

The model code for AGMD is presented in detail in Appendix III where the main equations used are reported.

The mean temperature T_m of the solution that enters the feed side of the module is calculated in [$^{\circ}\text{C}$] using the following equation:

$$T_m = \frac{(T_{hi} + T_{ci})}{2}$$

where,

T_{hi} : temperature of the hot feed side [$^{\circ}\text{C}$]

T_{ci} : temperature of the cold side of condensation section [$^{\circ}\text{C}$]

The mean vapour partial pressure P_m in [kPa] is calculated using the Antoine equation:

$$P_m = \exp \left(23.328 - \left(\frac{3841}{T_m - 45} \right) \right)$$

The water surface tension γ_w in [kN/m] is determined by:

$$\gamma_w = (-0.1769 \times T_m + 76.58)^{-6}$$

The membrane tortuosity τ is expressed by:

$$\tau = \frac{(2 - \varepsilon)^2}{\varepsilon}$$

where,

ε : the membrane porosity.

The latent heat of vapourisation H_{fg} in [kJ/kg] is calculated using the term:

$$H_{fg} = (1.7535 \times T_m) + 2024.3$$

The liquid entry pressure LEP [kPa] is then calculated by:

$$LEP = \left(\frac{-2 \times \gamma_w}{r_{memb}} \right) \times \cos \theta$$

where,

r_{memb} : membrane pore in [m].

The overall mass transfer coefficient C_w in [kg/m² s Pa] can be calculated using the following equation, if T_m is > 50;

$$C_w = \left(\left(\frac{2\varepsilon r_{memb}}{3\tau D_{memb}} \right) \right) \sqrt{\left(\frac{8 \times Mw_w}{p_i \times R_{constant} \times (T_m + 273)} \right)}$$

where,

D_{memb} : membrane thickness in [m]

$R_{constant}$: specific gas constant in [$\frac{kJ}{kmol}$]

Mw_w : molecular weight of the water in [$\frac{kg}{mol}$]

The overall mass transfer coefficient C_w when T_m is < 50 is determined by:

$$C_w = \frac{\varepsilon \times PD_{va} \times Mw_w}{\tau \times D_{mem} \times R_{constant} (T_m + 273) \times P_m}$$

where PD_{va} is the water-air diffusion coefficient and the average pressure of air inside the membrane is calculated as:

$$PD_{va} = 1.9851^{-5} \times (T_m^{2.072})$$

The Permeate flux J_p in [kg/m²h] is calculated by:

$$J_p = C_w \delta (T_{hi} - T_{ci})$$

where the δ is the relative viscosity which can be calculated using the term:

$$\delta = \left(\frac{H_{fg}}{R_{constant}} \times ((T_m + 273)^2) \right) \times P_m$$

The mass transfer coefficient K_m in [kJ/m s °C] is determined by using the term:

$$K_m = (J_p \times H_{fg}) / (T_{hi} - T_{ci}) \times 1$$

The membrane area A_{memb} in $[m^2]$ is calculated by:

$$A_{memb} = \frac{M_p}{J_p}$$

where M_p is permeate flow rate $[kg/h]$.

The feed mass flow rate M_f (in kg/hr) is calculated via:

$$M_f = (21.44 \times M_p) + 21.7$$

The brine loss M_b in kg/hr is expressed based on:

$$M_b = M_f - M_p$$

The salt rejection SR is calculated by:

$$SR = 1 - \left(\frac{S_p}{S_f} \right)$$

where:

S_p : product salinity ratio $\left[\frac{kg}{kg} \right]$

S_f : feed salinity ratio in $\left[\frac{kg}{kg} \right]$

The brine loss salinity S_b in $\left[\frac{kg}{kg} \right]$ is calculated by:

$$S_b = ((M_f \times S_f) - \frac{M_p \times S_p}{M_b})$$

The concentration factor C_f is calculated based on the following equation:

$$C_f = \frac{M_f}{M_f - M_p}$$

The water recovery ratio WRR can be determined by:

$$WRR = 100 \times \left(1 - \left(\frac{1}{C_f} \right) \right)$$

The energy transfer through the membrane Q_{memb} is expressed in $[kW]$ by:

$$Q_{memb} = Q_{conduction} + Q_{vaporization}$$

where,

$$Q_{vapourisation} = \frac{J_p \times H_{fg} \times A_{memb}}{3600}$$

$$Q_{conduction} = \left(\frac{k_{memb}}{D_{memb}} \right) \times A_{memb} \times T_m$$

The thermal conductivity k_{memb} of the membrane in [kW/m °C] varies for different membranes as follows:

$$k_{memb} = \varepsilon k_g + (1 - \varepsilon) \times K_p$$

where, k_g : is the gas thermal conductivity [kW/m °C] in the pores of the membrane and is calculated as follows:

$$k_g = ((0.01383 \times \exp(0.005486 \times T_m)) + (3.344 \times 10^{17} \times \exp(0.0986 \times T_m))) \times 10^{-3}$$

The gain ratio GOR as a function of specific feed flow rate in $[\frac{kg}{m^2h}]$ is calculated by:

$$GOR = \frac{M_p \times H_{fg}}{Q_{memb} \times 3600}$$

The thermal efficiency of the membrane η_{memb} is expressed based on:

$$\eta_{memb} = \frac{Q_{vaporization}}{Q_{memb}}$$

The number of pores NOP is calculated using the term:

$$NOP = 247.3 - 198.1 \times \cos(r_{memb} \times 1.13 \times 10^7) + 237.2 \times \sin(r_{memb} \times 1.13 \times 10^7) - 31.65 \times \cos(2 \times r_{memb} \times 1.13 \times 10^7) - 69.25 \times \sin(2 \times r_{memb} \times 1.13 \times 10^7)$$

The pump power W_{pump} is defined in [kW] by:

$$W_{pump} = \frac{M_f \times \Delta P}{\rho_w \times \eta_{pump} \times 3600} \times$$

where,

ρ_w : water density

η_{pump} : pump efficiency

The specific power consumption SPC in $[\frac{kWh^3}{m}]$ is calculated by:

$$SPC = \frac{1000 \times W_{pump}}{M_p}$$

3.4 The Proposed System Combinations

Different software models have been developed to compute each part of the system using the published literature and extant techniques. The following points summarise the input data for the developed models:

Solar radiation model:

- Latitude & longitude = [deg]
- Julian day = [#]
- Current time of the location = [h], [min], [sec]
- Tilt angle = [deg]
- Solar radiation model selection
 - ASHREA
 - HOTTEL

SP:

- Solar radiation = from the solar radiation model
- Wind speed = 0.1-10 [m/s] (varies based on time and location)
- Ambient temperature = (varies based on time and location)
- Initial temperature = 25 [°C] (set according to experiment)
- Area = [m²]
- Depth = [m]
- Cover material = conductivity, emissivity, absorptivity

AGMD:

- Membrane type = AQ24
- Feed salinity ratio = brackish and/or seawater
- Pumping efficiency = 75 [%]
- Membrane inlet feed temperature = [°C]

3.4.1 Solar Pond/PV Assisted AGMD (SGSP/PV/AGMD)

In this proposed model, the SP will be responsible for the thermal load needed to power the AGMD through the heat exchanger unit HEX unit. The system contains the SP, the HEX unit for energy and heat transfer, a pump for circulation and pressure drop, PV for electrical power generation and AGMD for the desalination process. (Figure 03.04)

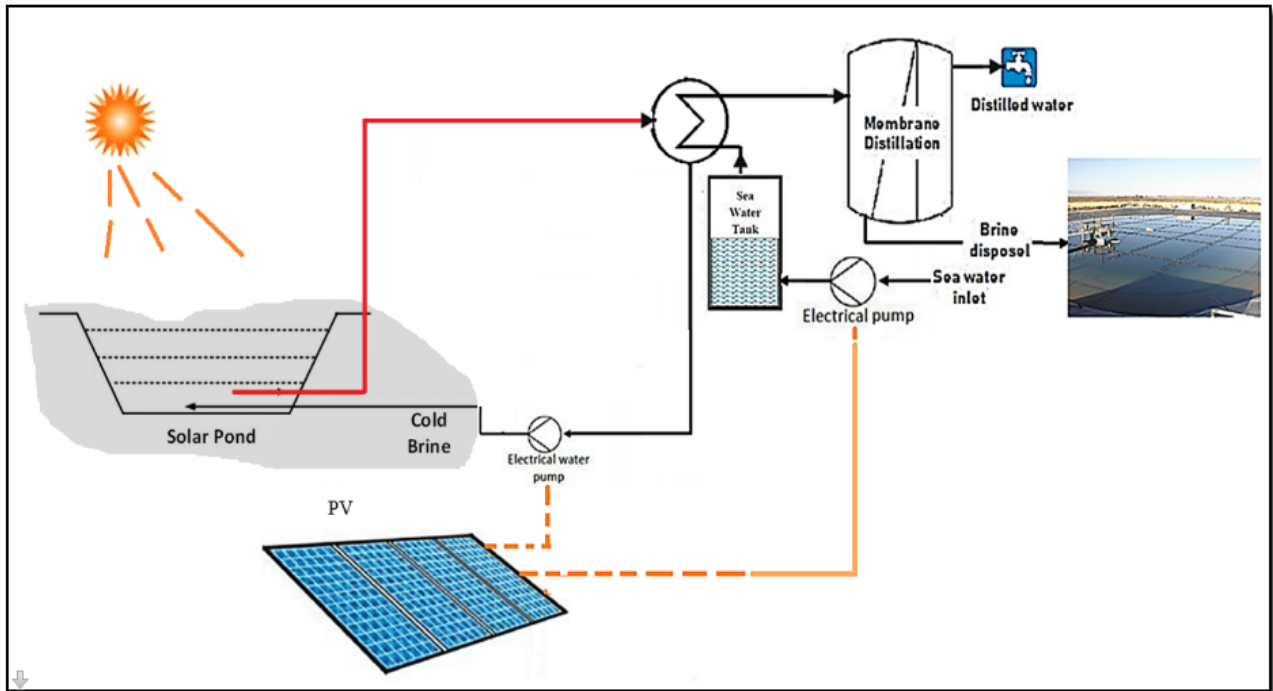


Figure 03.04 – Performance model SP/PV/AGMD

SP size has been considered as per the modular design for the experimental work conducted in Oman, having a size of 10 m x 14 m (as described in Table 03.04) and gradient layers with 0.4, 0.7, 0.8 metres in depth. An alternative SP was also considered, with the same total surface area, but different layer depths (Table 03.05).

Length	Width	UCZ	NCZ	LCZ
10 m	14 m	0.4 m	0.7 m	0.8 m

Table 03.04 –Dimensions of the nominal SP considered in this study

Length	Width	UCZ	NCZ	LCZ
10 m	14 m	0.2 m	0.4 m	0.3 m

Table 03.05 – Dimensions of the alternative SP considered in this study.

3.4.2 Solar FPC/PV Assisted AGMD (FPC/PV/AGMD)

In this performance model, the AGMD is assisted by Flat Plat Solar (FPC) Collector instead of the SP. The hot stream from the FPC will be responsible for the thermal power generation through the heat exchanger unit (HEX) to the AGMD. The HEX will increase the seawater temperature before entering the AGMD unit for the desalination process. The returned stream will be pumped back into the FPC field. The PV system will sustain the power needed for the water circulating pump, the AGMD pump, and the solar FPC pump. Figure 03.05 shows the schematic diagram of the proposed system.

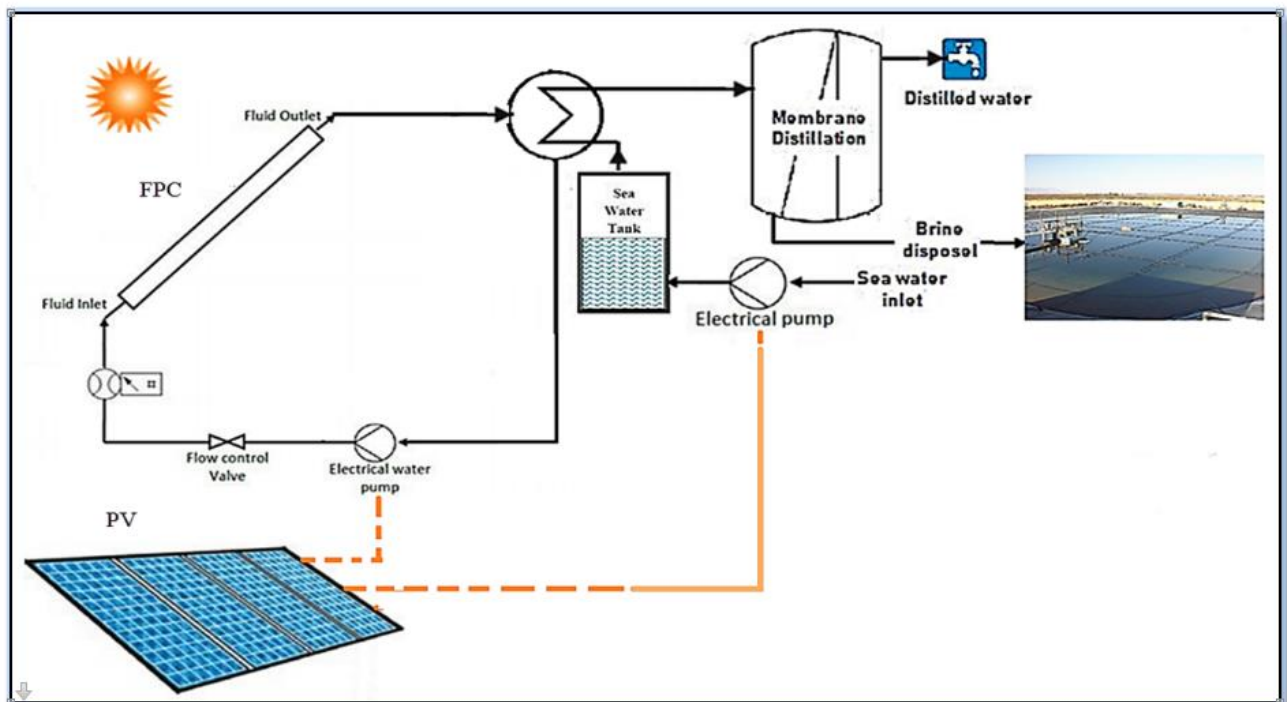


Figure 03.05 – Performance model FPC/PV/AGMD

3.5 Simulations

3.5.1 Environmental Operating Conditions

The study location coordinates are the experimental ones for Oman complete with latitude and longitude: **23.614328, 58.545284**. It is estimated, by reference, that the daily average global radiation in a typical day is in the range of 21-40 MJ/m². Figure 03.06 shows the seasonal variations of solar radiation on the specific location.

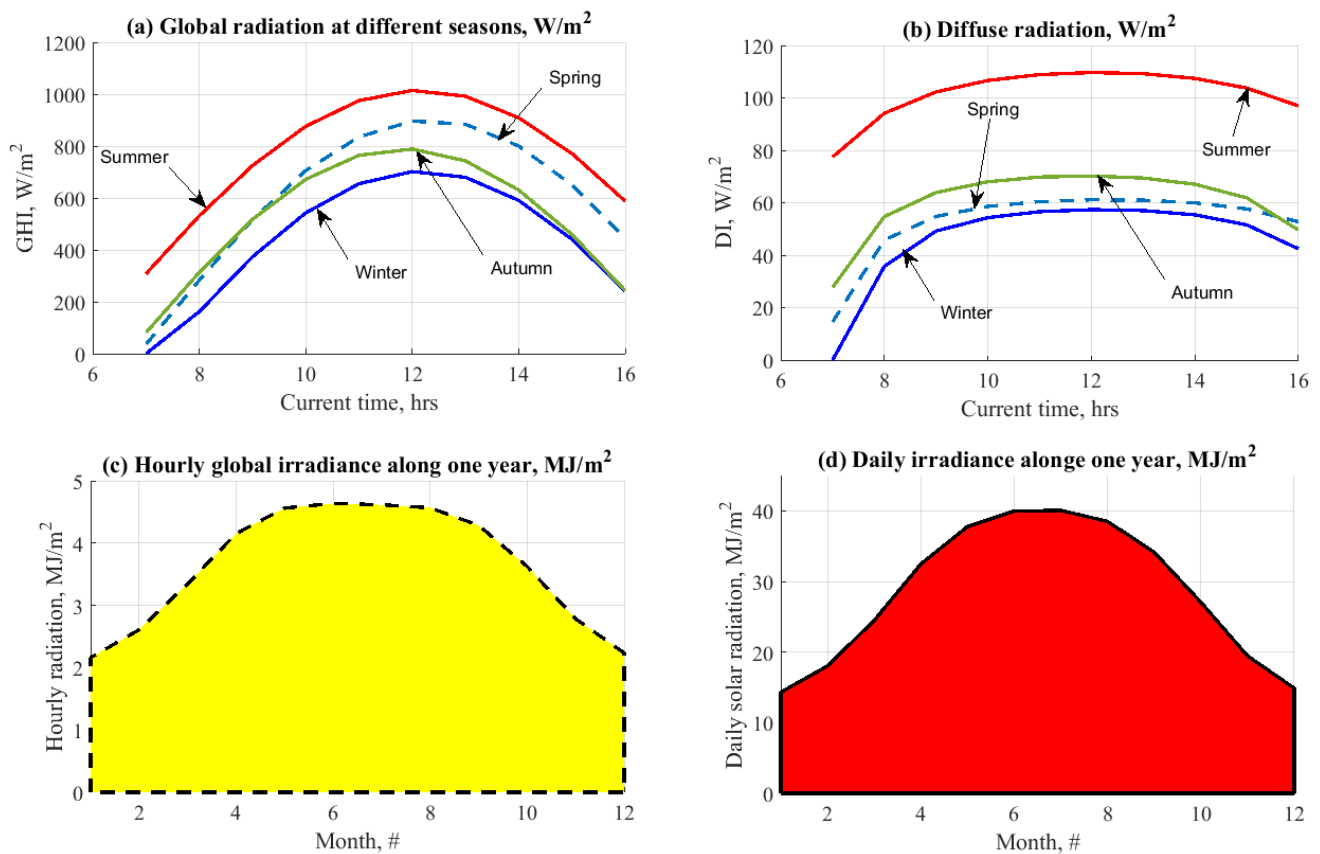


Figure 03.06 – Data results related to Global Radiation Irradiance (GHI) and Diffuse Irradiance (DI), both hourly [W/m²] and daily [MJ/m²] based on the selected location of Oman.

3.5.2 Solar Pond Results

Based on the calculation of the solar radiation model proposed, thermal power, losses, pond temperature, and performance are calculated for the proposed SP. The cover material has been added to discover the effect on pond performance. The following design specifications are taken into consideration:

- Pond characteristics UCZ, NCZ, and LCZ = 0.4, 0.7, 0.8 m
- Pond length/width = 10/14 m
- Cover thickness = 0.01 m
- Cover conductivity = 0.025 W/m °C
- Wind speed = 0.1~0.2 m/s (measured on site)
- Ambient temperature = (varies based on time and location)

Figure 03.07 shows the data variations related to solar flux in terms of instant average, daily average, hourly global and monthly average. It has been reported that summertime is the peak solar flux and such behaviour would strongly affect the SP's performance. Figure 03.08 shows the SP results based on the effect of solar radiation at the specified location. The performance of the SP offers an excellent match with the incidence of solar radiation throughout the year. For instance, Figure 03.08-a shows the behaviour of the solar flux entering the SP at various depths during the course of a single year. In winter, the flux was in the range of 150 to 160 W/m² while it ranges from 350-400 W/m² in summer.

The same effect is noted in Figure 03-08-b representing the pond's transmission (0.29-3.1). The pond energy and heat transmissions are increased during the summer months as expected due to the increase in incident solar radiation.

Figure 03.08-c shows the performance of the pond temperature throughout the year; the temperature is found to vary between 60°C and 67°C in winter and summer, respectively. Such temperatures are suitable for process heat applications.

Figure 03.08-d shows the variations in pond load or thermal power. In summer, the load varies between 20 and 35 kW_{th}. In winter, the pond power ranges between 5 and 15kW_{th} of thermal energy. The pond's behaviour clearly shows a direct correlation with incident solar radiation throughout the year.

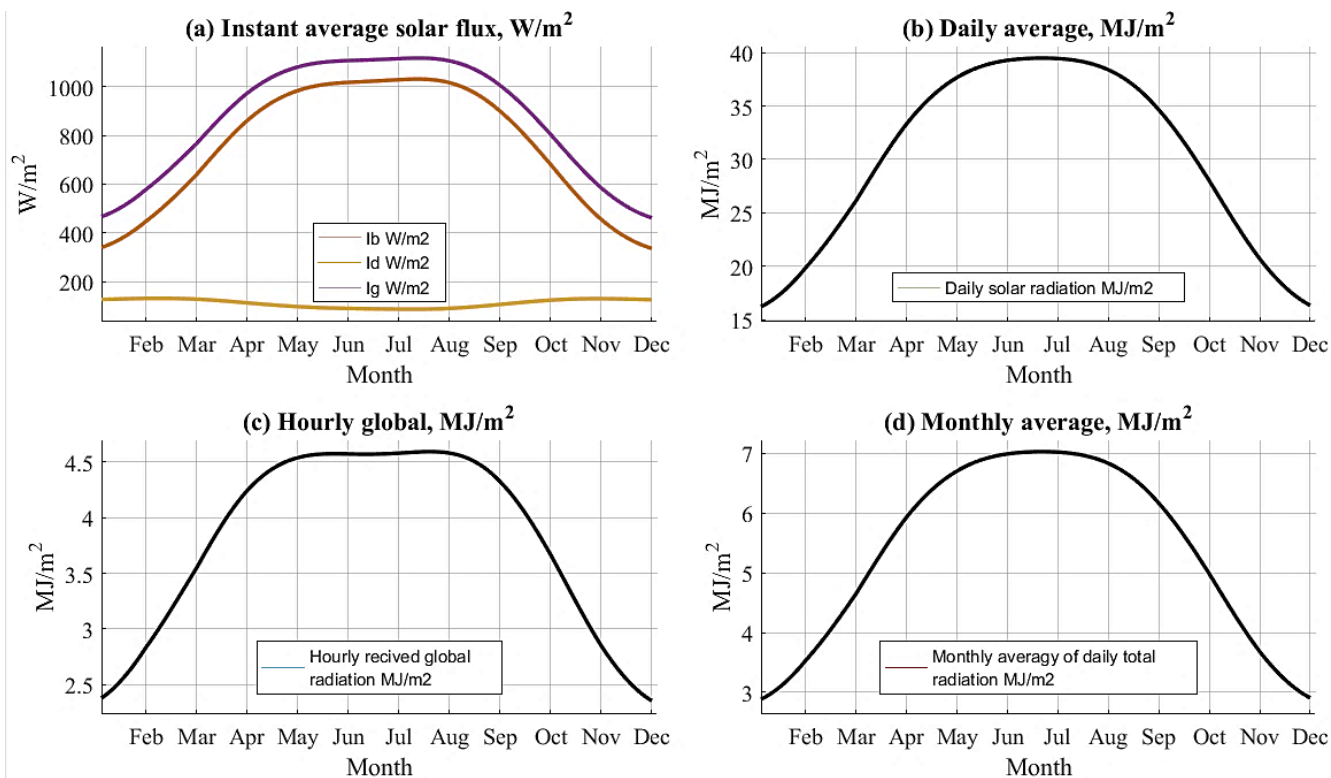


Figure 03.07 – Solar radiation data based on HOTTEL & ASHRAE models.

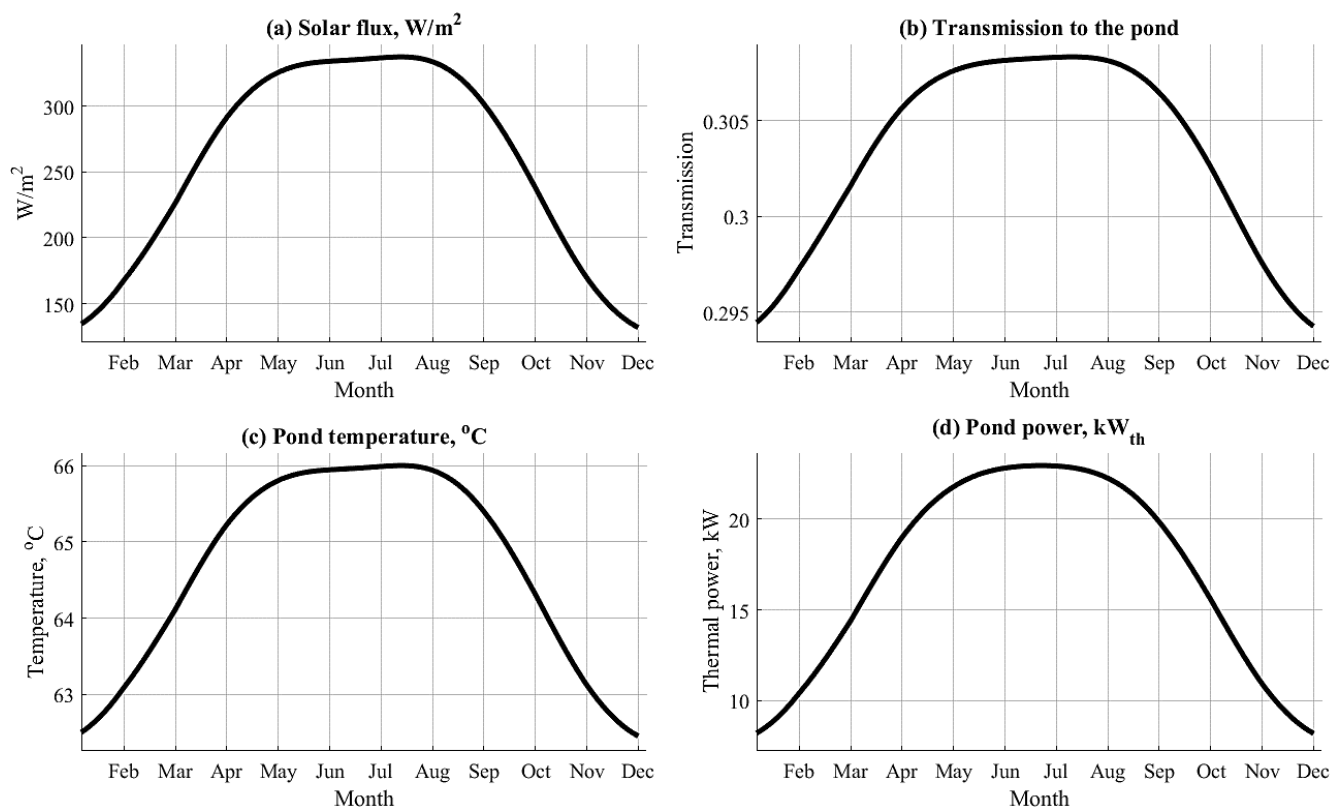


Figure 03.08 – Solar radiation data based on the effect of solar radiation on the selected location in Oman.

3.5.3 AGMD results

The Aquastill AGMD module with a 24 m² membrane and 5 m long channels has been considered in this study. Figure 03.09 shows the predicted performance data for the AGMD unit wherein its productivity is designed not to exceed 10 m³/day.

Figure 03.09 shows the effect of system productivity on (a) SPC; (b) Water Recovery Ratio (WRR); (c) Concentration Factor (CF); (d) Gain Ratio GOR; and (e) feed flow rate (FFF). Generally, the SPC shows an attractive result regarding the production rate. The WRR % is found not to exceed 5% and it would be predicted to increase with the production rate, as anticipated. The same effect was noticed in Figure 03.09-d, where the CF increases by increasing the production rate.

Figure 03.09-e shows the effect on the GOR (gain ratio = product/feed). Increasing the production rate would increase the GOR which would be considered a remarkable increase in the productivity of the AGMD unit.

Figure 03.09-f shows the variation in FFF [kg/h] based on the variation in production rate. Increasing the production rate would demand a greater FFF rate to the system. For instance, at 1 m³/day, the FFF rate is 1800 kg/h; whereas for 10 m³/day, the FFF was in the range ~8,500-8,700 kg/h.

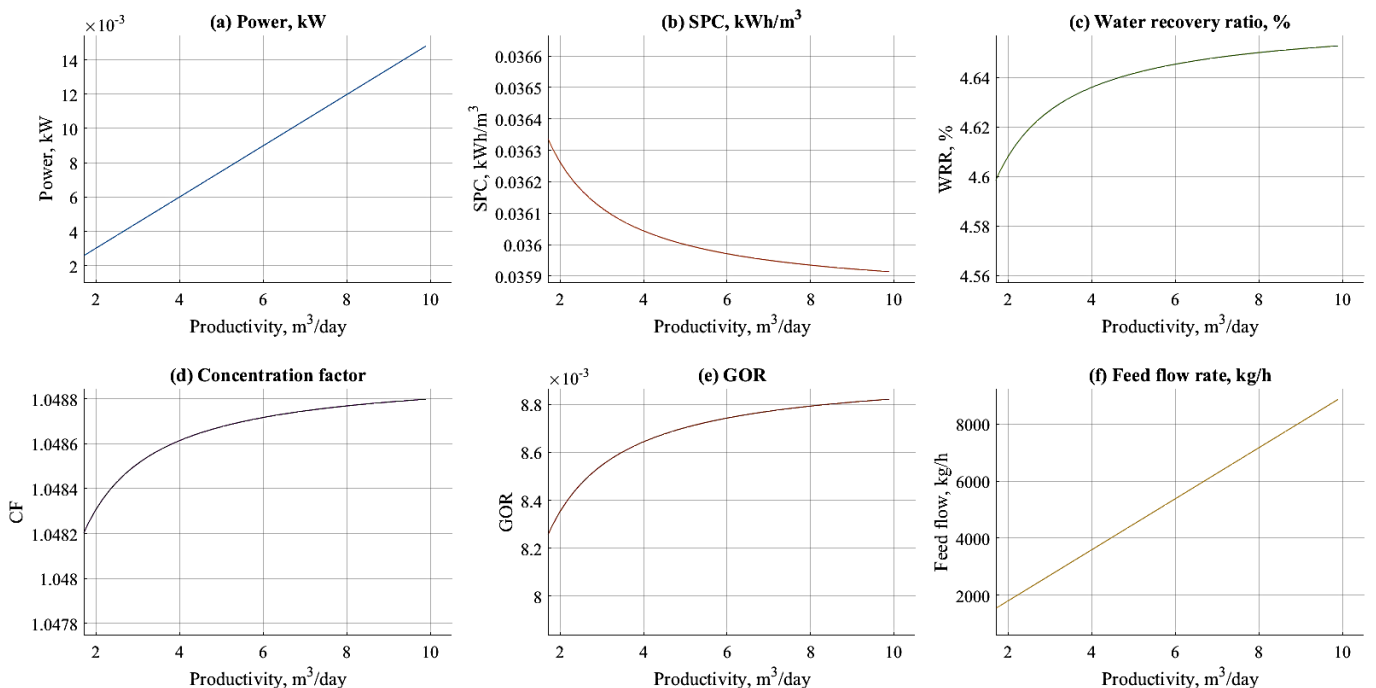


Figure 03.09 – Results for the AGMD based on productivity variation (1-10 m³/day).

3.5.4 The Data Comparison for the Proposed Models SGSP+AGMD vs. FPC+AGMD

The comparison between the systems introduced in section 3.4 has been addressed in this section. The main input parameters are the following:

- Location: Muscat, Oman
- SP area: 10m x 14m
 - UCZ = 0.4m & 0.2m
 - NCZ = 0.7m & 0.4m
 - LCZ = 0.8m & 0.3m
 - Cover material type: glass
- FPC: water working fluid
 - Area = 150m²
- AGMD:
 - AQ-7 with 7m²
 - AQ-24 with 24m²

Tables 03.06 and 03.07 show the results of FPC coupled with AGMD relative to the change in AGMD area from 7 m² to 24 m² over a year (monthly days). The results show that increasing the membrane area would increase the total productivity of the system and that the maximum allowable system productivity can be extracted during summer times (Jun, Jul, and Aug) for both types. Productivity achieved with AGMD AQ-24 is much higher than that achieved with AQ-7 (Figure 03.10).

Tables 03.08 and 03.09 list the results for SP with a cover combined with different depth profiles and AGMD AQ-7 over one year (monthly days). The findings indicate that changing the depth profile will marginally change the total productivity of the system and that the maximum system productivity can be extracted during the summer months (Jun, Jul, and Aug) for both types (Figure 03.11).

Tables 03.10 and 03.11 list the findings for the SP with cover combined with different depth profiles and AGMD AQ-24. The results obtained at various gradient depths and for different membrane areas show that decreasing the depth would slightly increase the thermal energy and water productivity, while increasing the membrane area would increase total productivity (Figure 03.12).

Month	Is, [W/m ²]	FPC temperature [°C]	AGMD temperature [°C]	GOR	Productivity [m ³ /day]
Jan	458.6	43.55	40.02	0.1724	9.565
Feb	578.7	49.64	45.2	0.1698	14.74
Mar	767.4	59.31	53.42	0.1659	25.15
Apr	967.9	69.93	62.44	0.1616	39.92
May	1081	76.17	67.75	0.1591	50.34
Jun	1107	77.67	69.02	0.1585	53.04
Jul	1115	78.13	69.41	0.1583	53.88
Aug	1105	77.59	68.95	0.1585	52.9
Sep	1004	71.92	64.13	0.1608	43.11
Oct	803.3	61.18	55	0.1651	27.49
Nov	584	49.91	45.42	0.1697	14.99
Dec	461.5	43.7	40.14	0.1723	9.679

Table 03.06 – Data based on FPC/PV/AGMD-AQ7.

Month	Is, [W/m ²]	FPC temperature [°C]	AGMD temperature [°C]	GOR	Productivity [m ³ /day]
Jan	458.6	43.55	40.02	1.143	32.79
Feb	578.7	49.64	45.2	1.138	50.52
Mar	767.4	59.31	53.42	1.13	86.22
Apr	967.9	69.93	62.44	1.121	138.5
May	1081	76.17	67.75	1.116	172.6
Jun	1107	77.67	69.02	1.115	181.8
Jul	1115	78.13	69.41	1.115	184.7
Aug	1105	77.59	68.95	1.115	181.4
Sep	1004	71.92	64.13	1.12	147.7
Oct	803.3	61.18	55	1.129	94.25
Nov	584	49.91	45.42	1.138	51.38
Dec	461.5	43.7	40.14	1.143	33.18

Table 03.07 – Data based on FPC/PV/AGMD-AQ24.

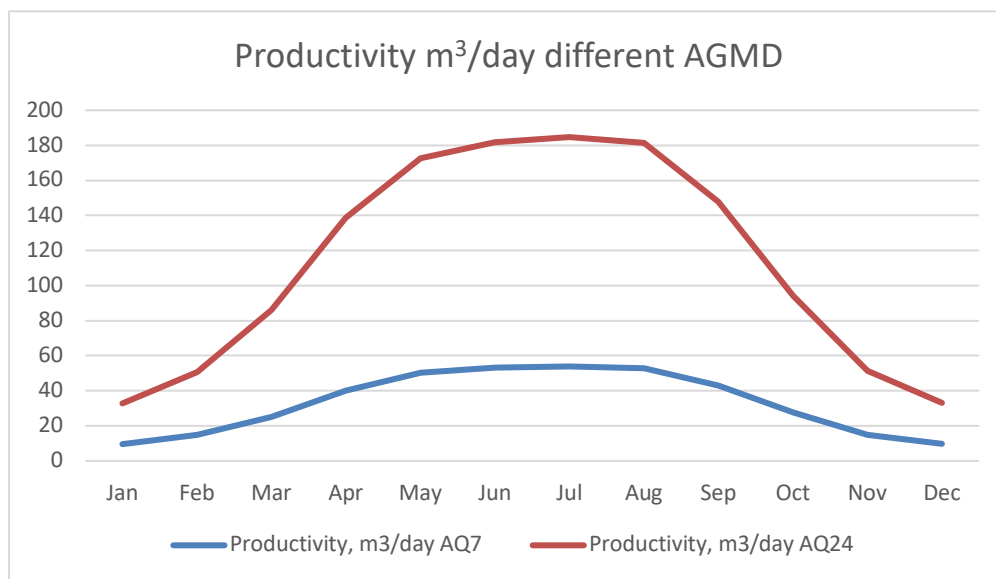


Figure 03.10 –Data based on FPC/PV/AGMD-AQ7 and AQ24 daily productivity in m³/day

Month	Is [W/m ²]	SP temperature [°C]	Outlet SP temperature [°C]	AGMD temperature [°C]	GOR	Productivity [m ³ /day]	Depth zones [m]
Jan	458.6	52.43	23.05	22.6	0.1835	0.7628	0.4+0.7+0.8
Feb	578.7	53.09	23.96	23.37	0.1831	1.023	0.4+0.7+0.8
Mar	767.4	54.11	25.44	24.62	0.1825	1.482	0.4+0.7+0.8
Apr	967.9	54.11	25.44	24.62	0.1825	2.127	0.4+0.7+0.8
May	1081	55.79	28.18	26.96	0.1813	2.452	0.4+0.7+0.8
Jun	1107	55.93	28.57	27.28	0.1812	2.6	0.4+0.7+0.8
Jul	1115	55.98	28.61	27.32	0.1812	2.616	0.4+0.7+0.8
Aug	1105	55.93	28.36	27.11	0.1813	2.519	0.4+0.7+0.8
Sep	1004	55.38	27.46	26.34	0.1816	2.181	0.4+0.7+0.8
Oct	803.3	54.3	25.87	24.99	0.1823	1.625	0.4+0.7+0.8
Nov	584	53.11	24.15	23.53	0.1831	1.079	0.4+0.7+0.8
Dec	461.5	52.45	23.13	22.66	0.1835	0.7854	0.4+0.7+0.8

Table 03.08 – Data based on SPwc (with cover)/PV/AGMD-AQ7 depth 0.4+0.7+0.8.

Month	Is, [W/m ²]	SP temperature [°C]	Outlet SP temperature [°C]	AGMD temperature [°C]	GOR	Productivity [m ³ /day]	Depth zones [m]
Jan	458.6	55.12	23.02	22.56	0.1836	0.7524	0.2+0.4+0.3
Feb	578.7	56.49	24.03	23.43	0.1831	1.044	0.2+0.4+0.3
Mar	767.4	58.64	25.68	24.83	0.1824	1.561	0.2+0.4+0.3
Apr	967.9	60.98	27.59	26.45	0.1816	2.229	0.2+0.4+0.3
May	1081	62.19	28.75	27.44	0.1811	2.673	0.2+0.4+0.3
Jun	1107	62.49	29.19	27.81	0.1809	2.847	0.2+0.4+0.3
Jul	1115	62.58	29.24	27.85	0.1809	2.865	0.2+0.4+0.3
Aug	1105	62.47	28.95	27.61	0.181	2.75	0.2+0.4+0.3
Sep	1004	61.33	27.94	26.75	0.1814	2.36	0.2+0.4+0.3
Oct	803.3	59.05	26.17	25.25	0.1822	1.726	0.2+0.4+0.3
Nov	584	56.55	24.25	23.61	0.183	1.108	0.2+0.4+0.3
Dec	461.5	55.15	23.11	22.64	0.1835	0.7784	0.2+0.4+0.3

Table 03.09 – Data based on SPwc/PV/AGMD-AQ7 depth 0.2+0.4+0.3.

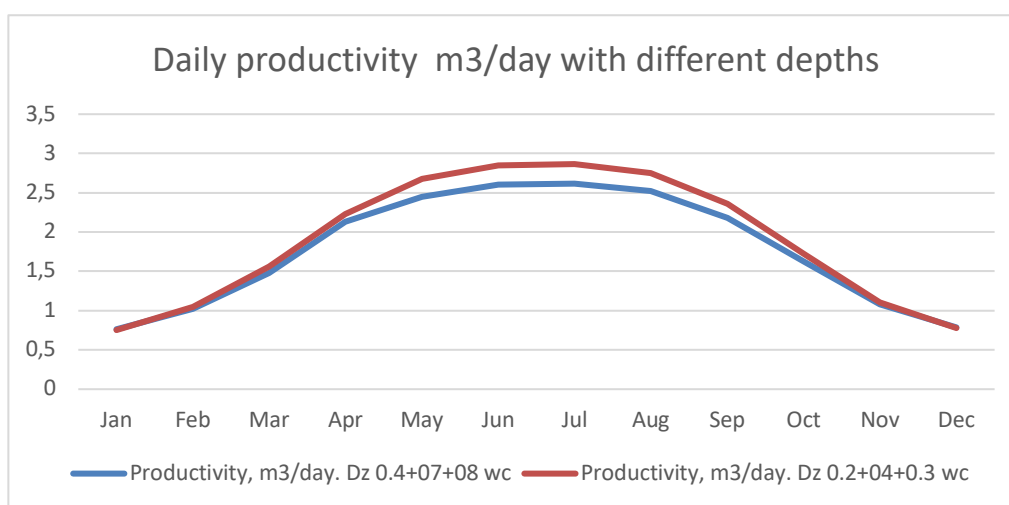


Figure 03.11 – Data based on SPwc/PV/AGMD-AQ7 at different depths daily productivity in m³/day.

Month	Is, [W/m ²]	SP temperature [°C]	Outlet SP temperature [°C]	AGMD temperature [°C]	GOR	Productivity [m ³ /day]	Depth zones [m]
Jan	458.6	52.43	23.05	22.6	1.164	2.615	0.4+0.7+0.8
Feb	578.7	53.09	23.96	23.37	1.163	3.508	0.4+0.7+0.8
Mar	767.4	54.11	25.44	24.62	1.162	5.081	0.4+0.7+0.8
Apr	967.9	54.11	25.44	24.62	1.161	7.087	0.4+0.7+0.8
May	1081	55.79	28.18	26.96	1.16	8.406	0.4+0.7+0.8
Jun	1107	55.93	28.57	27.28	1.16	8.914	0.4+0.7+0.8
Jul	1115	55.98	28.61	27.32	1.16	8.97	0.4+0.7+0.8
Aug	1105	55.93	28.36	27.11	1.16	8.637	0.4+0.7+0.8
Sep	1004	55.38	27.46	26.34	1.161	7.477	0.4+0.7+0.8
Oct	803.3	54.3	25.87	24.99	1.162	5.573	0.4+0.7+0.8
Nov	584	53.11	24.15	23.53	1.163	3.699	0.4+0.7+0.8
Dec	461.5	52.45	23.13	22.66	1.164	2.693	0.4+0.7+0.8

Table 03.10 – Data based on SPwc/PV/AGMD-AQ24 depth 0.4+0.7+0.8.

Month	Is, [W/m ²]	SP temperature [°C]	Outlet SP temperature [°C]	AGMD temperature [°C]	GOR	Productivity [m ³ /day]	Depth zones [m]
Jan	458.6	55.12	23.02	22.56	1.164	2.58	0.2+0.4+0.3
Feb	578.7	56.49	24.03	23.43	1.163	3.578	0.2+0.4+0.3
Mar	767.4	58.64	25.68	24.83	1.162	5.353	0.2+0.4+0.3
Apr	967.9	60.98	27.59	26.45	1.161	7.642	0.2+0.4+0.3
May	1081	62.19	28.75	27.44	1.16	9.165	0.2+0.4+0.3
Jun	1107	62.49	29.19	27.81	1.159	9.76	0.2+0.4+0.3
Jul	1115	62.58	29.24	27.85	1.159	9.823	0.2+0.4+0.3
Aug	1105	62.47	28.95	27.61	1.159	9.428	0.2+0.4+0.3
Sep	1004	61.33	27.94	26.75	1.16	8.091	0.2+0.4+0.3
Oct	803.3	59.05	26.17	25.25	1.162	5.919	0.2+0.4+0.3
Nov	584	56.55	24.25	23.61	1.163	3.8	0.2+0.4+0.3
Dec	461.5	55.15	23.11	22.64	1.164	2.669	0.2+0.4+0.3

Table 03.11 – Data results based on SPwc/PV/AGMD-AQ24 depth 0.2+0.4+0.3.

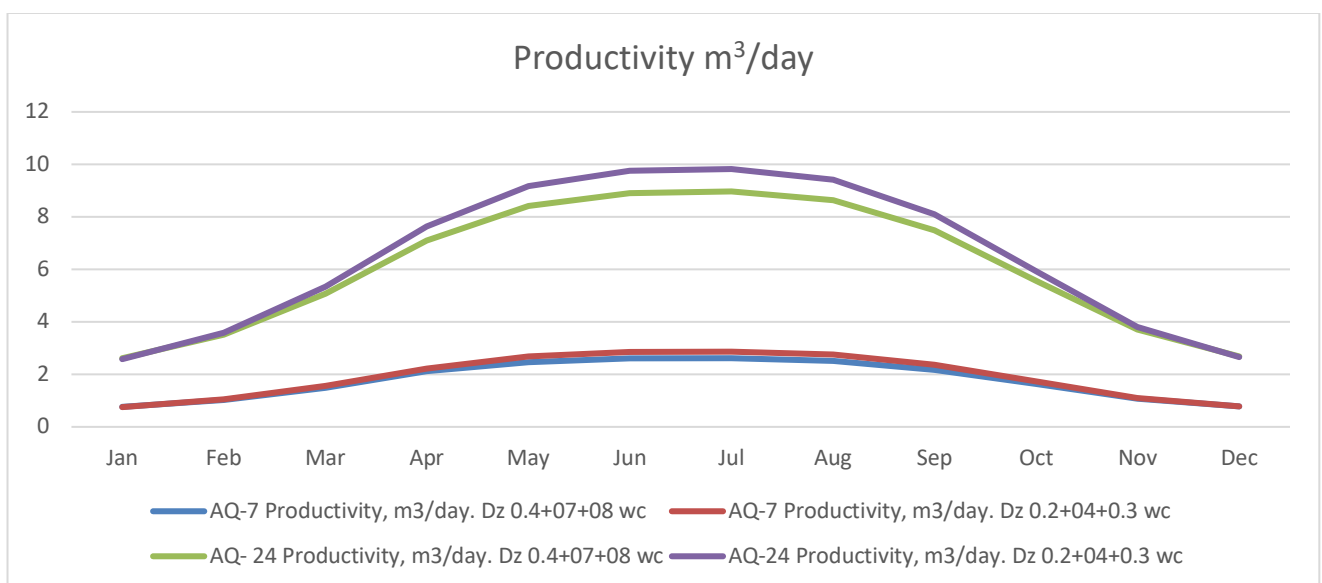


Figure 03.12 – Data based on SPwc/PV/AGMD-AQ7 and AQ-24 at different depths on daily productivity in m³/day.

Tables 03.12, 03.13, 03.14, and 03.15 show the outcome of the previous simulation for the uncovered SP. Figure 03.13 shows the data derived for all configurations based on the existence of the solar pond with cover (SPwc) or without cover (SPnc) with depth variations of (0.4+0.7+0.8) or (0.2+0.4+0.3). All data were obtained for an average salinity ratio of 80g/kg. Finally Figure 03.14 shows the effect of SP temperature on the system's productivity.

Month	Is, [W/m ²]	SP temperature [°C]	Outlet SP temperature [°C]	AGMD temperature [°C]	GOR	Productivity [m ³ /day]	Depth zones [m]
Jan	458.6	50.72	23.08	22.62	0.1835	0.7713	0.4+0.7+0.8
Feb	578.7	50.92	24	23.4	0.1831	1.034	0.4+0.7+0.8
Mar	767.4	51.24	25.49	24.67	0.1825	1.498	0.4+0.7+0.8
Apr	967.9	51.59	27.21	26.13	0.1817	2.09	0.4+0.7+0.8
May	1081	51.78	28.26	27.02	0.1813	2.479	0.4+0.7+0.8
Jun	1107	51.83	28.64	27.35	0.1811	2.629	0.4+0.7+0.8
Jul	1115	51.84	28.68	27.38	0.1811	2.645	0.4+0.7+0.8
Aug	1105	51.82	28.43	27.17	0.1812	2.547	0.4+0.7+0.8
Sep	1004	51.65	27.53	26.4	0.1816	2.205	0.4+0.7+0.8
Oct	803.3	51.3	25.93	25.04	0.1823	1.643	0.4+0.7+0.8
Nov	584	50.93	24.19	23.56	0.183	1.091	0.4+0.7+0.8
Dec	461.5	50.72	23.17	22.69	0.1835	0.794	0.4+0.7+0.8

Table 03.12 – Data based on SPnc (no cover) /PV/AGMD-AQ7 depth 0.4+0.7+0.8.

Month	Is, [W/m ²]	SP temperature [°C]	Outlet SP temperature [°C]	AGMD temperature [°C]	GOR	Productivity [m ³ /day]	Depth zones [m]
Jan	458.6	51.81	23.14	22.67	0.1835	0.787	0.2+0.4+0.3
Feb	578.7	52.31	24.19	23.56	0.183	1.091	0.2+0.4+0.3
Mar	767.4	53.12	25.89	25.01	0.1823	1.631	0.2+0.4+0.3
Apr	967.9	54	27.85	26.68	0.1815	2.327	0.2+0.4+0.3
May	1081	54.47	29.05	27.69	0.181	2.789	0.2+0.4+0.3
Jun	1107	54.58	29.49	28.07	0.1808	2.969	0.2+0.4+0.3
Jul	1115	54.62	29.54	28.11	0.1808	2.988	0.2+0.4+0.3
Aug	1105	54.58	29.25	27.86	0.1809	2.87	0.2+0.4+0.3
Sep	1004	54.14	28.21	26.98	0.1813	2.463	0.2+0.4+0.3
Oct	803.3	53.27	26.39	25.43	0.1821	1.801	0.2+0.4+0.3
Nov	584	52.34	24.4	23.74	0.183	1.156	0.2+0.4+0.3
Dec	461.5	51.82	23.23	22.75	0.1835	0.8134	0.2+0.4+0.3

Table 03.13 – Data based on SPnc/PV/AGMD-AQ7 depth 0.2+0.4+0.3.

Month	Is, [W/m ²]	SP temperature [°C]	Outlet SP temperature [°C]	AGMD temperature [°C]	GOR	Productivity [m ³ /day]	Depth zones [m]
Jan	458.6	50.72	23.08	22.62	1.164	2.644	0.4+0.7+0.8
Feb	578.7	50.92	24	23.4	1.163	3.547	0.4+0.7+0.8
Mar	767.4	51.24	25.24	24.67	1.162	5.138	0.4+0.7+0.8
Apr	967.9	51.59	27.21	26.13	1.161	7.167	0.4+0.7+0.8
May	1081	51.78	28.26	27.02	1.16	8.5	0.4+0.7+0.8
Jun	1107	51.83	28.64	27.35	1.16	9.012	0.4+0.7+0.8
Jul	1115	51.84	28.68	27.32	1.16	9.069	0.4+0.7+0.8
Aug	1105	51.82	28.43	27.17	1.16	8.734	0.4+0.7+0.8
Sep	1004	51.65	27.53	26.4	1.161	7.561	0.4+0.7+0.8
Oct	803.3	51.3	25.93	25.04	1.162	5.634	0.4+0.7+0.8
Nov	584	50.93	24.19	23.56	1.163	3.739	0.4+0.7+0.8
Dec	461.5	50.72	23.17	22.69	1.164	2.722	0.4+0.7+0.8

Table 03.14 – Data based on SPnc/PV/AGMD-AQ24 depth 0.4+0.7+0.8.

Month	Is, [W/m ²]	SP temperature [°C]	Outlet SP temperature [°C]	AGMD temperature [°C]	GOR	Productivity [m ³ /day]	Depth zones [m]
Jan	458.6	51.81	23.14	22.67	1.164	2.698	0.2+0.4+0.3
Feb	578.7	52.31	24.19	23.56	1.163	3.739	0.2+0.4+0.3
Mar	767.4	53.12	25.89	24.83	1.162	5.591	0.2+0.4+0.3
Apr	967.9	54	27.85	26.68	1.16	7.978	0.2+0.4+0.3
May	1081	54.47	29.05	27.69	1.159	9.564	0.2+0.4+0.3
Jun	1107	54.47	29.05	27.69	1.159	9.564	0.2+0.4+0.3
Jul	1115	54.62	29.54	28.11	1.159	10.25	0.2+0.4+0.3
Aug	1105	54.58	29.25	27.86	1.159	9.841	0.2+0.4+0.3
Sep	1004	54.14	28.21	26.98	1.16	8.446	0.2+0.4+0.3
Oct	803.3	53.27	26.39	25.43	1.161	6.175	0.2+0.4+0.3
Nov	584	52.34	24.4	23.74	1.163	3.965	0.2+0.4+0.3
Dec	461.5	51.82	23.23	22.75	1.164	2.789	0.2+0.4+0.3

Table 03.15 – Data based on SPnc/PV/AGMD-AQ24 depth 0.2+0.4+0.3.

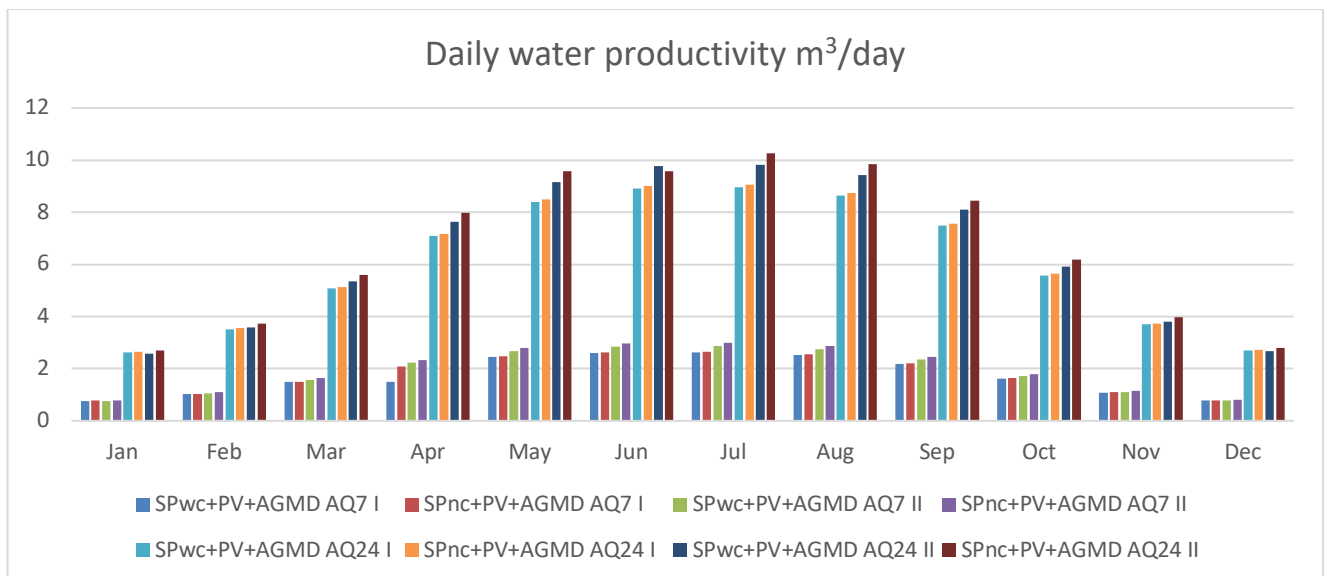


Figure 03.13 – Productivity based on the different configurations modelled.

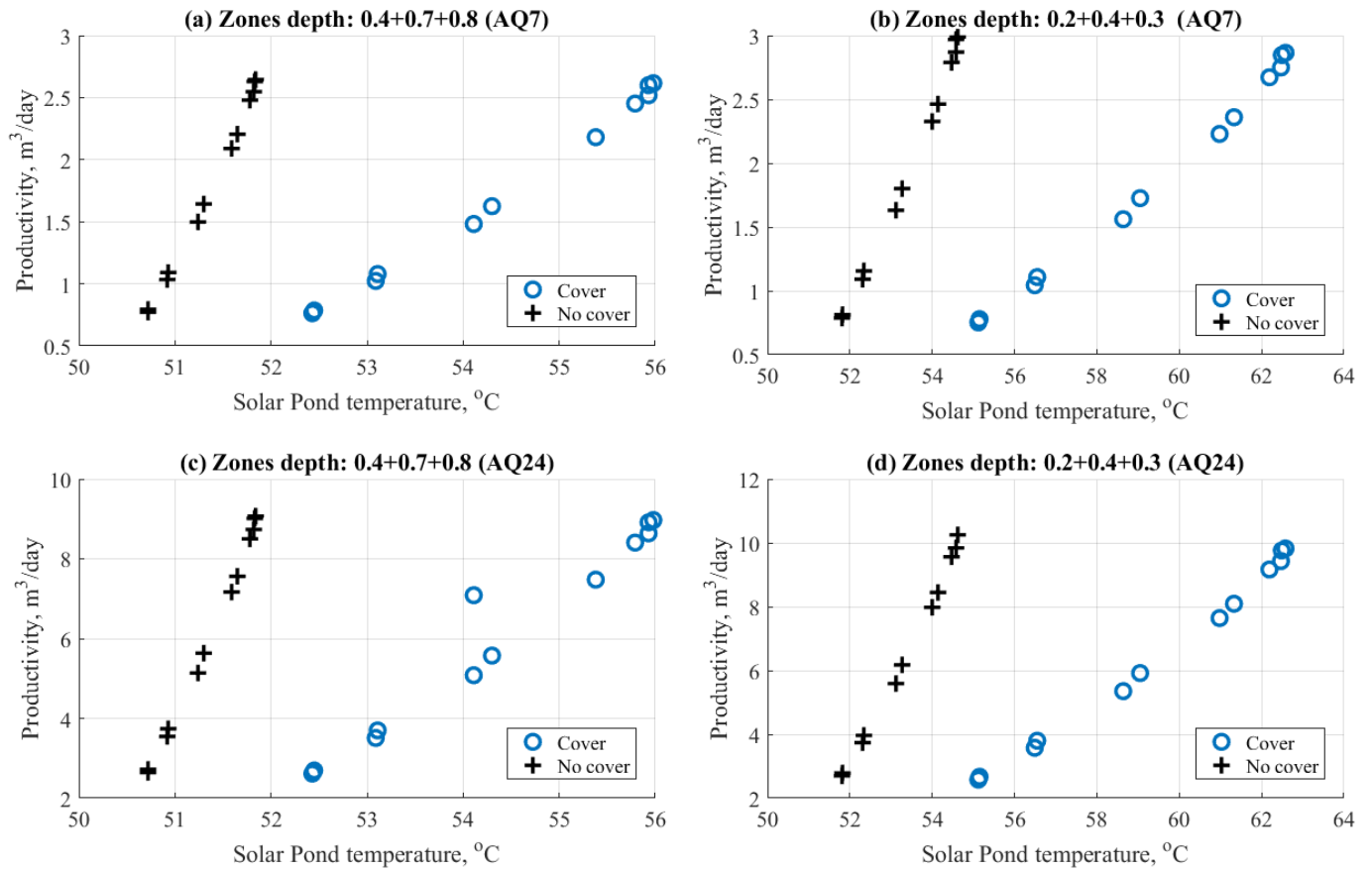


Figure 03.14 – Effect of SP temperature on system productivity based on the variation of the depth and the existence of the SP cover.

3.6 Conclusions

The performance modelling technique has thus far been used for the proposed SP and FPC combined with AGMD. This work has developed and presented the mathematical models for the units addressed. The meteorological data has been simulated based on a developed solar radiation model which simulates solar radiation that is instant, hourly global, monthly global, beam, diffuse and normal flux. The simulation data is designed according to Oman's known operating conditions. The performance findings can be outlined as follows:

- The SP temperature varies based on the effect of solar radiation throughout the year.
- The temperature of the SP varies between 60 and 67 °C.
- The SP load varies between 5 and 30 kW_{th}.
- For the AGMD, the WRR was found to vary between 4.6% and 5% based on the increase in production rate.

- The results were obtained at various zone depths and for different membrane areas. Decreasing the depth would increase the thermal energy and membrane productivity. Moreover, increasing membrane area would increase total productivity.
- Generally, FPC/PV/AGMD would yield remarkable productivity as compared to the SP/PV/AGMD system.
- The covered SP would reduce productivity by ~3% for the AQ24 type and by ~4% for the AQ7 type.

The results from the simulations clearly show that a small-scale SP combined with an MD is not a viable solution for water production in remote areas and that the use of a pond cover has a detrimental effect on water productivity. Water production using a SP is limited in volume and has an interesting production rate for a short period of the year (which is usually too hot for growing crops). On the other hand, simulating using flat solar panels is demonstrated to be a suitable option, even without an intermediate heat storage system, for water production and is one that could be subsequently used for irrigation. Real field test efficiency, capital and operational costs, maintenance costs and the predicted lifespan of the systems should also be appropriately addressed as harsh environmental conditions, such as sand and high temperatures, may drastically reduce the applicability of these solutions. While flat solar panels have been studied and are in use today across many arid regions in combination with solar stills, humidification-dehumidification systems and other technologies, the SP remains a prospective solution with only a few experimental trials to date. For this reason, an experimental SP with a cover has been designed and constructed in Oman, thereby confirming that harsh environmental conditions may not be neglected when choosing a suitable solar collector. The experimental trials described in the following chapter demonstrate that SP construction and management, despite outwardly appearing to be a simple solution, requires many efforts that further confirm its limited applicability. The use of flat panels or heat pipes for water and air heating have been chosen for implementation in Oman, and these are directly coupled with a novel solar distillation technology that will be analysed and described in Chapter 5.

4. Solar Pond Construction/Failure

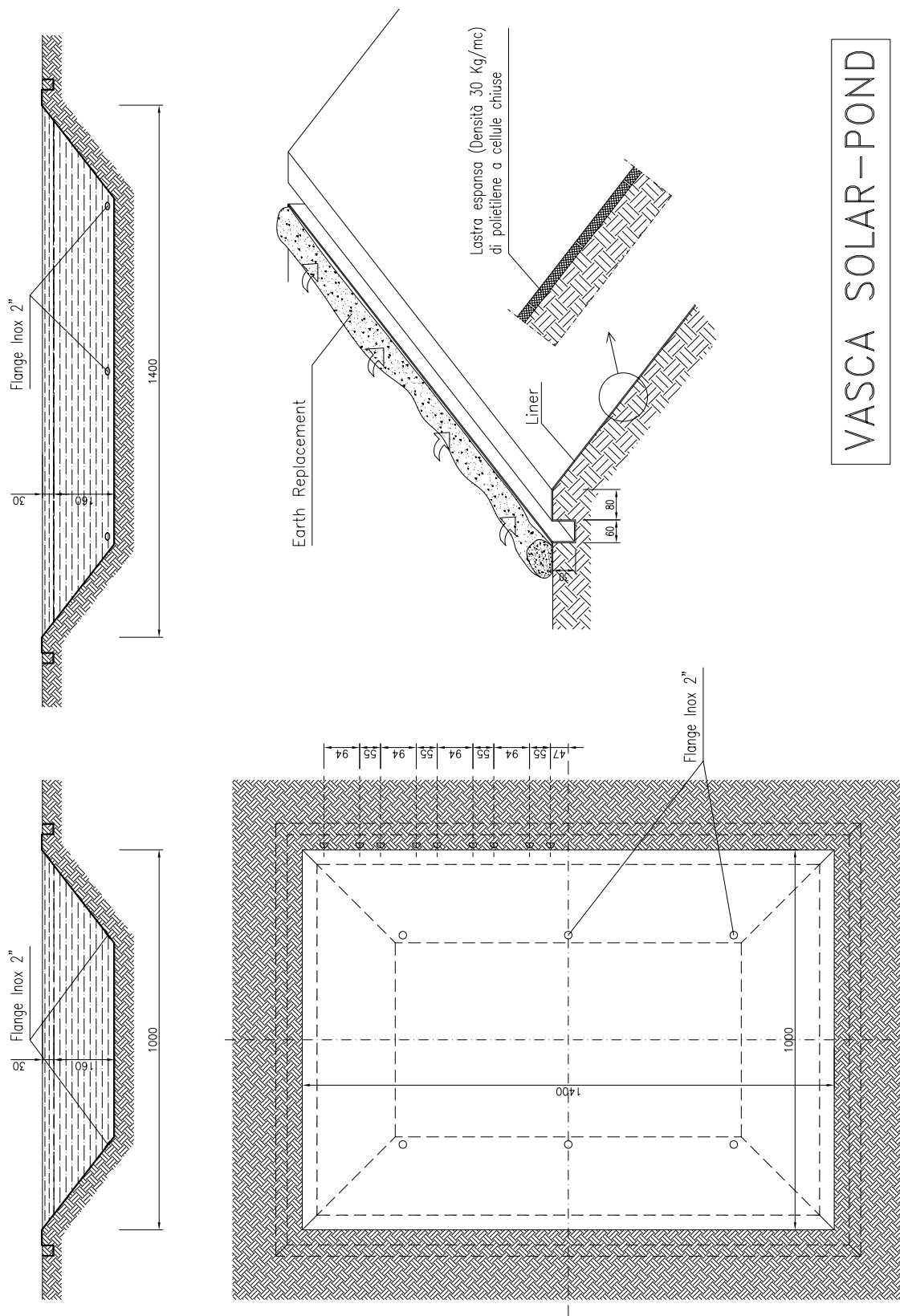
4.1 Introduction

Many papers can be found in the literature concerning the modelling of salinity gradient SPs and their simulations, although less attention has been focused on their detailed design, real construction, start-up or maintenance. For these reasons, a SP with a cover measuring 10 m x 14 m (Figure 04.01) has been built in Oman as a heat source for desalination and novel irrigation techniques.

Before designing and building the SP, several significant problems have been identified and adequately addressed, though not sufficiently to guarantee smooth construction and continuous use.

The SP was constructed with extreme difficulty and, even more problematic, were issues with its maintenance due to the practical troubles associated with its construction and operation. Consequently, it was decided to abandon this solution and instead opt for solar FPCs for the integration of new seawater desalination techniques.

There is no doubt that, in future, a SP could be used for such applications, although new materials will need to be developed alongside more efficient management. For remote areas, it is better to opt for simpler solutions, while for industrial applications and less adverse environments (e.g. sand, wind and excessive temperatures), its application can be further studied and, where possible, fully implemented.



4.2 Solar Pond Design, Construction, Operation and Data Collection

Most of the experimental work to date on SPs has concentrated on their design, application, thermal measurements, efficiency and investigations of the thermal performance of various types of SPs at a laboratory scale (Yadav et al. 2004; Sayer et al. 2016). The efficiency of a solar pond in collecting energy depends on the stability of the gradient zone and water clarity (Al-enezi 2012), thus maintaining the salinity gradient is essential for its successful operation. The salinity gradient is destroyed when care is not taken or there is a lack of proper insulation of the upper, lower or side zones. Solar pond design, construction, operation and data collection have been planned based on the previous experiment and are reported in the following paragraph.

4.2.1 Solar Pond Design Challenges

Innovative design in reducing heat losses from the top and bottom of Solar Ponds and increasing their overall efficiency has been considered and planned, and every single component that could have been improved with a new approach, compared with known technology, has been investigated and tentatively applied. In particular, attention has been given to the following main components or features:

- Top cover
- Bottom and side-liner
- Shape
- Salt type
- Turbidity
- Gradient construction & stability
- Heat extraction

4.2.1.1 Top Cover

Evaporation represents a significant challenge in the successful operation of Solar Ponds. The idea of using a cover to prevent evaporation and convective currents and, thereby, reduce heat losses from Solar Ponds has been proffered by some researchers. The use of such a cover has been applied or else studied for small-scale and SSPs, being impractical for wider ones. A preliminary application of a cover has been introduced for a shallow SP by Kudish et al. (1978), and further forms of cover,

whether liquid, floating objects or glazing materials such as glass, have been investigated and experimented with, as the effect of cover type has a fundamental impact on efficiency, durability and cost. The cover must be and remain transparent because, when it becomes opaque, despite continuing to be useful in the suppression of evaporation, it will not allow the penetration of solar radiation or temperature build-up in the pond.

The use of a shallow liquid layer of carboxymethyl cellulose (Jayaprakash et al. 2011) or a 5mm paraffin layer (Sayer et al. 2017) as cover to increase the stored energy of the pond and reduce evaporation have both been demonstrated to improve solar pond performance, although dust accumulation on the liquid surface represents a significant challenge which needs to be overcome, as the need to remove accumulated dust particles will also destabilise the liquid layer and destroy the pond's stability.

The use of double-glazing plastic instead of a liquid layer was introduced by Ali (1987) for a SSP. His conclusion confirmed reductions in heat loss and the optical efficiency of the pond. Following the experimental investigations of Bezir et al. (2008, 2009) using rotatable covers installed at the sides of the pond, both with and without a reflective covered surface and with insulated and reflective covers, their findings demonstrated that the cover, as a reflector, was more efficient than insulation, exhibiting a better performance at around 25%. Bozkurt et al. (2014) studied the effect of different transparent covers including glass, polycarbonate, and mica on the performance of a small cylindrical SP and found that the glass cover contributed the highest SP efficiency. These findings were confirmed by Sogukpinar et al. (2016) and Ganesh and Arumugam (2016). The use of glazing materials demonstrated, in general, an increase in the efficiency of the system due to the greenhouse effect, preventing heat losses from the top and increasing the temperature of the UCZ. Another critical outcome was the prevention of dust accumulation and the possibility of readily removing it.

The use of floating objects has been demonstrated to reduce evaporative losses from water reservoirs by up to 78% (Manges et al. 1966), yet most of the experimental investigations have been conducted using spheres which are opaque to solar radiation. Opaque plastic spheres and other opaque materials such as plastic and aluminised meshes, foamed rubber, or plastic sheeting have also been investigated by Assouline et al. (2010, 2011). Burstson et al. (2002) demonstrated that plastic domes have the same effect in reducing evaporation as opaque plastic domes. However, with transparent plastic domes, water surface temperatures were slightly higher than with opaque plastic domes. Ruskowitz et al. (2014) compared two non-opaque floating element designs (floating discs and floating hemispheres) and a continuous cover and found that floating discs were the most effective, covering 88% of the SP

and facilitating a 47% decrease in the evaporation rate and a 22% increase in heat content. The increase in heat content allows more heat to be withdrawn from the pond for use in external applications, thereby significantly improving the thermal efficiency of the SP. An increase in available heat was also obtained from the investigation of Silva et al. (2017) using floating discs on the surface of the SP. In these experiments, he found that the evaporation reduction efficiency was related to the cube root of the relative covered area and that, as the covered fraction of the surface area increased, the thicknesses of the UCZ and LCZ also increased as the NCZ thickness decreased. However, unlike the results from the studies using continuous coverage, the temperature of the LCZ had not risen.

An economic analysis showed that, although the evaporation reduction efficiency of SPs is smaller than that for natural water bodies or reservoirs, the benefits relating to the additional energy collected within the SP when reducing evaporation offset the smaller gains in water savings. Therefore, suppressing evaporation in SPs is a valuable approach in arid locations where there is no water to replenish the evaporative losses and improve its economic benefits.

According to the previous findings on the advantages of using a SP cover, a clear transparent continuous cover that reduces evaporative losses from the water surface by suppressing water-surface-to-air contact, while only minimally reducing the intensity of radiation penetration, was designed for the experimental work in Oman. The covering element developed was characterised by double-layer modules partly overlapping and fixed to one another across one connecting zone (Figure 04.02), being aware that a complete covering could have proven operationally challenging for such adverse weather conditions as sand, wind and high solar radiation as compared to transparent floating elements that would have allowed some evaporative losses, yet would have been easier to install and more easily scalable for field applications. The covering element was composed of polyurethane to be UV and saltwater resistant. It further contained a semi-transparent thermal insulating fluid to allow the transmission of solar radiation and prevent both evaporative and heat losses. The covering floating element had a specific mass of between 0.8 and 1.15 kg/dm³, lower than the density of the SP water as influenced by its salinity. The fluid employed was glycerine mixed with water at a concentration of between 80% to 100% and each modular covering element presented two connectors (Figure 04.02-n.09) to fill, discharge and, if necessary, change the transparent thermal fluid to investigate alternative products and dilutions. Each modular element was connected to the next one (Figure 04.02- n.10) with a fixing device. The top cover overlapped the bottom liner and was affixed to it via

rods (Figure 04.02-n.05). A partial supernatant layer of water was supposed to remain on the top of the cover to prevent the dust from adhering to the cover, thereby reducing its transparency.

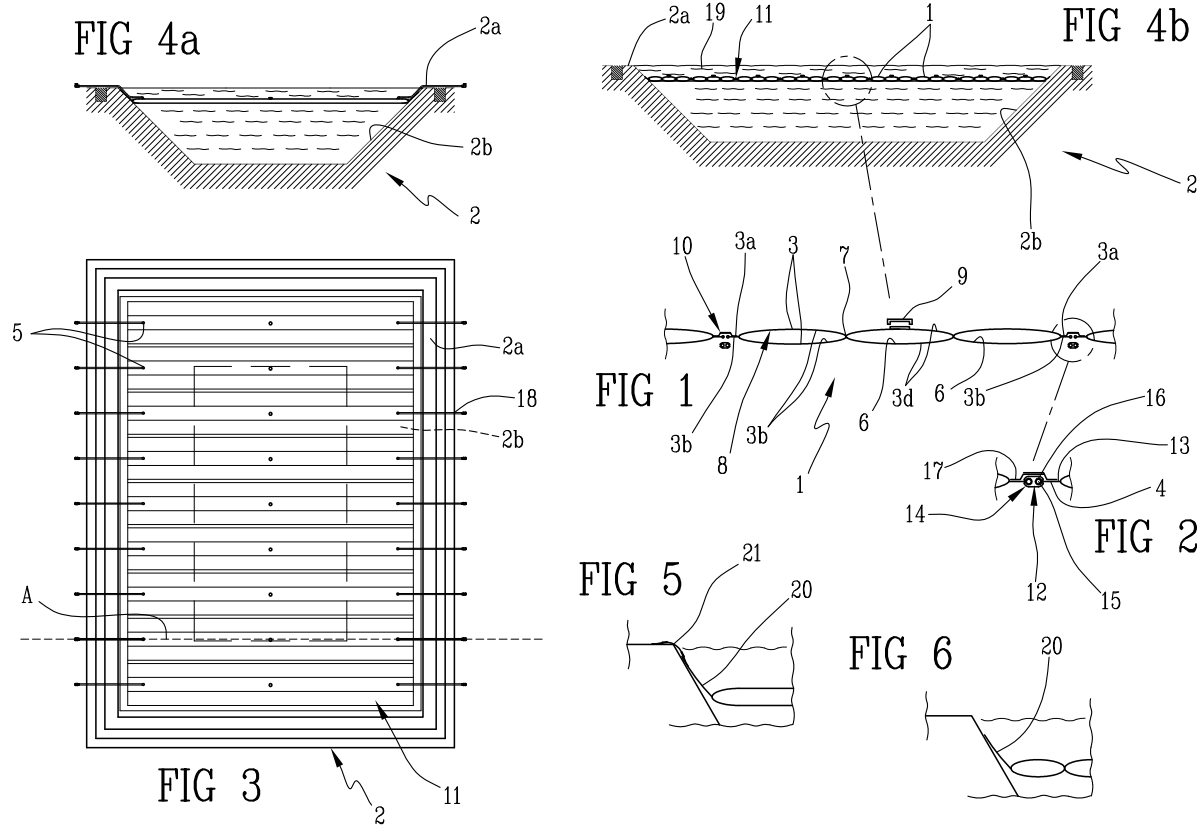


Figure 04.02 - Design of upper layer of the SP and means of fixing the top cover.

4.2.1.2 Bottom and Side Liners

SPs are usually contained within earth excavations and thus heat loss to the ground and sides are inevitable. The amount of heat loss to the ground has an important influence on the thermal efficiency of the SP system as demonstrated by Saxena et al. (2019). An important quantity of heat, around 50%, is lost to the ground below the SP (Ganguly et al. 2017) and sides due to the temperature gradient arising between the pond and the underlying earth.

Hull (1985) and Zang et al. (1990) demonstrated that ground heat losses are influenced by the soil's thermal properties and the mass flow rate of the water table beneath the Solar Pond. Many areas in the world with abundant solar radiation possess large ground thermal conductivity and/or an important moving water table. Thus, if a solar Pond is constructed in these areas, thermal loss to the ground would be vast while the residual heat stored in the solar pond would be far smaller. Thus it is

essential to investigate how to reduce heat losses to the ground can improve the heat efficiency of Solar Ponds situated in these areas. The selection of a proper liner has a significant effect on improving thermal performance. Therefore, the mechanical and thermal properties of the liner should be considered alongside such essential features as strength, longevity, cost-effectiveness, and resistance to saline and UV light. The chosen liner must produce a watertight barrier with adequate thermal insulation while at the same time preventing any contamination of aquifers. Plastic materials have been used with great success as liners for small prototypes, although experience with large Solar Ponds shows that such synthetic liners increase costs by about 30% (Jubran et al. 1996).

One of the first synthetic liner materials was tested at the El Paso SGSP of 3,000 m². It was an XR-5 geomembrane, one of the best-regarded, having been used across a range of challenging containment applications, whether for primary or secondary containment. XR-5 employs a unique proprietary blend of UV inhibitors and hydrocarbon resistant Elvaloy (Du Pont) to allow long-term immersion in hazardous chemicals, including caustic liquids that would destroy most conventional geomembrane liners. The XR-5 liner material has some of the most robust physical properties for a geomembrane liner, providing a highly resistant, non-degradable membrane surface. The high-quality reinforcement thread affords the liner extreme puncture and tear resistance, while its coating allows for high dimensional stability under high loads and extreme temperature fluctuations. XR-5 is also easily heat welded with a very high peel strength. Despite these extreme properties, the XR-5 membrane failed after seven years of use and was eventually replaced by a Geosynthetic Clay Liner (GCL) (Robbins et al. 1995). GCLs are factory manufactured hydraulic barriers consisting of a layer of bentonite (or other very low-permeability material) supported by geotextiles and geomembranes. These are mechanically held together by needling, stitching or chemical adhesives. Initially, a combination of two liners, specifically a flexible polypropylene geomembrane covered with PVC with a mass unit per area of 1.0 kg/m² and a GCL were selected. Unfortunately, the GCL only survived two years before a 0.1 cm fissure appeared in the polypropylene membrane at the pond's lateral edges. Occurring above water level, the deterioration of the material was attributed to UV exposure or such manufacturing defects as a loss of elasticity following the action of high temperature brines. Eventually, a new polypropylene-improved membrane, fabricated from a combination of two liners of flexible 60-mil polypropylene geomembrane of 0.15 cm thickness, seemed to have been successful (Lu et al. 2004). The 60-mil polypropylene geomembrane was a UV stabilised polyester scrim reinforced film with carbon black and UV resistance. This material is generally used for long-term water containment applications.

An alternative to synthetic materials and geomembranes, especially in remote areas and low-income communities, is the use of clays. This option reduces both the cost of construction and the risk of contamination of the subsoil and groundwater by hot brines. Underdeveloped nations can use this type of liner, although a battery of tests is recommended, including soil and water composition, permeability, plasticity, and X-ray diffraction analysis. In their experiment, Almanza et al. (1989) used a compacted clay liner to measure the thermal and mechanical properties of the clay and its ion exchange characteristics. They demonstrated for CH-type clay (an inorganic clay of high plasticity which exhibited a kaolinite structure) that the influence of a hot brine reduces the thermal conductivity and permeability during long periods of exposure. In their subsequent studies, Almanza et al. (1990), using Ca-montmorillonite bentonite, proved that the thermal conductivity and permeability of this clay was better than those of kaolinite clay. However, under drastic changes in temperature of 10°C or above, the clay starts to form small fissures that increase its permeability. Almanza and Castañeda (1993) studied the permeability of a calcic non-swelling clay liner under a hot NaCl brine (50°C). In the presence of a hot electrolyte, such as NaCl brine, this clay flocculates and makes the voids larger and therefore more permeable, demonstrating that not every Ca-clay is suitable for use as a liner for NaCl SPs. Silva and Almanza (2009) tested several compacted clay liners along with different additive materials. In their investigations, they analysed native clay soils with hillite, montmorillonite and halloysite; treated and non-treated bentonites in powder and granulated form; a mixture of zeolite and sodium bentonite; and industrial minerals composed primarily of halloysite, kaolinite and attapulgite selected clays.

Aqueous solutions of neutral salts (such as NaCl and KCl) at different concentrations and under various temperature gradients were used for compatibility testing of these specimens. The results indicated that those soil samples that contained more attapulgite (palygorskite) and less hillite and kaolinite clay minerals displayed good strength and water resistance. Liners with native clays could prove to be the solution to reducing the cost of large SPs, particularly in developing countries. However, one must first investigate the locally available material to ascertain whether it may be used in its native form or else blended into a soil amendment mixture. Another efficient and economic design for a liner comprises a polyethylene film of low density (LDPE) that is manufactured locally and placed between two compacted local clay layers as established by Raman and Kishore (1990) and Jubran et al. (1996). However, the polyethylene film displays certain disadvantages, including low joint reliability, small pieces, rigidity and low resistance to wrinkling.

Other research studied the effects of adding porous media to the bottom of the pond to reduce thermal losses and, consequently, salt diffusion. This porous media acts as a heat insulator, increasing the

LCZ temperature and heat storage capacity. The findings of Shi et al. (2011) showed that, where the ground thermal conductivity is considerable, a brine layer with porous media can serve as a heat insulator and thereby significantly increase the LCZ temperature and total heat storage capacity of the SP. Therefore, when the ground conditions are otherwise unsuitable for building a SP because of a critical moving water table, a brine layer with porous media can be considered to restrain heat transfer downward and improve the overall thermal performance. On the other hand, when the ground thermal conductivity is low, a brine layer in conjunction with porous media could not enhance the thermal performance of the SP and may even cause its performance to deteriorate, reducing its total heat storage capacity. It was also discovered that porous media repress the increases in turbidity observed during salt replenishment of the LCZ. Wang et al. (2014) experimentally and theoretically studied the development of adding a coal cinder (a burnt residue of coal) to the bottom of the SP to increase the LCZ temperature. Coal cinder is a cheap material with perfect thermal performance that can be readily found in any location.

The benefits of using coal cinders are an increase in solar radiation absorption and a commensurate decrease in heat losses. In their subsequent experimental studies, Wang et al. (2015) demonstrated that, within the experimental temperature range, the porous medium could delay salt diffusion upward. There were also some indications that the porous material seems to have an absorptive effect on salt, whereupon the lower the porosity of the medium, the more slowly salt diffuses. Wang et al. (2018) indicated that adding porous media with a low volume heat capacity and low heat diffusivity to LCZ is beneficial in attaining a higher temperature. Adding cinders enables maximal energy efficiency as compared to limestone and marble. Assari et al. (2017) used two layers of pebbles and ball bearings as a porous medium beneath the LCZ of a small experimental SP in Dezful, Iran. At the end of the test period, the results showed an enhancement in LCZ temperature from 71°C to 75°C, a 5.6% increase in temperature. The use of the porous medium not only increased the thermal stability of the pond but also reduced the variation of its maximum temperature. Hongsheng et al. (2020) studied the heat storage capacity of various porous materials, achieving a maximum temperature increase of around 6° C, 11.6% higher than a traditional pond. It was found that the optimal material was the coal sorbent owing to its large heat capacity and stacking density.

In alignment with the experimental findings mentioned above, different materials, previously used as SP liners were compared and contrasted with newer ones, both technically and economically, to ascertain their viability. A PET recyclable highly consistent material extruded structural foam named Gurit® Kerdyn® Green (by Gurit) (Table 04.01) was selected. The main advantages of such a product are:

- Highly adaptable
- 100% recyclable
- A thermoplastic core material with a good balance of mechanical properties, temperature resistance, density and cost
- Stable at high temperatures
- Provides outstanding chemical resistance and good adhesion, ideal for wind energy, marine, industrial, and transportation applications
- Of low thermal conductivity

Properties	Standard	Unit	Average values	Remark
Density	ISO 845	kg/m ³	80	-
Compressive Strength	ISO 844	MPa	1,2	Thickness according standard (50 mm)
Compressive Modulus	ISO 844	MPa	50	Thickness according standard (50 mm)
Shear Strength	ISO 1922	MPa	0,56	Thickness according standard (25 mm)
Shear Modulus	ISO 1922	MPa	22	Thickness according standard (25 mm)
Tensile Strength	ASTM C297	MPa	1,1	Thickness according standard (25 mm)
Tensile Modulus	ASTM C297	MPa	61	Thickness according standard (25 mm)
Thermal conductivity	DIN EN 12667	W/(m·K)	0,0317	Thickness 25 mm

Table 04.01 – Technical specifications of the extruded structural foam named Gurit® Kerdyn® Green (by Gurit).

Despite showing excellent thermal insulation properties, the material failed to produce a barrier of adequate water-tightness at the connecting interface during preliminary experimental tests. Different bonding materials, as reported in Table 04.02, have also been implemented without success, as external influences such as high temperature, saltwater, etc., harmed its bonding properties. All chosen adhesive systems were easy to apply and had a short installation time. The product's high price makes it even more unsustainable for this application.

Sample No.	Bond
1	3M Marine Hybrid glue 4000 UV
2	3M Marine polyurethane glue and sealing agent 4200 FC
3	3M adhesive tape Type 1 (grey) without using primer
4	3M adhesive tape Type 1 (grey) with primer
5	3M adhesive tape Type 2 (white) without using primer
6	3M adhesive tape Type 2 (white) with primer
7	No bonding. Only demonstration of the tongue and groove connection

Table 04.02 – Overview of samples for bonding application tests.



Figure 04.04 - Open and closed tongue and groove connection - Sample 7.

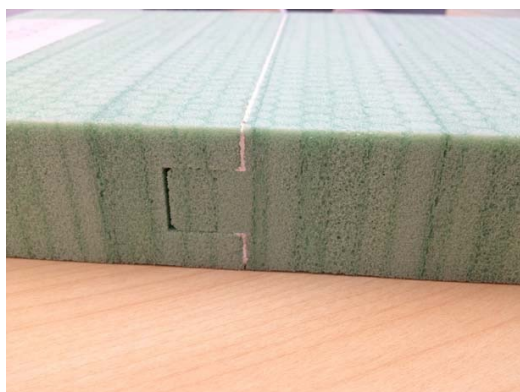


Figure 04.05 - Tongue and groove connection with glue - Sample 1.



Figure 04.06 - Tongue and groove connection with adhesive type - Samples 3,4.

Eventually, after a thorough investigation into other prospective liner materials, a polyether polyurethane liner was selected. Polyether polyurethane is an elastomer, meaning that it possesses elastic properties and offers a good price relative to its performance (Table 04.03).

Resistance	Characteristics
Abrasion Resistance	Excellent impingement abrasion resistance.
Heat Resistance	Low susceptibility to dynamic heat build-up.
Cut and Tear Resistance	High tensile strength and high cut and tear resistance.
Water and Moisture Resistance	Excellent hydrolytic stability.
Salt Resistance	Degree of degradation in salty water is dependent on the degree of crosslinking (to be further investigated).
UV Resistance	Tribological properties, in terms of wear resistance, are affected by UV exposure (to be further investigated).
Oil, Fuel and Solvent Resistance	Resistant to attack from harsh chemicals.

Table 04.03 – Performance properties of polyether polyurethane.

The polyether polyurethane material used had a mass of 1,300 g/m², breaking strength of 4,500 N/5 cm and a tearing capacity of 450 N. Material colour was cream on one side and black on the opposite side exposed to the sun to enhance solar radiation. The final material price was 8,000 € for a liner measuring 160 m² (50 €/m²).

No insulation material was placed underneath the liner to avoid additional costs incurred during excavation and pond preparation. Due to the unstable sandy soil, it would have been also very difficult to construct a stable base for the pond using insulation material provided in foils. An alternative option could have been to use a spray solution such as formaldehyde urea, or even asphalt, but this solution would have made the system less environmentally friendly.

4.2.1.3 Shape

SP shape impacts performance by reducing the shading effect and attendant heat losses. The most popular forms for salinity gradient SPs are either circular or rectangular. Geometric shape also has an essential impact on the performance of smaller ponds although it has an insignificant impact on the efficiency of larger commercial SPs owing to the diminishing perimeter-to-area ratio. SP geometry can be studied by analysing the horizontal and vertical cross-sections.

The horizontal cross-section has an important impact on the shading effect.

Dehgahn et al. (2013) and Assari et al. (2015) conducted an experimental investigation of the energetic and exegetic performance of two SPs with similar cross-sections and volumes, reaching contradictory conclusions. One of these ponds was square, while the other was circular. Dehghani et

al. concluded that a circular SP had better energy performance as compared to square designs due to a lower perimeter-to-area ratio, thereby demonstrating that a circular pond has higher efficiency as compared to a square one (25.8% vs. 23.65%). Both units had similar dimensions, with cross-sectional areas of 3 m² and 1.5 m², respectively. Assari et al. (2015) came to the opposite conclusion, affirming that the rectangular pond has better performance if the angles of the pond are chosen appropriately. Their square SP reached a higher maximum temperature than the circular one (74°C vs. 71°C). Assari et al. (2015) also indicated that the arrangement of the pond location is essential for square ponds whereas it is of no importance to circular ones due to its geometric symmetry. In fact, the rectangular pond should be positioned so that its width runs along the north-south axis to reduce the shading effect. The shading effect depends on other factors such as geographical location, radiation angle, the pond's dimensions, and date and time of year. Therefore, the pond should be designed considering a range of these factors to decrease the shadow cast across the pond. Khalilian et al. (2017) further investigated the energy efficiency of a square horizontal SP to experimentally validate a shading model. The authors discovered that the highest energy efficiencies for the NCZ and LCZ, both with and without shading, occur in July and are 9.32% and 6.57%, respectively. The shading of the side walls dramatically impacts energy efficiency, so it is essential to choose the right angle of the walls to enhance the pond's efficiency. Aramesh et al. (2017), using experimental data from previous studies, presented a novel model to calculate the energy efficiency of a rectangular SP with shading effect considerations, confirming that the shading effect inside the pond significantly affects the energy storage performance of the pond, especially for small ones, with the experimental data and theoretical results indicating that the energy efficiencies were 28.11% and 30.94% for the month of August, respectively.

The geometry of the vertical cross-section also has an important impact on heat losses, shading effects, and heat storage.

The effects of vertical cross-section on heat losses and, indirectly, on the salt concentration profile, were investigated theoretically by Akbarzadehet et al. (1984). The authors showed that sloping walls increased the concentration gradient at the bottom of NCZ and decreased the gradient at the top. Jaefarzadeh et al. (2004) studied the shading effect for a vertical wall of a square pond and its impact on the reduction of the sunny area was incorporated into the model, thereby demonstrating the importance of the wall shading effect on the performance of the pond, especially for smaller ponds. Liu et al. (2015) proposed a trapezoidal cross-section pond with a surface of 2.4 m×2.4 m and a bottom area of 1.0 m×1.0 m. The temperature of the trapezoidal pool was higher than that of the rectangular cross-sectional pool, with a maximum difference of about 5°C. The sidewall heat flux of

the trapezoidal pool is higher at the UCZ and NCZ. In contrast, at the LCZ, the trapezoidal structure helps improve the temperature performance of the SP because there is less water in the trapezoidal pond than in the rectangular. The sloped sidewall can both overcome the effects of shadow on radiation transmission and reduce the heat dissipation area, thereby increasing the temperature of the SP. Sayer et al. (2017) modelled equations to predict the salt concentration over time for both trapezoidal and rectangular cross-sections and compared the results with previous experimental experiences. Considering that there was no salt accumulation in the NCZ and no salt injection into the LCZ, they illustrated that the trapezoidal cross-section pond dissipated less heat but needed more time to reach a uniform concentration.

According to previous considerations, the experimental SP in Oman, which is classed as a small SP due to its limited dimensions of 10 m x 14 m (140 m²), has been constructed with a rectangular shape and trapezoidal vertical cross-section to minimise the wall shading effect. The pond has been positioned with its width aligned in the north-south direction and the slope of the inclined sidewalls is 35° towards the ground plane. The rectangular shape also helped in constructing the bottom liner and cover during the ground preparation works. The SP was constructed after excavating 3 m below ground level. The pond's bottom and side sand walls were compacted, compressing them mechanically with locally available machinery.

4.2.1.4 Salt Type

Salt gradient SPs are based on the principle of reducing heat losses by suppressing convection losses to the atmosphere. The salt concentration increases with depth, from a very low value at the surface to near saturation at the bottom. The concentration stratification is achieved during construction by dissolving salt at different salinity levels. One of the main considerations of the SP is the nature of the salt used in creating the salt gradient. Many kinds of salts have been tested for small-scale applications, while for larger ones, NaCl or natural brine are the only viable options due to their ready availability and reasonable cost. There are many coastal locations and salt lakes where the natural brine is present, and NaCl can also readily be obtained in coastal areas using the brine waste from local desalination plants. The salt is used to build the gradient and should be constantly added into the pond to restore losses due to evaporation or accumulation in the pond.

Several investigations have been conducted on the efficiency and economic aspects of using NaCl, natural brine or fertiliser salts. Hassairi et al. (2001) compared two ponds, one using NaCl solution and the other containing natural brine taken from the salt lakes present in the south-east of Tunisia. The outcome of the experimental work was that the maximum temperature reached near the bottom

of the pond with the NaCl solution was 55°C, whereas it was only 47°C with natural brine. Nie et al. (2011) investigated the behaviour of an experimental SP located on the Qinghai-Tibet plateau which was filled with natural brine. It had a surface area of 2,500 m², a depth of 3 m and a trapezoid cross-section. They noted that the LCZ temperature of the SP reached a maximum of 39.1°C with an average temperature increase of 0.69°C per day. The economic aspects of building a solar pond for desalination and energy production in the coastal area of Abu Dhabi, using natural brine instead of NaCl, were performed by Howari et al. (2008). Their calculations showed that the cost of production of one m³ of fresh-water ranges from 0.74 to 1.19 \$/m³ based on the assumption that salt is cheap and readily available, although it can decrease to between 0.68 and 1.10 \$/m³ if salt is free of charge (from the hypersaline lagoons of Abu Dhabi). Natural brine has a low thermal efficiency as compared with NaCl, and it may be appropriate to use it in some regions where it is freely available.

Other alternative salts can be used in preference to natural brine and NaCl, especially considering the risk of spillage and soil contamination with its attendant negative environmental impact upon agricultural land. Another reason could be that NaCl has no alternative use after being employed in a solar pond, and the disposal of salt which has diffused into top layers is difficult. Generally, ponds using NaCl need an evaporation pond almost equivalent in size for the recovery of the salt diffused to the top zone of the pond, making their use even more expensive.

Some alternative products that can potentially replace NaCl have been investigated. Some may offer good thermal capacity and environmental and economic viability, including fertiliser salts. Fertilisers which are suitable for use in a solar pond should have ready availability and a low price; good solubility to allow a high increase in density with a relatively low amount of product; good brine transparency; be of low maintenance and encourage only minimal algal formation. Various salts, including magnesium chloride (MgCl₂), potassium nitrate (KNO₃), ammonium nitrate (NH₄NO₃), sodium nitrate (NaNO₃) and fertiliser salts as urea (NH₂CO · NH₂) satisfy most of the aforementioned criteria and hence are considered suitable for use in a solar pond.

Hull (1986) studied the potential use of ammonium salts, including ammonium nitrate, ammonium phosphate and ammonium sulphate (Hull et al. 1989), as these all have thermal efficiencies sufficiently close to those of NaCl. Ammonium nitrate helps to solve the problem of salt discharge at the end of the shelf-life, being widely used as a fertiliser. It also prevents algal formation due to the precipitation of soluble phosphates. In contrast, ammonium phosphate is unsuitable for Solar Ponds because of its poor brine transparency. Ammonium sulphate's thermal behaviour was better than that

of ammonium nitrate and, like NaCl (for temperature gradients of between 50 and 300 K/m and salinity gradients of between 200 and 1400 kg/m³), gradient erosion and growth of the gradient zone were generally in line with the Nielsen boundary criterion for NaCl. To control algal formation and maintain transparency, the use of sodium hypochlorite was implemented.

Pawar et al. (1995) introduced the use of fertiliser grade urea (NH₂CONH₂) and compared it with NaCl and MgCl₂ ponds. It exhibited similar behaviour, the experiments demonstrating the effectiveness of urea in suppressing convection within the pond from the NCZ. Moreover, the temperature differential of 23°C between the upper and lower zones was obtained with a salinity difference of 35% without any instabilities arising within the gradient zone. The brine solution remained transparent and there was no algal formation.

Murthy and Pandey (2002) proposed using muriate of potash (MOP), a potassic fertiliser salt found to have properties comparable to those of NaCl at a lower cost than urea. Although urea has higher solubility and offers a lower density increase than NaCl, MOP eventually requires higher quantities in its installation, leading to higher costs. An experimental study on the use of MOP as a replacement medium for NaCl was further conducted by Murthy and Pandey (2003), confirming the suitability of MOP in generating stable temperature gradients which were comparable to those of NaCl. Another advantage of MOP is that the removed salts in the upper zone of the pond can be reused as a crop supplement instead of being disposed of as waste, although no investigation was conducted into the formation of algae.

Kurt et al. (2006), across two different studies, investigated both experimentally and theoretically the use of sodium carbonate (Na₂CO₃). Their resulting one-dimensional mathematical model confirmed their experimental investigations, demonstrating that the density gradient, achieved using Na₂CO₃, can suppress convection from the bottom layer to the surface of the pond and trap incident solar radiation as heat energy in the LCZ over a long period. After investigating different density gradients using Na₂CO₃, a 16% salinity solution was necessary and sufficient to successfully store the heat and create a temperature differential between the bottom and the pond's surface of 12 °C. Berkani et al. (2015) compared both numerically and experimentally the use of NaCl, Na₂CO₃, and CaCl₂, showing that both CaCl₂ and Na₂CO₃ can improve solar pond performance, especially within the NCZ. The CaCl₂ pond responds thermally more quickly than the two other ponds below saturation. They also demonstrated that the pond is warmer in the centre and colder near the walls, indicating a significant heat transfer in the horizontal direction, thereby requiring good pond wall insulation.

Bozkurt et al. (2015) conducted an experimental investigation into an MgCl_2 saturated solar pond. According to the results of their study, the maximum energy and exergy efficiencies were 27.41% and 26.04% for the heat storage zone, respectively, and 19.71% and 17.45% for the NCZ in August. Not only were fertiliser salts suitable for use in a SP, but there are also some other alternative candidate salts such as potassium aluminium sulphate dodeca-hydrate ($\text{KAl}(\text{SO}_4)_2 \cdot 12\text{H}_2\text{O}$), as reported by Vitner et al. (1984), which can successfully increase energy storage capabilities. Over the past few years, the use of nanofluids to enhance thermal conductivity has been applied to many heat transfer systems such as flat plate solar collectors or heat pipes, as nanofluids are almost opaque to light waves, thereby enhancing solar absorption. The use of CuO and Al_2O_3 at low concentrations of up to 10% in water can dramatically improve thermal conductivity.

Karunamurthy et al. (2012) investigated the use of nanoparticles in enhancing the efficiency of a SGSP. First, they adopted paraffin as a phase change material (PCM) due to its high storage density. Unfortunately, due to its poor thermal conductivity, they had to combine it with CuO nanofluids resulting in improved thermal conductivity; the higher the concentration, the better the performance. Other nanofluids have been investigated as a nanofluid pond is an excellent solar energy storage device. Despite its viable solar absorption characteristics, as compared to a conventional SP, it however presents a greater cost and the difficulty of disposing of the solution during its operation and end of life.

In remote and coastal areas, in particular, the use of traditional NaCl and natural brine solutions in constructing a salt gradient is preferred. In 2002 Oman had 14 desalination plants run by Petroleum Development Oman (PDO) across eight locations with a capacity of more than $7,000 \text{ m}^3/\text{d}$ of fresh-water when large quantities of reject brine are produced. The need to minimise the environmental impact of the rejected brine is however a big challenge for PDO. The company developed different disposal options such as reinjection, lined and unlined evaporation ponds, and natural depressions such as lakes. The abundance and low cost of NaCl make it a suitable choice in building salt gradients.

4.2.1.5 Turbidity

Water turbidity plays a critical role in the thermal performance of SPs, as high turbidity levels can prevent ponds from storing energy. Therefore, the turbidity levels within the pond must be regularly monitored and kept as low as possible. Water turbidity hinders radiation propagation, decreasing the light flux that reaches the NCZ and LCZ. Heat extraction and heat transfer to the bottom and surrounding walls can reduce the LCZ. External factors such as water evaporation, wind, and rain

may erode the UCZ. The LCZ and UCZ will then together increase convection eroding the NCZ and reducing thermal performance.

Wang et al. (1995) studied the thermal performance of a SP using a one-dimensional theoretical model and determined the correlation between the effect of a uniform turbidity distribution on solar radiation flux. The results indicated that water clarity plays a critical role on thermal performance for salt gradient SPs. Punyasena et al. (2003) studied the effect of wind and rain on SP performance and its capacity to destabilise the pond causing erosion of the NCZ and establishment of a uniform density and salinity. Xie et al. (2006) demonstrated that increasing turbidity will accelerate the decline of NCZ from the UCZ but will reduce the deterioration of NCZ from LCZ because, thanks to the increase in turbidity, the UCZ can absorb more solar radiation. Thus its temperature will increase while the LCZ will receive less solar radiation and its temperature will drop causing a fall in thermal performance. Atiz et al. (2014) experimented with the effects of turbidity on system performance, comparing two different ponds and evaluating their respective energetic efficiencies under both calm and turbid currents. Dirt deposition over time, for instance by sand, insects, algae, dust or any other particle moved by the wind, greatly affected performance, which was found to range from 28.40% for clear water to 22.27% for turbid water. Husain et al. (2004), in contradiction to previously mentioned studies, affirmed that a reflective bottom with an optimum value of turbidity might actually improve the efficiency of the pond as turbidity may, in fact, reflect the amount of heat radiated from the bottom of the pond and help to retain it in the lower part of the pond. Determining the optimum turbidity value is very important in compensating for the losses due to reflectivity and also in improving heat storage. Turbidity can, in this case, be controlled for by dosing a coagulant or other artificial medium. Since SPs must operate in an open environment to maximise solar radiation use, they will always be subject to such external factors as wind, rain, and sandstorms if positioned in a desertic area. This will inevitably reduce the pond's thermal efficiency or even destroy it. Solar radiation will also increase algal and microbial growth which further undermine water clearness. Due to the prevailing destructive influences of turbidity on the performance of SPs, the discovery of appropriate strategies is of great importance. Several studies have focused on how to control turbidity through additives and chemicals. Li et al. (2010) experimented with the use of Alum ($\text{KAl}(\text{SO}_4)_2 \cdot 12\text{H}_2\text{O}$) in reducing turbidity in a seawater SP, demonstrating that its strong capacity in promoting flocculation not only helps to reduce turbidity, but also the growth of algae and bacteria, thereby guaranteeing long-lived limpidity. Valderrama et al. (2011), using an experimental pond built in Catalunya, Spain, successfully employed HCl to control the clarity of the pond; while Malik et al. (2011) tested chemical and biological treatments to maintain clarity in NaCl and MgCl_2 SPs. Algal

and bacterial growth, enhanced by the highly organic solution, were the main drivers of the increase in turbidity. HCl was initially used as a shock treatment to kill the algae and then brine shrimps were introduced to maintain water clarity. Gasulla et al. (2011) used chlorine and copper ethylamine complex (Cupricide), concluding that Cupricide is more effective and ecologically friendly than chlorine in maintaining pond clarity. Provision of an acidic pond environment been shown to be adequate in maintaining limpidity, as algal growth is enhanced at a pH of between 5.5 and 8 and reduced if the pH is maintained below 4.5. Maintaining the clarity of the pond through the addition of chemicals and additives is very important, but it should be done through the consideration of solutions with a low environmental and economic impact. More attention should be placed on the use of biological and natural treatments. The use of the pond cover can prevent the entry of solid particles such as sand, insects and dust, because they can be easily removed, clearing the cover while algae growth should be considered as the main concern to avoid pond turbidity.

4.2.1.6 Gradient Construction & Stability

The construction of the salinity gradient and its stability is one of the primary challenges in guaranteeing good thermal performance from a SP. As such, it is essential to effectively and efficiently construct an accurate salinity distribution profile. Several studies have been addressed to investigate the salinity gradient construction, starting from the first injection filling technic introduced by Zangrando (1980), whereupon the pond was first filled up to half of its depth with a highly concentrated saline solution (to build the storage layer), after which fresh-water, or water of a lower salinity, was injected via a horizontal diffuser (Figure 04.07) into the top of the pond. The saline solution with the desired concentration was prepared with an additional shallow or evaporation pond close to the main pond.

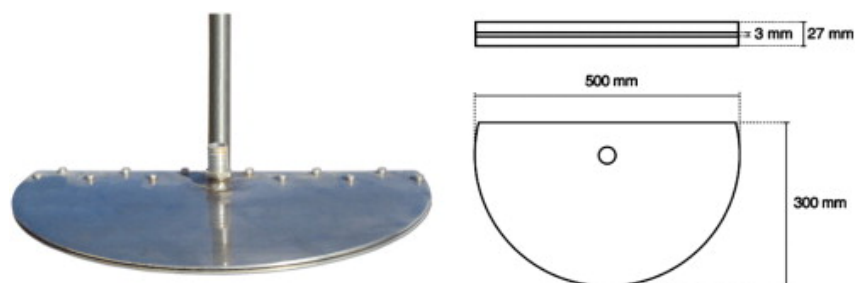


Figure 04.07 – Design of horizontal diffuser (Valderrama et al. 2011). Reproduced with permission of the rights holder Elsevier B.V.

Valderrama et al. (2011) and Leblanc et al. (2011) gave a detailed description of how the speed of the upward-lifting of the diffuser is vital in reaching the desired salinity gradient according to the Froude number (Fr) which represents the ratio of kinetic energy to gravitational potential energy of fluid injected into the pond. This number has been determined to be 18 or below, which means that the diffuser's speed should be twice the speed of the rising of the pond. The method mentioned above is generally known as the *redistribution method* by Faqeha et al. (2019) and is used for medium to large SPs. Two other methods that can be used to establish the salinity gradient are the natural diffusion and the stacking method.

The natural diffusion method consists of filling the lower part of the pond to nearly half of its volume with a high saline solution and the upper part with fresh-water. As salt will continuously diffuse from the lower part to the upper one, salt needs to be injected into the lower section while fresh-water is added to the surface to build the gradient. The last method of constructing a salinity gradient and the most frequently used, owing to its simplicity, is the *stacking method*.

In this method, the saline is injected into the pond from the lower part to the top with an incrementally decreasing salt concentration. In the lower part of the pond, within the LCZ, the salt solution concentration will be near the saturation point. Over the course of the following layers, it will steadily diminish until becoming of low salinity or pure fresh-water at the pond's surface.

The staking method was used to establish both the salinity and thermal gradients in the experimental SP in Oman. Prior to the filling process, trucks transported the necessary amount of brine from the nearest desalination plant to the facility. A small evaporation pond was constructed close to the main pond where the desired saline concentration was created before being introduced (Figure 04.08).



Figure 04.08 - Evaporation pond showing preparation of water salinity before injection into the main SP.

The injection process was split into four solution layers of decreasing salinity plus a supernatant layer of fresh-water, each layer having a reduced depth (Figure 04.09). These layers were added gradually into the pond through the use of a low flow rate pump (25 lpm) and a plastic hose. This was fitted at the end with a plastic diffuser in an attempt to reduce layer intermixing during the pond filling process. Each layer took approximately two days to add and the salinity and temperature of each layer was measured to understand the correct construction of the gradient.

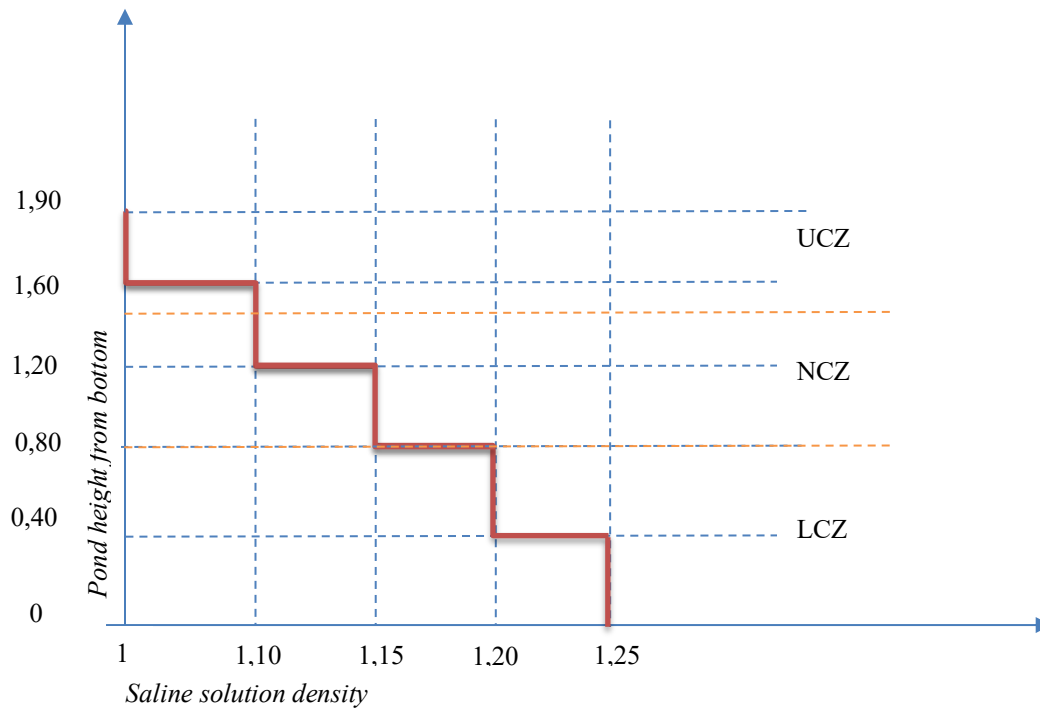


Figure 04.09 - Pond gradient layers.

Despite the initial stability of the first pond layers, the final saline solution to be introduced destabilised the gradient and created homogeneous salinity. Unfortunately, it was impossible to restart the reconstruction of the salinity gradient due to the need to conform with the seasonal sowing of the crops and the required growing period as per the experimental contract. It was then decided to maintain a mixed saline solution in the pond in the hope that the pond cover would prevent evaporation and instil stability rather than the salinity gradient.

4.2.1.7 Heat Extraction

The final parameter in designing and constructing a SP of high efficiency and stability is in collecting and storing useful heat at a suitable temperature which can later be extracted and made available for the required purpose. Many studies have focused on heat extraction methods to maintain pond gradient stability, and these studies can be classified into two main categories, namely *direct heat extraction*, wherein the hot saline of the LCZ is pumped from the pond and the heat is extracted through an external heat exchanger before returning the solution back to the LCZ, and *indirect heat extraction*, whereupon the heat is exchanged through a heat exchanger installed inside the pond via the use of a heat transfer fluid.

The direct heat extraction method has a cost advantage and is a more straightforward implementation as compared to the indirect mode, since the heat exchanger is positioned outside the pond and can be easily maintained in case of failure. As such it is not subject to a highly corrosive medium. The brine solution must be extracted and reinjected into the pond without disturbing the saline gradient, creating only minimal liquid movement. Kumar et al. (1999), in their experimental SP in India, used an external heat exchanger, demonstrating that the heat transfer coefficient was higher and the heat exchanger could be more compact than a submerged one. An extraction double plate diffuser to withdraw the brine was mounted 20 cm below the LCZ-NCZ interface, while another double plate diffuser was placed at the bottom of the pond 20 cm below the first at a depth of 3 metres to return the colder brine after the heat exchange process had concluded. The diffuser and brine flow rate design were chosen according to the Bulk Richardson Number and Local Richardson Number. According to Zangrando (1980), the values of Bulk Richardson and Local Richardson numbers were around 109 and 500, respectively, to avoid any disturbance of gradient. They also determined that fouling due to saturated brine flow within the heat exchanger is a significant problem and that a proper material should be chosen. In their case they used cupro-nickel for the tubes and carbon steel for the diffuser. A similar configuration was also described by Lu et al. (2001) for the heat extraction process at the El Paso SP. Angeli et al. (2006) created a computational fluid dynamic model to study heat extraction in an innovative U-shaped SP with an external heat exchanger located between the inlet and outlet sides of the pond, employing the slow movement of the brine without the need for any pump. The injection of the concentrated brine at the boundary between the LCZ and NCZ also improved the stabilisation of the salinity gradient. Yaakob et al. (2011; 2016) modelled and experimentally compared heat extraction from the NCZ of the SP using small pumps for extraction and reinjection at different levels. The introduction of a passive thermosiphon without any pump demonstrated that such a device could be applied to a large-scale SP, thereby achieving an efficiency increase of up to 30%.

The indirect heat extraction method has also been analysed by several investigations and can be considered an alternative conventional method through which to extract heat from the SP. The heat exchanger is usually positioned inside the pond within the storage zone near the gradient layer but can also be placed in the LCZ or at the boundary between the two. Thermal energy is transported outside the pond thanks to a heat transfer fluid and can be sent to an external heat exchanger or a storage tank.

Jaefarzadeh et al. (2006) studied the thermal energy extraction from a small SP using fresh-water recirculation through a heat exchanger placed in the LCZ and recovered with an external heat

exchanger. Their results showed a thermal efficiency of 10% although this can reach 22% for larger ponds. Andrews et al. (2005) reported an alternative method for extracting heat from the NCZ rather than the LCZ, demonstrating that heat extraction from the gradient layer can reduce heat losses to the surface and increase SP efficiency in delivering heat at relatively high temperature up to 50% as compared to extracting it solely from the LCZ. The heat exchanger is positioned so as to cover the entire NCZ and to receive a transfer fluid at low temperature, near to the ambient temperature at the top of the NCZ, releasing it from the bottom of the NCZ at a higher temperature close to that of the LCZ. Further experimental research into the possibility of extracting heat from the gradient layer was carried out by Leblanc et al. (2010), determining an increase in the overall efficiency of the pond of up to 55% as compared to extraction from LCZ. From this experimental study, in agreement with modelling, convection currents were found to be localised and not to have any significant effect on the layer density. Dah et al. (2010) demonstrated both numerically and experimentally that, for small SPs of less than 1 m², heat extraction efficiency could also be considerably improved although this would be at the expense of reduced stability within the lower convecting zone.

Aramesh et al. (2017) constructed a transient modelling method to predict the behaviour of the SP during the heat extraction process from the LCZ and observed that it was in agreement with the experimental data. As the heat was supposed to be extracted from a tube in the middle of LCZ at different extraction rates and operation times, the authors found that the heat extraction rate was maximal up to 40% of the operational time, although afterwards it decreased drastically from 40% to 70% to become near to zero after 70%. In their subsequent studies, Aramesh et al. (2017) investigated and compared the influence of using water-based nanofluids at different concentrations to extract heat from the pond, determining that the best performance was achieved by a SWCNT nanofluid at its threshold concentration. Alcaraz et al. (2016) compared (in an experimental SP built in Spain with a surface area of 50 m²) the efficiency of heat extraction, from both the gradient and heat storage zones, of two heat exchangers, one covering the entire lateral wall area of the pond and the other positioned at the bottom of the pond. The heat exchangers were used independently and in combination, and the result was that the efficiency increases when the heat is taken from the latter heat exchanger alone. Tundee et al. (2010) introduced the use of heat pipes made of copper with a single evaporator and condensator to extract the heat from the LCZ of the experimental SP built in North-Eastern Thailand. Through their theoretical model, and subsequently confirmed by experimental results, they investigated the performance of the heat exchanger by varying the velocity of inlet air used to extract heat from the condenser end of the heat pipe. Air velocity was found to have a significant impact, with an increase of 43% when air velocity was reduced from 5 m/s to 1 m/s. Following on from this

previous work, Ziapour et al. (2016; 2017) simulated an advanced design for a large-scale SGSP power plant, using two-phase closed thermosiphons as compared to an oversized size heat exchanger. The two-phase mode thermosiphon demonstrated not only technical advantages due to its passive mode of operation, but also a comparatively high heat transfer capacity, proving to be a more economic solution.

All the studies and experimental work on heat extraction to date have been based primarily on achieving the best extraction efficiency for a SP. A few others investigated the real effects of heat extraction on the stability of the SP and of optimising the heat that can be seasonally extracted from the SP and according to operational requirements. In Oman, the SP was introduced to be coupled with agricultural production. The principal idea was to use direct heat extraction with an external heat exchanger to heat the groundwater and ambient air for the enhanced evaporation humidification-condensation process highlighted in Chapter 5. Unfortunately, SP construction represented a significant challenge. Due to the consequent maintenance problems, it was decided to abandon it and instead utilise conventional solar thermal technologies such as heat pipes and flat plate collectors.

4.3 Solar Pond Construction Challenges & Conclusions

4.3.1 Solar Pond installation

Installation of the SP in Oman presented a significant challenge for several reasons which are as yet not adequately described within the broadly available literature. The principal issues identified are summarised below:

- Unstable sandy ground to fix the lower and sideliners
- High daily diurnal temperature range
- Difficulties in fixing the cover
- Sandstorms and winds cause cover transparency to deteriorate and create turbidity in the water
- Gradient layer mixing

The excavation works for preparation of the ground were performed using a crawler excavator. Sand dunes of approximately 50 cm in height above the soil were created around the excavation perimeter to protect the pond from the dust and sand carried from the surrounding ground by the wind. The laying of the liner on the bottom and at the sides of the pond was effected with extreme difficulties due to a bottom surface that was not completely flat. Further, the high diurnal temperature range made

it impossible to lay the liner. It was necessary to postpone all installations to night time to enable positioning and placement of the liner (Figure 04.10). Weather conditions were very challenging due to extremely high temperatures and solar irradiation during the daytime, making it nearly impossible to work or touch any items exposed to the sun.



Figure 04.10 - SP installation over-night to avoid heat and hot surfaces.

The upper layer (cover) was fixed to the sides of the pond before filling the pond with water (Figure 04.11).



Figure 04.11- Fixing of the upper layer.

The cover filling and discharging tubes were arranged so as to allow the injection of the glycerine mix. During the erection of the cover, part of the surrounding sand started to fall into the pond making it nearly impossible for it to be removed. Some of the hinges became loose and the fixing material

became very weak and fragile because of exposure to high temperatures. Connecting parts and rods started to break down and needed to be fixed or replaced with new ones (Figure 04.12).



Figure 04.12 - Broken fixing parts during installation process.

After the cover was in the correct position, the pond filling operations started according to the procedure described in section 4.2.1.6. Once the pond was filled up to the predicted level, the cover partitions started to be refilled with glycerine solution but due to the deformations caused again by high temperature, the cover deformations didn't allow the complete shading of the top of the pond (Figure 04.13).



Figure 04.13 - Installation of the upper cover.

The cover started floating although some of the water remained above the cover. Once again, it was shown that the idea put forward in the literature for a cover containing liquid is best although practical problems are encountered when implemented on a pond even on this limited scale.

Thus, SP installation at scale is very problematic. The final structure was completely different to that which was planned. The SP was not properly covered, meaning that any considerations for improving its efficiencies were in vain and rendering its management and maintenance nearly impossible. It was shown that the SP cover needed a better design, one that considers the need for easy onsite installation. However, such considerations are seldom, if ever, discussed in the literature.

Solar pond deterioration began during the installation phase, with most of the sand trapped between the cover modules and the pond floor. The planned approach to remove the sand from the connection point of the different cover modules with a suction pump did not work. The cover quickly became entirely covered by sand and weakened by the intense solar radiation. Therefore, there was an increase in the pond temperature during the first few days after installation, although most of this acquired heat was lost overnight due to the low level of insulation. After running the solar pond for one month, it became apparent that the use of the pond had failed and an alternative and more reliable solution was needed. Clearly, whilst this region is attractive for solar pond construction, at least in theory, practical limitations and difficulties preclude its use without significant expense. Whilst this represents a failure, we consider that the identification and reporting of these significant practical difficulties substantially contributes to the wider knowledge base of Solar Ponds under the Gulf conditions. Most studies are theoretical and therefore completely ignore the practical engineering aspects.



Figure 04.14 - Deterioration of the solar pond cover after a few weeks.

4.3.2 Conclusions

The use of this solar pond as a heat storage medium combined with irrigation was demonstrated to be both unsuccessful and unsatisfactory. It proved impossible to measure the pond data or develop procedures on how to run it efficiently as the experimental solar pond never reached thermal capacity. Most of the difficulties encountered arose during construction and installation. These were due to a lack of experience and information on construction, a challenging local environment due to very high ambient temperature, solar radiation, and the abundance of sand. As alluded to above, the design of the complete system works well on paper although, when confronted with real installation issues, reveals many unforeseen problems. It would be difficult to overcome these problems through a simple redesign unless the cost of materials and construction are drastically increased, making its use both unsuitable for the required application and prohibitively expensive.

The operation of the pond in this project proved to be troublesome. Dust collection on the top of the cover was a problem. Even though a dust removal technique was implemented it was not effective. Additionally, the dust rapidly reduced solar absorption, causing the cover to sink. Further, there was a stench caused by algal growth which required additional chemical additives to control.

It was concluded that solar pond construction in Oman is operationally limited by dust, a common problem not only in Oman but also in most Gulf countries. This problem severely limits the potential to deploy such ponds in regions where they are needed most. Addressing all these problems properly will make the SGSP a less economically viable option. Given that other solar thermal techniques are now available at a reasonable cost, including heat pipes (HPs) and Flat Solar Panels (FPCs), these alternative techniques were implemented in subsequent trials.

5. Experimental Design and Results from Seawater Irrigation and Seawater Distillation techniques

5.1 Introduction

One of the most important concerns today, especially for arid regions and remote areas, is the shortage of fresh-water either for drinking or agriculture use. Traditional desalination processes such as MSF, MED, VC and RO are suitable for large and medium capacity fresh-water production but require high levels of investment to build which most of regions cannot afford as their need is for decentralised, low-capacity, low-cost desalination solutions. To address these problems, over the past few decades cheaper solar-powered desalination systems for fresh-water production have been developed based on humidification and dehumidification processes. These have become more popular throughout the world and have been presented and modelled in many studies although only a few similar systems have actually been produced and tested. These small-scale standalone desalination systems, having lower production costs, are more environmentally friendly and versatile, yet can be used in various environments, are relatively simple to design, and require less space and time to implement. These systems would provide small, remote communities in arid regions with the necessary fresh-water to drink and irrigate small areas of land, enabling a range of crops to be farmed. This, in turn, could benefit the sustainability of these communities and support their local economies.

This chapter outlines a novel arrangement of an integrated system for solar desalination and irrigation/drinking water production, in which the ground serves as a condenser for humid air flowing through a system of buried pipes under the soil and the condensed fresh-water is supplied directly to the root zone. This system is not entirely new, as it was initially studied by Gustafsson and Lindblom (2001), although there have been some improvements to the system that were not outlined in previous studies. This study aims to prove in the field, theoretically model and take near-market production, innovative condensation irrigation techniques like Seawater Irrigation (SWI) and Seawater Distillation (SWD). These are used for growing high-value crops, wheat and trees in remote arid regions and developing countries that would otherwise typically lack options for irrigation. Most of these regions do not have sufficient electrical power to produce distilled water via conventional water desalination processes. The high capital cost of the techniques mentioned above is far beyond the economic means of most people living in these regions, especially those who base their livelihoods on agricultural products. Given such a problematic socio-economic situation, the present work aims to design new technologies which are able to produce distilled water for drinking purposes via SWD or directly link production to agriculture through SWI. These technologies should be comprised of cheap, durable and locally available materials to reduce the initial costs and be viable for an extended period with minimum maintenance and ready local availability of spare parts for repairs.

These technologies enable the cultivation of crops in hot and arid regions, where fresh-water is not otherwise available. By simply heating the salty/brackish water and air with solar energy, enhancing water evaporation by underwater air injection and then cooling the resulting saturated gas mixture until the water condenses directly in the soil at the roots of the plants (SWI) irrigation becomes possible. Alternatively, by collecting the condensate on the inside of shaded tents both irrigation and potable water become possible via SWD. The use of the subsurface irrigation system also presents further advantages, including reducing water losses through surface evaporation and deep percolation (Camp 1998). These are problems for conventional irrigation, increasing soil aeration, making harvesting easier and preventing surface crusts (Lindblom 2006).

These systems are based on the difference in the water vapour carrying capacity of air at different temperatures (Figure 05.01). For example, if air is heated to 40°C and becomes saturated, its vapour carrying capacity is 50 g/kg of dry air. When the same air is cooled under the soil and reaches a temperature of 20°C the air vapour holding capacity is reduced to 15 g/kg. Thus 35 g of water are released to the soil by condensation for every kg of air and this can be absorbed by the roots of the crops.

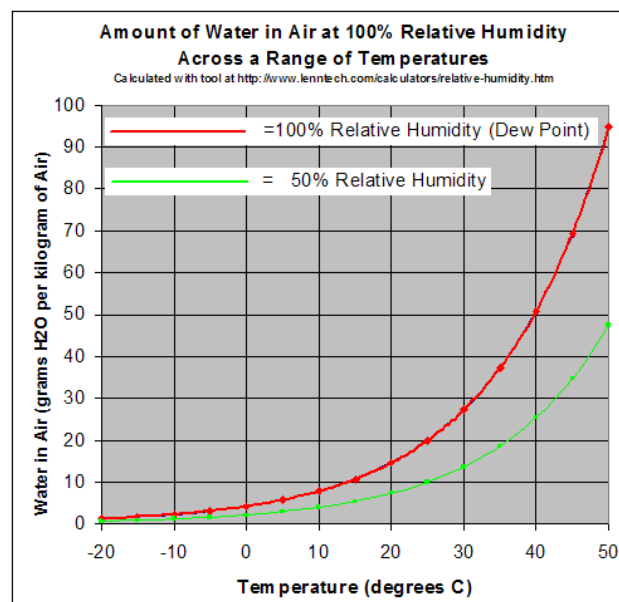


Figure 05.01 –Water vapour carrying capacity of air at different temperatures.

The manner and amount of irrigation water produced and transferred to the soil is the main focus of this chapter, including economic investigations and a discussion of future developments. To demonstrate the potential of such technologies, it is important to understand the processes governing water production and irrigation efficiency. In fact, despite the fact that the principles behind the humidification-condensation process are very simple, the theory and parameters involved are

complex, so the study requires an important experimental component. Chapter 5, after considering prior works, starts describing the experimental part of the process, consisting of the design of the experiment, a description of the experiments and their results, and, in Chapter 6, the experiment is modelled and a comparison with prior works and experimental results made.

Numerical and thermodynamic analysis of SWD and SWI techniques to determine the mass and heat transfer (with elements of conduction, convection, radiation and evaporation) of water, air, and soil across the different parts of the system (air and water heating, humidification and condensation) have been studied and models for simulating the experimented systems produced to determine irrigation potential and analyse specific parameters influencing the production yields. The results of the resultant models have then been compared with the experimental data recorded from real field applications in Oman as well as prior studies, thereby demonstrating that the results obtained from the theoretical models are in excellent agreement with those obtained experimentally.

5.2 Previous Works

The idea of heating and moistening air and seawater with solar energy and condensing water vapour directly by the roots of plants in underground horizontally buried drainage pipes is not entirely new in literature, initial studies on the subject were carried out in the mid-1980s at Luleå University of Technology (LTU) by Widegren (1986), Nordell (1987), Göhlman (1987) and were further investigated by Gustafsson and Lindblom (2001) and by Lindblom and Nordell (2003, 2006, 2007, 2011, 2012).

Widegren (1986) performed an initial design study for a condensation irrigation system to irrigate 1 ha of land. In his design, the humid airflow was driven by an electric fan that would consume power in the range of 3-10 kW, and condensation was envisaged to occur underground in a system composed of 200 pipes 50 m in length and 0.1 m in diameter. An experimental small-scale irrigation system based on Widegren's findings was then constructed by Nordell (1987) for a greenhouse in Övertorneå at the Hietala Market gardens, Sweden. In this experiment, warm, humidified air was sent to condense in underground perforated pipes during the day to water cucumber plants and aerate the soil. At night the greenhouse was heated by recirculating the residual heat within the lines, thereby extending the growing season.

Independently of these studies based in Sweden, Hausherr and Ruess (1993) built a condensation irrigation system in Margrethen, Switzerland, in which seawater and air passing through sun-exposed tubes increased their temperature and water evaporated and was subsequently condensed in underground drainage perforated pipes to water tomatoes and lettuce. A photovoltaic system was used to provide electric power to drive the air fans and the seawater pump, with a primary energy need of 14 kWh/m³ of condensed water. The quantity of conventional fresh-water needed to irrigate the tomatoes was drastically reduced to 50% of that previously used and the quality of the condensate was high, with few or no salt ions, as confirmed by the growth of thale cress (*Arabidopsis thaliana*) which is a very salt sensitive plant and therefore represents a good water quality indicator. (Ghars et al. 2008).

The next development of the technology was back in Sweden where Gustafsson and Lindblom (2001) in their master's thesis further investigated the feasibility of underground condensation of water from humid air for subsurface irrigation and drinking water production. In their work they improved the governing equations of the system, including the cooling process in the pipes, adding the calculation model of the heat transfer distribution through the soil, giving indication of water production and economic estimation of the cost of the system. In their model incoming air sweeps over the water surface of a solar still becoming saturated due to convection mass transfer and exits the system at the opposite side before being sent for condensation in underground perforated pipes. They found that the modelled irrigation system, when air is cooled from 70°C to 40°C is more water-efficient than the previous model. This had the possibility of being commercially competitive, especially in arid lands, in growing a range of crops, offering a potential irrigation productivity of 4.6 mm/m²/day with an energy consumption of 1.6 kWh/m³. The diameter and length of the experimental pipes considered were 100 mm and 8 m, respectively, while the pipes were buried at a depth of 0.40 m.

They also conducted a small-scale field experiment at Çukurova University in Adana, Turkey to understand the cooling process of humid air in an ordinary PVC pipe and compared it to a drainage pipe made of PVC but with slits for water penetration. The temperature distribution in the soil and pain in experience for planning and setting up a future real field large-scale experiment were evaluated. The air flow was generated using a simple computer fan and water was heated with four electrical resistances. To reduce the need for energy for the drinking system, they also investigated the possibility of creating a self-induced flow through the pipes by means of a solar chimney. Due to

the low accuracy of the instrumentation used, the results were merely indicative of the process potential that required accurate experimental data.

In several studies and experimental investigations, Lindblom and Nordell (2003, 2006a) contributed to our understanding of the CI and its governing parameters. They further studied and investigated underground and overhead irrigation (dew irrigation) as driven by a humidification-dehumidification. In their system, a traditional solar still was used to humidify ambient air flowing over the saline or an unpotable water surface of the still and increase its evaporation rate. The warm and humid air was then conveyed from the still through an underground pipe system where it was cooled by the colder soil and the vapour precipitated as fresh-water inside the pipes (Figure 05.02). The fresh-water produced could be harvested for drinking purposes or else released directly to the soil directly through underground perforated pipes for irrigation. The perforations in the pipes enabled the fresh-water produced to percolate into the soil, while part of the humid air could flow through the soil, condensing in the cooler ground and supplying soil aeration that helped crops to grow. The results of their new simulations improved upon the previous models available, confirming once again the advantages of the proposed system as compared with other traditional irrigation methods. These advantages included a higher irrigation rate, arising partially due to reduced water losses through surface evaporation and deep percolation, and increased soil aeration, while providing a low-tech/low-cost design.

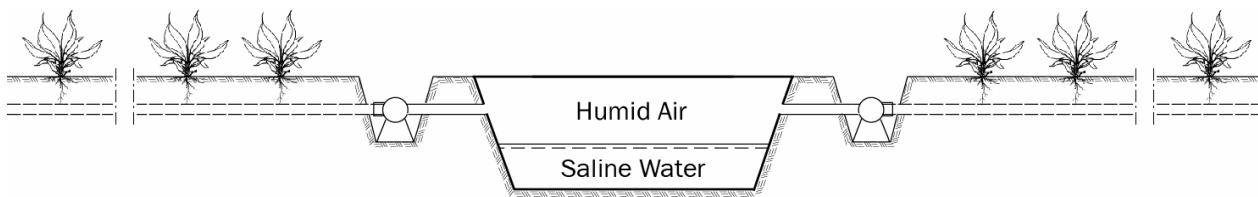


Figure 05.02 - Outline of the CI system. Ambient air is warmed and humidified by solar thermal energy and led into buried pipes, where it is cooled and dehumidified (Lindblom and Nordell 2006). Reproduced with permission of the rights holder Elsevier B.V.

In their following studies they also investigated the use of dew irrigation, wherein vertical standpipes were connected to the horizontal subterranean pipes so that, when the warm humid air stored in the underground pipes followed the vertical vent pipes to reach the colder atmospheric air, especially at night, the water condensed and created an artificial form of drizzle or small water droplets that precipitated and thus irrigated the soil (Figure 05.03).

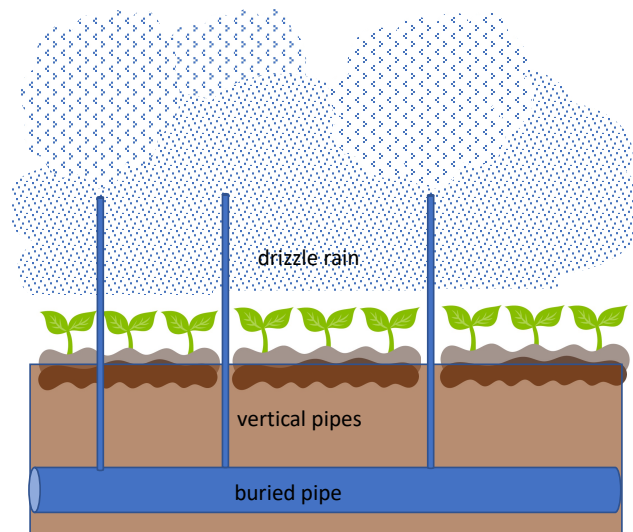


Figure 05.03 - Vertical pipes conduct warm, humid air to the colder ambient outside air at night. As the air from the pipes meets the colder air outside, water condenses and creates an artificial drizzle rain.

Comparing the results obtained they affirmed that subsurface irrigation, especially in arid regions, should be preferred to overland irrigation as it eliminates water losses through surface run-off and so water production is more effective during warmer sunny days when irrigation is mostly needed. The soil temperature during daylight, at certain depths, is normally lower than the ambient air temperature, and fresh-water can then be produced throughout the day, while overhead irrigation produces its best results when air is stored during the day and released at night.

They also discovered with their models that, for subsurface irrigation, the heat transported by the hot humid air while flowing along the underground pipes will warm the soil around the pipes, thereby reducing the water production efficiency of the system. The design of the system should be constructed to have, at the end of the daily operation, a maximum pipe temperature of 40° to 45°C. In fact, a soil temperature lower than 40°C is favourable for crop sowing and growing, while a greater temperature may limit plant shelf-life. On the other hand, a pipe temperature above 45°C will have a favourable impact, limiting the growth of crop roots into the pipes and protecting them from blocking airflow (Hatfield et al. 2015). Root distance from the pipes will not limit their capability to absorb water owing to capillary forces, diffusion, and root suction.

To reduce soil temperature, according to Lindblom and Nordell's findings and calculations, it is very important to choose the correct pipe diameter, soil depth and spacing (Figure 05.04) and to use the possibility of injecting cold air through the piping system during the hottest part of the day or at night.

They indicated how the heat is distributed and transported in the soil around the condensation, as influenced by soil permeability, moisture, solar radiation and crop type.

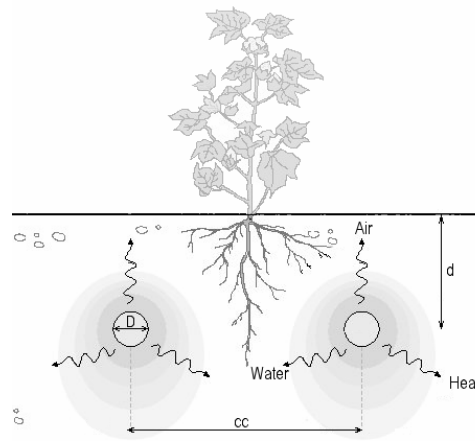


Figure 05.04 – Section of buried drainage pipes. The pipe diameter D , depth d and spacing cc are indicated (Lindblom and Nordell 2007). Reproduced with permission of the rights holder Elsevier B.V.

Their numerical modelling determined that the main parameters affecting the water production efficiency were inlet air temperature and relative humidity.

The modelling suggests that the condensation rate of the system, at steady external conditions and without considering seasonal variations in metrological conditions, especially rain and wind are not included, decreases rapidly during the first 15 days of operation, due to the increased ground temperature around the pipe and afterwards it approaches an asymptote (Figure 05.05).

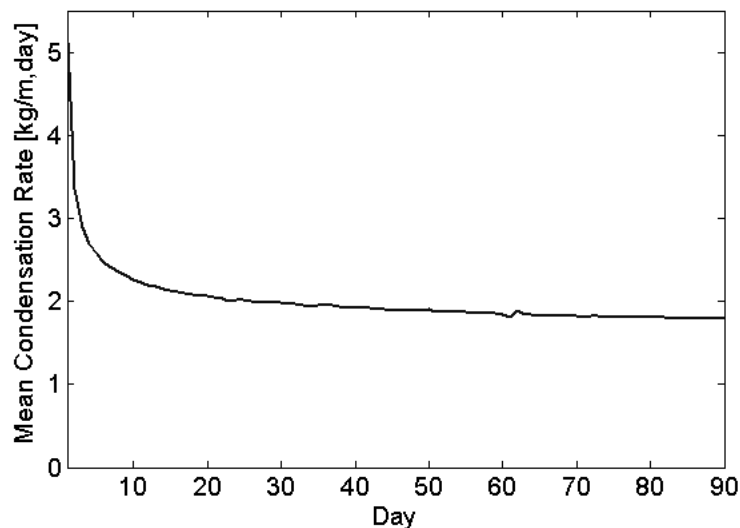


Figure 05.05 – Condensation rate for the system per pipe and unit length during the first 90 days (Lindblom and Nordell 2006). Reproduced with permission of the rights holder Elsevier B.V.

The condensation rate also decreases along the pipe (Figure 05.06) because the air cools down while flowing through the pipe, exchanging heat with the ground as the relative humidity decreases, so that short pipes have a relatively higher water production rate.

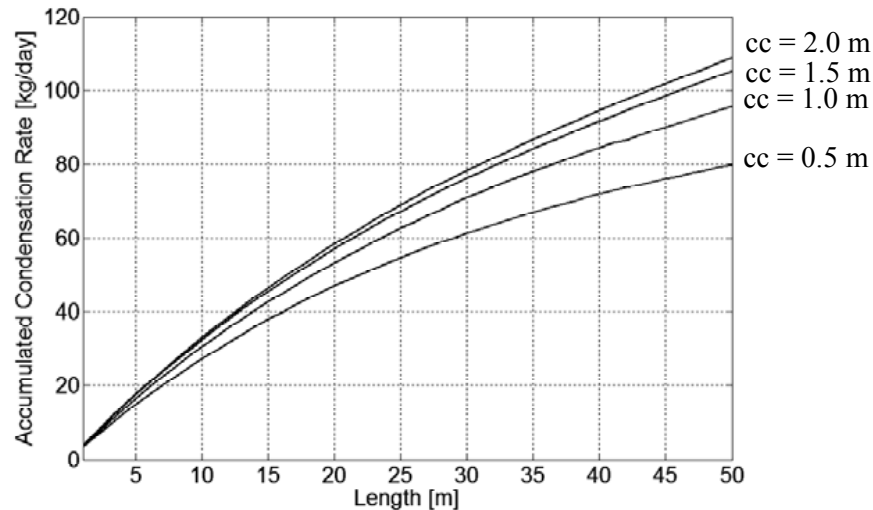


Figure 05.06 – Accumulated water production along the first 50 m of a drainage pipe in a system with different spacing (Lindblom and Nordell (2006)). Reproduced with permission of the rights holder Elsevier B.V.

According

to their modelling, daily fresh-water production for the drinking system was determined to be 1.8 kg/m of pipe per day with an energy consumption of 0.96 kWh/m³ of water produced, increasing to 3.1 kg/m/day for the subsurface irrigation system (irrigation yield of 2.3 mm/day) with an energy consumption of 0.4 kWh/m³ of condensed water. These results were achieved with the following air inlet from the solar still and design parameters (air velocity = 3.5 m/s; RH_{air} = 70%; T_{air} = 60° C, T_{soil} = 20°C pipe diameter = 0.2 m, pipe spacing= 1 m, pipe length = 50 m, pipe depth = 0.5 m, soil thermal conductivity= 2 W/m K), using the airflow at night to cool the soil and restore the starting values at the beginning of each day. The achieved productivity for the subsurface irrigation was shown to be consistent with their previous studies and sufficient for the growth requirements of crops. Further, the energy consumption per m³ was shown to be extremely promising for small-scale production, being better than large-scale MED or MSF plants with an energy consumption of 17.1 and 11.9 kWh/m³, respectively, while large-scale RO yielded consumption rates of 4.3 and 4.4 kWh/m³ (Antonyan, 2019).

Based on the modelling data, it can be noted that drinking water production has a lower efficiency than underground irrigation because the heat is transferred less efficiently to the soil, having a lower

thermal conductivity and negligible mass transport. The maximum soil temperature around the pipes is less critical in this system because no crops are considered and thus inlet air temperature can be significantly increased to obtain a higher level of water production.

Increasing the inlet air temperature from 60°C to 72°C (+20%) will improve drinking water production by more than 40% from 1.8 to 2.8 kg/m/day. There would be more than a 90% increase for subsurface irrigation, from 3.1 kg/m/day to 5.86 kg/m/day (irrigation yield of 4.1 mm/day), but in this second case the increased air temperature and, consequently soil temperature, may create impossible conditions for crop growth. Thus a 20% higher relative humidity instead will be preferred, increasing the soil condensation rate by 26% to 3.89 kg/m/day without harming the crops.

All these simulations have been made considering a constant air inlet temperature from the solar still of 60°C and a soil temperature at 20°C. However, in a warmer climate, the mean soil temperature will be much higher, therefore reducing initial water production by condensation although this will be partially compensated for by the higher inlet air temperature and moisture carrying capability.

In their subsequent mathematical model (2006b), Lindblom and Nordell studied the system's productivity in sandy soil, realising and affirming that many factors influence productivity. These are very difficult to consider in the modelling and should be investigated experimentally.

Even though their sandy soil model failed to consider the effect of solar radiation (negative impact of increasing soil temperature and reducing condensation during daylight), precipitation (positive effect with a cooling of the soil and an increase in condensation), and many other factors, they gave an acceptable prediction of the heat and mass transfer of water vapour in the soil and ground conductivity, determining the significant parameters and their effect on system productivity.

According to their models, low soil moisture and permeability decreased the initial condensation rate rapidly, since the heat dissipation in the soil near the pipe was reduced due to the less efficient transport of heat and mass. Thus the soil near the pipe was heated faster, while the soil permeability was also reduced as the ground became moist. Surface evaporation (the vapour flux is 10-fold higher than water transport into the soil) was higher during the day and dependent on soil temperature, ambient air temperature and humidity, reaching its peak at the end of the daily irrigation period when the soil temperature was at its highest.

These models also accounted for deep percolation to the groundwater table due to gravitational forces and this factor, when combined with surface evaporation, reduced the effective irrigation yield. The models did not consider the soil with any vegetation which would have helped to reduce soil temperature through root suction and enhance the water movement to the rooting zone. The reduction

in the depth of the piping system and increasing the spacing would also have increased the condensation rate with a concomitant reduction in the irrigation yield.

Based on Lindblom and Nordell's studies, a full-scale plant was built at the Center for Solar Energy Studies in Tripoli, Libya and other experiments were carried out by the National Research Institute for Agricultural Engineering in Tunisia but, unfortunately, there was no publication of the results of such experiments or any comparative analysis with the system's modelling.

The only minor down-scale laboratory experiment reported was performed by Lindblom and Nordell (2011) to assess the irrigation yield, water and heat transport of humidified air flowing through a single drainage pipe buried inside a thermally insulated sandbox. However, the experimental investigation was limited to a constant inlet airflow rate. Despite the limited testing, it was confirmed that the results were in line with Lindblom and Nordell's previous modelling and that the airflow temperature has the most significant impact upon the irrigation yield with an "exponential ratio with the vapour content carrying capability while incoming airflow velocity and humidity have a linear correlation".

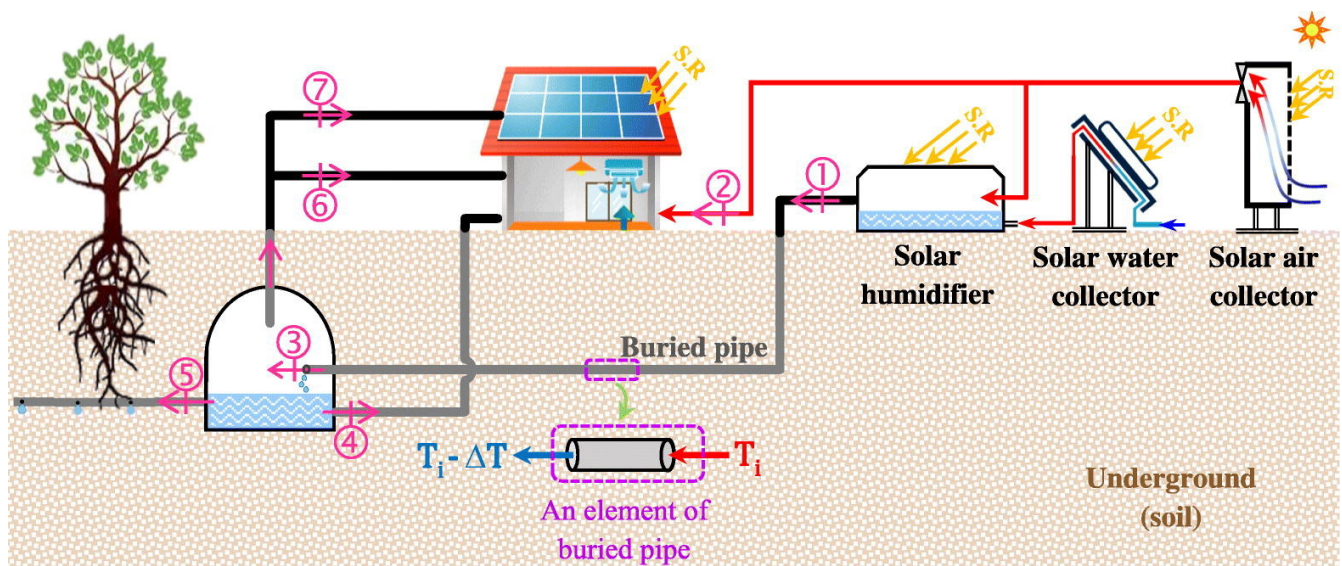
Another important outcome of the experiment was achieved by applying a plastic cover to the soil, thereby demonstrating that reducing gas transport through the soil significantly reduces mass and heat transfer and lowers the irrigation yield by around 53%. It is therefore essential to always guarantee gas transfer to the soil, although this mainly happens only from the upper part of the circumference of the drainage pipe as, without it, soil moisture will reduce further vapour condensation in the pipe.

Okati et al. (2016) further improved upon the previous studies and performed a sensitivity analysis on incoming system parameters within the humidification part of the unit, including inlet air velocity, air temperature and air humidity, demonstrating that water productivity matched previously modelled results and experiments. They concentrated their efforts specifically on the humidification part of the system rather than upon mass and heat transmission to the soil, knowing that how the air was heated and humidified before dehumidification in the subsurface irrigation pipes greatly affected the efficiency and economic feasibility of the system. They analysed the effect of humidifier length, the temperature of the saline in the still, and inlet air velocity, reporting that increasing inlet air temperature to the solar humidifier commensurately increased the productivity of the system exponentially while increasing the air velocity reduced it, as the air did not have sufficient time to absorb humidity while flowing over the warm salty water of the humidifier. Consequently, it entered

the dehumidification part with less water vapour. The temperature of the salty water in the solar humidifier also played an important role in being able to increase the inlet air temperature before flowing out of the solar humidifier to the dehumidification section.

In their following publication, Okati et al. (2018) introduced a further improvement to the modelling of the air humidification system by integrating a low-cost solar water collector to increase the salty water temperature before entry into the solar still, thereby improving the heat available for transfer to the air flowing over the still. They also determined that increasing air velocity entering the solar humidifier may have a positive effect if combined with an increase in the length of the humidifier and longer tubes in the condenser, even though it would lead to a larger system footprint and higher capital investment.

Okati et al. (2019) further improved upon the previous modelling by introducing a flat plate solar air collector to warm the inlet air before entry into the solar humidifier (Figure 05.07).



- | | |
|---|---|
| ① Saturated air from solar humidifier | ② Heated air (for ventilation in cold season) |
| ③ Dehumidified air | ④ Distilled water (for domestic uses) |
| ⑤ Distilled water (for agricultural uses) | ⑥ Dehumidified air (for heating or cooling-HVAC system) |
| ⑦ Dehumidified air (for PV/T cooling) | |

Figure 05.07 – Humidification-dehumidification system (Okati et al. 2019). Reproduced with permission of the rights holder Elsevier B.V.

They also estimated that the humidification chamber length required for the air flowing over the surface to reach the same temperature as the water present in the still is between 10 and 15 metres, and that the maximum length needed to reach saturation is 20 metres. Investigating the effect of the

air and water collector on fresh-water production, they found that when the inlet air temperature at the solar humidifier increases from 15°C to 40°C (Figure 05.08), the amount of water produced increased by 4.45%, and when the water temperature in the solar humidifier was increased from 20 to 40°C, fresh-water production increased by 74.46%. A further increase in water temperature from 40° to 50°C increased the yield by another 30.35% (Figure 05.09).

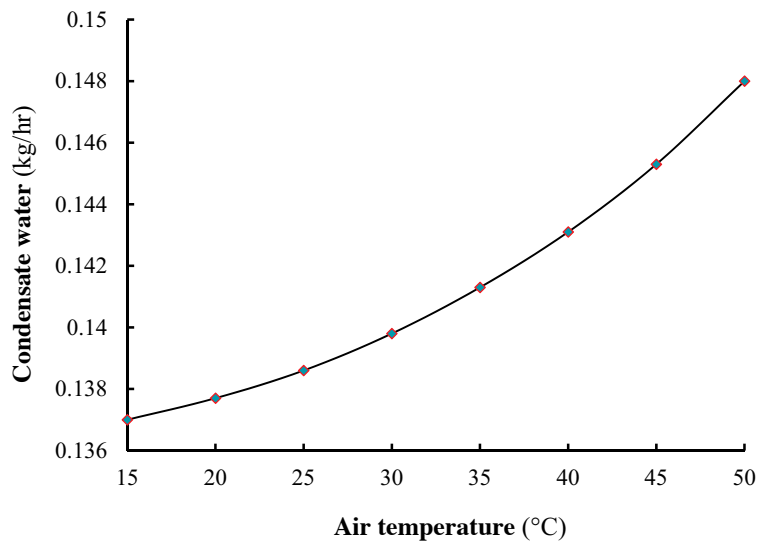


Figure 05.08– Effect of solar collector's outlet air temperature on the mass flow rate of the fresh-water produced (Okati et al. 2019). Reproduced with permission of the rights holder Elsevier B.V.

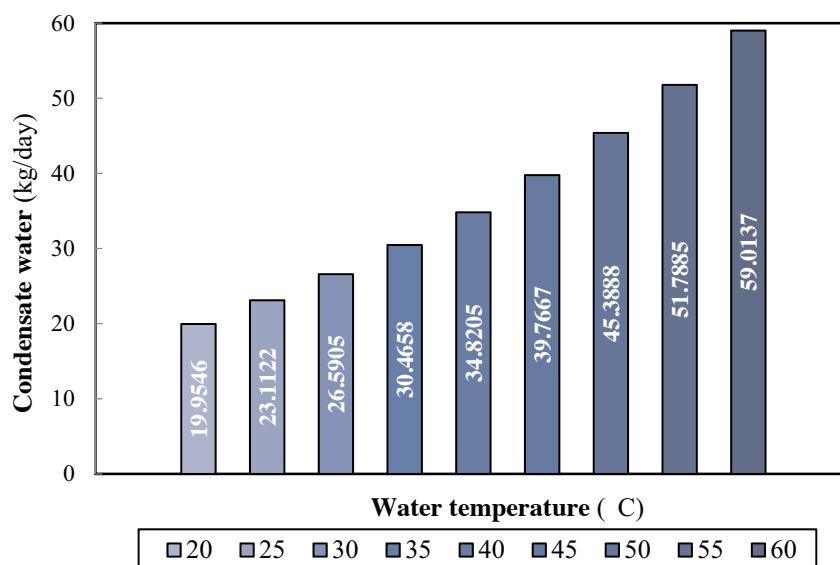


Figure 05.09 – Effect of solar collector's outlet water temperature on the mass flow rate of the fresh-water produced (Okati et al. 2019). Reproduced with permission of the rights holder Elsevier B.V.

All the aforementioned references modelled and calculated the increase in the water-carrying capacity in the humidifier for air flowing over the surface of salty or brackish water under saturated conditions. However, other ways in which hot air and water can be mixed have been proposed to increase the humidity of the air sent to the condenser, although these have yet to be combined with subsurface irrigation. While they may not improve the system's efficiency, they may contribute to reducing the cost of the water produced.

It is worth mentioning some of these approaches, as they have been partially integrated into the following design of the experiment. These may be summarised as follows. One important component of these studies focused on increasing the humidification performance firstly by spraying hot water into hot air (Farid and Al-Hajaj 1996; Al-Hallaj et al. 1998; Nafey et al. 2004; Ben Amara et al. 2004; Chafik 2002, 2003; Farid et al. 2002). These authors demonstrated that water production depends strongly on water temperature, airflow rate and the ratio between the flow of water and the flow of air (Seifert et al. 2013). Secondly, by using a packed column as a contact medium between the air and water as part of a counter-current flow system (Al-Enezi 2006; Ettouney 2005, 2006; Alnaimat et al. 2005; Dai and Zhang 2000), it was revealed that the production rate of the system is strongly affected by the water temperature and airflow rate, although only slightly affected by the submerged ratio of the packed column (Oueslati 2017). The efficiency of the spraying system was very limited in a single-stage system, while it was acceptable in a multi-stage system wherein the air goes through a series of air heating and air humidification processes. However, such an approach is more complex and costly. The packed column system, albeit more efficient, also requires some technical skills and appears challenging in terms of its implementation in remote arid regions where there is no access to technology or skilled staff.

In a third approach, other studies have focused on the performance of sparging hot air into hot water. The simplest way of mixing hot air and water is via a solar bubble column, a system in which hot air, pre-heated by solar energy, enters a humidifier driven by a blower or air compressor through a submerged nozzle. Here it is mixed with pre-heated water, humidified and sent to the condensation stage.

An experimental investigation into the effect of forcing air through hot water contained in a closed tank via a perforated end of an inlet tube was presented by Lashin et al. (1996), although any modelling or calculations were not mentioned. It was confirmed experimentally that, when airflow exiting submerged perforated tube passes through hot water, it increased its rate of vapourisation

although predicted correlations were not provided. Lashin et al.'s experimental trials have highlighted the importance of keeping the water level above that of the perforated tube to a maximum height of 18.6 cm to avoid any reduction in the evaporation rate due to an increase in the pressure head of the water which reduces the blower mass flow rate (the higher the water temperature, the higher the rate of evaporation).

Kabeel et al. (2014) performed further studies and experiments at the Faculty of Engineering of Kafrelsheikh University, Egypt, relating to the effect of submerged airflow patterns in a solar still on air humidification by analysing three types of forced air circulation systems, namely up, down and up and down natural air circulations. They reported that a forced down circulation gave a higher humidification performance.

El-Agouz et al. (2008) studied the performance of an electrically heated single-stage bubble column humidification-dehumidification desalination system, wherein both ambient and pre-heated air passing through seawater were analysed to determine the difference in humid air vapour content.

The results obtained with an evaporator of cross-sectional area 500 mm x 250 mm showed that the vapour content difference (Figure 05.10) and the humidification efficiency (Figure 05.11) of the system were strongly affected by saline temperature within the evaporator chamber. The headwater difference, air velocity and inlet air temperature to the evaporator chamber were found to have a negligible effect on the difference in vapour content.

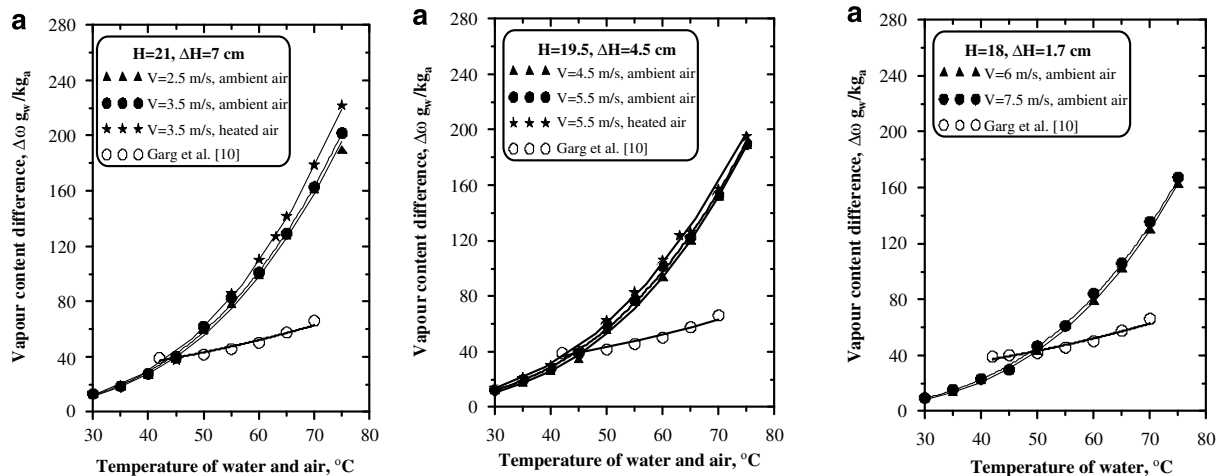


Figure 05.10 – The effect of the water and air temperatures on vapour content difference at different headwater ΔH and air velocities (El-Agouz et al. 2008). Reproduced with permission of the rights holder Elsevier Ltd.

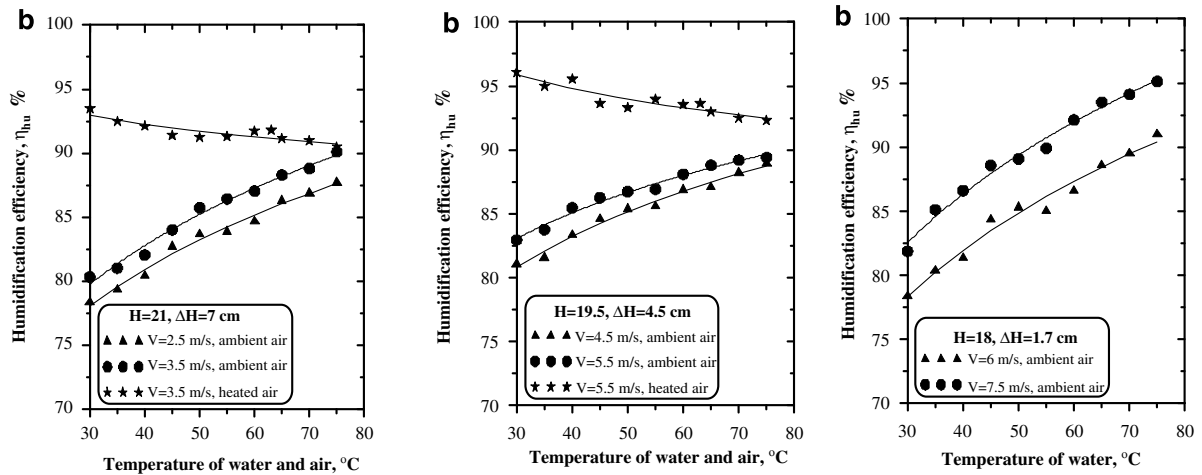


Figure 05.11 –The effect of the water and air temperatures on the humidification efficiency at different headwater ΔH and air velocities (El-Agouz et al. 2008). Reproduced with permission of the rights holder Elsevier Ltd.

Considering that, in the heated air experiment, the incoming air and water were heated to the same temperature (within the airflow range studied), the maximum vapour content difference of the air was approximately 85 g_w/kg_{air} at 55 °C; 110 g_w/kg_{air} at 60 °C; and 222 g_w/kg_{air} at 75°C. The vapour differences obtained were high as compared to the findings of Garg et al. (2003) for a single-stage system, although they were very similar for multi-stage systems used by Ben Amara et al. (2004) who, after the eight heating-humidifying stages obtained 110 g_w/kg_{air} at 60 °C. Chafik (2002, 2003), after the fifteenth heating-humidifying stage, obtained 75 g_w/kg_{air} at 55 °C and 138 g_w/kg_{air} at 60 °C. In his subsequent experiments, using an evaporator with a cross-sectional area of 400 mm × 300 mm, El-Agouz (2010) evaluated the influence of the temperature, saline level, and airflow rate on the desalination performance, finding a correlation between the aforementioned parameters and the system's global productivity. The effects of water temperature and airflow rate in the evaporator chamber on the productivity of the system are shown in Figure 05.12. It is clear from the figure that, as the water temperature increased, the average productivity was raised. On the other hand, the average productivity increased commensurate with the increase in airflow rate. When the temperature of the seawater in the evaporator chamber was 86°C the average productivity of the system was, respectively, 3.41 kg_w/h with 4.2 kg_{air}/h, 6.8 kg_w/h with 8.4 kg_{air}/h, and 7.45 kg_w/h with 8.22 kg_{air}/h.

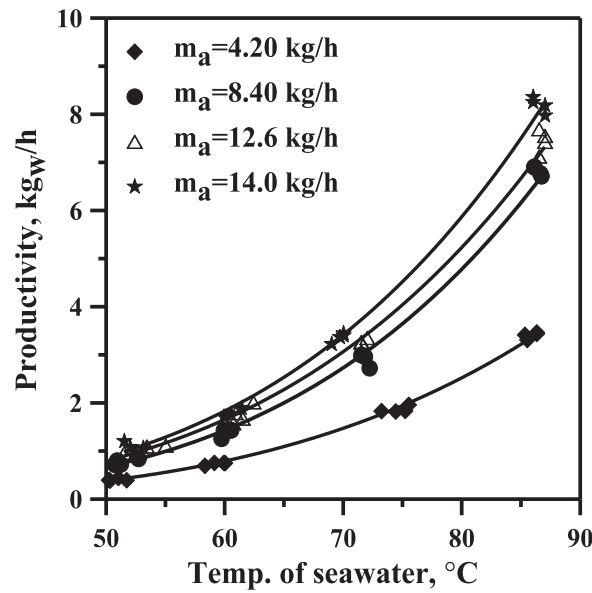


Figure 05.12 – The effect of the temperatures of seawater on productivity at different air flow rates (El-Agouz 2010). Reproduced with permission of the rights holder Elsevier Ltd.

El-Agouz (2010) also gave a cost estimation of the water produced with such a system, taking into consideration that all the required energy would have been provided from the local power grid without access to renewable sources either for power or for water heating. At a LCE (Levelised Cost of Energy) of 0.06 \$/ kWh, he determined the cost of water production as ranging from 0.080 to 0.095 \$/kg.

Srithar et al. (2017) experimented with a solar bubble column humidification-dehumidification desalination system fabricated in the manner of a conventional single-basin/single-slope solar still with a cross-sectional area of 500 x 500 mm and the inclusion of bubble pipe in the basin for air supply. The bubble column humidifier was tested with a direct ambient and pre-heated air supply (Figure 05.13-a) prior to entry into the humidifier. The system was equipped with an additional integrated solar air heater of dimensions 0.750 × 0.950 mm (Figure 05.013-b). Preliminary experiments were conducted to study firstly the efficiency of the solar bubble column humidifier and then the humidifier connected with a dehumidifier to analyse overall system performance. Analysing the effect of ambient and pre-heated air supply, both with and without turbulator, they found a considerable enhancement of the specific humidity of the outlet air (1.22-fold) when the pre-heated air supply was used as compared to systems with the ambient air supply at peak radiation hours.

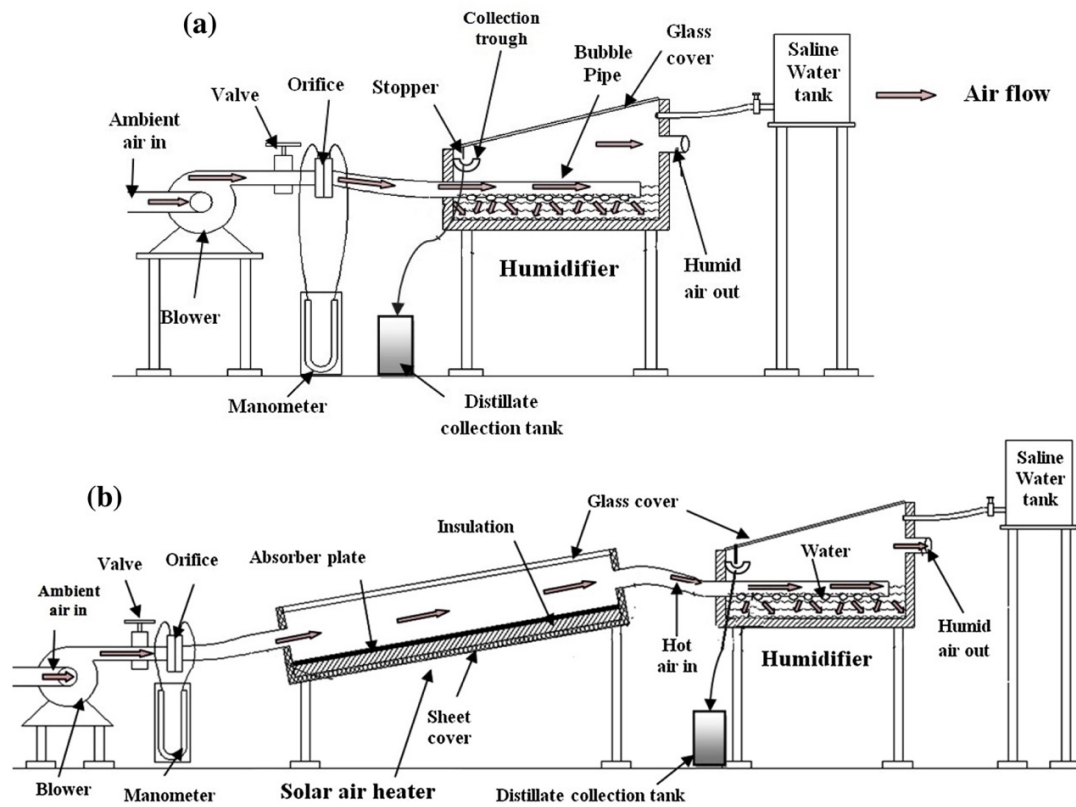


Figure 05.13 – Schematic view of bubble column humidifier with (a) direct air supply (b) pre-heated air supply. (Srithar et al. 2017). Reproduced with permission of the rights holder Elsevier Ltd.

Srithar et al. (2017) studied the effect of water height above the bubble pipe and air mass flow rate for the humidifier. The best performance was achieved with an 8 cm water column height. This increase in water column height reduced the water temperature which then required more time to be heated during the day, further reducing the column height from 12 to 8 cm, increasing both the water temperature and the specific air humidity by 21.17% at peak solar hours. They also found that increasing the air mass flow rate resulted in an augmented velocity at the nozzles and air-water mixing rate in the humidifier, leading to greater heat and mass transfer between the air and water in the humidifier, thus enhancing specific humidity. Maximum specific humidity gains were recorded for a solar air heater with turbulators, providing a maximum specific humidity gain of $187 \text{ g}_w/\text{kg}_{\text{air}}$, whereas the humidifier integrated with the solar air heater without turbulator had a maximum specific humidity gain of $11 \text{ g}_w/\text{kg}_{\text{air}}$. The authors reported a peak distillate output of $20.61 \text{ kg}/\text{m}^2/\text{day}$.

The extant literature has been analysed in detail to define the optimal design of the experiment, with the objective of increasing systemic humidification efficiency while guaranteeing the use of cheap and accessible technology and the need for only limited maintenance. The modelling and outcomes of the preceding publications have provided the groundwork for optimisation of the humidification-dehumidification process for subsurface irrigation. This formed the basis for the experiments

presented in this Chapter and for the modelling described in Chapter 6. Although based on the previous research there were some crucial novelties introduced to improve air saturation within the humidification chamber and reduce the system's footprint, construction costs and maintenance.

5.3 Design of the Experiment of SWI and SWD

The experiment aims to demonstrate that both SWI and SWD represent an efficient and reliable method suitable for deployment in remote arid regions to produce fresh-water for direct subsurface irrigation or drinking purposes, either alone or in combination with other irrigation techniques. Previous research and literature discovered and analysed the main parameters involved in the humidification-dehumidification process and tried to model the system and its governing equations in a complex way. The proposed system, with innovations tested in the field, was essential to better understand and demonstrate behaviour under real-world conditions. The encouraging results of these experiments in terms of water productivity and limited energy requirements confirmed the advantages that these technologies could offer in solving the problem of water scarcity in these regions.

SWI and SWD techniques are both based on a humidification-condensation process. The SWI system was developed using a soil matrix for condensation for direct subsurface irrigation while, in the SWD system, the soil matrix is removed and the soil channels covered with a plastic material to enhance condensation. For both cases, an FPC collector (air and water type) is used to increase the temperature of the incoming water and air to the system.

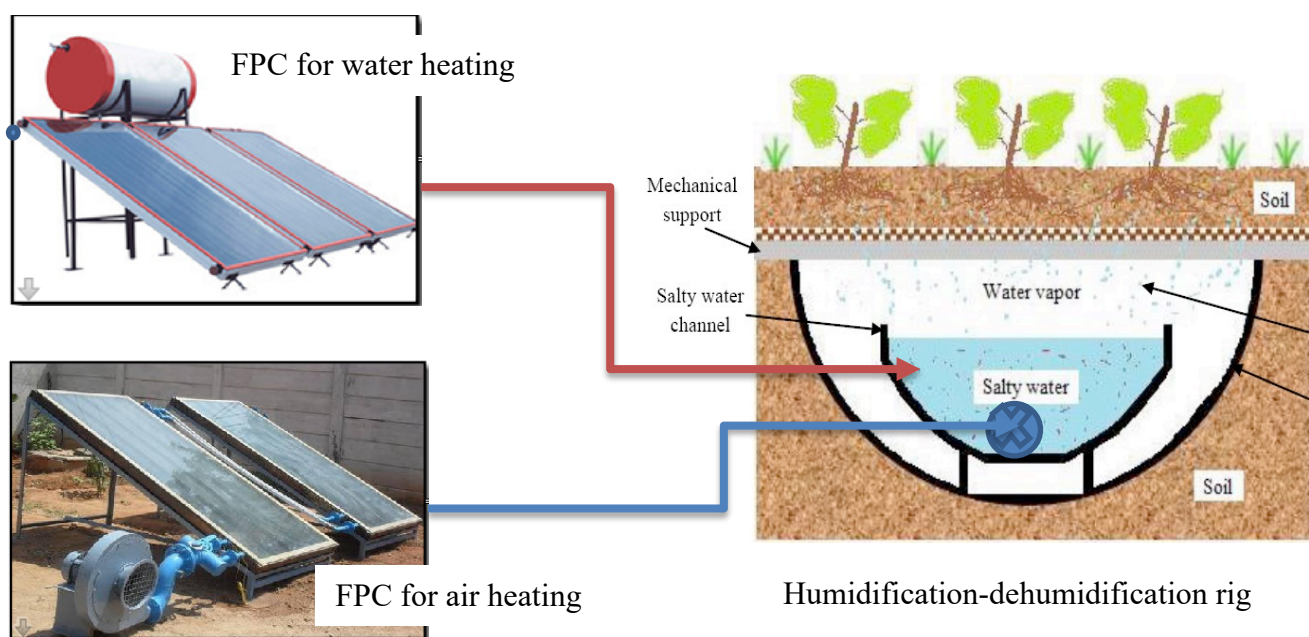


Figure 05.14 – SWI – Seawater irrigation system.

The SWI system is comprised of the following main parts (Figure 05.14):

- a) Flate Plate Collector for water heating
- b) Flate Plate Collector for air heating
- c) Humidification/dehumidification rig

The system process is as follows (SWI, Figure 05.15; Figure 05.16):

1. Salty water is stored in a sun-exposed tank positioned at a higher level than the rig (1). Its temperature is increased by the sun and through a heat exchanger (2) is connected to an FPC (3), driven by a closed-cycle water loop. The FPC collector can be replaced by a SP, heat pipe, SC, or electric resistance. A low-cost SC and FPC for water heating have been tested in these experiments.
2. When the salty feed water in the tank reaches the desired temperature, the cycle of operation begins and salty water is transferred via a primary pump (4) or simply by using a different water head between the starting tank and the lowest point at the end of the rig, to the humidification-dehumidification (5) part of the system, ultimately flowing through a subsurface semicircular open pipe built under the soil (sec. A-A, (6)). An external secondary pipe is also present to avoid soil contamination in case of salty water spillage from the main pipe (sec. A-A, (7)).
3. The salty feed water is controlled in both its temperature and flow rate and is continuously recirculated (8) between the semi-circular pipes and the water storage tank until the salt concentration becomes too high due to evaporation. It is then discharged (9) and replaced by a new batch of saline/brackish water, thereby starting a new cycle.
4. At the same time, ambient air is stored within a sun-exposed tank (10) heated through an FPC for air heating (11) before being compressed by the use of an air compressor or air fan (12) and sent into submerged perforated pipes (sec. A-A, (13)) lying beneath the salted water level of the semi-circular open pipes (sec. A-A, (6)) under the soil in which the hot salty water continuously flows.
5. The pressurised hot air passing through the salty hot water above creates air bubbles that cause turbulence and the appearance of small water droplets that enhance both water evaporation and air humidification to the point of saturation (sec. A-A, (14)).
6. When saturated water vapour (sec. A-A, (14)) reaches the soil above (which is initially at a lower temperature) it condenses on the lower soil subsurface (sec. A-A, (15)) and produces distilled water which is transferred to the soil and subsequently absorbed. Part of the saturated water vapour is also released into the air to avoid increasing the intra-rig pressure (9).

7. Soil is prevented from falling into the semi-circular open pipes by a structural mesh (sec. A-A, (16)) and a membrane layer that serves to absorb the condensed water and allow it to pass into the soil slowly via capillary action.

8. The soil is placed on top of the membrane layer and cultivation commences (sec. A-A (17)). The amount of fresh-water reaching the soil and passing through the soil to the crops is regulated by controlling both the water/air temperature and flow rate. A schematic view of the cross-section of the rig is illustrated in Figure 05.16.

The following experiment of SWD system (SWD, Figure 05.17, Figure 05.18) is obtained removing the soil mesh, the membrane and the soil above the semi-circular water pipe and covering the rig with a plastic tent (sec. B-B, (18)), in which saturated vapour can condensate and precipitate on the sides of the tent to be collected in its lower inner part (sec. B-B, (19)), as for a traditional solar still. An additional shader or wet pad is used to create a colder surface for condensation and can be added to the outer part of the covering tent (sec. B-B (20)).

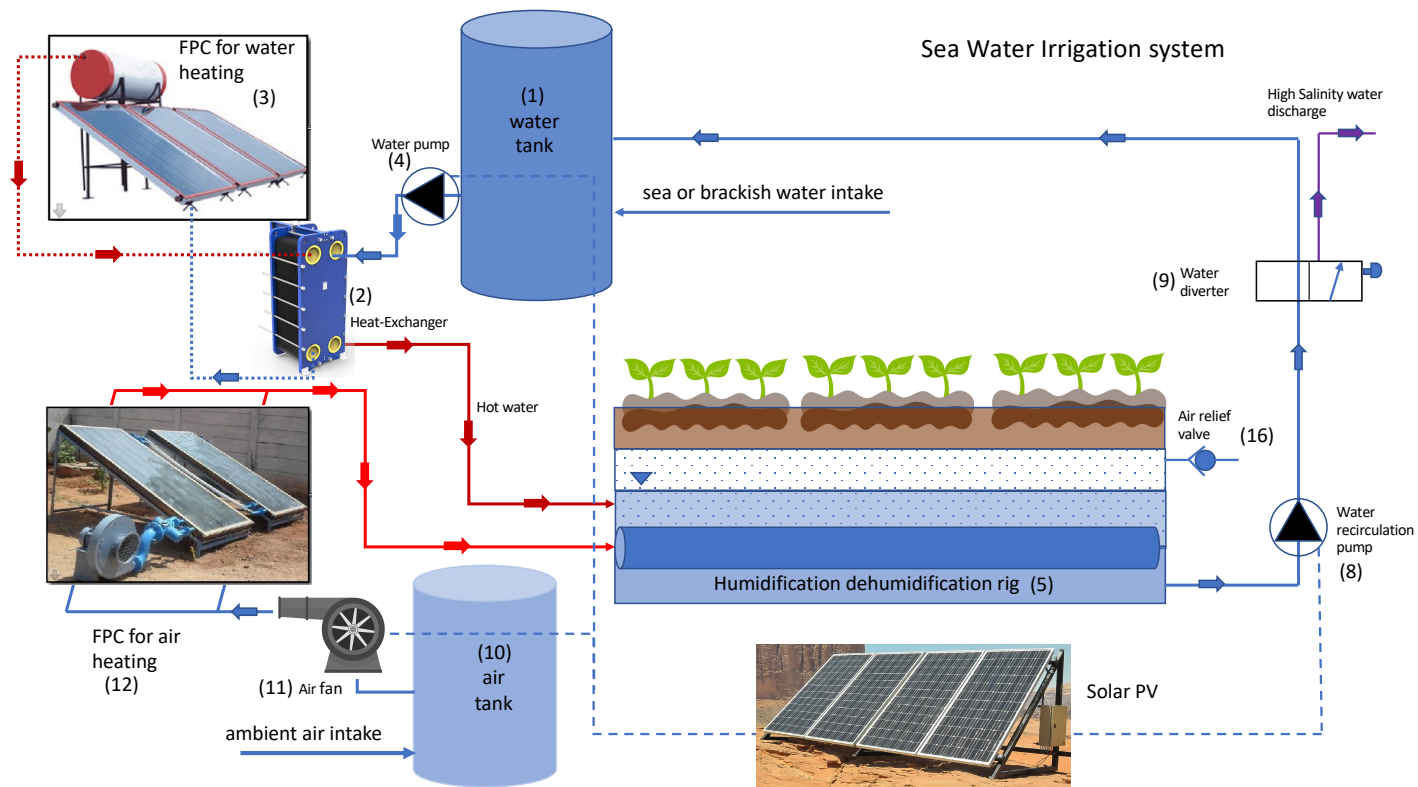


Figure 05.15 – SWI system.

SWI - Humidification Dehumidification rig section A-A

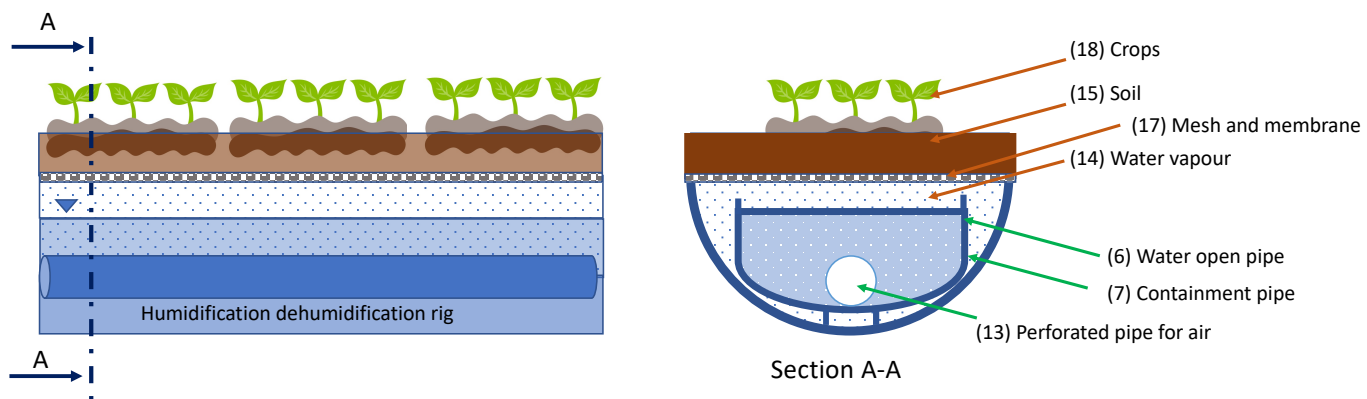


Figure 05.16 – SWI system rig section A-A.

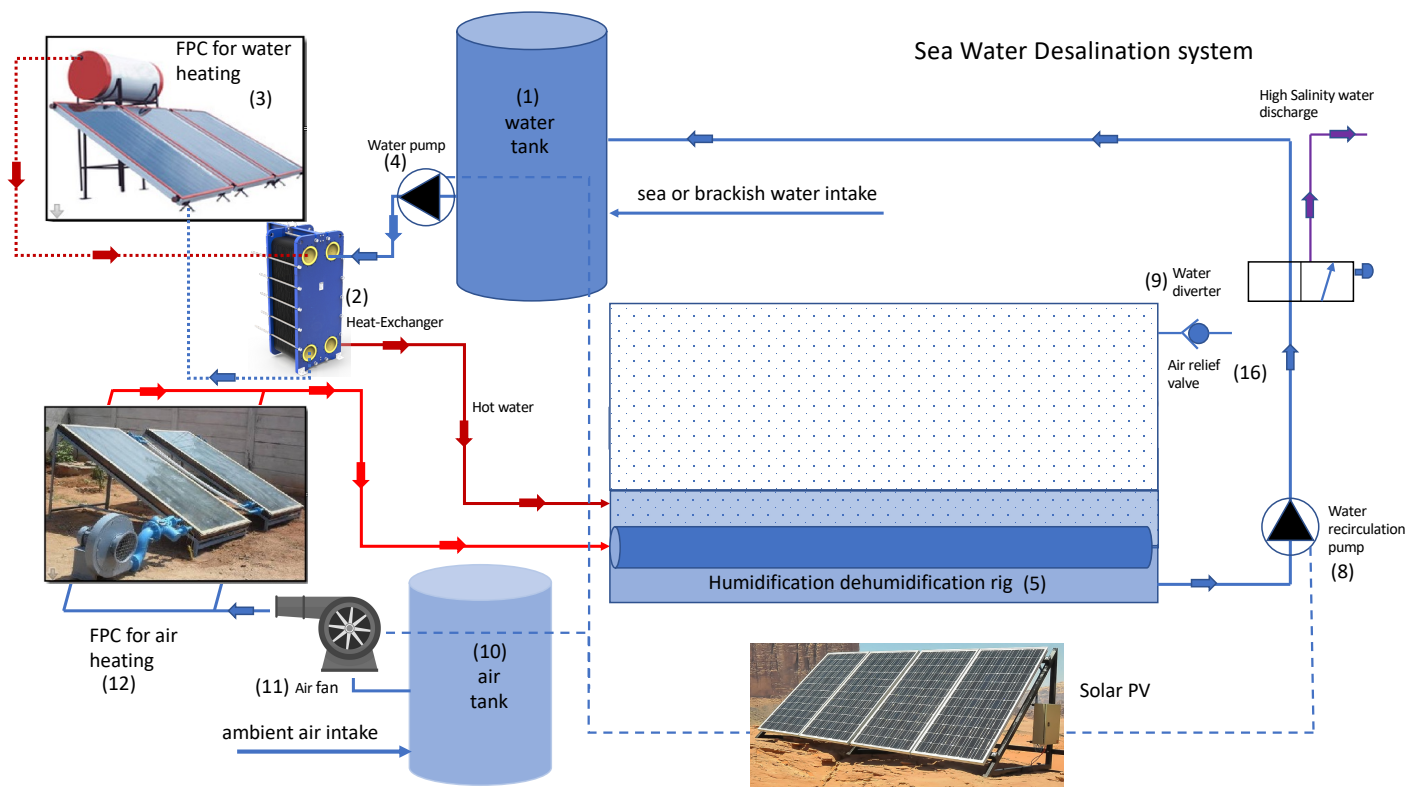


Figure 05.17 – SWD system.

SWD - Humidification Dehumidification rig section B-B

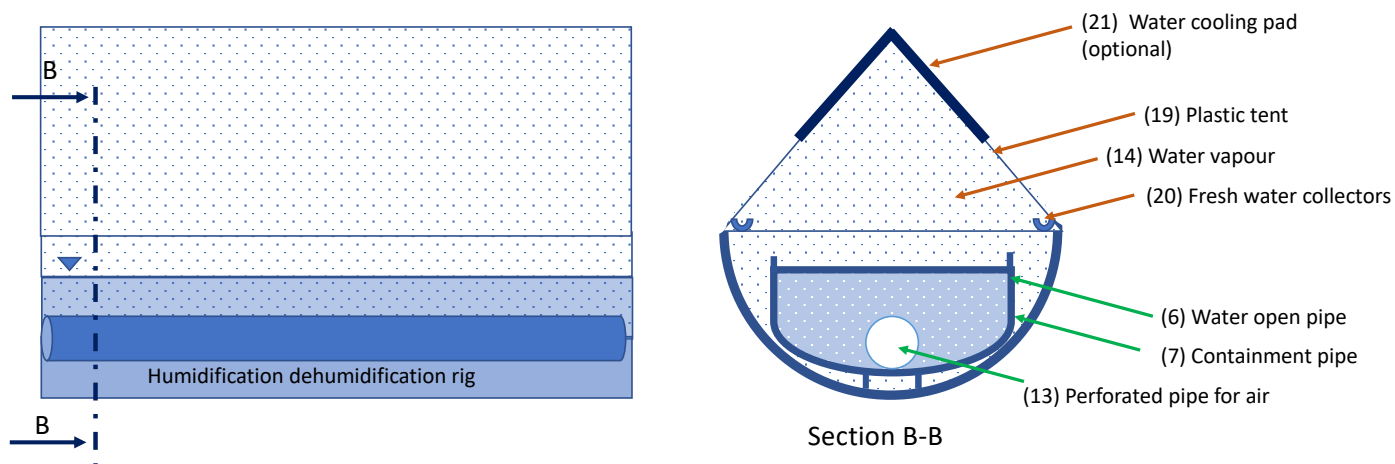


Figure 05.18 – SWD system rig section B-B.

5.4. Novelties of the Experiments

The experiments have been designed to test in field many systems novelties, not only from a technical aspect, but also in an attempt to understand the economics underlying the implemented solution, one which may guarantee favourable conditions for the deployment of the proposed systems for irrigation or fresh-water production in remote arid lands.

The humidification-dehumidification process works based on the difference in water vapour carrying capacity of air at different temperatures, such that the main parameters affecting its productivity are outlet air temperature, humidity at the humidifier, and the condensation temperature at the condenser. The way in which air is heated and humidified before being condensed greatly affects the efficiency of the system and, consequently, its economic feasibility. In the experimental field tests, the following novel adaptations were tested:

1. Flat solar panels that are independent in terms of air and water heating have been introduced to increase the inlet air and salty water temperatures. Most of the previous work used a less efficient solar still as a humidifier to improve the air humidity and temperature and the salty water temperature. The aforementioned solutions required wider, less efficient and more expensive solar stills to transfer sufficient heat and moisture to the air flowing over the still water surface.
2. Hot air is injected under the hot salty water flowing into the semicircular pipes of the rig through a bubbling system or solar bubble column to increase outlet air humidity. This enhances water evaporation and air humidification in the upper part of the rig. In the previous solution, the water temperature, air temperature and humidity were all increasing, facilitating airflow over the salty water surface of the solar still.
3. Evaporation, humidification, and condensation are concurrent and coincident in the upper part of the semicircular pipe, thereby reducing systemic heat loss, footprint and capital cost. In all previous documented simulations and modelling, humidification and dehumidification were spatially separated with substantive heat losses arising during humidified airflow along the condensation pipes.
4. Hot water flowing through the rig provides constant heat transfer to the incoming hot air from the FPC, guaranteeing a constant air temperature and humidity distribution along the pipe independent of its length. Salty water pre-heating by an FPC and heat exchanger also reduces the need for keeping a low water depth in the circulating pipe. In the previous experiment, humidity was reduced along the pipe during heat transfer to the soil as the hot air was flowing along the pipe.

For subsurface irrigation experiments, other important adaptations have been introduced:

5. Perforated underground pipes for air dehumidification have been replaced by direct soil condensation and the soil is placed directly above the semicircular pipe of the rig. The space between the salty water level and the lower soil subsurface offers widespread evaporation and a high condensation volume. Therefore there will be a homogeneous distribution of humidity throughout the soil. Temperature distribution to the soil will also be more uniform and not concentrated around the pipe, while the airflow and water flow regulation will be more manageable, enabling a better control of process parameters.
6. Soil texture in the experimental tests has been modified and optimised to increase water permeability and retention within the soil, thereby allowing a better heat transfer to the ambient soil and a reduction in soil temperature. In all previous studies, the behaviour of the soil has been investigated numerically although never through experiments.
7. During the experiments, different membrane layers have been proposed and tested under the soil to retain moisture and slowly release it back into the soil.

The results of the aforementioned developments have been investigated experimentally and the results collated for comparison with previous work. This data was then used to build models capable of predicting the behaviour of the system.

5.5 Experimental Design of SWI & SWD

The possibility of testing effective use of the SWI and SWD approaches was made feasible thanks to an opportunity offered by the Omani MoAF in cooperation with a private British company (Aquama Ltd.).

The location chosen for the experimental work in Oman was the area of the Omani Directorate General of Agricultural and Animal Research based in Al Rumays. There are, in fact, many government farms located in the southern reaches of the Batinah region, lying within 50-60 km of the capital Muscat. Due to their ideal location and optimal road connections to Muscat this enables them to supply the capital region with vegetables.

The soils of Rumays are considered very marginal, as they are shallow, highly calcareous, and poor in available nutrients. Water for irrigation is mainly taken from groundwater and it normally has medium to high salinity due to seawater intrusion. Thus it needs to be desalinated before being fed to the crops. Water availability in these areas is limited and thus should be managed carefully to avoid wastage. Normally sprinklers and drip irrigation methods are used in these farms. Irrigation frequency should be designed so as to provide the right level of soil moisture, soil temperature, water quality, water consumption and evapotranspiration. All of these parameters should be properly addressed, and evening and nocturnal irrigation should be preferred to reduce evaporation losses.

For all the above-mentioned limitations and restrictions, it is very important to experiment with new irrigation techniques which may be easily implemented in the area to be able to provide water and consequently ensure food security within the region.

SWI and SWD have been addressed systematically in terms of experimental trials and their drawbacks. The techniques were studied through a series of pilot experiments and final experiments were used to validate the process and determine the specific conditions that influence their overall efficiency and productivity.

Oman is a country facing serious problems associated with water resources as, each year, increased demands are being placed upon its scarce water resources. Agricultural, commercial, recreational, domestic, and growing industrial use are exacerbating problems of water quantity and quality. The

current project addresses this issue and was designed to focus on proving, in the field, novel SWI and SWD techniques, taking them from concept to near-market products, including their commercial exploitation in Oman.

5.5.1 Experimental Design of SWI

The project has involved the construction and installation as well as field trials of SWI techniques for growing crops and plants without any genetic modifications or changes to the plants' physiology. This has been addressed through several objectives and practical measures, including field trials of the SWI technique for growing high-value crops such as tomatoes and cucumbers. The project has also integrated the use of solar thermal technologies for heating feed air and water into the system, initially using the designed and constructed SP as presented in Chapter 4. Following the failure of the solar pond, the following objectives have been addressed in the experimental work of the SWI:

- a) Evaluate the feasibility of using the SWI technique for practical applications.
- b) Evaluate the SWI technique for soil moisture improvement and crop growth.
- c) Identify the parameters that influence SWI productivity.
- d) Investigate the type of crops that can be irrigated using this technique.
- e) Identify those areas which can be developed to improve the performance of SWI techniques.
- f) Determine the optimum conditions to accelerate soil wetting.

The timeline of the experiments and primary objective of the investigation is reported in following Tables 05.01 and Table 05.02, while methodology and results are indicated in the specific sections.

<u>Stage</u>	<u>Trial</u>	<u>Investigation</u>	<u>Timeline</u>
STAGE I Pilot experiments aimed at soil moisture improvements	Trial I	Investigate the effect of soil texture and composition on the development of moisture level.	Q2.2015
	Trial II	Investigate the influence of using silica gel in building up soil moisture.	Q3.2015
	Trial III	Investigate the influence of peat moss in retaining soil moisture (failed).	Q4.2015

Table 05.01 – SWI – Project timeline and partial objectives of Stage I.

<u>Stage</u>	<u>Trial</u>	<u>Investigation</u>	<u>Timeline</u>
STAGE II Main experiment	Trial I	Investigate the influence of using peat moss to retain soil moisture.	Q3.2016
	Trial II	Investigate the influence of acrylate in retaining soil moisture and in the use of solar thermal technologies.	Q4.2016/Q1.2017
	Trial III	Investigate increasing soil porosity and the use of ventilation pipes.	Q1.2017

Table 05.02 – SWI – Project timeline and partial objectives of Stage II.

5.5.1.1 Stage I – Pilot Experiments Aimed at Achieving Soil Moisture Improvements

This part of the project was devoted to investigating the main parameters influencing soil moisture improvements. Soil water content is, in fact, essential for crop germination and growth and, during long drought periods, the soil water storage decreases to values where water is no longer available to crops leading to severe drought stress and wilting. To control the available water content of soils, the water retention curve (WRC), which describes the capacity of soils to hold water at different water potentials, is measured. Soil biogeochemistry, and in particular soil organic matter content, influences the WRC of soils, with a positive correlation arising between soil organic matter content and its water holding capacity (Franzluebber 2002; Brady et al. 1999). However, other important biogeochemical processes affecting WRC have not yet been studied or are else not described within the available literature and so experimental work is needed to evaluate their influences. The use of different organic and inorganic substrates allows plants to optimise nutrient uptake to ensure sufficient growth and development to optimise water and oxygen retention. Different substrates could have direct and/or indirect effects on plant growth and development, providing nutrients for crop production but also affecting the physical, chemical, and biological functions of the soil itself. Soil conditioners, both natural and synthetic, contribute greatly to providing a reservoir of soil water to plants ‘on demand’ within the upper layers of the soil where the root systems normally develop. These organic materials do not only serve as buffers against temporary drought stress and reduce the risk of plant failure during establishment (De Boodt 1975; Johnson et al. 1990), but they also increase the soil’s physical properties. One of these substances is Coco Peat, a finely processed coconut husk produced from the inner fibres, pith and organic grits. This is readily available in Oman and can be directly incorporated into the soil to improve water retention and aeration and also to decrease the risk of soil fungus and root diseases (Managecraft 2001). Peat moss, a dark fibrous and compact material produced from

decomposed organic substances, improves water drainage in clay soil and helps lean, sandy soils to retain water as peat moss naturally absorbs water, slowly releasing it to plants, in addition to helping to balance the soil's water retention and drainage. Peat moss also increases soil aeration which in turn improves plant health. It further provides a sterile medium, which is ideal for crop growth.

The short lifespan of organic soil conditioners has led to an increased interest in synthetic soil conditioners. Synthetic soil conditioners do not interact directly with the soil matrices but instead form aqueous gels and act as water reservoirs for the plant-soil system in which roots can grow and draw water when required. Many inorganic soil conditioners have been investigated. De Boodt (1975) and Azzam (1980) studied the behaviour of polyacrylamides with low levels of carboxylic groups; Quchi et al. (1989) and Bouranis et al. (1995) concentrated their research on a potassium-based polymer; while Bowman et al. (1990) focused on sodium-based polymers. Potassium-based polymers have been demonstrated to be better as compared to other soil conditioners because they are completely and immediately available to plants.

Yangyuoru et al. (2006) further investigated the use of synthetic crystal potassium-based copolymers, liquid synthetic and organic coco peat and their effects on the growth performance of maize on five Ghanaian soil series. Crystal potassium-based copolymers dramatically increased the water retention capacity of the soil by 400 times its weight and absorbed it faster than all its predecessors. The soil conditioning improved dry matter yields by 92%, 4%, and 81%, respectively on sandy/clay/loam soils. Liquid synthetic conditioner however showed much lower retention rates than expected, probably due to leaching of this liquid polymeric absorbent into the soil. The use of sodium polyacrylate super water-absorbent polymer (SAP) and its capacity to retain water has been investigated experimentally in Oman together with the use of other natural soil amendments such as perlite and silica gel which are not extensively referenced within the literature. However, they are cheap and readily available in the region. The idea of using natural substances which are cheap and locally available, that are not harmful to the environment and thus cannot poison the crops was one of the main targets of this investigation.

Perlite is a baked volcanic rock that provides an airy substrate, increases water drainage, and improves the structure of the soil. It can be broadly used because it is germ-free and stimulates root development. Perlite is not a fertiliser and adds no nutritional or microbial value to plants or soil, but it can store nutrients for a short period when they otherwise might be washed away immediately. Its benefits derive from keeping the soil structure loose and light. Perlite is filled with many tiny cavities that hold water (like a sponge), making it efficient in delivering moisture to plant roots. All of these

nooks and crannies enable perlite to hold three to four times its weight in water while, at the same time, the cavities render perlite porous, so that it drains excess water more readily than other media, thereby preventing the soil from becoming waterlogged and thus preventing root rot and fungal diseases. Perlite is commonly used in potting soil and soilless cultures to keep the soil structure loose and well-draining without the risk of compaction over time. When combined with peat moss or coco peat, it can be used as a basic seed starting mix that supports healthy seedling development.

Silica gel is essentially an amorphous and porous form of sand (silicon dioxide), consisting of an irregular three-dimensional framework of alternating silicon and oxygen atoms that can absorb from 40% up to 500% of its mass in water (Matichenkov et al. 2001; Iler 1973). It was suggested that silica gel conditioning may help plants to survive drought (Gong et al. 2012; Pei et al. 2010), but there is relatively little literature demonstrating that its addition to soils could potentially increase its WHC, normally due to the existing porosity and the nature of bonding within the soil. Tentative work by Schaller et al. (2020a) analysed the effect of silica gel on WHC for different soil types and observed that, with increases in silica content by 1%, 5% and 15% [g /g], WHC increased by >3%, >15% and >25%, both for pure sand and sandy clay loam. The enhanced water retention upon silica gel addition can be explained by the water adsorption capacity of the added silica. In a second study, Schaller et al. (2020b) also confirmed another advantage of using silica in mitigating phosphorus (P) availability which is essential for crop growth. Increasing silica availability in soils leads to a mobilisation of Fe (II)-P phases from mineral surfaces, thereby increasing P availability/mobility in soils. There could also be side effects of the P increase in soil. For example, this may lead to an excess of phosphate whose potential side effects have yet to be investigated. Despite the low level of knowledge in terms of the application of such amendments to the soil, silica can be considered a promising option for increasing water and nutrient availability, especially in sandy soils where water storage capacities are low and interactions with organic carbon are less likely to compete with Si at sorption sites. The analysis is mainly related to sandy soils, but more complex soil systems should be tested to understand interactions arising between soil solutions, including organic matter and clay minerals, as this may be important for both the WHC and sorption of phosphate in non-sandy soils.

Sodium polyacrylate (SAP) is a type of superabsorbent polymer that can increase moisture availability to plants. It mixes with soil to increase the soil's capacity to hold water (forming an aqueous gel that stays in the soil for months as it is insoluble), making its stored water slowly available to plants. Due to its hydrophilic properties, SAP can swell up in demi-water up to hundreds of times its dry weight, depending on the soil type, thereby enhancing soil water retention (Dhliwayo 1993; Wang et al. 1990; Choudhary 1995). The use of such superabsorbent polymers has been studied

for many years to increase the WHC of coarse soils (Johnson 1984; El-Amir et al. 1991; Sabrah et al. 1993; Sharma et al. 1996; El-Hady et al. 2006; Geesing et al. 2004), demonstrating that its capacity to provide water to crops depends on the water retained by the polymer that is easily available to plants, the pressure the soil exerts on the polymers and the presence of soluble salts. De Varennes et al. (1997) demonstrated that plant-available water, as estimated by the difference between the amount of water retained at -10 and -1500 kPa, increased three-fold when a polyacrylate polymer was incorporated into a sandy soil as a 0.2% mixture with dry soil as compared with unconditioned soil. However, the expansion of the polymers and their capacity to retain water is greatly affected by the pressure exerted by the soil. In fact, water retention was reduced from 258 to 65 g of water per gramme of dry polymer when a polyacrylate polymer was uniformly incorporated into 20 cm high soil columns. The high cost of many polymers has usually restricted their use to high-value crops, yet little is known about the agricultural use of sodium polyacrylate. As it is relatively cheap, it will form part of the study. The efficient management of soil moisture and, consequently, of WRC is important for agricultural production, especially in areas with scarce water resources.

A series of pilot experiments have been executed to investigate the WRC of different types of soils and their combination using a specific rig that has been built for the purpose. The experimental rig is made from stainless steel and consists of 3 canals of 0.6 m (width) x 0.4 m (depth) x 3 m (length) as designed in Figure 05.19. Each of the 3 canals is independent and is provided with:

- feed-in and feed-out piping for seawater
- feed-in and feed-out piping for air
- underwater perforated piping to release air and enhance evaporation
- incoming water valve to control the water flow rate
- incoming air valve to control the air flow rate

All three canals are connected to the main unit providing:

- air blower connection to control the incoming airflow rate
- electric resistance to increase feed-in water temperature

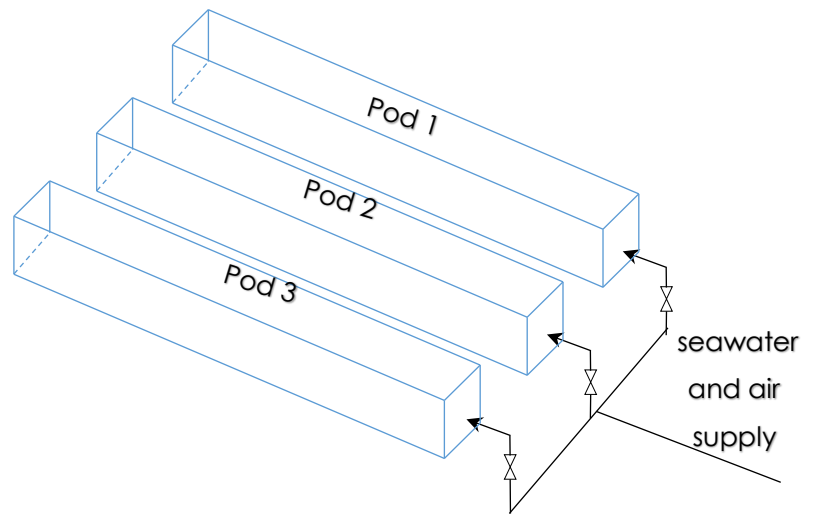
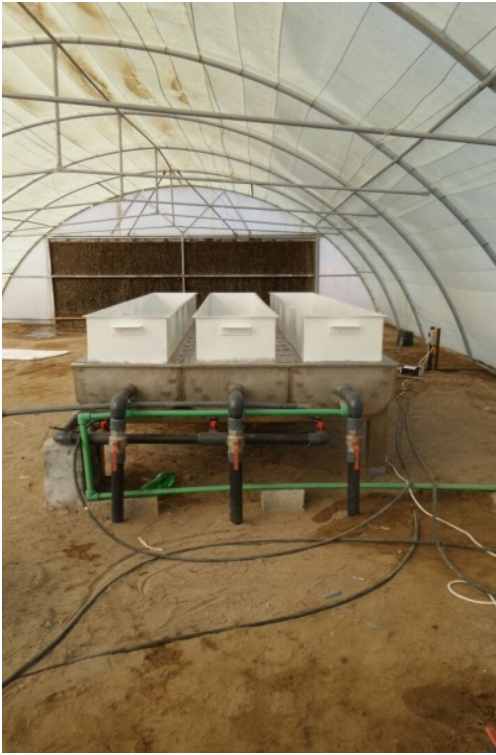


Figure 05.19 – SWI – Rig for pilot experiments.

Different types of soil have been analysed and tested to determine which types of soil build-up substantial moisture content. For each type of soil, the following methodology has been followed:

- Carry out soil chemical and physical characterisation.
- Determine soil water saturation.
- Monitor soil parameters, temperature, salinity, and moisture during the experiment.

Soil composition is identified by knowing the content of sand, silt and clay as reported in Table 05.03, taking into consideration the knowledge that the perfect soil is normally a loam which is a balanced mix of all three soil substrates, namely clay, sand, and silt. Clay, in fact, is a very fine particulate material and, when wet, prevents water from flowing through. Sand provides adequate air spaces and pathways for water to flow through, whereas silt is a light particle that erodes easily but contributes to good farmland.

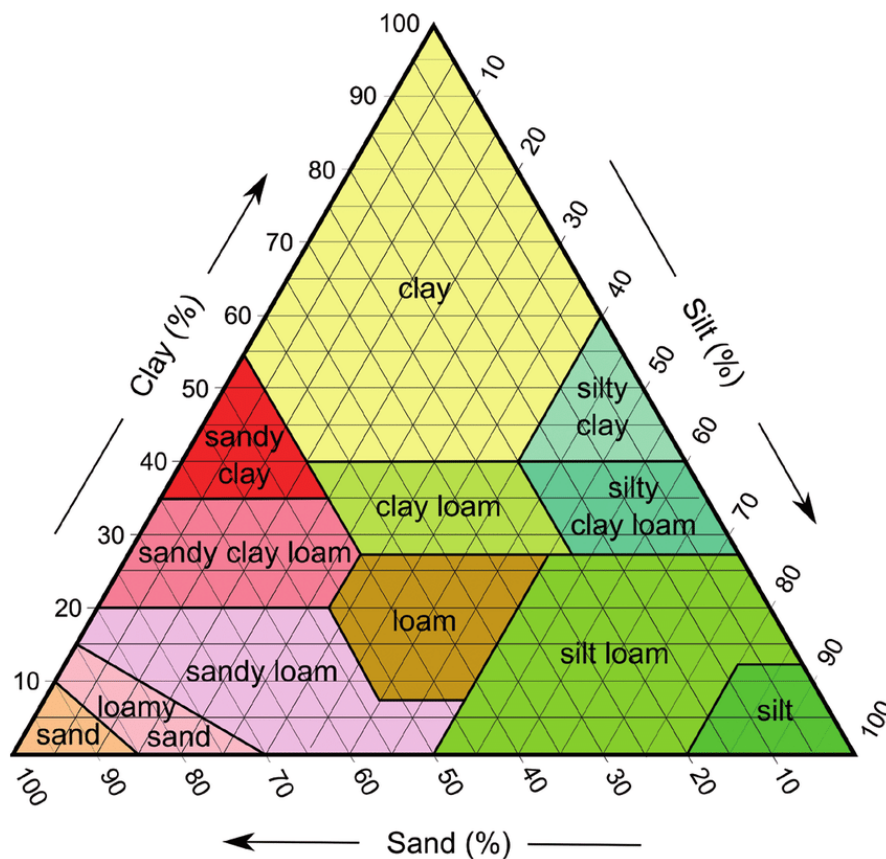


Table 05.03 – A soil texture diagram showing soil types according to their clay, silt and sand composition (redrawn from the USDA webpage: <http://soils.usda.gov/education/resources/lessons/texture/>. Credit Mikenorton).

The typical soil types that can be found in Oman are as reported in Table 05.04 together with their specific compositions.

Type	Coarse sand (%)	Fine sand (%)	Silt (%)	Clay (%)	Soil texture
1	0	45.7	28.6	25.7	Loam
2	10.3	67.4	14.6	7.7	Loamy sand
3	12.6	81.1	4.6	1.7	Sand

Table 05.04 - Examined soil texture present in Oman.

To improve soil moisture retention capabilities, different combinations of soil samples for testing have been created and are presented in Table 05.05. These new combinations present different quantities of the aforementioned soil texture with the addition of other soil conditioners.

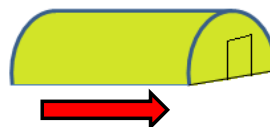
Sample	Composition
Sample 1	Loam
Sample 2	Loamy sand
Sample 3	Sand
Sample 4	Loam (60%) + Sand (40%)
Sample 5	Loamy sand (60%) + Sand (40%)
Sample 6	Sand (80%) + Coco Peat (20 %)
Sample 7	Loam (60%) + Sand (30%) + Coco Peat (10 %)
Sample 8	Loamy Sand (60%) + Sand (30%) + Coco Peat (10%)

Table 05.05 - Examined soil compositions.

Stage I/Trial I

The objective of these initial pilot experiments is to investigate the effect of soil texture and composition on the development of moisture levels within the soil. The pilot experiments were performed in a greenhouse to control and guarantee stable testing conditions. The experimental canals were designed to accommodate 10 soil samples, each of the following dimensions (length 30 cm; height 30 cm; and width 40 cm). Each soil sample was duplicated, one being tested with a cotton absorbing layer below the soil sample and the other without the cotton absorbing layer (Figure 05.20). The cotton layer was used to increase the water storage capability under the soil surface and it was noticed that, after running the experimental rig for a few minutes, the lower surface of the soil became wet, as predicted, yet it prevented other water from passing through the soil. Thus the cotton layer may provide a good substrate for storing water and releasing it back slowly into the soil, although this remains to be carefully investigated. The incoming airflow rate was set to 10 m³/h, while salty water was left flowing under the soil samples at a very low speed as created by the water head due to the slight inclination of the rig. The results obtained under the ambient conditions of these experimental trials are shown in the following Figures 05.21 (weather station), Figure 05.22 (rig conditions) and Figures 05.23a to 05.23e (sample soil moisture content).

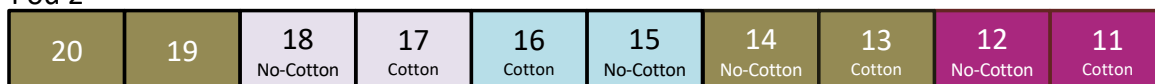
Arrangement of samples in GH



Pod 1



Pod 2



Pod 3

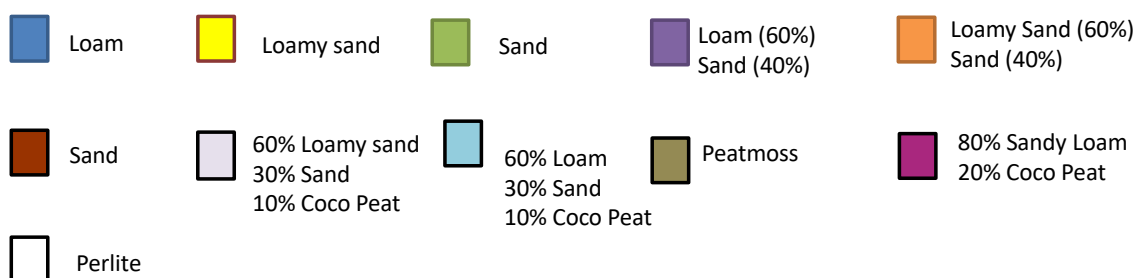
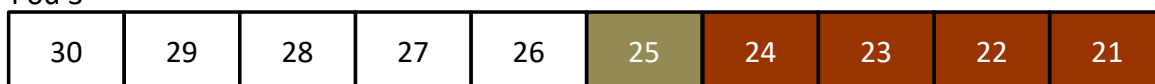
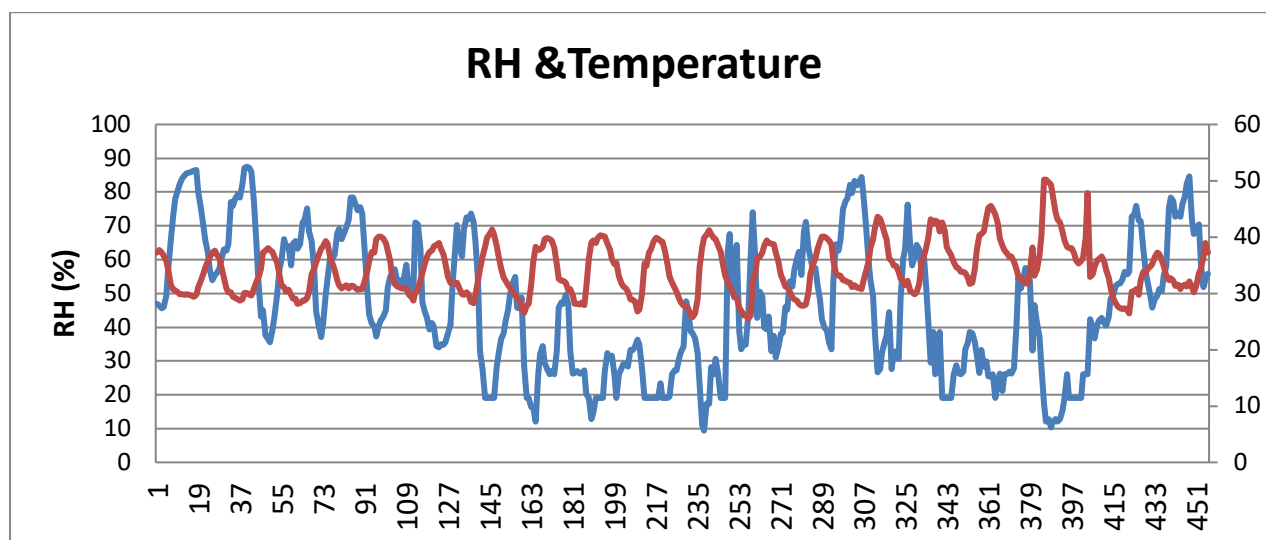


Figure 05.20 – Arrangement of soil samples inside the irrigation canals - Stage I/trial I.



• Temperature	• Relative Humidity
Min= 25.5C after 280hr (30/6/2015 at 5:00 AM)	Min= 9.4% after 261hr (29/6/2015 at 10:00 AM)
Max= 50.2C after 385 hr (7/5/2015 at 1:00PM)	Max= 87.5% after 40hr (20/6/2015 at 4:00 AM)

Figure 05.21 – Weather station data (Stage I/trial I).

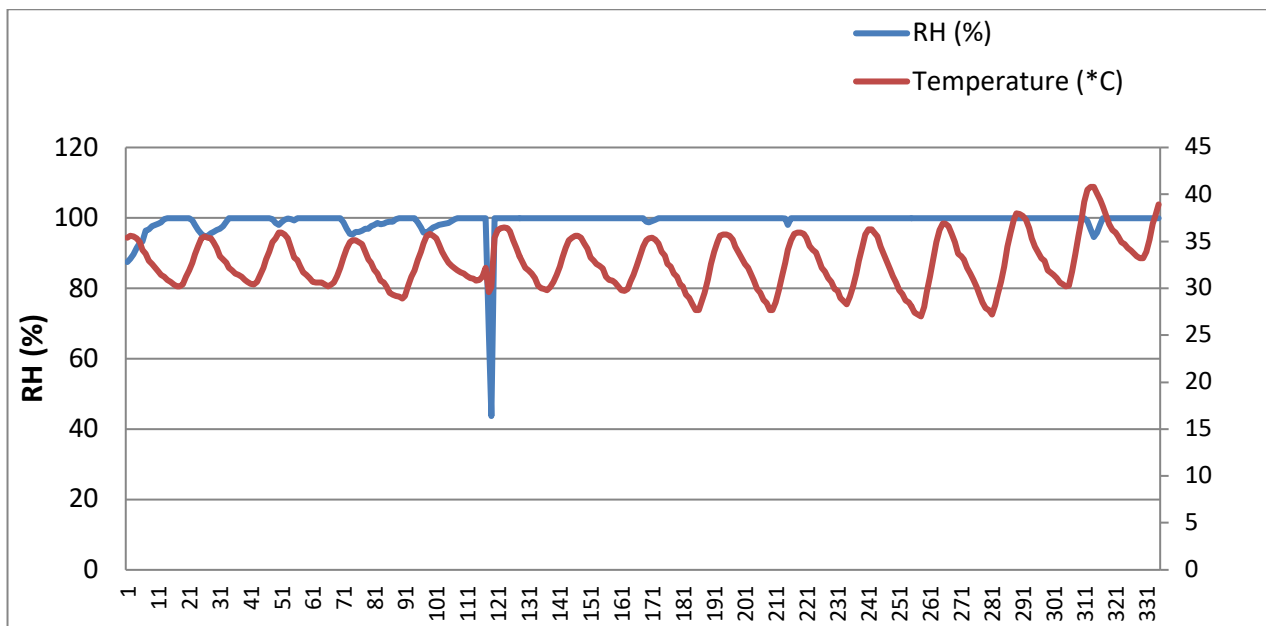


Figure 05.22 – Temperature and humidity % inside the pods (Stage I/trial I).

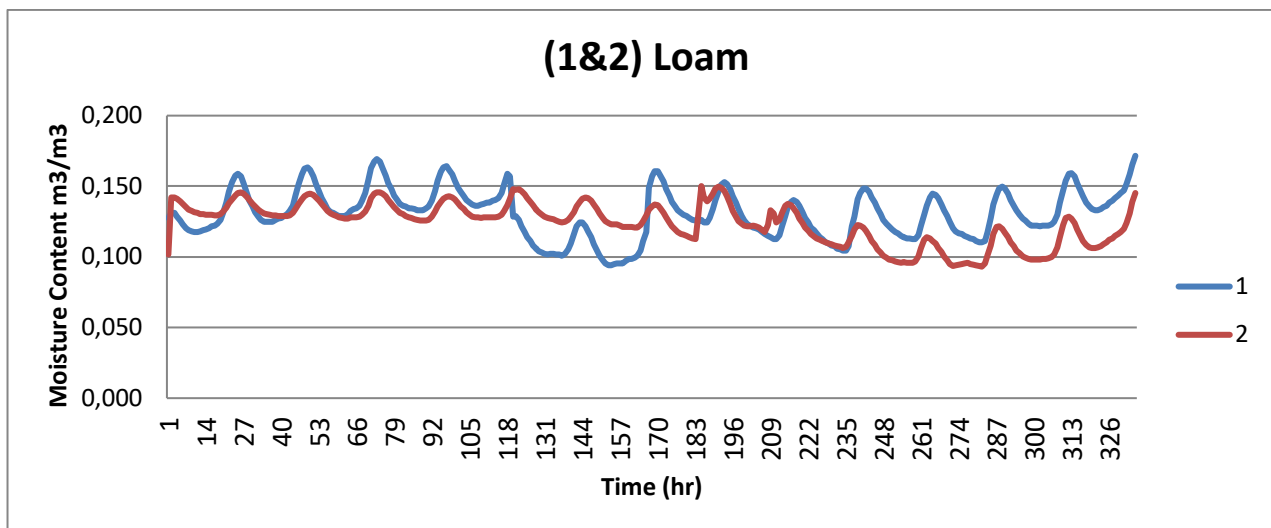


Figure 05.23a – Moisture content of loam – Sample 1(Pod1.1 and Pod 1.2).

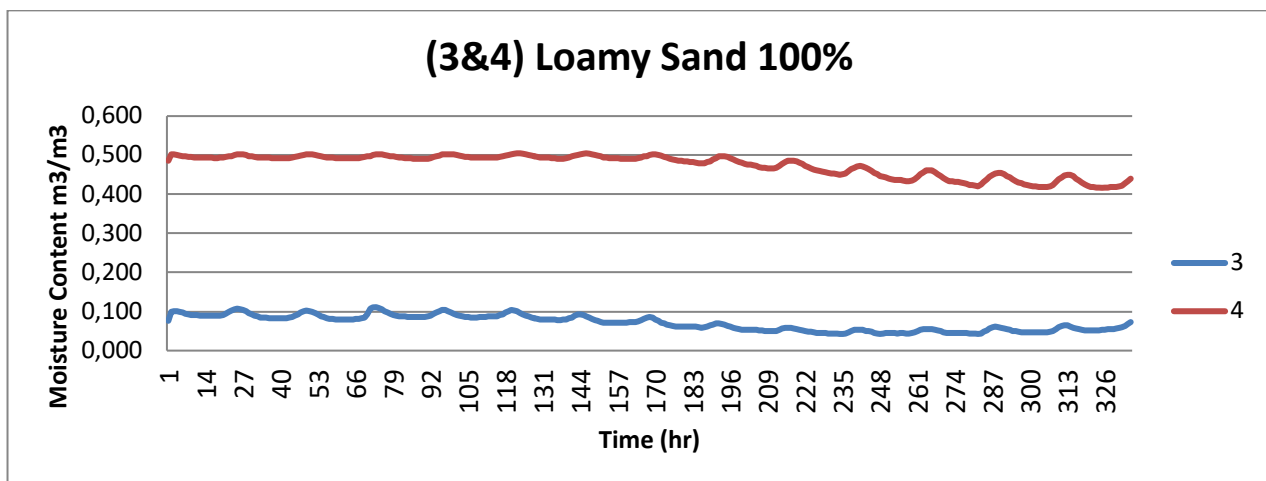


Figure 05.23b – Moisture content loamy sand - Sample 2 (Pod1.3 and Pod 1.4).

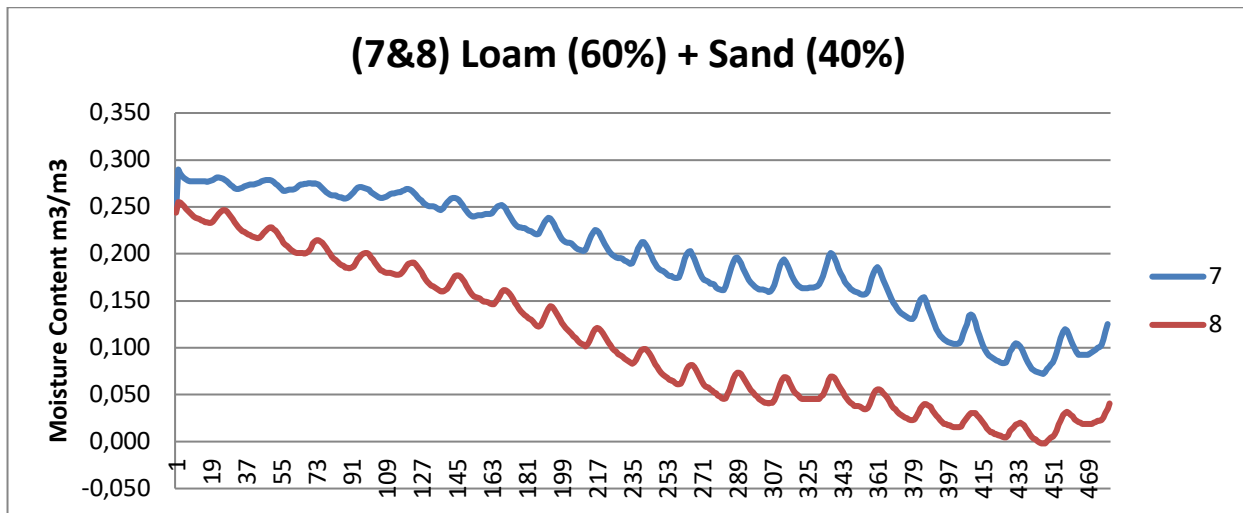


Figure 05.23c – Moisture content of loam (60%) + sand (40%) - Sample 4 (Pod1.7 and Pod 1.8).

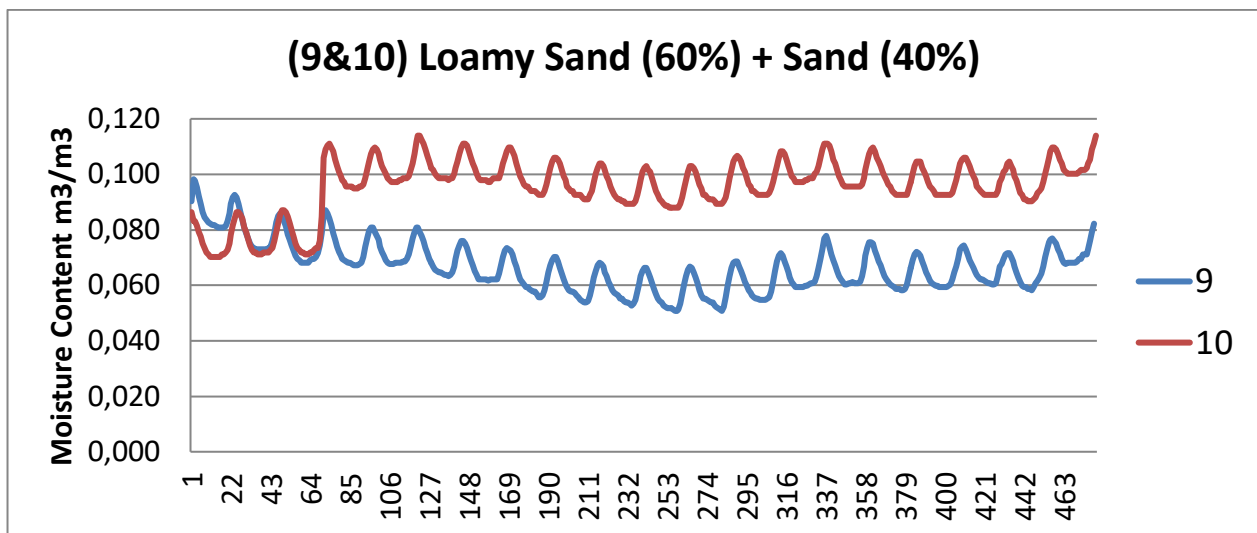


Figure 05.23d – Moisture content of loamy sand (60%) + sand (40%) - Sample 5 (Pod1.9 and Pod 1.10).

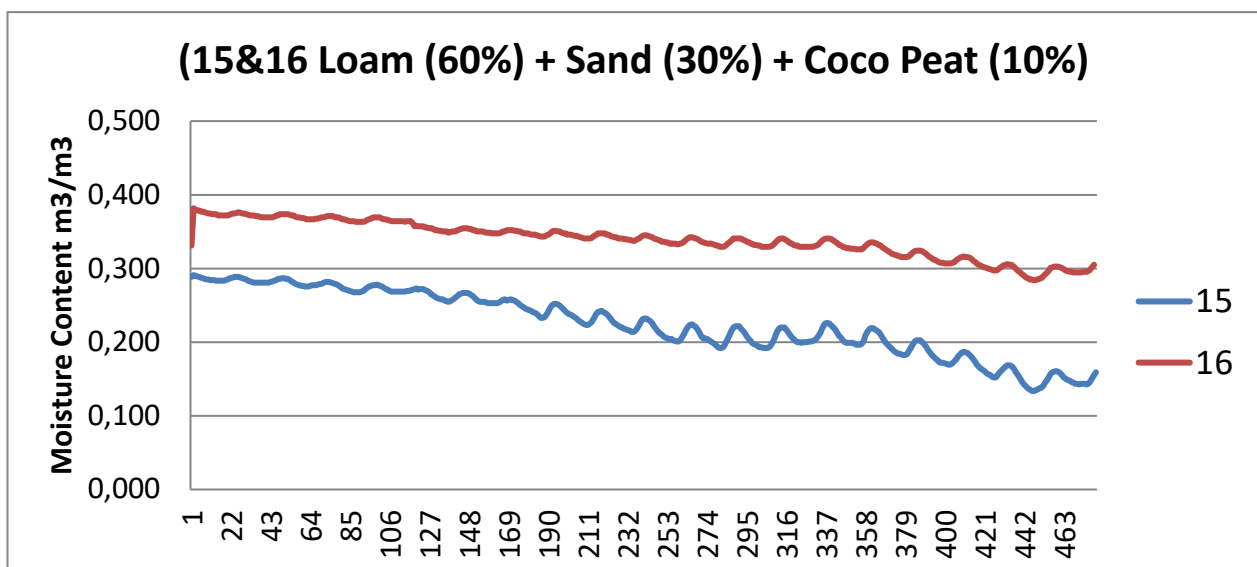


Figure 05.23e – Moisture content of loamy (60%) + sand (30%) + Coco Peat (10%) - Sample 8 (Pod 2.15 and Pod 2.16).

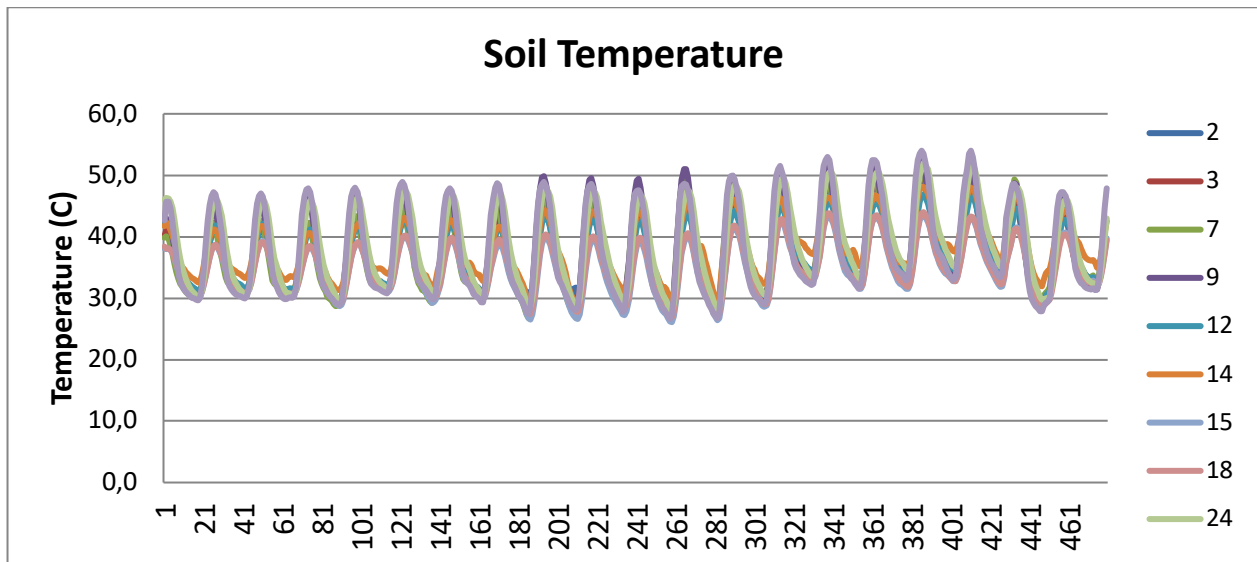


Figure 05.24 – Soil temperatures as measured during the experiment.

The main results from these initial pilot experiments may be summarised as follows:

- (i) The type of soil texture and composition plays an essential role in building up soil moisture.
- (ii) The moisture content of soil samples decreases over time.
- (iii) The cotton layer beneath the soil in most of the soil compositions enhances soil moisture content.
- (iv) Better moisture content was achieved by using loamy sand soil 100% (Figure 05.23b) or a combination of loam, sand and coco peat (Figure 05.23e).
- (v) Average soil temperatures during the experiments were 40°C and reached a maximum of 51°C, while the air temperature was around 40 °C (Figure 05.24).

It was evident, after the initial trial experiments, that soil temperature must be properly controlled to avoid any excess temperature that may harm crop growth or cultivation. Maximum temperature was reached at midday when the solar radiation and outside temperatures are at their peaks. It would have been advisable to stop the system during this part of the day to avoid bringing more heat to the soil.

Stage I/Trial II

This second part of the pilot experiments was designed to investigate the use of silica gel as a soil conditioner and to study its capacity to build up soil moisture, either alone or in combination with the previously tested cotton layers. During these trials, the soil samples from trial I were rearranged in the irrigation canals as shown in Figure 05.25 and the airflow rate was increased to 25 m³/h.

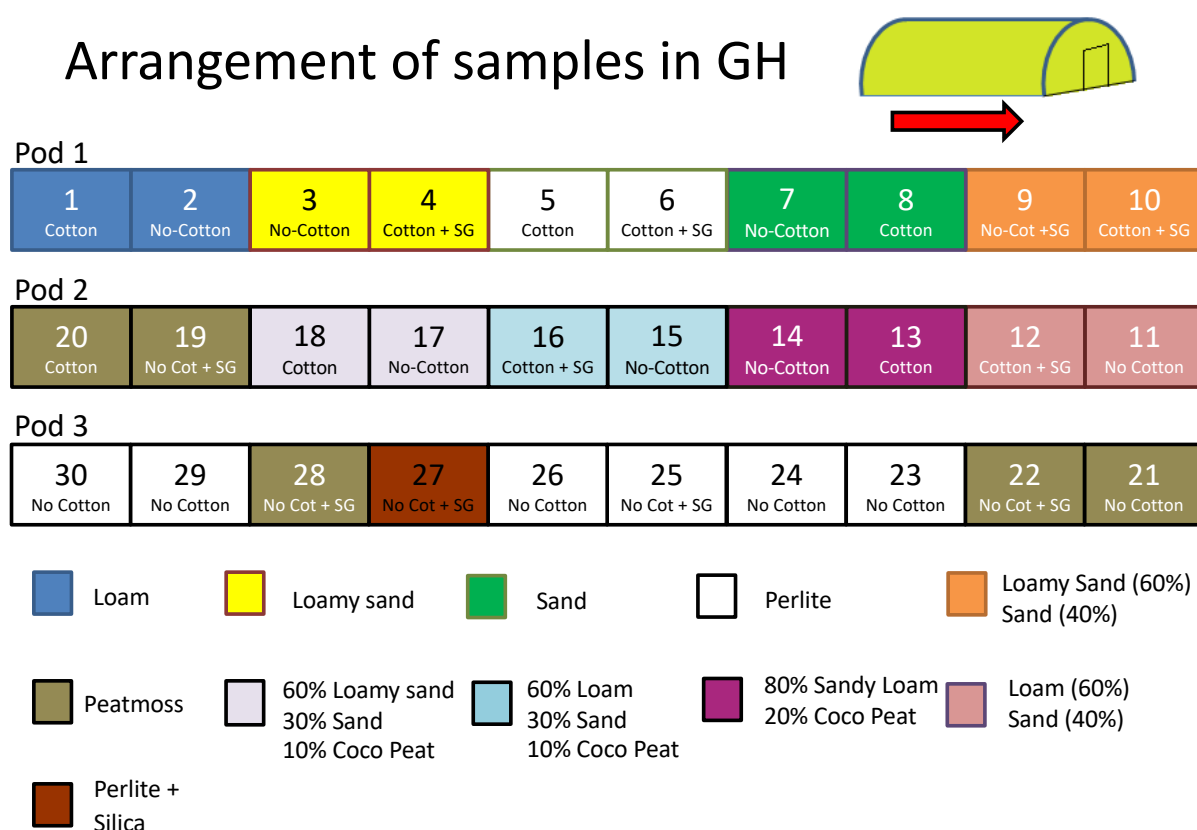


Figure 05.25 – Arrangement of soil samples inside the irrigation canals (with silica gel) – Stage I/Trial II.

The main outcomes of the experiment during trial II can be summarised as follows:

- (i) There were no significant effects on the build-up of moisture content when using the silica gel soil conditioner. However, the building up of the moisture was faster than for trial I.
- (ii) The main increase in soil moisture content was achieved for the following reasons:
 - a) increasing the air flow rate;
 - b) removing the individual cover of each sample as numbered in the channels above.

It was also found that soil moisture can penetrate best and fastest with a soil layer thickness of approximately 15 cm in height. The soil temperature during the experiment remained within the same range as for the previous trial I, with an average soil temperature of 40°C.

During trial II, other pilot experiments were performed, such as planting cucumbers and adding fertilisers to the soil. A liquid fertiliser was added to each plant (8 g of NPK (20-20-20)/ 4 litres of water) >> EC= 2.1 ds/m 60 ml. Unfortunately, during the tests, some soil samples in Pod 3 faced water overflow that caused the soil's salinity to increase due to the direct contact between the seawater and the soil. The influence of water overflow is shown in Table 05.06.

Sample No.	EC (ds/m)	pH
1	7.96	7.1
2	5.29	7.2
3	0.72	7.5
4	2.32	7.4
7	1.05	7.4
8	1.51	7.4
9	2.71	7.3
10	3.92	7.3
11	1.74	7.4
12	0.55	7.6
13	4.04	7.5
15	3.64	7.6
17	1.56	7.7

Table 05.06 – Measured soil sample conductivity and pH.

Stage I/Trial III

The final part of the pilot experiments was designed to investigate the use of peat moss as a soil conditioner. The irrigation canals were rearranged as shown in Figure 05.26, wherein some soil samples from trial II were ignored and Pod 3 was designed so that it had only three soil samples with greater dimensions (length 100 cm; height 30 cm; width 40 cm). The three soil samples were:

- Sand + peat moss
- Loamy sand + peat moss
- Sandy loam + peat moss

Unfortunately, another water overflow occurred during this trial which affected the growth of the plants because the soil became contaminated with saline and the test had to be cancelled.

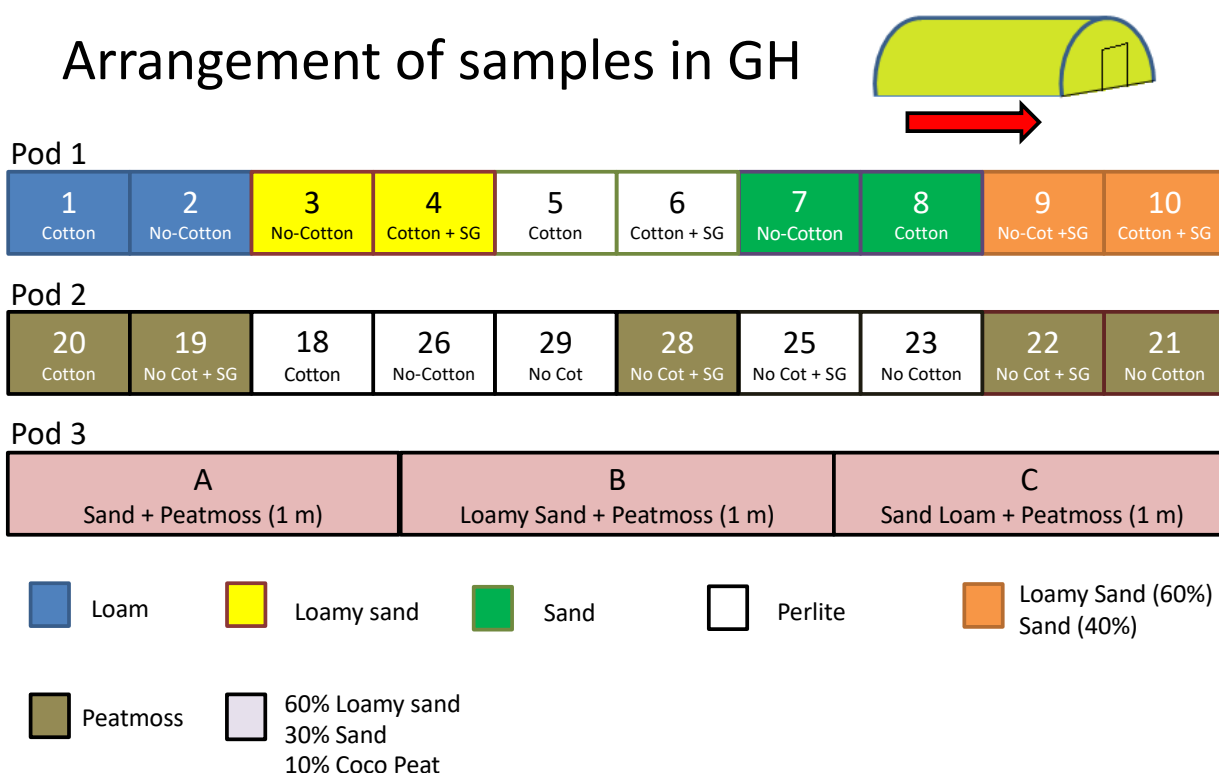


Figure 05.26 – Arrangement of soil samples inside the irrigation canals– Stage I/ Trial III.

5.5.1.2 Stage II – Main Experiments and Field Investigations

Using the data and experience acquired from the previous pilot experiments, it was possible to prepare a full field test investigation and begin crop production. The main experiment was divided into different testing stages. The first stage followed the pilot experiment with the aim of optimising soil composition and process parameters. The second was the integration of solar thermal technologies to improve the productivity and find ideal conditions for crop sowing and growing. Accordingly, it was necessary to design and build a new rig to perform these main experiments.

Stage II/Trial I

This first part of the main experiment was devoted to investigating the use of peat moss to increase the capability of the soil to retain moisture following the failure of the pilot rig due to salty water overflow.

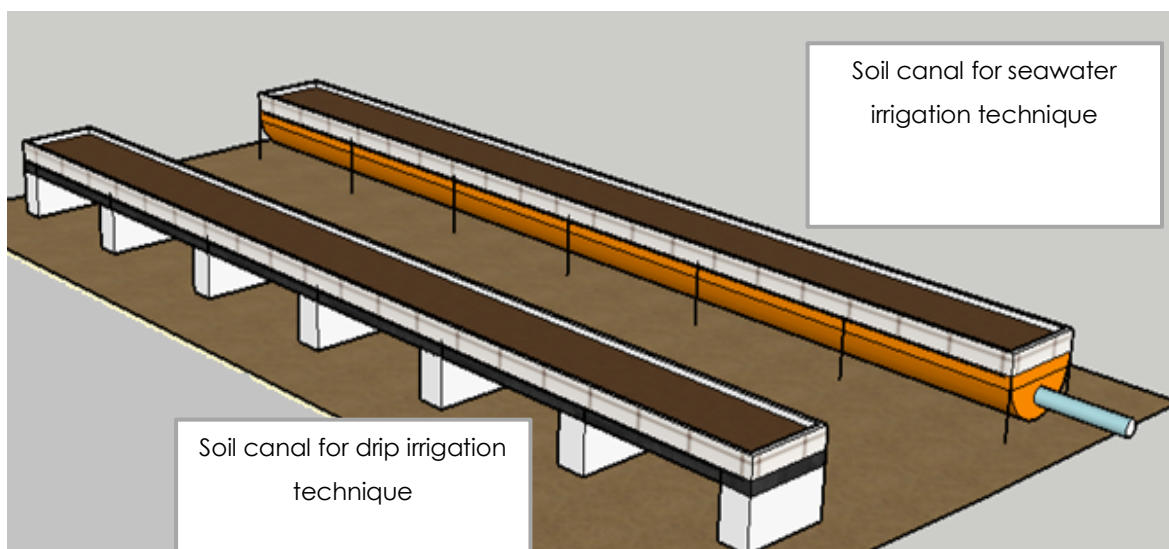


Figure 05.27 - Seawater Irrigation Test Rig: Stage II/Trial I.

Methodology

- Construction of two identical testing rigs (circa. 600 cm x 40 cm x 15 cm; Figure 05.27).
 - The test sections were constructed and evaluated inside the greenhouse to ensure the same climatic conditions for both.
 - One test section was used for the drip irrigation technique, while the other was used for the direct SWI technique.

- Introduction of an external salty water storage tank exposed to the sun and a heat exchanger connected to an FPC to increase the temperature of saltwater flowing into the rig (Figure 05.28).
- Select suitable soil type for both test sections with the capacity to retain soil moisture.
 - The soil type selected was sandy loam, one of the most dominant soil types in Oman. Soil specifications are as presented in Table 05.07.
 - The soil was mixed with peat moss (as soil conditioner) to improve water holding capacity.
 - The soil thickness was selected to be 15 cm based on previous results so that the moisture could penetrate easily and swiftly across the whole thickness (Figure 05.29).
- Three different crops were used in each test section, namely cucumber, tomatoes, and lettuce.

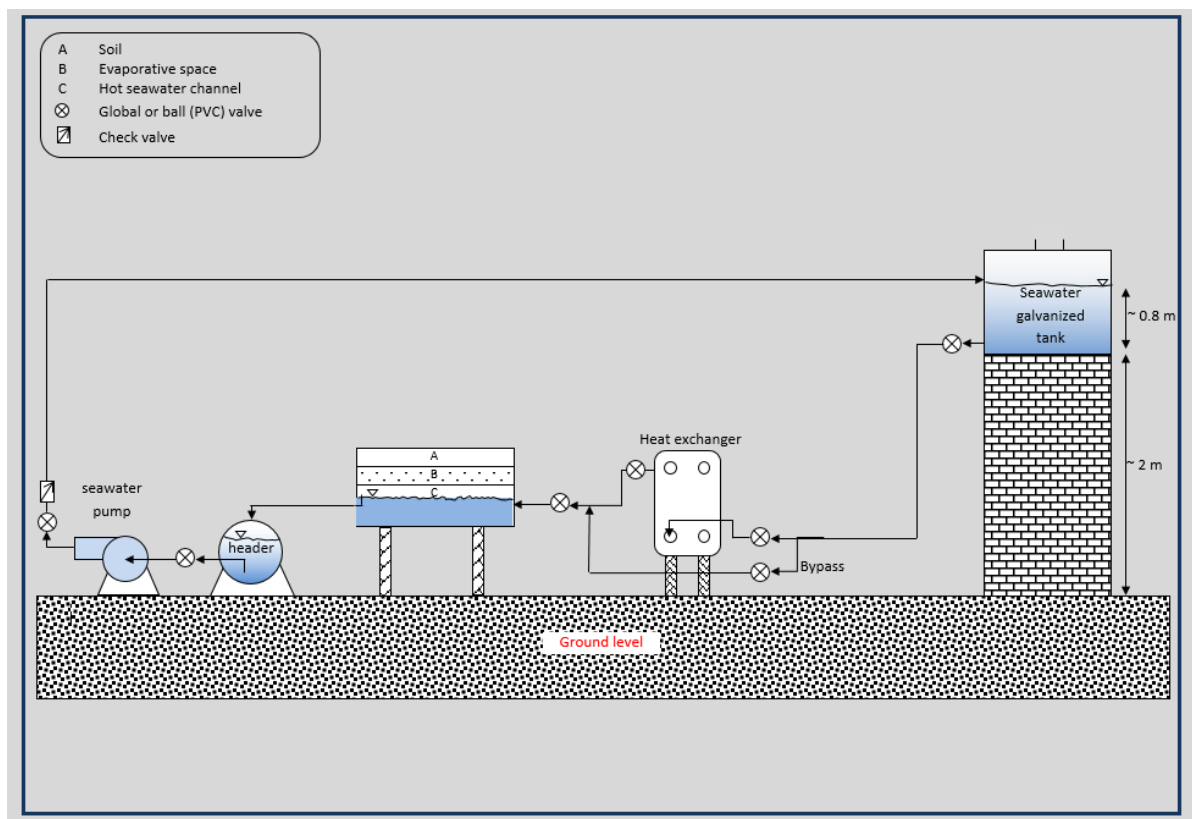


Figure 05.28 - Diagram of the new rig with salty water pre-heating.

Experimental and Performance Evaluation

- Conduct chemical and physical characterisations of the soil.
- Monitor soil parameters including temperature, salinity and moisture (in at least at three different locations for each test section).
- Crop growth monitoring.
- Fertilise the soil regularly based on the requirement of each crop.
- Monitor the temperature and the humidity of the air inside the rigs.
- Investigate the effect of air flow rate and temperature on the evaporation rate.
- Investigate the influence of feedwater temperature on soil moisture content.
- Record all the operating conditions of the soil, water, and air at hourly intervals.

Soil name	Sand (%)	Silt (%)	Clay (%)	Feel when moist
Sandy Loam	72	15	13	Gritty

Table 05.07- Soil Texture used for experiment Stage II/Trial I.



Figure 05.29 - Soil thickness in the canal.

Results Analysis of Trial I

The main outcomes of Trial I are summarised below:

- i. Low moisture level. The soil moisture content was far below the levels seen in previous pilot experiments (Figure 05.30).
- ii. High salinity level. The salinity of the soil, especially at the bottom layer of the rig, increased sharply. In other words, the salt content in the soil is very high, suggesting a possible direct contact between the seawater and the soil due, probably to the high air flow rate (Figure 05.31).
- iii. Low water temperature. The higher water flow rate is considered to be the cause of the low heat transfer rate through the plate heat exchanger and, consequently, of the lower recorded seawater temperature (Figure 05.32).

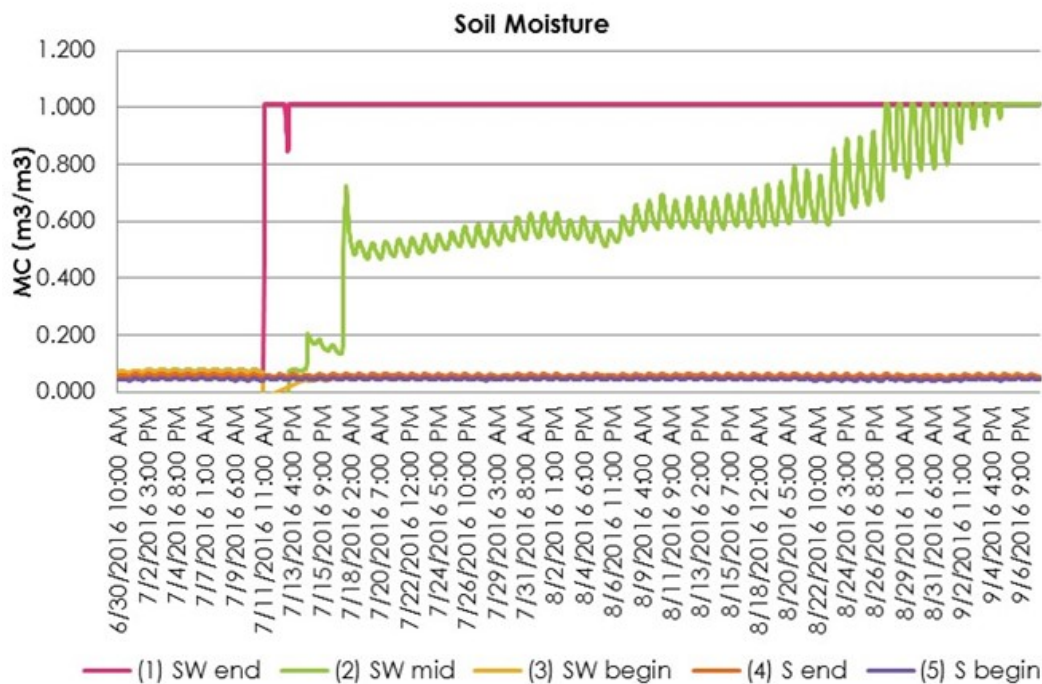


Figure 05.30 - Soil moisture during the test period - Stage II/Trial I.

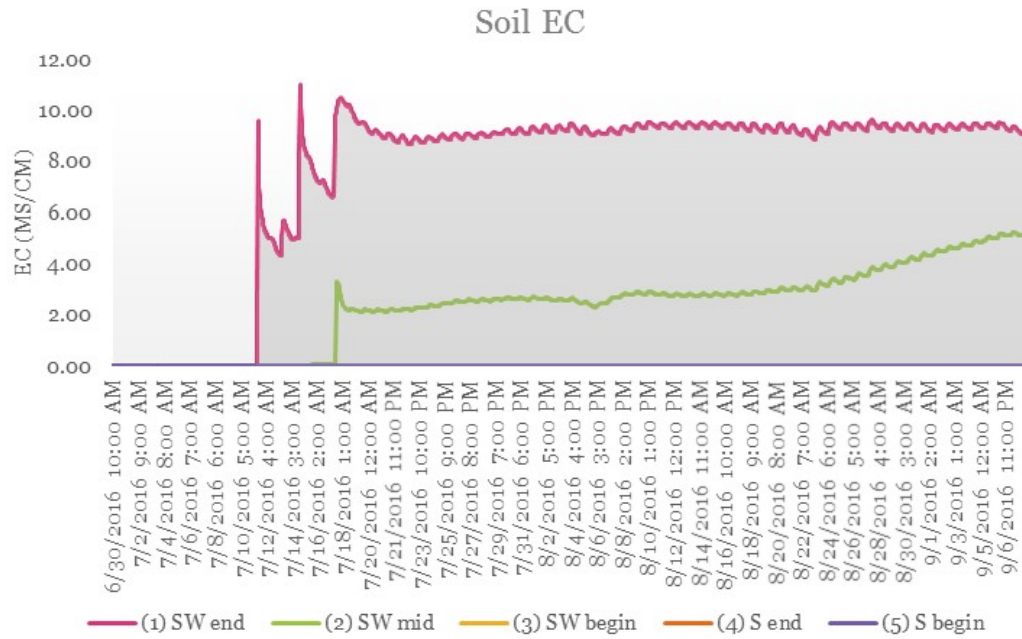


Figure 05.31 - Soil salinity during the test period - Stage II/Trial I.

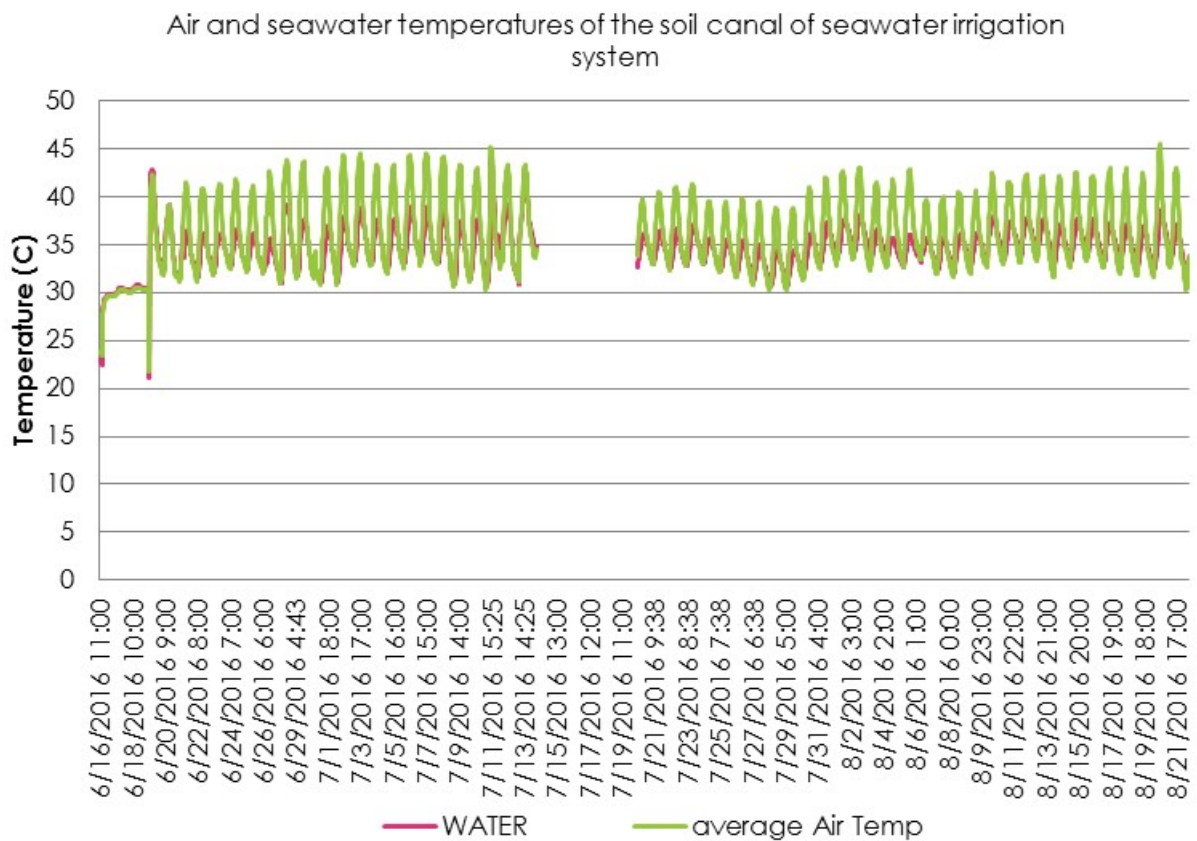


Figure 05.32 - Air and seawater temperatures inside the canal of the irrigation system - Stage II/Trial I.

Technical Problems and Recommended Solutions

i. Low moisture level in the soil

➤ Reasons:

- The supply seawater temperature was very low at around 35° C.

➤ Implemented solutions during the execution of the tests:

- Increasing the supply seawater temperature through the utilisation of a small FPC for water heating.
 - Results: No significant increase in seawater temperature was observed. The low thermal conductivity of the FPC and the higher flow rate of the pump reduced the heat transfer rate to the seawater.
- Increasing the supply seawater temperature through the utilisation of the SP and the heat exchanger.
 - Results: No significant increase in seawater temperature was observed. The maximum temperature in the SP was 45°C at the bottom level, although most of the heat was lost during extraction to the heat exchanger plate.

➤ Recommended solutions for Trial II:

- Replace the submersible pump with a low flow rate centrifugal pump.
 - Reason: The current submersible pump has a higher flow rate of 9 m³/h which is the cause of the low heat transfer rate through the plate heat exchanger and, consequently, of the lower seawater temperature observed.
 - The low flowrate centrifugal pump will enhance the heat transfer rate through the heat exchanger and increase the seawater temperature.
- Use HPs instead of FPC to absorb the solar energy and increase the temperature of the heat exchanger plate.
- Use acrylate seeds as a water vapour absorber material to be distributed in the soil (Figure 05.33 shows the suggested distribution method).
- Increase the air flow rate to the rig.
 - Reason: This could lead to an increase in the evaporation rate below the soil.
- Wetting the textile mesh layer. This would create a condensation layer that could accelerate the water vapour condensation process.

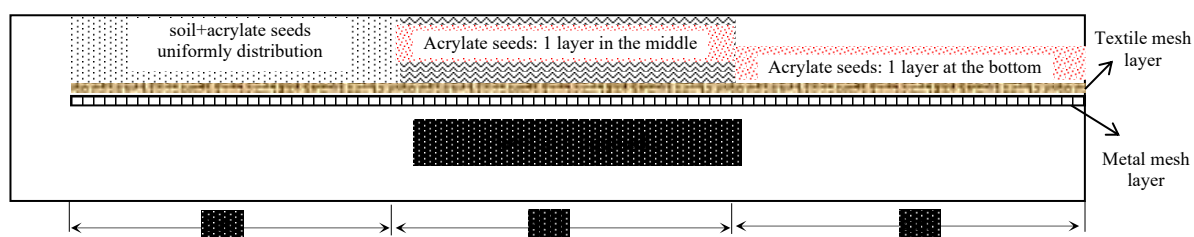


Figure 05.33 - Air and seawater temperatures inside the canal of the irrigation system - Stage II/Trial I.

ii. High salinity level

➤ Reasons:

- Unexpected overflow in the test rig (for a short period) caused direct contact between the seawater and the soil.

➤ Recommended solutions:

- Replace the submersible pump with a low flow rate centrifugal pump.
- Increase the distance between the soil and the salty water level. This would also help in increasing the evaporating space volume and the distance between the salty water level in the canal and the soil. This would also avoid salty water droplets leaving the air to reach the soil.
- Stop the tests and replace the soil with a fresh batch to return to a zero level of salinity.

An overview of all modifications implemented in the following field test is represented in Table 05.08.

Recommended Solutions and Expected Results of Trial II			
No.	Recommended Solutions	Functionality	Expected Results
1.	Replacing the submersible pump with a low flow rate centrifugal pump	To supply water to the rig passing through the heat exchanger	<ul style="list-style-type: none"> ▪ Avoiding overflow in the rig. ▪ Increasing the supply seawater temperature.
2.	Changing the piping network	Circulating seawater in the system	<ul style="list-style-type: none"> ▪ Reducing both thermal losses and pressure losses.
3.	Using heat pipes	Solar energy absorber	<ul style="list-style-type: none"> ▪ Increasing the supply seawater temperature

4.	Using Acrylate seeds	Water vapour absorber	▪ Enhancing the building up of the soil moisture.
5.	Increasing air flow rate	Water vapour transporter	▪ Increasing the percentage of water vapour in the rig.
6.	Increasing the distance between the soil and the seawater level	Evaporation space	▪ Increasing the evaporating space volume.

Table 05.08 - Summary of the recommended solutions to facilitate the progress of the main experiment that will be used in Stage II/trial II.

Stage II/Trial II

The second stage of the main experiment began after implementing the required modifications to the rig. This second stage was devoted to investigating the capacity of the soil to retain moisture after the addition of new conditioning agents, such as acrylate, and increasing the incoming water and air temperature. SWI is based on the well-known principles of evaporation and condensation. Thus increasing the water temperature increases the evaporation rate and this could be achieved by using solar energy in Oman where it is abundant, providing that the capital cost of the solar system is kept low and that its operation is continuous and trouble-free.

Methodology

- Redesign and construction of new water piping system according to the results and suggestions from previous experimental work (Stage II/Trial I; Figure 05.34).
 - Three test sections were constructed and tested inside the greenhouse to ensure the same climatic conditions for both.
 - One test section was used for SWI without using acrylate as a water-absorbent polymer.
 - One test section was used for SWI with acrylate.
 - One test section was used for the drip irrigation technique.
 - The evaporating space inside the canal was increased by 10 cm to avoid direct contact between salty water droplets and the soil (as shown in Figure 05.35).

- A plastic mesh layer has been installed over the pipe of the supplied air to break down any droplets of water before they can reach the lower surface of the soil as shown in Figure 05.36.
- Select suitable type of soil for all test sections.
 - The soil type selected was sandy loam.
 - The soil has been mixed with acrylate to improve its water retention capacity.
 - The soil thickness was maintained at 15 cm as for the previous experiment.
- Three different crops were used in each test section, specifically cucumber, tomatoes, and lettuce.

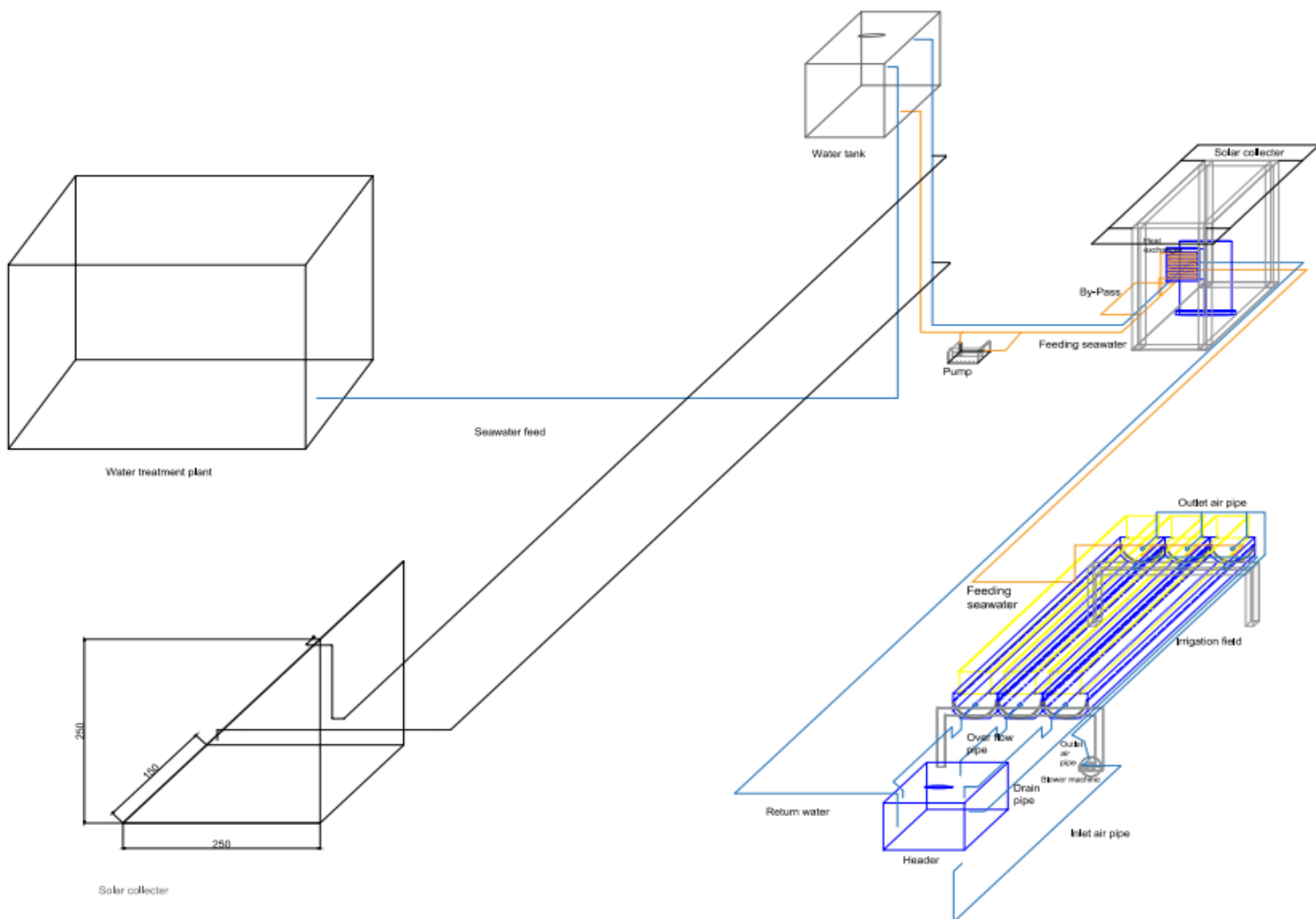


Figure 05.34 - Engineering drawing of the SWI technique - Stage II/Trial II.

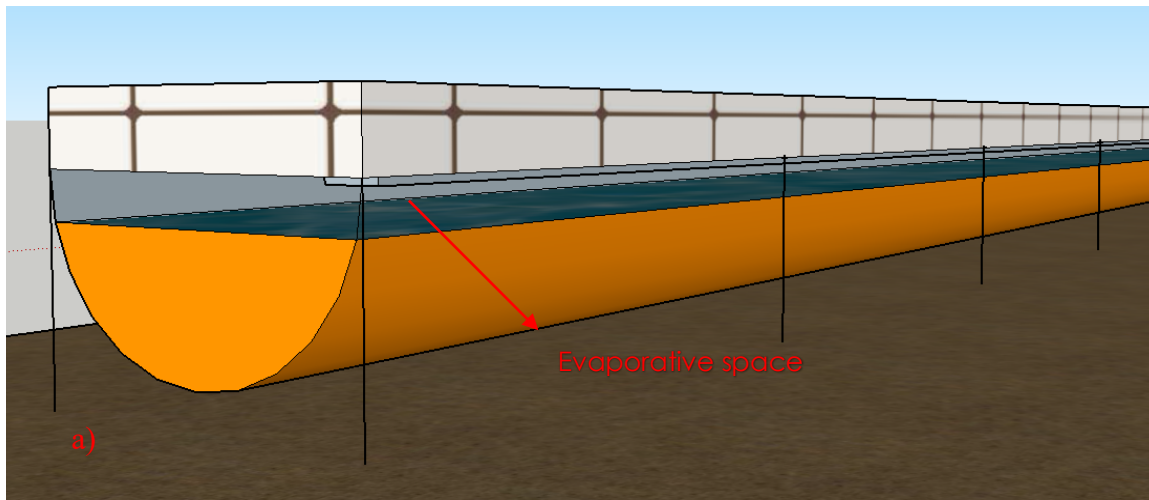


Figure 05.35 - Evaporating space inside the canal.

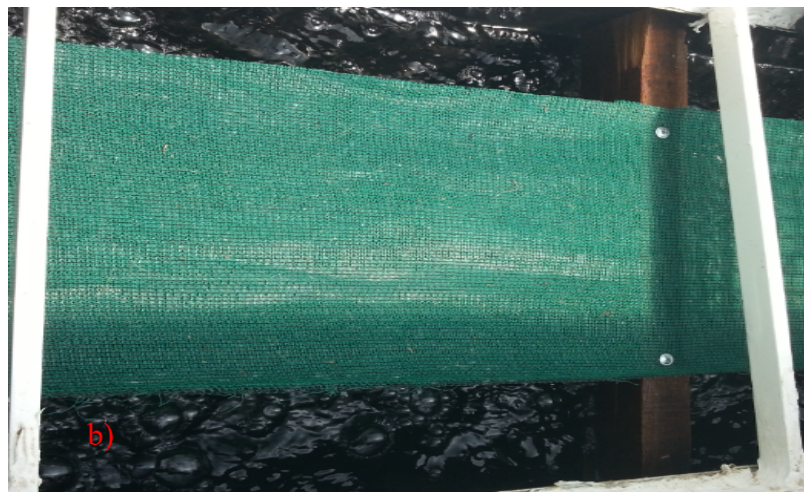


Figure 05.36 - Plastic mesh layer to break down the water droplets.

Experimental and Performance Evaluation

- Investigate the use of acrylate as a water-saving super absorbent polymer.
 - It has been confirmed experimentally that acrylate can absorb water up to 43 times its own weight within an exposure time of one hour and has a water evaporation rate of 3.34 ml/min. Different experimental sets have been designed and examined to determine:
 - i) The best way to deploy the acrylate (i.e., beneath the soil and/or homogenous mixing within the soil);
 - ii) The optimal amount of acrylate that could increase soil moisture effectively.
- Investigation of the use of solar thermal energy to increase the incoming water temperature.

- Some technical problems associated with the effect of sand on the solar flat plate and heat exchanger were resolved during the set up of the new testing rig. Two electrical resistances of 3 kW were installed to increase the salty water temperature for testing. In addition, HPs and low-cost solar concentrators (SCCs) were implemented as shown in Figures 05.37 and 05.38.
- A tentative and specifically designed SCC system was built, self-made from locally available low-cost components, including waste satellite dishes covered with a solar reflective tape. This helps to focus solar irradiation and increases its heating effect. Remarkably a high localised temperature of about 90°C was reached after a few minutes of using the system although, for real-world applications, it would need to be increased in size to provide enough heat for water or air heating.
 - Monitor soil parameters such as temperature, salinity and moisture (in at least at three different levels of each test section).
 - Crop growth monitoring.
 - Fertilise the soil regularly based on the requirement of each crop.
 - Record all the operating conditions of the soil, water and air at regular hourly intervals.



Figure 05.37 - Heat pipe system.



Figure 05.38 - SCC system.

Results Analysis of Trial II

The obtained results in Trail II are as summarised below:

- i. Low moisture level and long moisture build-up period. The soil moisture content was low and a build-up of soil moisture occurred slowly and this might require a long period to reach an optimal level (Figure 05.39, Figure 05.40, Figure 05.41).

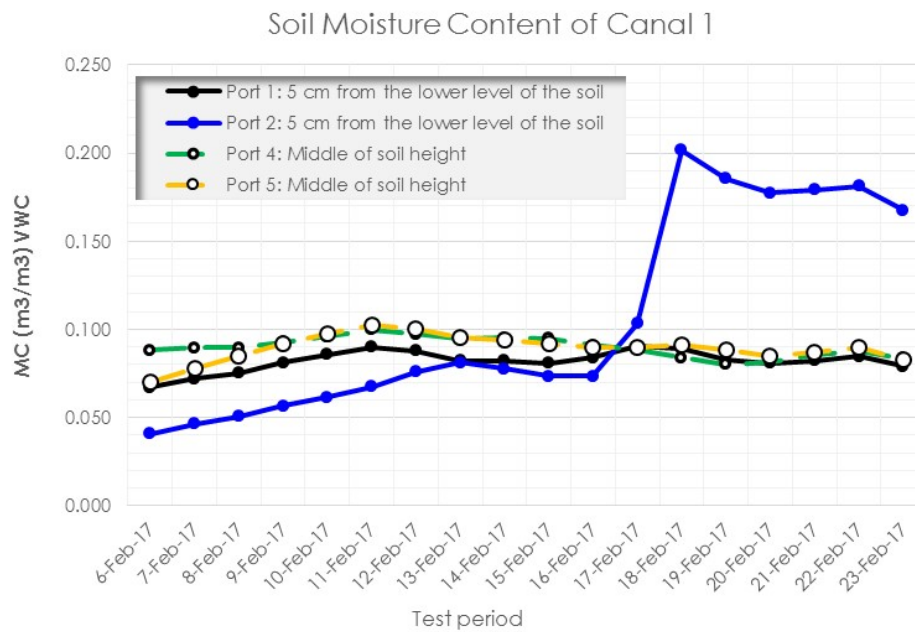


Figure 05.39 - Soil moisture of canal #1- Stage II/Trial II.

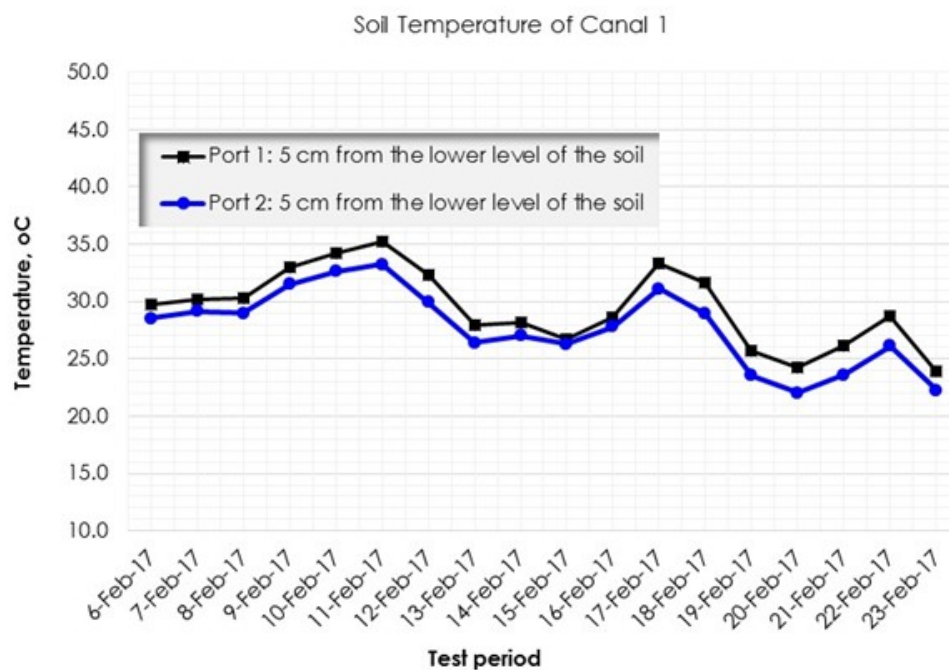


Figure 05.40 - Soil temperature of canal #1 - Stage II/Trial II.

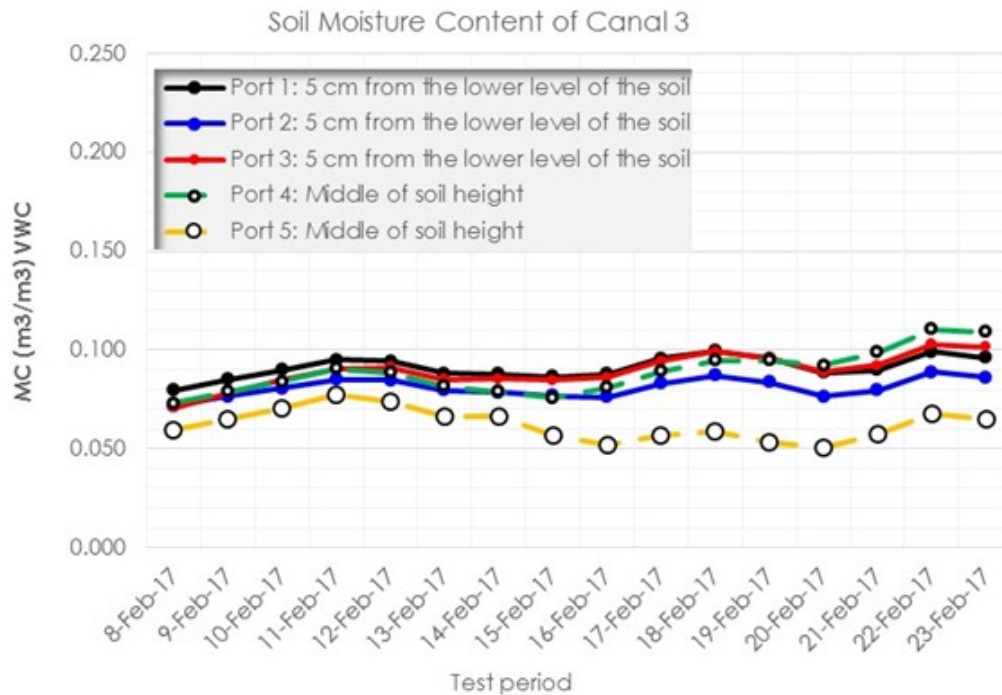


Figure 05.41 – Soil moisture of canal #3 - Stage II/Trial II.

Technical Problems and Recommended Solutions

i. Low moisture level and long moisture build-up period

➤ Reasons:

- Low-grade soil porosity could have prevented the penetration of water vapour. This was perhaps because the soil composition was 72% and 13% clay (as given in Table 05.07).
- Once the lower layer of the soil became wet it developed resistance to the direction of the water vapour path.
- The homogenous distribution of the acrylate in the soil had no significant influence on the build-up of soil moisture. However, having a uniform layer of acrylates in the soil assisted in absorbing moisture. On the other hand, once acrylate absorbs water, a higher pressure is required to compress the acrylate and release the moisture to the soil.

➤ Recommended solutions for main experiment or Trial III:

- Increase soil porosity by mixing perlite and peat moss in the soil.
 - Reason: A lighter soil composition may allow improved soil aeration and moisture build-up (Figure 05.42).

- Using ventilation pipes buried in the soil.
 - Reason: To allow the water vapour generated in the evaporating space of the canal to be uniformly distributed throughout the soil (Figure 05.43).



Perlite



Peatmoss



Soil: Sandy loam



Modified Soil: SLWP

Figure 05.42 - Modified soil to increase porosity - main experiment.



Figure 05.43 - Ventilation pipes below the soil - main experiment.

Main Experiment of SWI (Stage II/Trial III)

All pilot tests and analyses aimed to identify the best conditions for crop sowing and growing in Oman. The main experiment was the occasion to test in the field all previous findings to see their effect across a seasonal cultivation period and to monitor and record all process parameters for future modelling and analysis.

Methodology

- Modifications and re-arrangement of the experimental rig of previous Stage II/Trial II
 - 3 test sections have been constructed and tested inside the greenhouse to have the same climatic conditions.
 - Two test sections were used for SWI with new arrangements (canals 1 + 3).
 - One test section was used for the drip irrigation technique.
- Use of ventilation pipes within the soil to allow the generated vapour in the evaporating space of the canal to be uniformly distributed throughout the soil.
- Select a suitable type of soil for all test sections.
 - The soil type selected was sandy loam, as in the previous experiment.
 - The soil was mixed with peat moss and perlite (soil conditioners) to improve soil porosity and allow a better distribution of irrigation water in the soil.
 - The soil thickness was maintained at 15 cm as per the previous experiment.

Experimentation and Performance Evaluation

- Investigate in the field the use of ventilation pipes, taking into consideration the following design issues:
 - i) That the pipes should be made of PVC to avoid corrosion as they will be in direct contact with water vapour and the soil (also reducing cost).
 - ii) They should have a small size to avoid blocking the area that is required for plant roots as these will try to develop and reach the water, eventually blocking the pipes.
- Monitor soil parameters such as temperature, salinity, and moisture (in at least at three different levels of each test section).
- Monitor water and air incoming temperature and airspeed.
- Crop growth monitoring.

- Record soil, water, and air operating conditions at regular hourly intervals.

Results Analysis of Trial III

The results obtained from the main experiment are as summarised below:

- i. Fast build-up of soil moisture. The soil moisture builds up in channels 1 and 3 (Figures 05.44 to 05.52) which has been demonstrated to be sufficient for crop planting. The main reason related to it was a:
 - a. Low fluctuation in soil temperature helping to build up moisture levels sharply.
 - b. Increasing supplied air flow rate from 36 to 40 m³/h, thereby increasing water vapour penetration.
- ii. Short plant shelf-life at high temperatures. It has been concluded that the soil temperature plays a decisive role during the transplantation period of the plants. After the soil moisture reached an acceptable level suitable for planting, two types of plants were selected for testing, namely tomato and lettuce (as shown in Figure 05.53). Unfortunately, the shelf-life of most of the plants was very short, except for the lettuce in some specific areas of the canal (corners) as shown in Figure 05.47.

From the data presented in Figures 05.46, 05.49 and 05.52, it can be seen that soil temperatures reached 40°C. The effect of such high soil temperatures can be summarised through the following two effects:

- It will increase the level of evaporation of the moisture from the soil (i.e., reducing the build-up of soil moisture).
- It will develop uncomfortable growing conditions for the plants. The germination of most of the vegetables requires temperatures below 40°C as shown in Table 05.09.

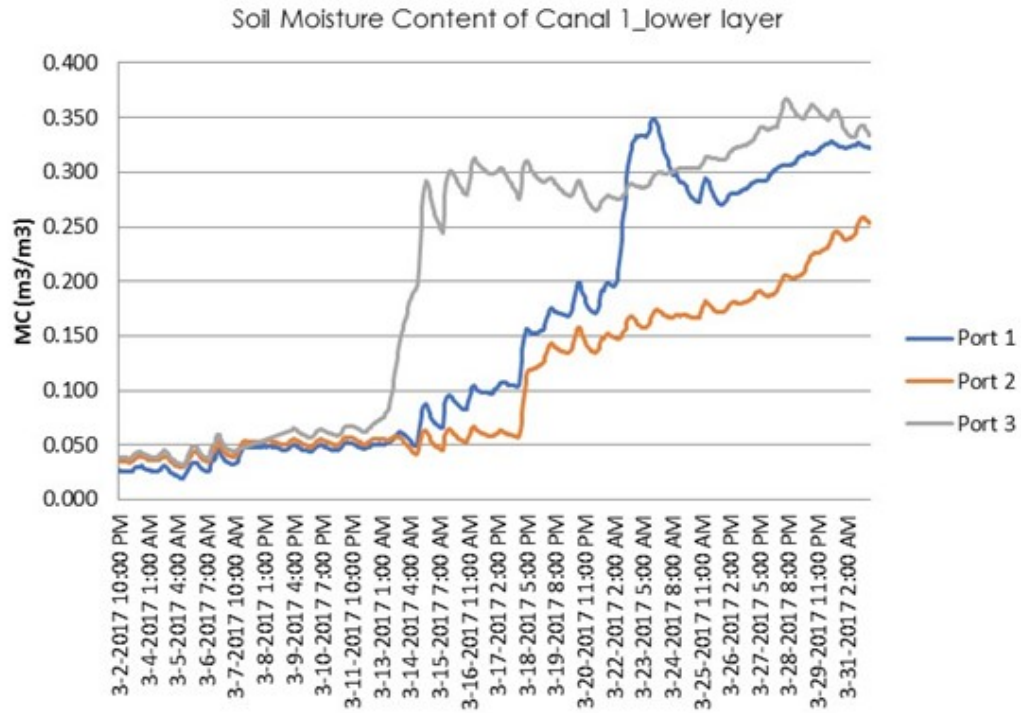


Figure 05.44 - Soil moisture of the lower layer in canal #1- Stage II/Trial III (March 2017).

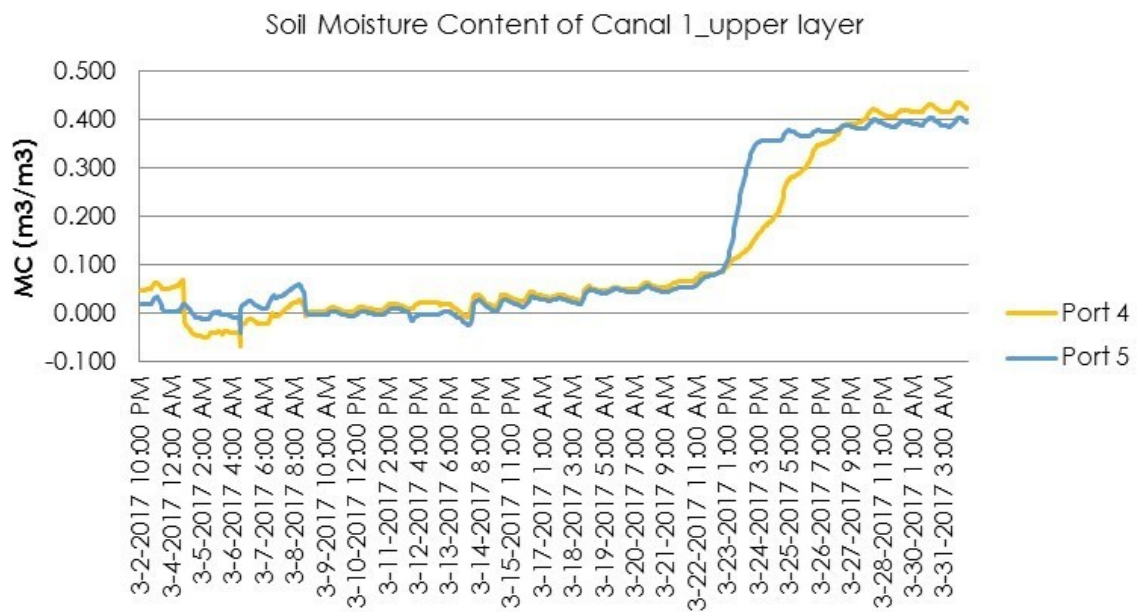


Figure 05.45 - Soil moisture in the upper layer in canal #1- Stage II/Trial III (March 2017).

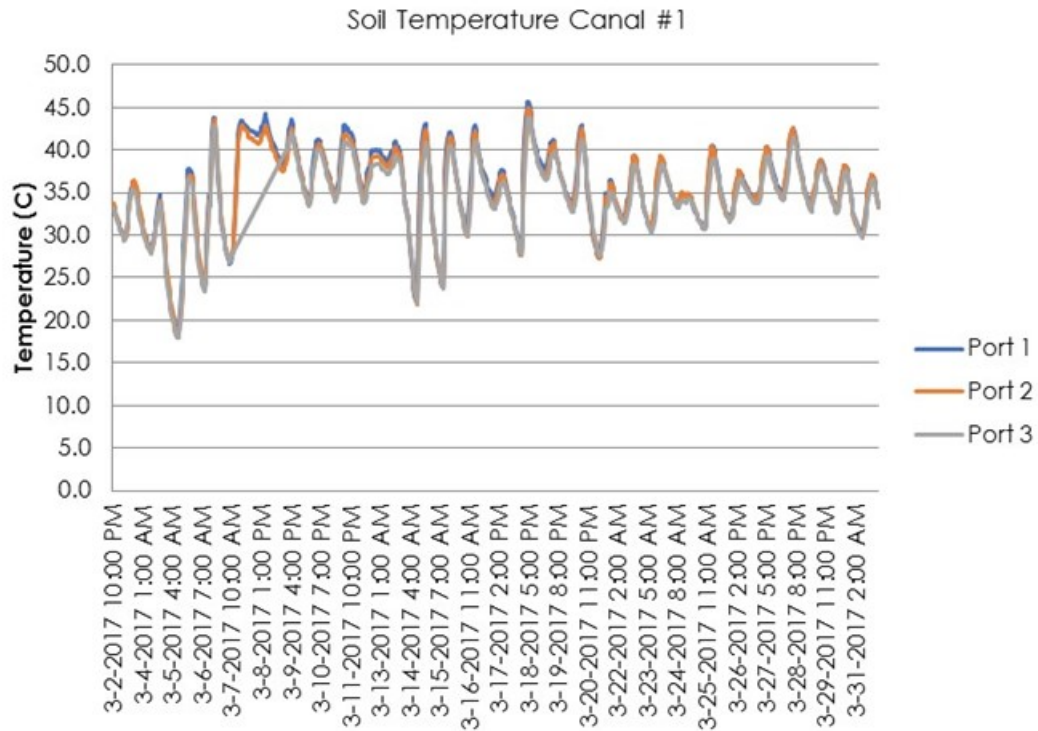


Figure 05.46 - Soil temperature of canal #1- Stage II/Trial III (March 2017).

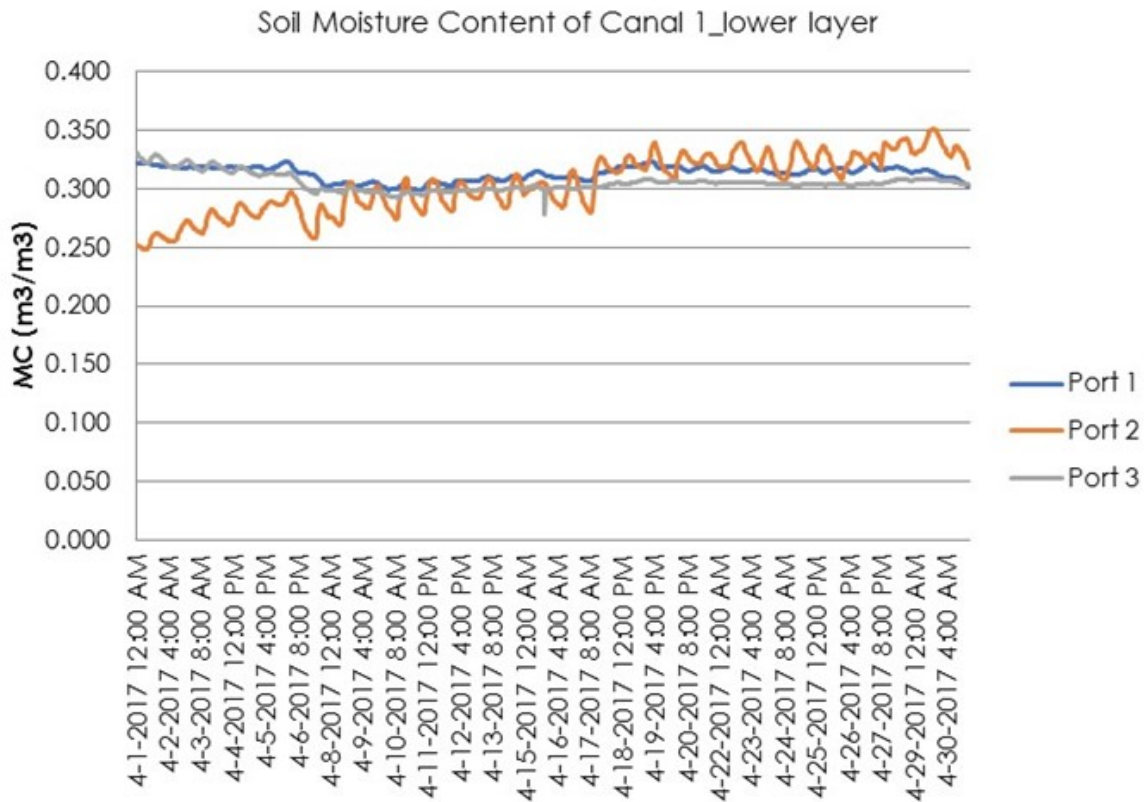


Figure 05.47 - Soil moisture of the lower layer in canal #1- Stage II/Trial III (April 2017).

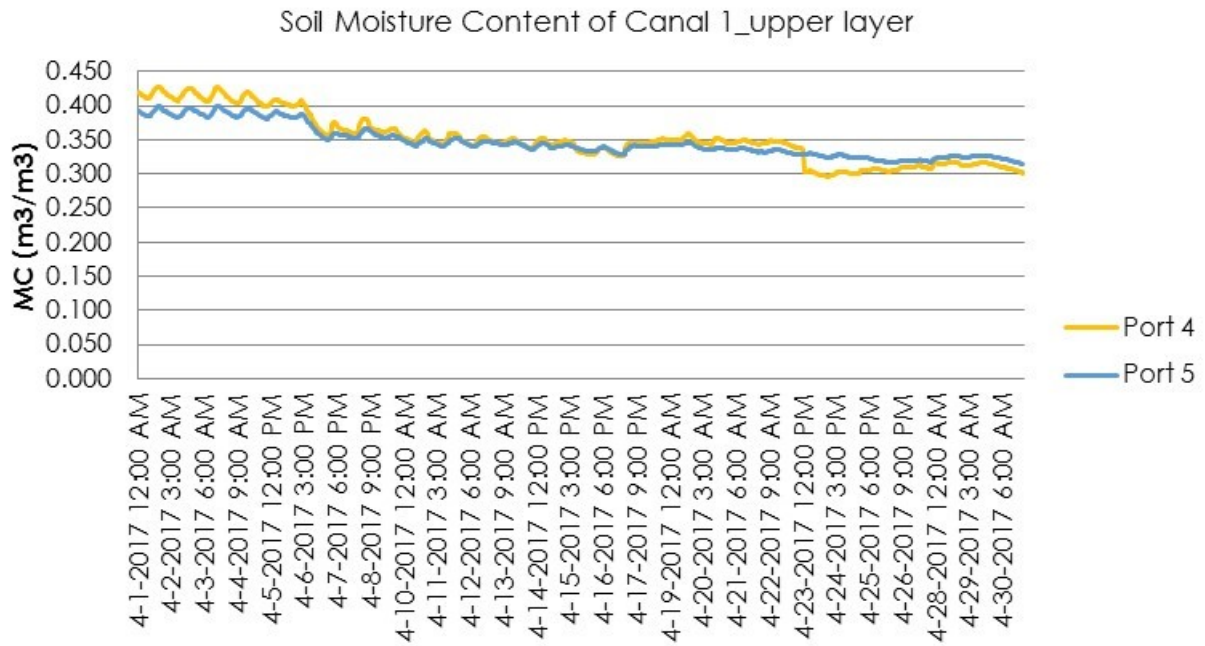


Figure 05.48 - Soil moisture of the upper layer in canal #1- Stage II/Trial III (April 2017).

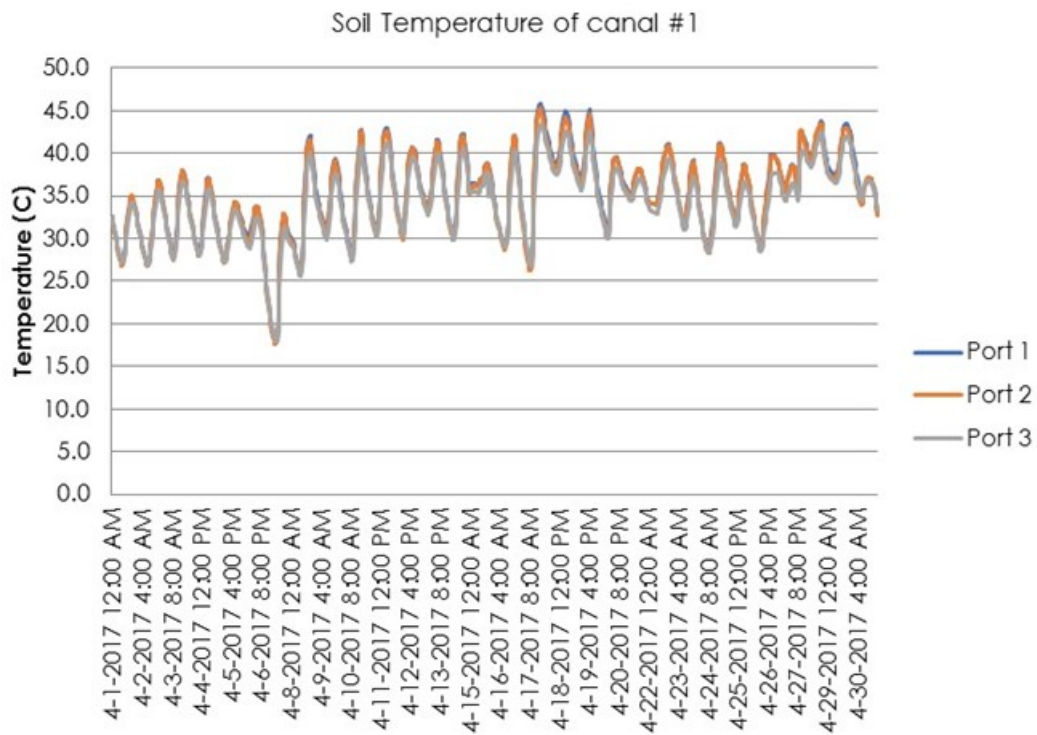


Figure 05.49 - Soil temperature of canal #1- Stage II/Trial III (April 2017).

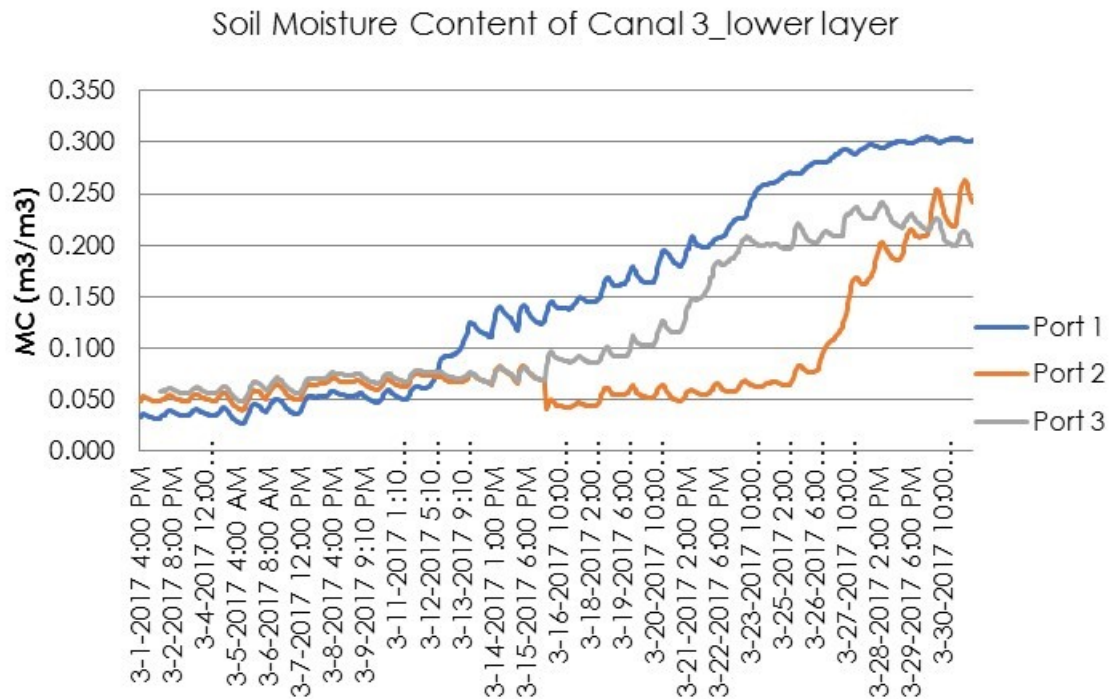


Figure 05.50 - Soil moisture of the lower layer in canal #3 - Stage II/Trial III (March 2017).

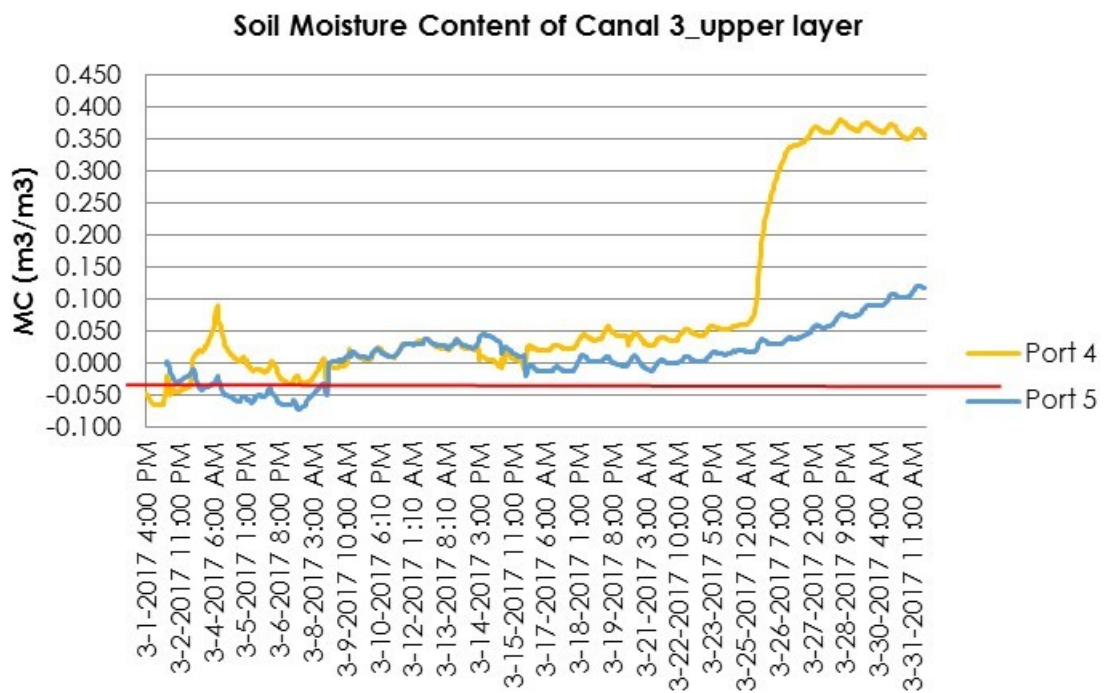


Figure 05.51 - Soil moisture of the upper layer in canal #3 - Stage II/Trial III (March 2017).

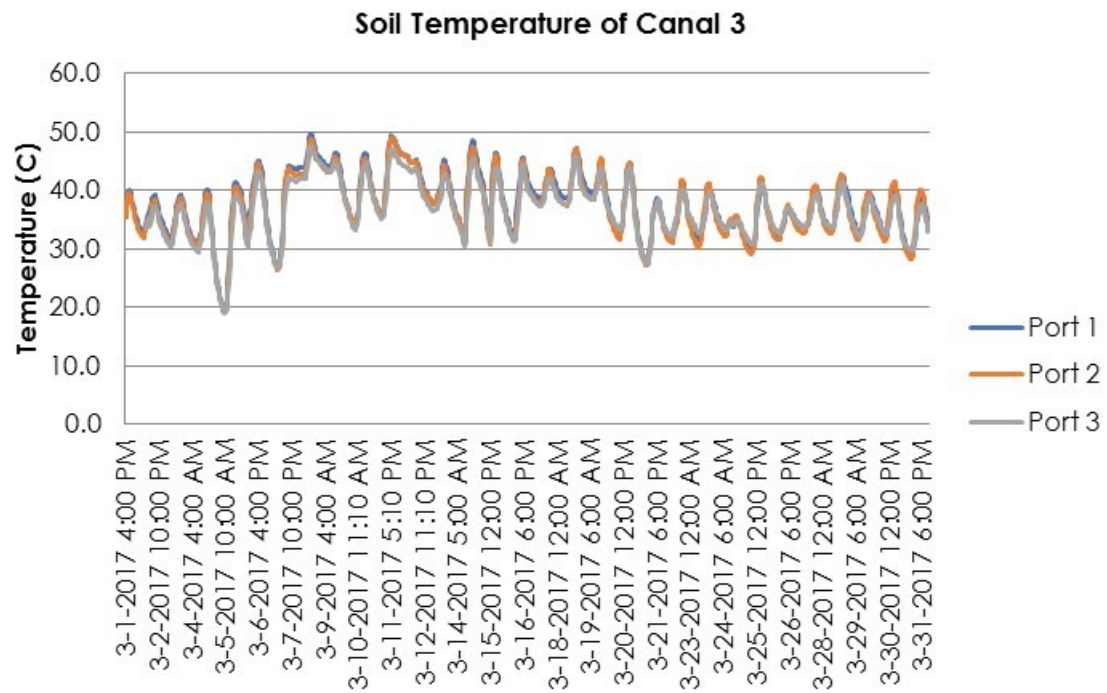


Figure 05.52 - Soil temperature of canal #3- Stage II/Trial III (March 2017).



Figure 05.53 - Transplantation of tomatoes and lettuce in Canals 1 and Canal 3 - Stage II/Trial III.



Figure 05.54 - Lettuce transplantation.

Crop	Minimum	Optimum	Range Optimum	Maximum
Bean	15.5	15.5-29.5	26.6	35
Carrot	4.44	7.22-29.5	26.6	35
Lettuce	1.66	4.44-26.6	23.88	35
Onion	1.66	10-35	23.88	35
Tomato	10	15.5-29.5	29.5	35
Cucumber	15.5	15.5-35	35	40.55

Table 05.09 - Soil temperature conditions for vegetable seed germination (°C) (Harrington et al. 1972).

Technical Problems and Solutions

ii. Short plant shelf-life at high temperature

➤ Reasons:

- High soil temperature due to high incoming water temperature and heat transmission from water vapour to the soil, especially during the hot season and the hottest part of the day.

➤ Implemented solutions:

- Closing the salty water flow rate through the experimental rig when an uncomfortable soil temperature is reached.
- Shut down the heat exchanger to reduce salty water temperature.
- Cool the soil by circulating cold water through coils inside the soil when the soil temperature is too high.

The application of the solutions mentioned above resulted in a significant improvement in tomato and lettuce growth, as shown in Figures 05.55 and 05.56. Similar results were obtained with several other crops indicating a positive outcome of the experiment and a validation of the technology (Figures 05.57, 05.58, and 05.59).

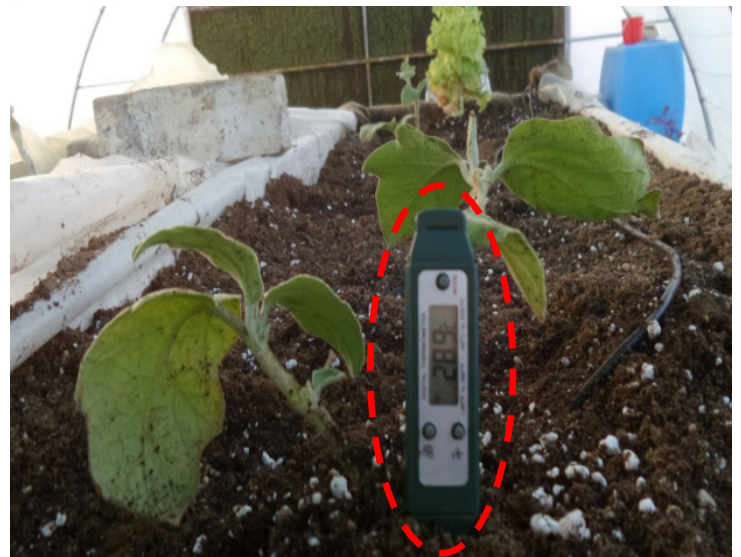


Figure 05.55 - Plants and the soil temperature of main experiment - Stage II/ Trial III.



Figure 05.56 - Stages of growing lettuce - Stage II/ Trial III.



Figure 05.57 - Significant growth of crops - Stage II/Trial III.



Figure 05.58 - Germination stages of the seeds - Stage II /Trial III.

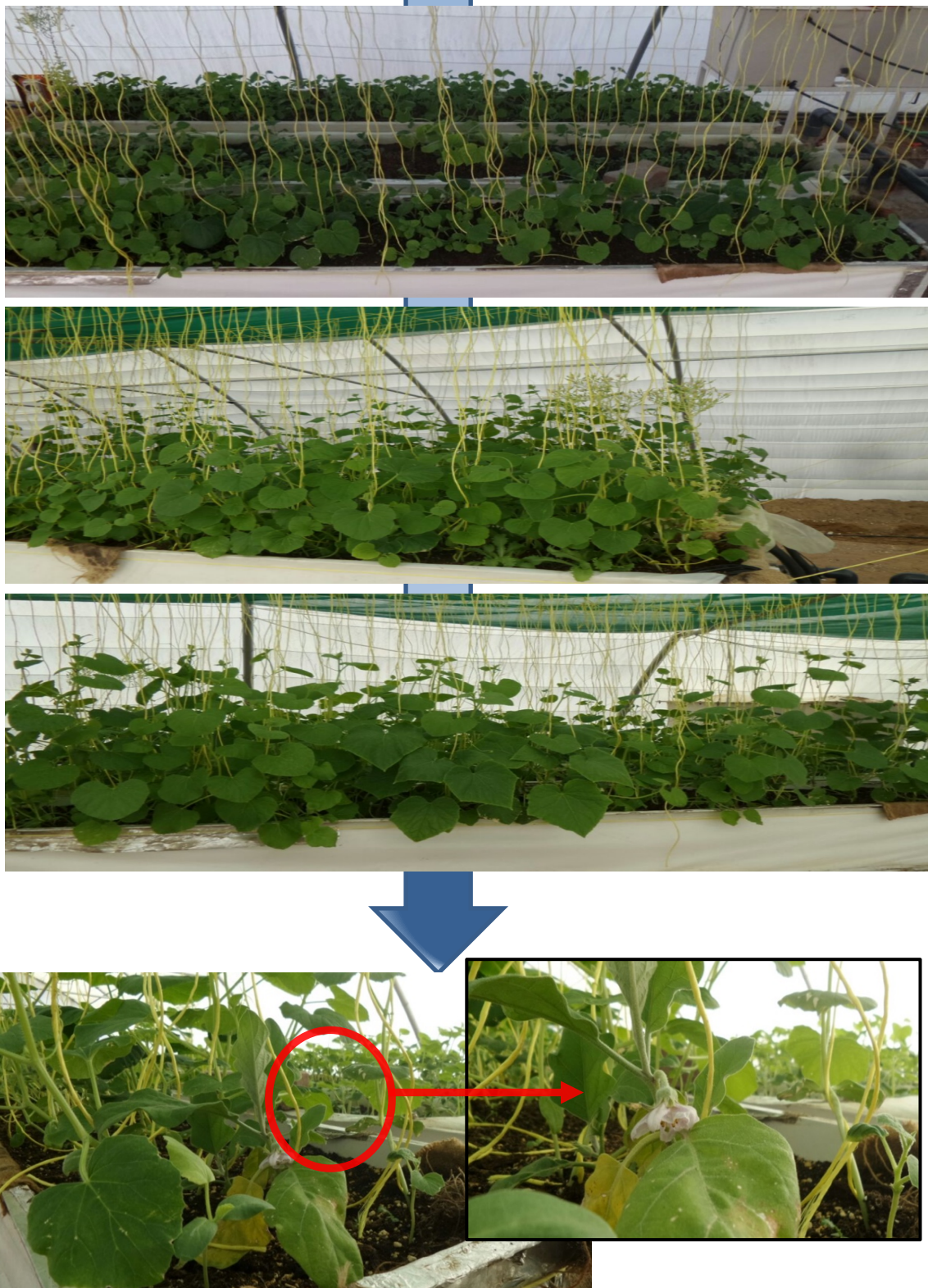


Figure 05.59 - Significant growth of crops in the main experiment - Stage II/Trial III.

5.5.1.3 Seawater Irrigation Project Outcome

The main experimental success was in demonstrating that SWI can be used to grow crops in arid regions and be competitive with drip irrigation approaches, producing irrigation water of sufficiently low salinity. It is capable of building up the soil moisture and is a feasible technology for scaling up to commercial levels of production pending some modifications and improvements. To increase the water productivity per unit area of the system and reduce both operating and capital costs, RES must be used for the power supply (e.g., solar PV panels for powering the pump and air blower/compressor) and employing cheap plastic materials to reduce capital costs. The experiments have also indicated that these techniques are best suited for a controlled environment such as a greenhouse, wherein the operating conditions can be easily kept under control. Greenhouse farming also confers the advantages of increasing water productivity and reducing both operating and capital costs, as well as reducing the growing area required for plants using vertical farming techniques. The achievements of the main experimental project may be summarised as follows:

1. SWI techniques can be practically applied for crop irrigation. The technique has already been tested within real-world operating conditions inside a greenhouse under extreme environmental conditions.
2. Building up soil moisture has been achieved successfully. The collected data and crop growth support this conclusion. It should be noted that it was not possible to reach the harvesting stage of the crops because the project period ended and we were unable to extend this further.
3. Soil moisture is sufficient for seed germination and transplantation.
4. Soil temperature plays an important role during transplantation and should be kept carefully under control.
5. Increasing feed seawater temperature enhances soil moisture by increasing evaporation.
6. Increasing the flow rate of the supplied air greatly enhances the SWI process by increasing the evaporation rate.
7. The soil type, in terms of soil porosity, has a significant influence on the SWI process.
8. It has been concluded that sandy loam soil, the most widespread in Oman, is not suitable for the SWI technique. For this reason, the soil has been modified by increasing its porosity and ability to absorb more moisture. This supports the main conclusion that the soil type in terms of soil porosity and composition has a significant influence on the efficacy of the SWI technique.
9. Mixing the soil with peat moss and perlite (soil conditioners) improves soil porosity and allows a better distribution of irrigation water in the soil.

5.5.2 Experimental Design of SWD

Trials of alternative technologies for seawater desalination were undertaken in Oman together with the development and testing of SWI technologies. Specifically, SWD technologies, including subsurface drip irrigation (SDI), were investigated and, while SWI was addressed to the cultivation of high-value crops, such distillation techniques are mainly directed towards date palm and tree irrigation. The date palm is the primary agricultural crop of Oman and comprises 80% of all fruit crops produced, covering 50% of the total agricultural area of the country (Al-Yahyai et al. 2015). Oman is, in fact, one of the largest producers of dates in the world and there are over seven million date palms that are primarily located within the northern governorates of the sultanate. Traditional cultivation methods are based on small farms as palm cultivation is a labour-intensive industry that makes a valuable contribution to improving and sustaining livelihoods, especially in poorer rural areas. Unfortunately, due to the lack of available fresh-water for irrigation, most of these farms have since been abandoned and date palms are left to die.

Date palms not only constitute a vital socio-economic cultivation for Oman, but also provide numerous environmental benefits such as resistance to land erosion (FAO 2012) and thus play an essential role in the fight to stave off climate change, as these trees absorb greater amounts of carbon dioxide than many other trees due to their large size (Sharif et al. 2010). Among all the crops cultivated in Oman, date palms are the primary consumers of water, followed by Rhodes grass and alfalfa along with other fruits and vegetables. In 1998, the date palm trees consumed 558,000,000 m³ of water, accounting for 38% of total irrigation water (Al-Mulla et al. 2017). Besides dominating the irrigation water supplies, 84% of date palm trees are currently irrigated utilising a flooding irrigation system that leads to a loss of half the water supplied. This may occasionally rise to as much as 60% when the soil is of heavy texture. Modern irrigation systems are growing in popularity for date palms (FAO 2008), yet they are not widely used. Drip and bubbler irrigation methods predominate, while sprinkler and micro-sprinkler irrigation systems are not commonly deployed despite their popularity in neighbouring countries, especially on sandy soils where palms are widely grown. The question of how much water date palms use is a crucial one, particularly in arid countries, both for individual farmers seeking to maximise their income and for governments who wish to plan the best use of their limited water resources. Unfortunately, there are few published studies on water consumption by date palms and the data available is mostly theoretical. Consumption patterns are heavily influenced by many parameters, including palm type, age, soil type, year, season, location, etc. Scientists for the Omani Ministry of Agriculture calculated that, in 2015, a typical date palm cultivated using traditional flood irrigation techniques will use 60 litres of water a day in cooler months and up to 210 litres daily

during the height of summer. However, it should be noted that SDI cuts consumption dramatically, and scientists suggest that the use of SDI could reduce water consumption by as much as 60%. Delivering water through pipes directly to the trees' roots prevents evaporation, percolation and other losses commonly incurred as water moves through the irrigation furrows associated with traditional watering methods. Newer SWD techniques based on MD and enhanced evaporation have been experimented with in Oman to seek a viable alternative to the current inefficient flood irrigation techniques in use, especially as regards whether they are competitive or can be integrated with actual drip irrigation systems.

5.5.2.1 Scope, Objectives and Timeline

This project has involved the construction, installation and field trials of SWD techniques for growing date palms and trees. The initial idea of using MD as a source of fresh-water was abandoned after a few negative results and this technology was replaced by experimental trials using simultaneous evaporation and condensation processes enhanced by hot air injection to produce low-cost fresh-water suitable for drip irrigation.

The following objectives have been addressed in the experimental work:

- a) Application and investigation of a low capital cost SWD technique.
- b) Systematic examination of the performance of this technique.
- c) Identification of the parameters that influence the performance of the SWD unit.
- d) Evaluate the feasibility of using the technique for practical applications.
- e) Identification of areas that can be developed to improve the performance of SWD.
- f) Determination of the optimal operating conditions to increase potable water production via this technique.
- g) Identification of the optimal environmental conditions for the best thermal performance of the technique.

The timeline of the experiments and primary objective of investigation was as reported in Table 05.10

<u>Stage</u>	<u>Part I</u>	<u>Investigation</u>	<u>Timeline</u>
STAGE I	Trial I	Investigate MD unit	Q4. 2016
STAGE II	Part I	Investigate simultaneous evaporation and condensation processes	Q3. 2016
	Part II	Investigate simultaneous evaporation and condensation processes	Q1. 2017

Table 05.10 – SWD – Project timeline and partial objectives of SWD.

5.5.2.1 Stage I: MD unit

In this stage, an existing and consolidated water distillation technology, such as solar MD, was applied with the basic idea of reducing evaporation and distributive losses of fresh-water to date palms and trees and to organise a micro-desalination system using small MD units situated in close proximity to the trees and date palms (Figure 05.60).

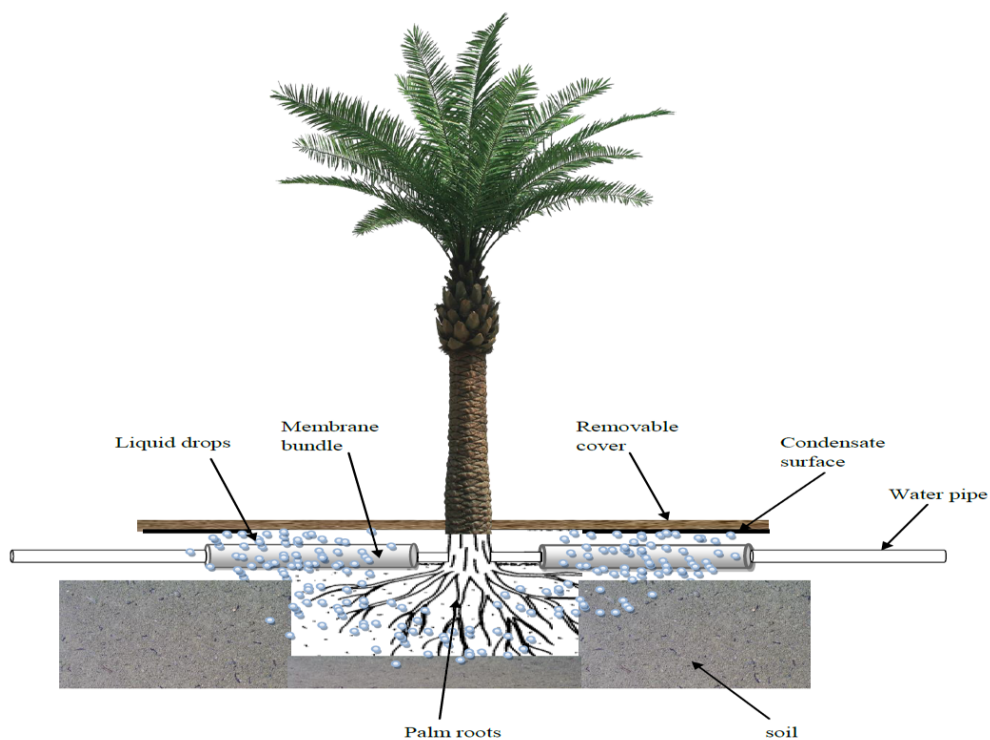


Figure 05.60 – SWD – Localised MD - Stage I.

MD is a thermally driven membrane separation process in which only vapour molecules are transported across porous hydrophobic membranes. The driving force is the vapour pressure difference arising between the hot liquid feed side and the cold permeate side of the membrane

(Alkhudhiri et al. 2011). The main competitive advantage of MD is that distillation occurs below the boiling point of the feed solution. The DCMD used in this trial is the simplest known MD configuration, wherein the hot solution (feed) is in direct contact with the hot membrane side surface (Figure 05.61). Therefore, evaporation takes place at the feed-membrane surface, and the vapour is moved by the pressure differential across the membrane to the permeate side where it condenses inside the membrane module. Because of the hydrophobic characteristics, the feed itself cannot penetrate the membrane (as only the gas phase can exist within the membrane pores).

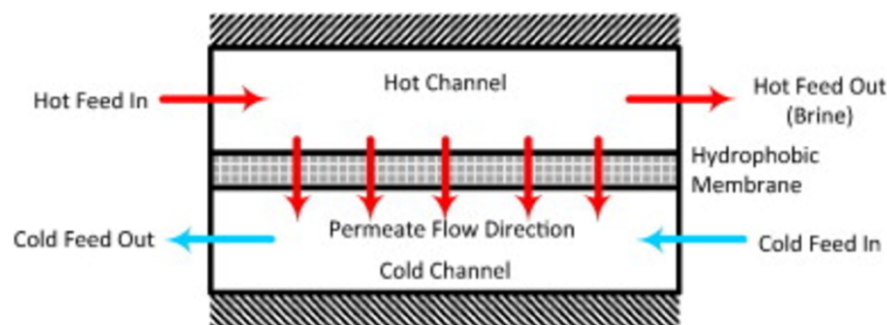


Figure 05.61 - Direct contact membrane desalination unit (DCMD).

Small size DCMD membranes appear to be a suitable application although, after several trials, the results were not encouraging. It has since been discovered that DCMD presents the following disadvantages when used in small units:

- Low productivity – productivity of DCMD is minimal and, to achieve a suitable production rate, a large membrane surface area is needed.
- High costs – despite the MD unit being a well-researched technique, it is still not a cost-effective technology for date palm/tree irrigation as compared with current soil irrigation techniques.
- Short membrane shelf-life – the membrane's durability is questionable as the membrane loses its hydrophobicity after a short time (after less than six months of use), rendering the technique both impractical and expensive as the cost of the membrane is high.

Since the project aimed to identify and investigate a low-cost and straightforward irrigation method for date palms and trees, follow-up MD studies were abandoned and a new technique employing an enhanced water evaporation system with a controlled aeration process was considered as an alternative solution. In this configuration, the water produced is collected in the first stage and drip irrigation may be applied subsequently.

5.5.2.2 Stage II: Simultaneous Evaporation and Condensation Processes (Part I)

To address the limitations of the MD unit of stage I, a new idea was implemented to meet the project objectives. The novelty of the concept is based on the simultaneous evaporation and condensation of water vapour produced in an enclosed space due to the heating and humidification of the surrounding air passing through hot seawater (a controlled aeration process).

To investigate the performance of the concept, a small test prototype of 0.5 m (width) x 0.25 m (depth) x 5 m (length) has been designed and constructed (Figures 05.62 - 05.63).

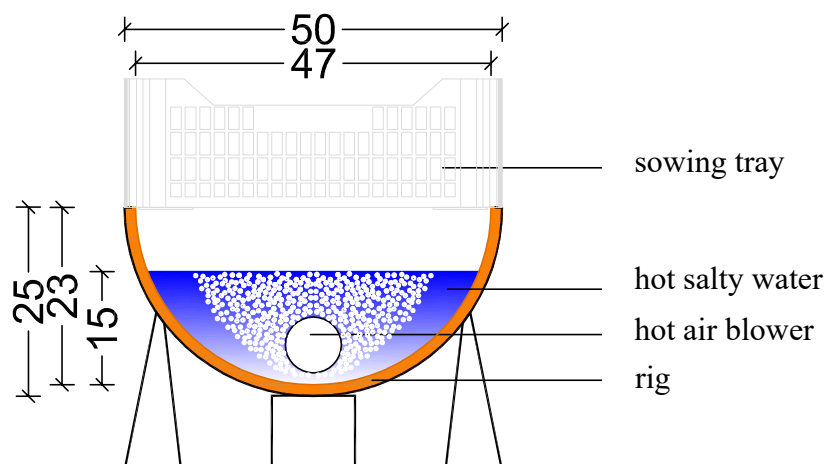


Figure 05.62 – Rig dimensions [cm] of prototype of SWD - Stage II/part I.



Figure 05.63 – Image of prototype of SWD - Stage II/part I.

The prototype is designed to have a tent shape to increase the contact surfaces area for the water vapour. A metal structure is used to affix the plastic sheets and serve as a suitable frame that can withstand the air flow pressures. The prototype was equipped with sensors to measure the water temperature, air temperature, and RH at different locations as depicted in Figure 05.64. These sensors will help to analyse the unit's performance and refine this technique.

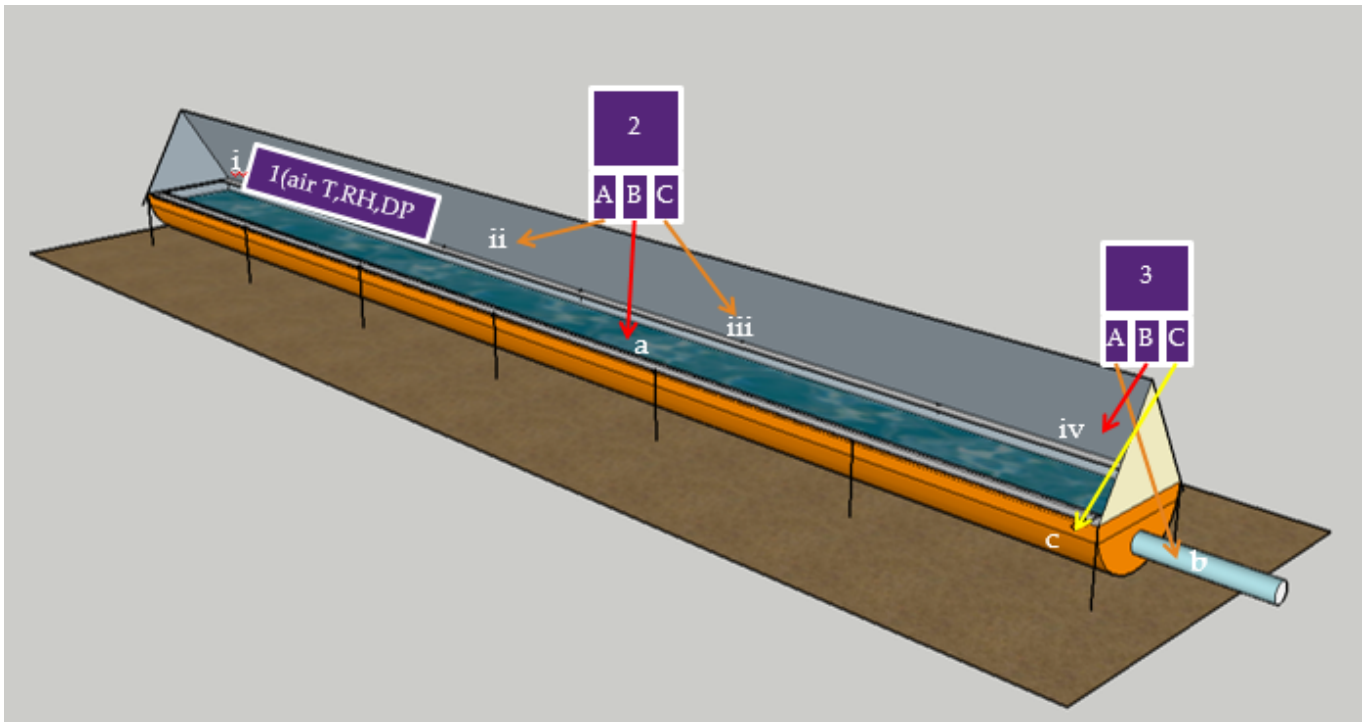


Figure 05.64 - Prototype A of SWD– inside the greenhouse plus sensors (rig design) - Stage II/part I.

It was decided that two prototypes should be constructed for better evaluation. Prototype A was deployed inside the greenhouse, while prototype B was positioned outside the greenhouse. Prototype A (Figure 05.65) was tested without the mesh and drip water cooling system, while prototype B (Figures 05.66 - 6.67) was equipped with a textile mesh and drip cooling water system. The purpose of using a wet textile mesh outside the tent was to create a cold layer that could accelerate the water vapour condensation process.



Figure 05.65 - Prototype A of SWD - inside the greenhouse plus sensors (real)- Stage II/part I.

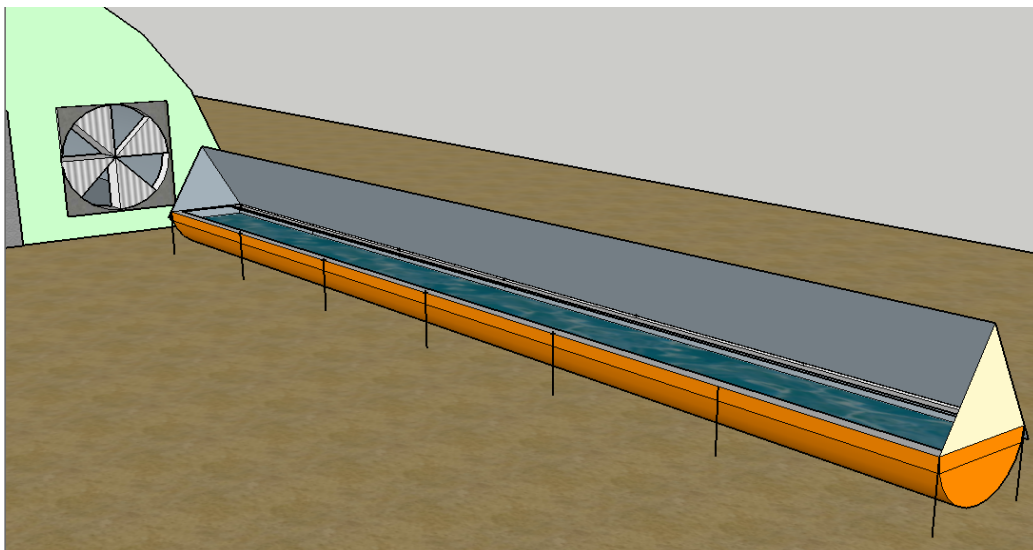


Figure 05.66 - Prototype B of SWD I - outside the greenhouse (rig design) - Stage II/part.



Figure 05.67 - Prototype A of SWD - outside the greenhouse (real) - Stage II/part I.

The experimental test was run with the following operating conditions:

- Hot water flow rate: 1.25 m³/h
- Air flow rate: 55 m³/h
- Air compressor power: 2.2 kW
- Incoming water temperature: 35°C
- Air Temperature (IGH): 28-42°C
- Air Temperature (OGH): 30-52°C
- RH (IGH): 55-85%
- RH (OGH): 49-52%

The results obtained in this stage are summarised in the following figures. The data presented in Figure 05.68 shows that prototype A's productivity fluctuated during the test period. This is expected behaviour due to the variation in environmental conditions represented by air dry bulb temperature and air RH.

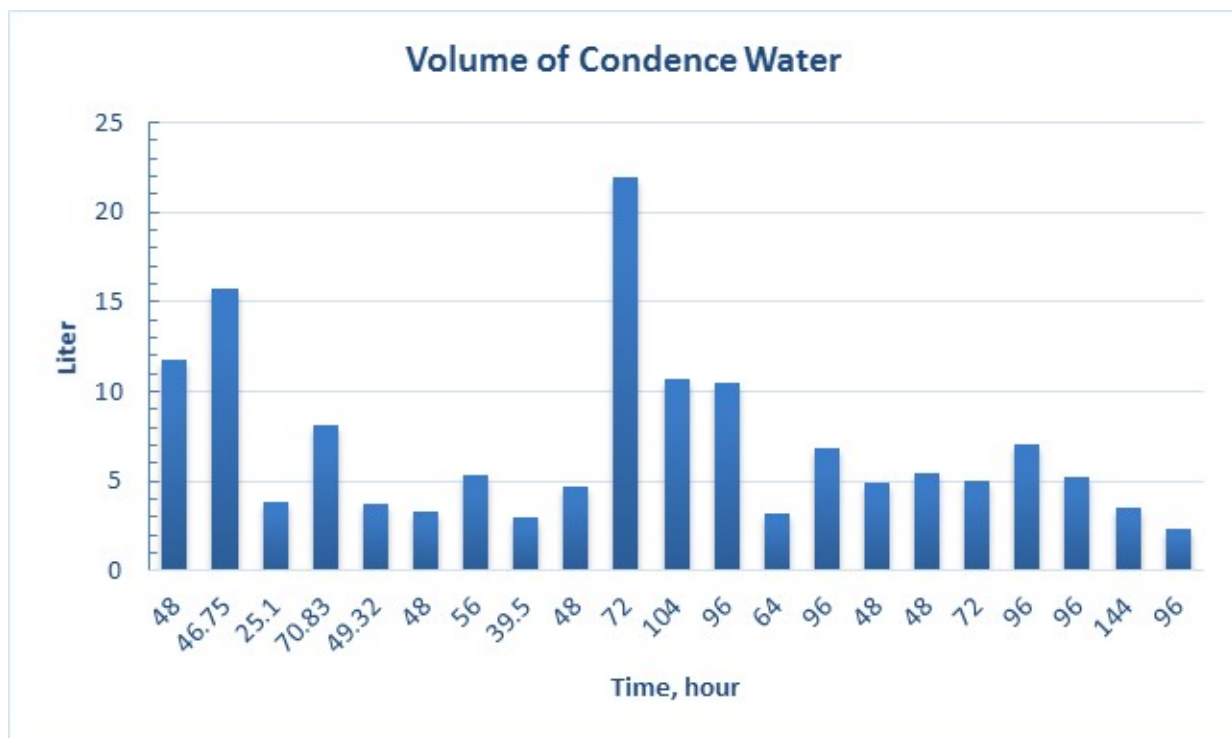


Figure 05.68 - Prototype A of SWD - volume of condensate water - Stage II/part I.

Despite the low incoming seawater temperature (average temp. 35°C as shown in Figure 05.69), the fresh-water collected by this technique was at an acceptable level under these operating conditions.

The collected water reached a maximum yield of 8.06 l/day (3.22 l/m² day) with an average value of 2.69 l/day (1.07 l/m² day) as revealed in the daily performance of prototype A. The collected water from prototype B was less than that of prototype A, but this was mainly because prototype B was not perfectly sealed, causing the vapour to escape and reduce the evaporating rate.

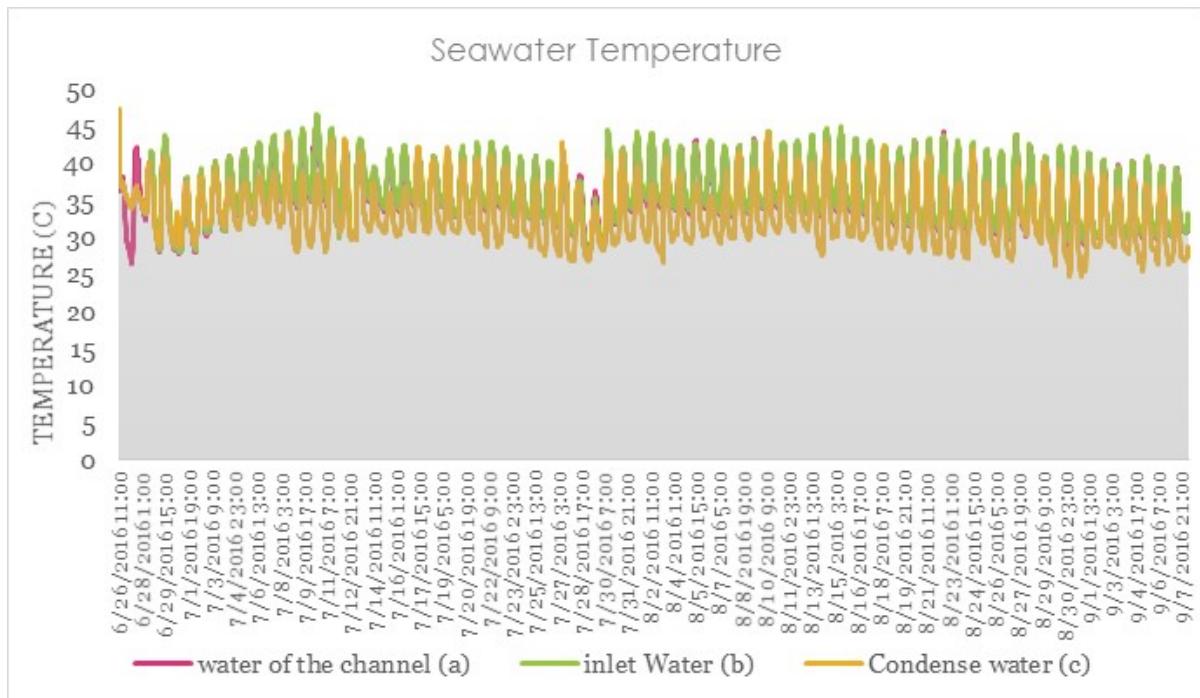


Figure 05.69 - Prototype A of SWD - seawater temperature - Stage II/part I.

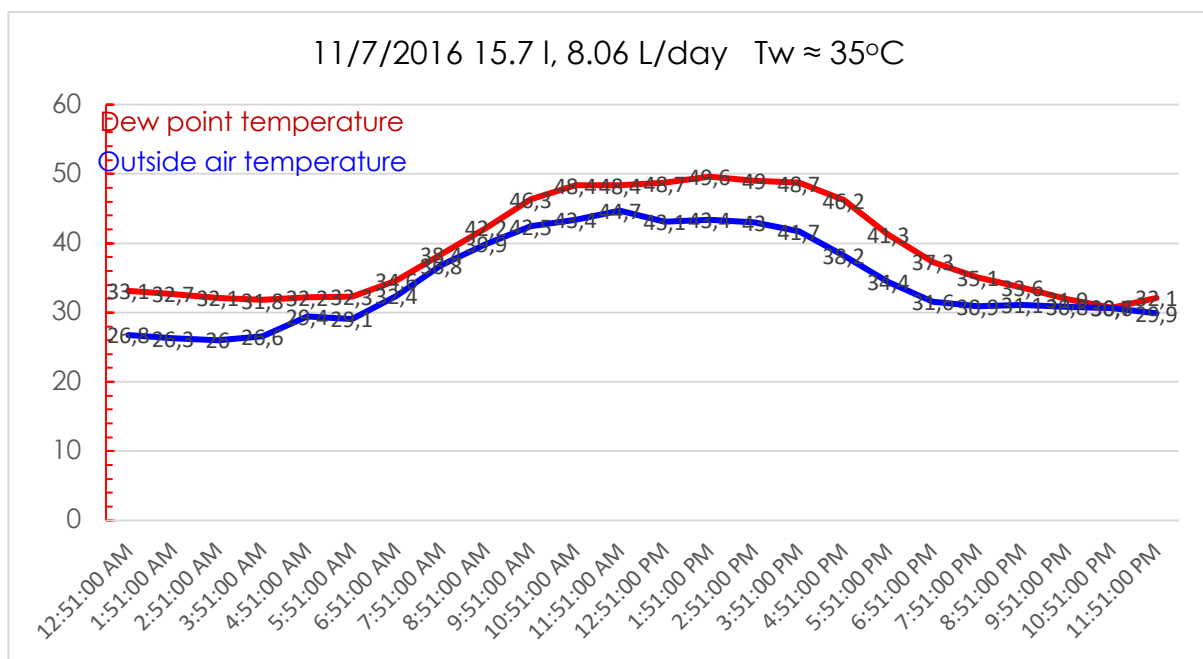


Figure 05.70 - Prototype A of SWD – daily performance - Stage II/part I.

The results obtained are indicative of the potential of the SWD technique as summarised below:

- ✓ The air temperature inside the tent and the relative humidity (RH) faced a significant increase as compared to the temperature of the surrounding air. This is a clear indicator of the performance of the evaporating process. Since this technique depends on simultaneous evaporation and condensation of water vapour produced in an enclosed space, the system's productivity is strongly dependent on increasing the evaporation rate inside the tent. Three important factors may be used to evaluate the evaporating process; specifically the air temperature, flow rate and the RH inside the tent. The higher the air temperature, flow rate and RH, the higher the evaporation rate.
- ✓ The slight difference arising between the dew point temperature of the air inside the tent and the external air dry-bulb temperature (2-8°C) affected the condensation rate significantly (Figures 05.71, 05.72 and 05.73). Increasing the difference will increase the condensation rate.
- ✓ The feed seawater temperature has a significant effect on the condensation rate as it directly impacts the air dry-bulb temperature inside the tent.

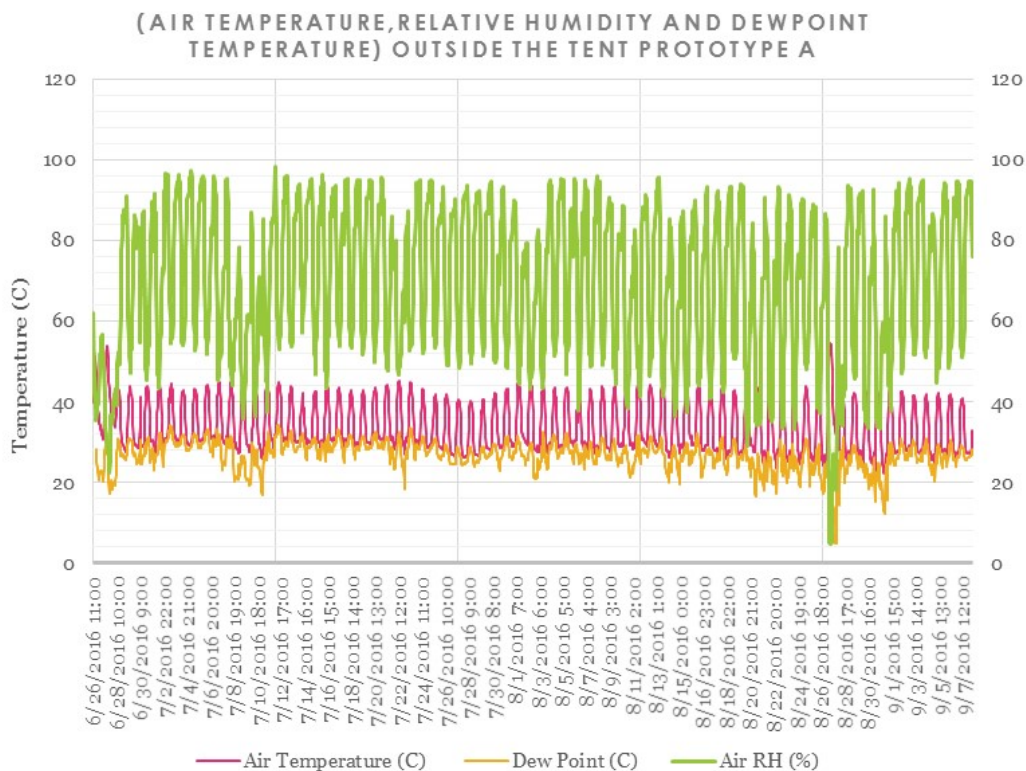


Figure 05.71 - Prototype A of SWD - air properties outside the tent - Stage II/part I.

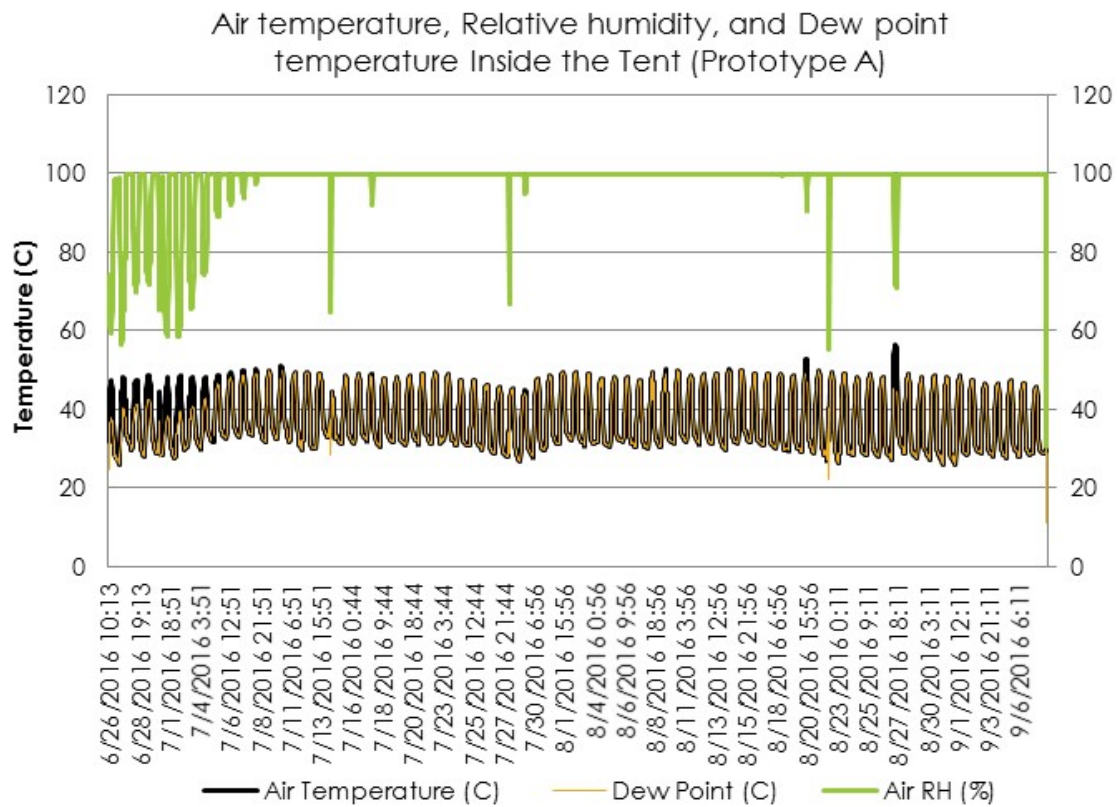


Figure 05.72 - Prototype A of SWD - air properties inside the tent - Stage II/part I.

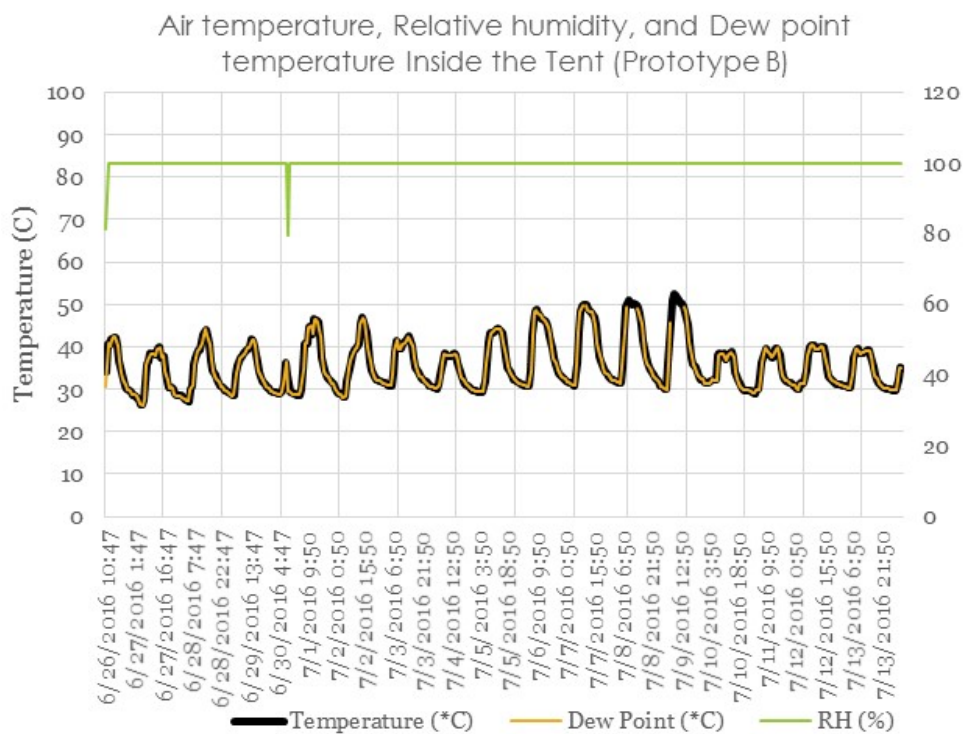


Figure 05.73 - Prototype B of SWD - air properties inside the tent - Stage II/part I.

In general, the proposed water collection technique utilised in Stage II/Part I failed to reach the targeted productivity as reported in the overview of results presented in Table 05.11.

After carefully studying and analysing the experimental data, it was found that the production of water by this technique is strongly influenced by the:

- i) Seawater feed temperature in a non-linear manner; and,
- ii) Surrounding environmental conditions represented by the air dry-bulb temperature in an inverse relationship.

In other words, the evaporation process can be enhanced by increasing the seawater feed temperature and this can easily be achieved using a direct solar thermal heating system.

The condensation process can also be enhanced by cooling and using a SAP such as acrylate to absorb the water vapour. The system should be designed for the SAP to absorb the water vapour of the incoming humid air from the water evaporation unit, as this could help to enhance performance efficiency of the whole system by cost-effectively increasing the water yield.

In addition, it was found that the durability of the plastic sheets was poor and so it was decided to use thicker and harder plastic sheets to resolve this issue.

Summary of Seawater Distillation Project (Stage II/ Part I)

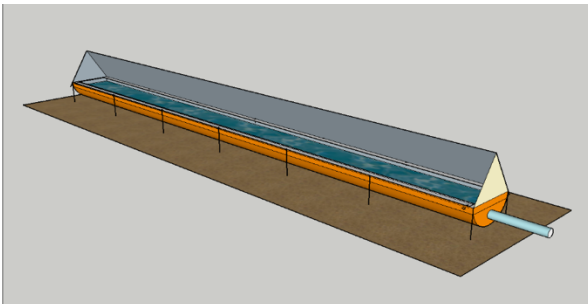
	SWD STAGE II /PART I	
<p>Utilisation Material:</p> <ul style="list-style-type: none">Plastic sheets type: Nylon 1mm ThickCanal size: 5 m x 0.5 m x 0.25 mPiping system: PVC, 1’’ ODSupply air equipment: Compressor <p>Operating Conditions:</p> <ul style="list-style-type: none">Hot water flow rate: 1.25 m³/hAir flow rate: 55 m³/hAir compressor power: 2.2 kWWater temperature: 35°- 50°CAir Temperature (IGH): 28°C-42°CAir Temperature (OGH): 30°C-52°CRH (IGH): 55-85%RH (OGH): 49-52% <p>Technical Information:</p> <ol style="list-style-type: none">Durability of the sheets lowProductivity lowWater salinity acceptable <p>IGH: Inside the greenhouse - PROTOTYPE A OGH Outside the greenhouse - PROTOTYPE B</p>	<div><div>8.6 l/day</div><div>Productivity</div></div> <div><div>7.8</div><div>pH</div></div> <div><div>2.5 m²</div><div>Evaporation area</div></div> <div><div>0.84 ds/m</div><div>Conductivity</div></div> <div><div>7 m x 2.5 m x 2 m</div><div>Required space</div></div> <div><div>32 l/day</div><div>Productivity [target value]</div></div>	
<p>Feasibility Remarks:</p> <ol style="list-style-type: none">Practically not feasible due to lower productivity value rate.Produced water is not sufficient for surface water irrigation.Direct exposure to the sun affected the durability of the Tent’s material (Nylon).		

Table 05.11 - SWD– results of experimental work - Stage II/part I.

Other technical solutions have been introduced into the system and were tested in Stage II/Part II, all of which were oriented to increase the productivity and shelf-life of the unit. Some of the implemented modifications and their expected improvements are listed in the following Table 05.12:

Recommended Solution	Functionality	Expected Results	STAGE II
Wetting the shading textile mesh layer	Creating an efficient condensation surface	<ul style="list-style-type: none"> Creates a condensation layer that could accelerate water vapour condensation process. 	PART I
Using new and strong plastic sheet for the tent	Making a larger evaporating space	<ul style="list-style-type: none"> Increase operating lifetime of the sheet and the unit. 	PART II
Shading the tent (see Figure 05.67)	Reducing the tent surface temperature	<ul style="list-style-type: none"> A cavity of natural convection will be developed between the wall and the shaded surfaces. 	
Increasing seawater feed temperature	Increases the evaporation rate	<ul style="list-style-type: none"> Increase the water vapour dew point temperature to be above the outside dry bulb temperature. Allowing the air to hold more moisture. 	
Increasing air flow rate	Increases the evaporation rate	<ul style="list-style-type: none"> Increase the amount of water vapour content in the air. 	

Table 05.12 - Recommended modifications to enhance the productivity of the SWD technique - Stage II/part II.

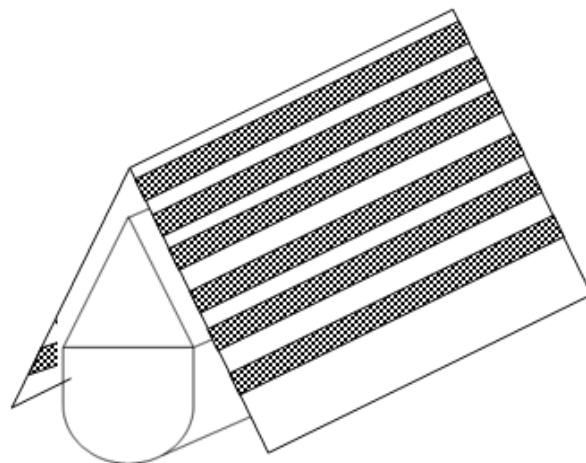


Figure 05.74 - Sketch of the proposed shaded shell of the tent.

5.5.2.3 Stage II: Simultaneous Evaporation and Condensation Processes (Part II)

After analysing the results from the first pilot experiment and implementing the required modifications to the system's configuration, the second part of the experiment was devoted to investigating the possibility of enhancing the underperformance of the previous distillation unit.

Methodology

- Construction of a new test rig to be used for testing inside the greenhouse.
 - *Nota bene*: due to the high velocity of the air leaving the fan, it was decided to support the tent with a more robust structure (Figures 05.75 and 05.76).
- It was decided to reconstruct the second test rig so as to be identical to the new one for a better evaluation procedure.
- The indoor test rig was first tested without mesh and drip water cooling system and afterwards it was then equipped with a drip water cooling system.
- To minimise water losses from the system it was decided to seal the rig to avoid vapour escape and leakage.

Experimental and Performance Evaluation

- Monitor the air temperature inside the tent.
- Investigate the effect of air flow rate and temperature on the evaporation rate.
- Investigate the influence of feed water temperature on water production.
- Evaluate the impact of environmental conditions on the evaporation and condensation processes.
- Record all the operating conditions of water and air twice per day.

The recommended technical solutions, as suggested by previous results, needed to enhance the performance of the distillation unit have been implemented and are as described below in Table 05.13.

No.	Technical solution	Modifications	Target
1.	Increasing supply seawater temperature	<ul style="list-style-type: none"> ▪ Adding two 300W electrical heaters ▪ Installing heat pipe system as a solar collector system 	<ul style="list-style-type: none"> ▪ To be able to increase and control the water temperature. It was possible to increase and control the water temperature to reach 70°C. ▪ Using solar energy to increase seawater feed temperature.
2.	Decreasing the contact air temperature at the outer surface of the tent (i.e., cooling)	<ul style="list-style-type: none"> ▪ Shading the tent using plastic mesh cover as a shell layer 	<ul style="list-style-type: none"> ▪ Creating a cavity in which a natural convective layer can be developed, which could enhance cooling of the outer surface of the tent.
3.	Decreasing the water level inside the canal of the tent	<ul style="list-style-type: none"> ▪ Lowering the supply water pipe by 5 cm 	<ul style="list-style-type: none"> ▪ Lowering the seawater level inside the canal of the tent. This would prevent the generated air bubbles from carrying salinity to the condensate surface as well as avoiding overflow.
4.	Increasing the contact surface area for both evaporation and condensation	<ul style="list-style-type: none"> ▪ Design and construct a bigger tent frame structure 	<ul style="list-style-type: none"> ▪ The greater the contact surface area, the greater the condensation rate.
5.	Using a thicker and harder plastic sheet	<ul style="list-style-type: none"> ▪ Installing the acrylic sheet which has: ▪ Modulus of Elasticity of 30,000 kg/cm³ ▪ High working temperature up to 85°C ▪ Specific gravity of 1.19 	<ul style="list-style-type: none"> ▪ Increasing the prototype's durability. ▪ Provide better thermal conditions. ▪ Developing a prototype that could withstand the local harsh environmental conditions.
6.	Increasing air flow rate	<ul style="list-style-type: none"> ▪ Installing a new air blower with lower power consumption and high air flow rate 	<ul style="list-style-type: none"> ▪ Increasing evaporation and the amount of water content in the air.

Table 05.13 - Technical solutions, required modifications, and their targets for Stage II/Part II.



Figure 05.75: Frame structure of Prototype A (tent inside the greenhouse).



Figure 05.76: Acrylic sheets used for constructing the tent.

Analysis of Results from Stage II/Part II

The obtained results are summarised as follows:

- i. Significant increase in water productivity. New tests have been carried out and partial data are presented in Figure 05.77 showing a considerable increase in the new unit's water productivity. The rate of water produced was higher than for the previous test, reaching an average value of 27 L/day (10.8 L/m² day) with a very low level of conductivity and mid-range pH (7.2). There were some days in which the tests were stopped for additional modifications.

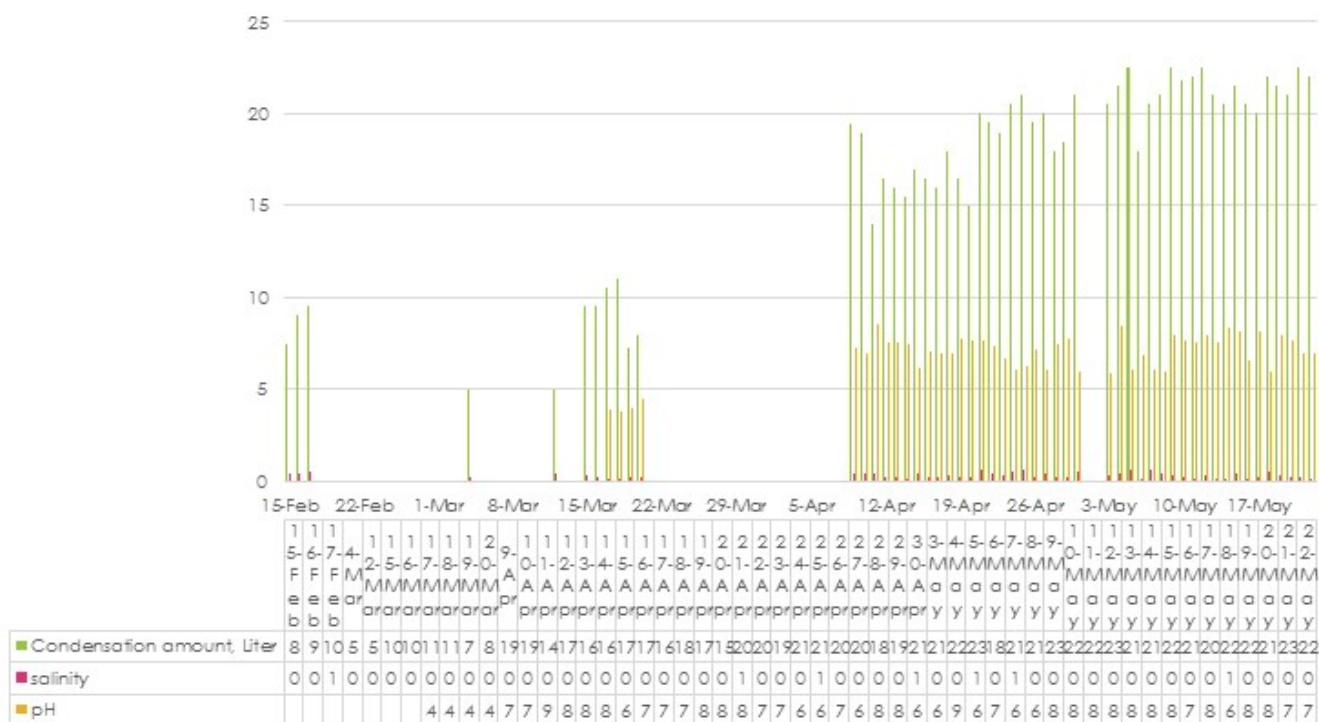


Figure 05.77 - Condensate water inside the tent and its physical properties - Stage II/Part II.

ii. Lowering the air temperature inside the greenhouse increases water productivity.

Owing to the higher air temperature inside the greenhouse, it was decided to cover the external part of the greenhouse with a gypsum layer as shown in Figure 05.78. This was intended to reduce solar irradiation and consequently lower the air temperature inside the greenhouse from 69 °C to 48.5°C.



Figure 05.78 - Gypsum protective layer over the sheets of the greenhouse - Stage II/Part II.

Cooling the air inside the greenhouse by 30% resulted in a *circa* 22% increase in the condensation rate (equivalent to an additional 6 L/day or 2.4 L/m² day). Lowering the air temperature of the greenhouse will accelerate the condensation rate where the air temperature falls below the dew point. Figure 05.79 shows the creation of water droplets on the rig tent surface.

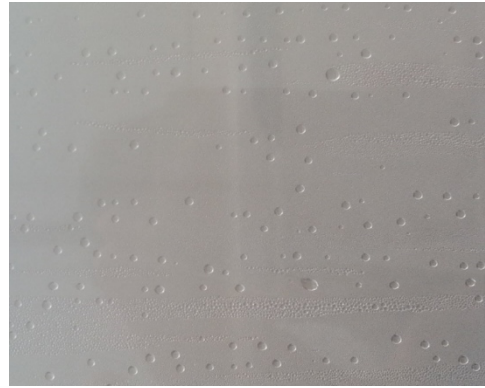


Figure 05.79 - Water droplet on the acrylic sheet of the tent.

In general, the proposed water collection technique demonstrated important productivity and could be used as a cheap alternative for fresh-water production in arid countries. A brief report of the overall results achieved is presented in Table 5.14. The experimental results provide information on the conditions needed to develop commercial scale modelling of the system, enabling a prediction of productivity for varying input parameters.

Summary of the Seawater Distillation Unit (Stage II/Part II)


	<p>SWD STAGE II/PART II</p>										
<p>Utilisation Material:</p> <ul style="list-style-type: none"> Plastic sheets type: Acrylic sheets size 1.22 m x 2.44 m, 4 mm thick Canal size: 5 m x 0.5 m x 0.25 m Piping system: PVC, 1" OD Supply air equipment: Air blower <p>Operating Conditions:</p> <ul style="list-style-type: none"> Hot water flow rate: 1.5 m³/h Air flow rate: 65 m³/h Air compressor power: 1.1 kW Water temperature: 42°C-58°C Air Temperature (IGH): 36°C- 40.5°C Air Temperature (IT): 39°C- 48.3°C RH (IGH): 30-40% RH (IT): 80-100% <p>Technical Information:</p> <table> <tr> <td>6</td><td>Durability of the sheets</td><td>high</td></tr> <tr> <td>7</td><td>Productivity</td><td>high</td></tr> <tr> <td>8</td><td>Water conductivity</td><td>low</td></tr> </table> <p>IGH: Inside the greenhouse IT: Inside the tent</p>	6	Durability of the sheets	high	7	Productivity	high	8	Water conductivity	low	<p>27 L/day</p>	<p>7.2</p>
6	Durability of the sheets	high									
7	Productivity	high									
8	Water conductivity	low									
	Productivity	pH									
	<p>2.5 m²</p>	<p>0.332 ds/m</p>									
	Evaporation area	Conductivity									
	<p>7m x 2.5 m x 2 m</p>	<p>51.5 L/day</p>									
	Required space	Productivity [design value]									
<p>Feasibility Remarks:</p> <ol style="list-style-type: none"> Low-cost technique for producing very low salinity (irrigation) water. The produced water can be used for drip irrigation technique; or, It can be used to assist the hydroponic irrigation technique. The water requirement for various crops and trees using the hydroponic irrigation technique is detailed in Table 05.15. The high durability of the tent allows to use this technique under severe environmental conditions. This conclusion is based on the current test as well as the manufacturer's data which gives the maximum recommended operating temperature (up to 85°C). The very low conductivity level refers to very low salinity of the water produced which means that no effect on soil salinity will be incurred. The condensate can be used to build up the soil moisture using pipes beneath the soil. 											

Table 05.14 - SWD– results of experimental work - Stage II/part II.

Crop/Tree	Litres/day
750 cucumber plants inside greenhouse over a three-month season will require about 50 m ³ of water.	560
Dates palm outside GH	140
Lemon outside GH	110
Banana outside GH	160

Table 05.15 - Water requirements using Hydroponic Irrigation Technique.

6. Modelling of the Experiment and Comparison with Experimental Results for SWI and SWD.

6.1 Introduction

Based on the experimental data, results from the Chapter 5 and the modelling of similar systems within the literature, this chapter seeks to find mathematical models which are able to simulate and predict the effect of variable system parameters on fresh-water production. These include inlet water temperature, inlet air temperature and air velocity as recorded and studied in the field experiments. The results of the models are then compared to experimental data and the models then used to predict system productivity with a view to scaling up towards large commercial units. Finally, the results from the model are compared with those from previous studies and experimental data found within the literature.

6.2 SWI and SWD System Models

Detailed thermodynamic models and mass and heat conservation equations, as already defined and employed in most prior studies, are developed for each part of the system and the resulting computational and mathematical models of the proposed system are then solved by Matlab software.

The main components of the proposed systems are:

- Flat plate solar collector for air heating.
- Flat plate solar collector for water heating.
- Integrated humidification-dehumidification unit for both SWI and SWD.

The mass and heat transfer occurring through the soil during SWI (Lindblom 2012) are not reproduced here, although assumptions about soil properties are based on her conclusions. Soil is considered to be optimised for condensation and heat transfer with the addition of artificial conditioners.

The effect of air inflation is also not presented in the model as it is assumed that its effect is that all air present within the evaporation condensation chamber will become saturated, and thus the temperature will be constant along the rig due to heat transport by the hot salty water flowing in the rig.

The primary assumptions used for developing the computational models are as follows:

- The overall system modelling is time-variant, wherein incident solar radiation is integrated as a function of time and not considered as an average value. During the day the system is operational, while at night it is assumed to be closed. The initial starting values for each day are thus plausible according to the experiment.
- The model for a solar FPC for water and air is time-variant and is run so as to achieve maximum outgoing water and air temperatures.
- Heat losses in the system are ignored (i.e. no energy is stored in the rig or any other component).
- The pressure drop within the system device is neglected, aside from that occurring across the air release valve.
- The total mass of water and humid air is preserved along the rig.
- Air and vapour are considered to behave as perfect gases.
- The air, once in contact with the salty water, is considered to be saturated with water vapour.
- Variations in kinetic and potential energy are negligible (Okati et al. 2018; 2019).

If the components of the system are connected appropriately then the mass flow rate in the system is constant, irrespective of the arrangement of water and/or air heater/humidification-condensation unit in the system.

6.2.1 Flat Plate Solar Collector (Air & Water)

In this section, the equations pertaining to the flat plate solar collector used for increasing the temperature of the integrated humidification-dehumidification inlet water and air are written in order of the relative Matlab code as presented in Appendix III (Okati et al. 2016; 2018; 2019).

The amount of useful thermal load absorbed by the gas (air or water vapour [kW]) from the collector is given by the following Eq. (1):

$$Q_{th,a} = M_f \times C_{pa} \times (T_{co} - T_{ci}) \quad (1)$$

where T_{co} and T_{ci} are the inlet and outlet temperatures through the FPC [°C], and M_f is the mass flow rate of the fluid (either air or water) [kg/s] and C_{pa} is the air specific heat capacity as a function of temperature measured in [J/kg °C].

According to the following equation, known as the Hottel-Whillier-Bliss Equation, when we consider overall heat loss in the solar collector, the effective heat produced by the FPC at time t will be (Eq.2):

$$Q_{th,total} = A_c \times [I_s \times \tau\alpha - U_L (T_p - T_{amb})] \quad (2)$$

where A_c is the collector area [m²], I_s is the incident solar radiation as a function of time [W/m²], $\tau\alpha$ is the transmittance absorptance of the unit, U_L is the FPC's overall heat loss coefficient, and T_p and T_{amb} are the plate and ambient temperature [°C], respectively.

Considering now Eqs. (1) and (2), the temperature of the FPC outer fluid T_{co} [°C] can be obtained from the following Eq. (3):

$$T_{co} = \frac{A_c \times [I_s \times \tau\alpha - U_L (T_p - T_{amb})]}{M_f \times C_{pa}} + T_{ci} \quad (3)$$

where U_L can be calculated as follows:

$$U_L = \frac{U_T}{A_c \times (T_p - T_{amb})} = \frac{U_l + U_e + U_b}{A_c \times (T_p - T_{amb})} \quad (4)$$

The total losses U_T will consist of the overall energy losses by convection to the glass cover above U_l , the edge losses U_e , and the energy conducted through the bottom insulation U_b .

The main heat transfer loss U_l [W/m² °C] can be calculated from Tabor (1958) via Eqns. (5), (6), (7), (8), (9), (10):

$$U_l = \left(\left(\left(\left(\frac{NG}{\left(\frac{c}{T_{mp}+273} \right) \times \left(\frac{T_{mp}-T_{amb}}{NG+f} \right)^e} \right) + \left(\frac{1}{h_w} \right) \right)^{-1} \right) + \left(\frac{\sigma \times (T_{mp}+273+T_{amb}+273) \times \left((T_{mp}+273)^2 + (T_{amb}+273)^2 \right)}{\left((\varepsilon_p + 0.00591 \times NG \times h_w)^{-1} \right) + \left(\frac{(2 \times NG) + f - 1 + (0.133 \times \varepsilon_p)}{\varepsilon_g} \right) - NG} \right) \right) \quad (5)$$

where T_{mp} is the mean plate temperature, ε_g is the glass emissivity, ε_p is the emissivity of the plate, NG is the number of the glass cover, ε_p is the emissivity of the plate, and σ is the Boltzmann constant.

The parameters can be calculated as follows:

h_w is the heat transfer coefficient for air flowing over the outside surface of the glass cover and depends primarily on wind velocity [$\text{W/m}^2 \text{K}$]. It can be calculated after Klein et al. (1974).

$$h_w = 5.7 + 3.8 \times V_w \quad (6)$$

where V_w is the wind speed [$\frac{m}{s}$]

$$f = (1 + 0.089 \times h_w - 0.1166 \times h_w \times \varepsilon_p) \times (1 + 0.07866 \times NG) \quad (7)$$

$$C = 520 \times (1 - 0.000051 \times \beta^2) \quad (8)$$

$$e = 0.43 \times \left(1 - \left(\frac{100}{T_{mp} + 273} \right) \right) \quad (9)$$

$$\sigma = 5.67 \times (10^{-8}) \quad (10)$$

where β is the tilt angle.

Heat losses from edges U_e in [$\text{W/m}^2 \text{ }^\circ\text{C}$] can be computed according to Whillier (1953) in the following Eqns. (11), (12):

$$U_e = h_e \times A_p \times (T_p - T_{amb}) \quad (11)$$

where, A_p is the perimeter area of the collector and h_e is the coefficient heat transfer by convection in [$\text{W/m}^2 \text{K}$] arising between the edges of the FPC and the ambient and can be defined according as:

$$h_e \cong 0.5 \quad (12)$$

U_b , the heat losses from the bottom insulation U_b [$\text{W/m}^2 \text{ }^\circ\text{C}$] can be calculated from Tabor (1958) via Eqns. (13), (14):

$$U_b = \frac{A_c \times (T_p - T_{amb})}{\frac{\delta}{k} + \frac{1}{h_b}} \quad (13)$$

where δ is the thickness and k is the thermal conduction coefficient of the insulation below the collector plate, and h_b the coefficient heat transfer by convection [$\text{W/m}^2 \text{K}$] between the insulated bottom surface and the ambient. According to Tabor:

$$h_b \cong 12.5 \text{ to } 25 \quad (14)$$

All following values can be calculated:

T_{mpn} , new mean plate temperature [°C] from Eqn. (15):

$$T_{mpn} = \left(\frac{\left(A_c \times \frac{I_s}{1000} \right) - Q_{th}}{A_c \times \frac{U_T}{1000}} \right) + T_{amb} \quad (15)$$

T_p , plate temperature, [°C], Eqn. (16):

$$T_p = \left(0.88 \times \frac{I_s}{U_T} \right) + T_{amb} \quad (16)$$

F , efficiency factor, Eqn. (17):

$$F = \frac{\tanh\left(M_f \times \left(\frac{W-De}{2}\right)\right)}{M_f \times \left(\frac{W-De}{2}\right)} \quad (17)$$

FR , heat removal factor, Eqn. (18):

$$FR = \left(\frac{M_f \times C_{pa}}{A_c \times \left(\frac{U_T}{1000}\right)} \right) \times \left(1 - \exp\left(-1 \times \left(\frac{A_c \times \left(\frac{U_T}{1000}\right) \times F}{M_f \times C_{pa}}\right)\right) \right) \quad (18)$$

FF , the flow factor, Eqn. (19):

$$FF = \frac{FR}{F} \quad (19)$$

Q_u , useful energy [kW], Eqn. (20):

$$Q_u = A_c \times FR \times \left(\left(\frac{I_s}{1000} \right) - \left(\left(\frac{U_T}{1000} \right) \times (T_{ci} - T_{amb}) \right) \right) \quad (20)$$

T_{fm} , the mean fluid temperature, is then calculated by Eq. (21):

$$T_{fm} = T_{ci} + \left(\left(\frac{Q_u}{A_c \times \left(\frac{U_T}{1000}\right) \times FR} \right) \times (1 - FF) \right) \quad (21)$$

T_{co} , the calculated outlet collector temperature [°C] of the air is obtained from Eqn. (22):

$$T_{co} = (2 \times T_{fm}) - T_{ci} \quad (22)$$

Then, η (thermal efficiency) is determined by Eqn. (23):

$$\eta = \frac{1000 \times Q_u}{I_s \times A_c} \quad (23)$$

For the flat plate solar collector used to increase air temperature, an FPC system having an equivalent diameter (expressed in [m]) is considered, where W is the width and H is the height Eqn. (24):

$$D_e = \frac{4 \times W \times H}{2 \times W} \quad (24)$$

The FPC water heater is considered to be identical to the air heater except that we are replacing the air channel with a water tube configuration. An FPC system of equivalent diameter $D_e = D_t$ is therefore modelled.

6.2.2 SWI with membrane model

After writing the flat plate solar collector equations to increase air and water temperature, the equations related to the humidification-dehumidification unit are defined. Such unit is responsible both for increasing the inlet air humidity and reducing the outlet humidity after condensation. The prior modelling for humidification presented by Lindblom (2006) and Okati et al. (2018), (2019) is implemented but without the contribution of solar radiation, since mixing of hot air and water will happen directly in underground pipes shaded to radiation by the ground above.

For the Sea Water Irrigation unit, the following mathematical model equations are written in order of the relative Matlab code presented in Appendix III to calculate the unit's productivity; a schematic of the unit is reported below (Figure 06.01).

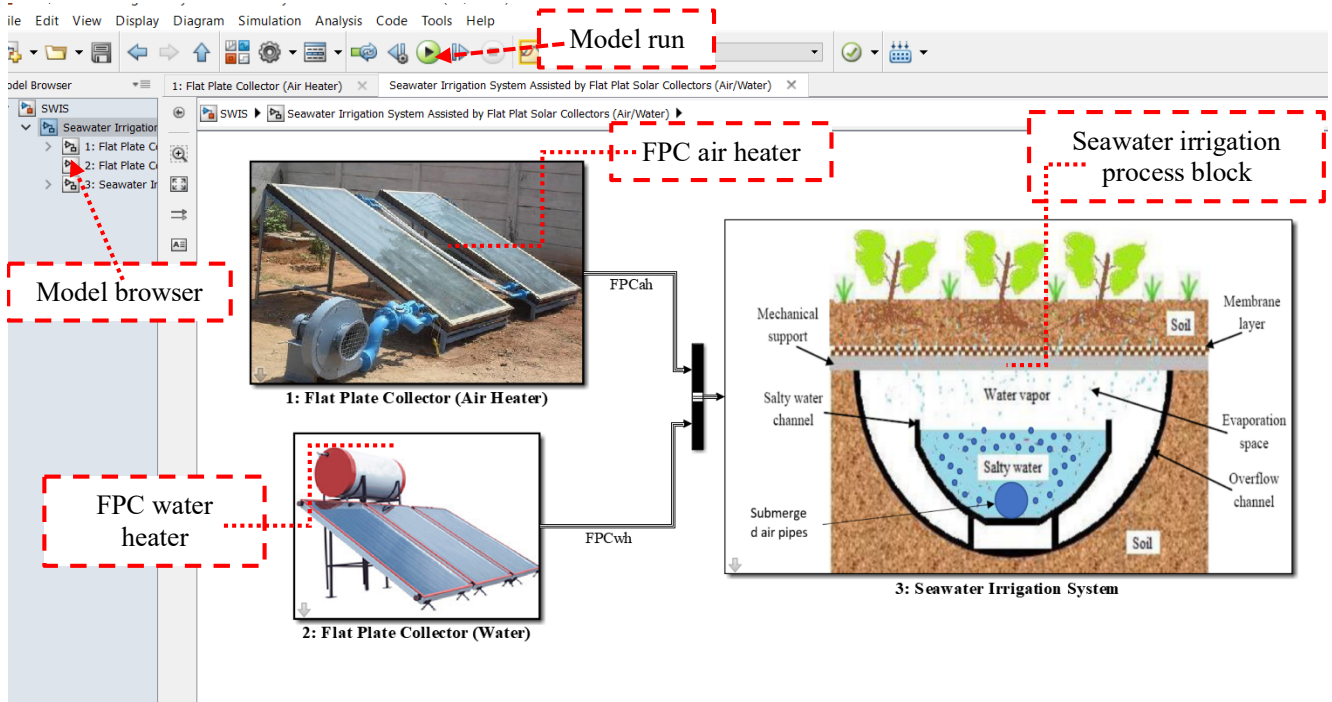


Figure 06.01 – SWI - system model under Matlab/Simulink toolbox environment.

The first law of thermodynamics and mass and energy balance equations for the first part of the system, where humidification takes place and hot air and hot water exiting the FPC for air and water heating enter in contact in the rig, is implemented.

A small volume of water and air encompassing the rig chamber with length dx is considered (Figure 06.02) the equation will then be as presented in the Eq. (25) and Eq. (26):

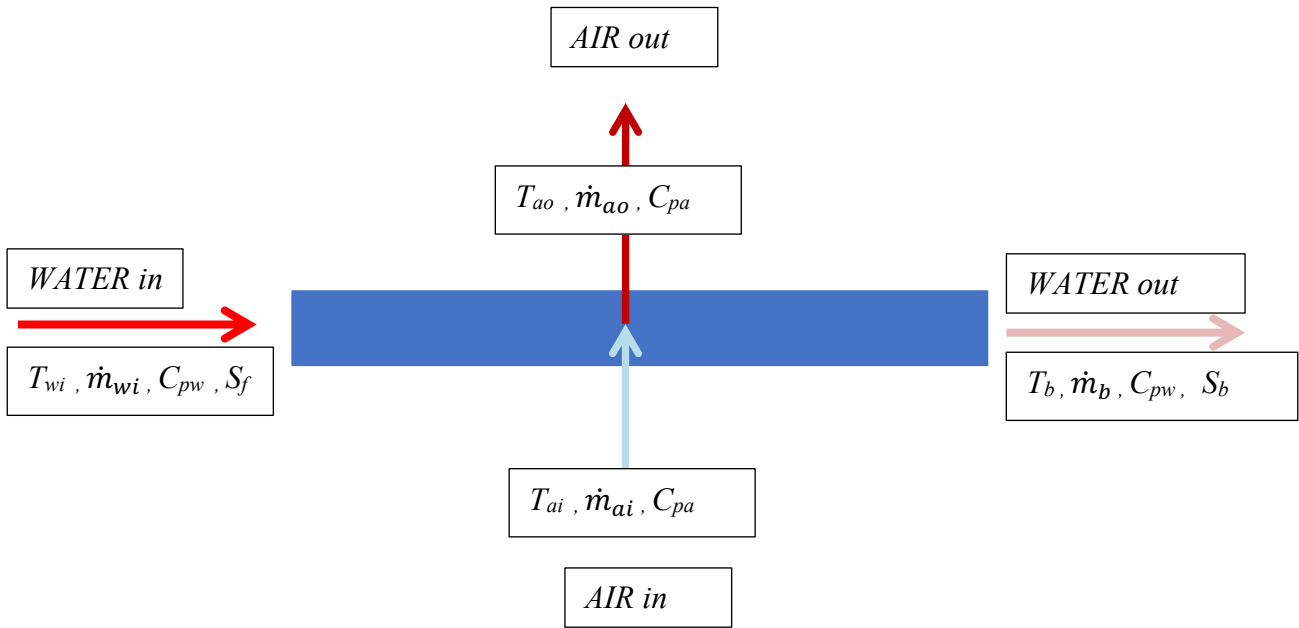


Figure 06.02 – Schematic of the thermodynamic equation for the humidification part of the process.

$$\dot{Q}_{c.v} + \sum \dot{m}_i \times h_i = \sum \dot{m}_o \times h_o \quad (25)$$

$$(\dot{m}_{ai} \times C_{pa} \times T_{ai}) - (\dot{m}_v \times C_{pa} \times T_v) = (\dot{m}_b \times C_{pw} \times T_b) - (\dot{m}_{wi} \times C_{pw} \times T_{wi}) \quad (26)$$

Assuming a constant dry bulb temperature [$^{\circ}\text{C}$], where T_v is the vapour temperature, T_{ai} is the inlet air temperature from the air heater unit, and T_{wi} is the inlet water feed temperature from the water heating unit [$^{\circ}\text{C}$], all acting in as a function of time, and C_{pw} is the specific heat capacity of the water as a function of temperature and the salinity ratio of each stream, and C_{pa} is the air specific heat capacity as a function of temperature (both measured in [$\text{J/kg } ^{\circ}\text{C}$]), where \dot{m} is the mass flow rate of different fluids (i.e., air, vapour, brine or water) in the system.

$$T_v = T_{ai} \quad (27)$$

\dot{m}_v , the vapour mass flow rate is based on air saturation [kg/s] and is calculated by Eqn. (28):

$$\dot{m}_v = (\omega_{ao} - \omega_{ai}) \times \dot{m}_{ai} \quad (28)$$

Considering that ω_{ai} and ω_{ao} are the inlet and outlet specific humidity of the air, respectively, then, according to Eqns. (29) and (30):

$$\omega_{ai} = \frac{\dot{m}_{vi}}{\dot{m}_{ai}} \quad (29)$$

$$\omega_{ao} = \frac{\dot{m}_{vo}}{\dot{m}_{ai}} \quad (30)$$

\dot{m}_b , the brine flow rate in [kg/s] is dependent on the difference arising between the feed \dot{m}_{wi} and vapour \dot{m}_v released by the air:

$$\dot{m}_b = \dot{m}_{wi} - \dot{m}_v \quad (31)$$

S_b , the brine salinity ratio [g/kg] can thus be calculated as:

$$S_b = \frac{S_f \times \dot{m}_f}{\dot{m}_b \times 1} \quad (32)$$

where S_f is the feed salinity ratio.

The brine outlet temperature [°C] can be obtained from the energy balance arising across the membrane system and it is a function of the temperature and salinity ratio of each stream:

$$T_b = \left(\frac{(\dot{m}_{wi} \times C_{pw} \times T_{wi}) + (\dot{m}_{ai} \times C_{pa} \times T_{ai}) - (\dot{m}_v \times C_{pa} \times T_v)}{\dot{m}_b \times C_{pw}} \right) \quad (33)$$

After analysing the humidification component of the system and determining its primary parameters, the other important part of the unit is the dehumidification section where condensation occurs since the soil is at a lower temperature than that of the humid saturated air. Hence condensation occurs and desalinated water is produced directly at the soil interface.

For the dehumidification process, considering the soil as a condensing plate with soil plate area A_p [m²], where L [m] and W [m], are the length and width of the membrane plate, respectively:

$$A_p = L \times W \quad (34)$$

The conduction heat transfer is determined $[W/m^2 \text{ } ^\circ C]$, where k is the thermal conductivity $[W/m \text{ } ^\circ C]$:

$$Re = \frac{\dot{m}_v}{W \times \mu} \quad (35)$$

$$Pr = C_{pa} \times \frac{\mu}{k} \quad (36)$$

$$Nu = 0.332 \times (Re^{0.5}) \times (Pr^{0.333}) \quad (37)$$

$$h_c = \frac{Nu \times k_p}{L} \quad (38)$$

U , the overall heat coefficient $[W/m^2 \text{ } ^\circ C]$ can be calculated as follows:

$$U = \frac{1}{\left(\frac{X_p}{k_p}\right) + \left(\frac{1}{h_c}\right)} \quad (39)$$

where X_p is the membrane plate thickness $[m]$:

Considering the plate as a condenser unit, the number of transfer units can be then calculated as:

$$NTU = \frac{U \times A_p}{\dot{m}_{ai} \times C_{pa}} \quad (40)$$

The dehumidifier's effectiveness is determined by:

$$\varepsilon_{dh} = 1 - \exp(-NTU) \quad (41)$$

The thermal power of the membrane $[kW]$ is given by:

$$Q_{mem} = U \times A_p \times \frac{T_v - T_{soil}}{1000} \quad (42)$$

The outlet air temperature $[^\circ C]$ can be calculated as:

$$T_{ao} = T_v - \varepsilon_{dh} \times (T_v - T_{soil}) \quad (43)$$

The system's productivity, \dot{m}_v [kg/s] can be then calculated based on the specific humidity and air flow rate via:

$$\dot{m}_v = (w_{ai} - w_{ao}) \times \dot{m}_{ai} \quad (44)$$

The recovery ratio (RR) can be calculated based on the system's total productivity and inlet feed flow rate, as follows:

$$RR = \frac{\dot{m}_v}{\dot{m}_f} \quad (45)$$

6.2.3 SWD without Membrane Model (Still Cover Type)

For the SWD unit, the following mathematical model equations are written in order of the relative Matlab codes presented in Appendix III to calculate the productivity of the unit and a schematic of the unit is reported below (Figure 06.02). The humidification part of the model is identical to the SWI while the dehumidification component is considering the replacement of soil with the cover.

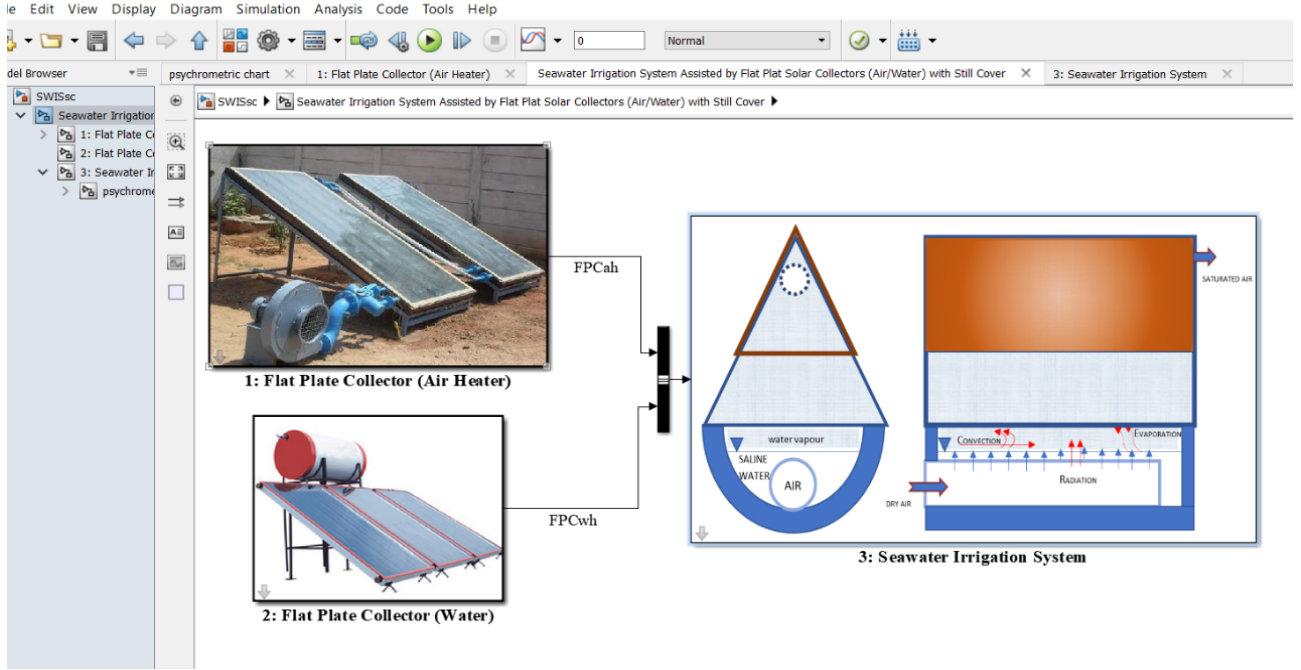


Figure 06.02 – SWD - system model under Matlab/Simulink toolbox environment.

For the dehumidification process, the still cover area A_c is calculated in $[m^2]$, where TA_c , L_c and W_c are the cover tilt angle, length, and width of the still cover:

$$A_c = L_c \times W_c \quad (46)$$

where the cover width, based on the tilt angle (TA_c) and still width can be calculated as follows:

$$W_c = 2 \times \left(\frac{W}{2 \times \cos(TA_c)} \right)$$

The conduction heat transfer is determined $[W/m^2 \text{ } ^\circ C]$, where k is the thermal conductivity $[W/m \text{ } ^\circ C]$:

$$Re = \frac{\dot{m}_v}{W \times \mu} \quad (47)$$

$$Pr = C_{pa} \times \frac{\mu}{k} \quad (48)$$

$$Nu = 0.332 \times (Re^{0.5}) \times (Pr^{0.333}) \quad (49)$$

$$h_c = \frac{Nu \times k_p}{L} \quad (50)$$

U , the overall heat coefficient [$W/m^2 \text{ } ^\circ C$], can be calculated as follows:

$$U = \frac{1}{\left(\frac{X_p}{k_p}\right) + \left(\frac{1}{h_c}\right)} \quad (51)$$

where X_p is the membrane plate thickness [m]. Considering the plate as a condenser unit, the number of transfer units can be then calculated:

$$NTU = \frac{U \times A_p}{\dot{m}_{ai} \times C_{pa}} \quad (52)$$

The dehumidifier effectiveness is given by:

$$\varepsilon_{dh} = 1 - \exp(-NTU) \quad (53)$$

The thermal power on the membrane [kW]:

$$Q_{mem} = U \times A_c \times \frac{T_v - T_{soil}}{1000} \quad (54)$$

The outlet air temperature [$^\circ C$] can be calculated for effectiveness:

$$T_{ao} = T_v - \varepsilon_{dh} \times (T_v - T_{soil}) \quad (55)$$

The system's productivity, \dot{m}_v , in [kg/s] can be then calculated based on the specific humidity and air flow rate:

$$\dot{m}_v = (w_{ai} - w_{ao}) \times \dot{m}_{ai} \quad (56)$$

The RR can be calculated based on the system's total productivity and inlet feed flow rate, as follows:

$$RR = \frac{\dot{m}_v}{\dot{m}_f} \quad (57)$$

6.2.4 The Developed Software Models

Engineering processes consist of several interactive stages. Using these stages within various process configurations enables tailored outcomes and functionality. Generally, to understand the behaviour of these processes under different operating conditions, a flexible and general computer programme is needed. Using such programme, many flow sheeting problems can be controlled. These problems can be broadly divided into two classes, namely (i) performance problems; and (ii) design problems. In the performance problem, the variables associated with the feed streams to a processing unit and all design parameters (such as surface module area, dimensions, etc.) are assumed to be known while the variables associated with the internal and output streams are unknown. In the design problem, some design parameters (e.g., areas, dimensions, voltage, current, number of cells, unit cost, etc.) and/or feed variables are left unspecified and become unknowns to be determined. What is left is generally known regarding the border streams of the process or the system and, in such a case, is the crux of the SWI and SWD modules (1st and 2nd configurations). In this work, the parameters of the SWI and SWD are calculated based on the performance technique of modelling. Therefore, the following assumptions have been made.

For FPC air heater:

- Solar irradiation = 700 W/m^2
- Wind speed = 0.1 m/s
- Ambient temperature = temperature of the day measured in the experiment
- Inlet FPC temperature = 25°C
- Inlet RH = 30%
- Air mass flow rate = 0.025 kg/s
- Area = 2 m^2
- Number of glass covers = 1
- Tilt angle of the FPC = 45°
- Glass cover, plate emittance = 0.88 & 0.95
- Edge overall loss and bottom loss heat transfer coefficient = $0.15 \text{ \& } 0.9 \text{ W/(m}^2 \text{ }^\circ\text{C)}$
- FPC channel length and height = $100 \text{ cm \& } 1 \text{ cm}$
- Plate thickness = 5 mm
- Plate thermal conductivity = $385 \text{ W/(m }^\circ\text{C)}$

For FPC water heater:

- Solar irradiation = 700 W/m^2
- Wind speed = 0.1 m/s

- Ambient temperature = temperature of the day measured in the experiment
- Inlet FPC temperature = 35°C
- Air flow rate = 0.1 kg/s
- Area = 23 m²
- Number of glass cover = 1
- Tilt angle of the FPC = 45
- Glass cover, plate emittance = 0.88 & 0.95
- Edge overall losses and bottom losses = 0.15 & 0.9 W/(m² °C)
- Tube spacing and diameter = 10 cm & 2 cm
- Plate thickness = 5 mm
- Plate thermal conductivity = 385W/m °C

For the SWI:

- Soil temperature = 25-35°C
- Feed salinity ratio = 10g/kg
- Target RH = 50-100%
- Membrane length = 5 m
- Membrane width = 0.5 m
- Membrane thickness = 0.1m
- Membrane conductivity = 80W/m °C

For the SWD with cover:

- Cover temperature = ~ambient temperature of the day measured in the experiment
- Feed salinity ratio = 10g/kg
- Target RH = 50-100%
- Cover length = 5 m
- Still width = 0.5 m
- Cover thickness = 0.001m
- Cover tilt angle = 45 deg
- Cover conductivity = 0.25W/m °C

6.2.5 Meteorological data of selected Omani locations

Oman is located in the south-eastern corner of the Arabian Peninsula bordering the Gulf of Oman. It neighbours the Arabian Sea, the Arabian Gulf, the United Arab Emirates, Yemen, and Saudi Arabia. This geographical location has granted Oman important access to one of the largest energy corridors in the world. The climate in Oman is hot and dry in the desert, while it is humid and hot along the long coastline. Every year a strong southwest summer monsoon season arrives in Oman, usually from May to September. Oman has one of the highest solar irradiation concentrations in the world, and solar energy has the potential to meet all of Oman's electricity requirements as well as being able to provide an important source of energy for desalination and irrigation. This would not only be sufficient for the entire country, but also affords the possibility of exporting it to the Gulf Cooperation Council (GCC), a political and economic union consisting of Bahrain, Kuwait, Oman, Qatar, Saudi Arabia, and the United Arab Emirates.

Oman receives daily solar irradiation ranging between 5,500 and 6,000 Wh/m²/day in July and 2,500 to 3,000 Wh/m² in January (Gastli and Charabi 2010). Furthermore, Oman has a mean wind speed of 6 m/s which, in theory, is sufficient for clean energy generation (Anagreh and Bataineh 2011). Notwithstanding the average wind speed, the wind used during our modelling was that measured at the experimental site (which had a lower value).

The data obtained has been used to predict the hourly wind and levels of solar irradiation across six sites in Oman, namely Al Khuwaimah, Al Halaniyat, Al Mazyounah, Haitam, Madha and Methane. These rural regions are suitable for the installation of the proposed systems alongside renewable electrical off-grid units, including PV (Raeco 2017). These rural locations are indicated in Figure 06.03 along with detailed geographical and meteorological information in Table 06.01.



Figure 06.03 – Sites in Oman investigated in terms of their suitability in terms of solar radiation.

	Al Khuwaimah	Al Halaniyat	Al Mazyounah	Haitam	Madha	Methane
Latitude	21.39 N	17.49 N	17.83 N	18.83 N	18.59 N	18.59 N
Longitude	59.20 E	55.97 E	52.62 E	56.92 E	56.33 E	52.45 E
Terrain form	Moderate to flat desert	Island (generally rugged and barren)	Moderate to flat desert	Flat, and desert, located in a coastal region	Mostly flat area located in a coastal region	Moderate to flat desert located near to the Yamen border
Terrain elevation	10 m	5 m	526 m	9 m	41 m	314 m
Geographical area	8.2 Km ²	56 Km ²	58 Km ²	86.1 Km ²	3.27 km ²	22.2 Km ²
Climate	Desert: Hot summer and warm winter	hot, humid weather in summer and warm weather in winter.	Desert: Hot summer and warm winter	Desert: hot, humid weather in summer and cold weather in winter.	Hot summer and warm winter	Desert: hot, dry weather in summer and cold weather in winter.
Air temperature	13 to 45°C	19 to 36°C	12 to 44°C	19 to 36°C	20 to 38°C	12 to 45°C
Direct normal irradiation (DNI)	5.7 to 6 kWh/m ²	5.5 to 6.2 kWh/m ²	6.2 to 6.6 kWh/m ²	5.6 to 6.2 kWh/m ²	5 to 5.5 kWh/m ²	6.0 to 6.5 kWh/m ²
Global horizontal irradiation (GHI)	6.0 to 6.4 kWh/m ²	6.2 to 6.4 kWh/m ²	6.5 to 6.8 kWh/m ²	6 to 6.4 kWh/m ²	5.8 to 6.0 kWh/m ²	6.4 to 6.6 kWh/m ²
Diffuse horizontal irradiation (DIF)	1.6 to 1.8 kWh/m ²	1.7 to 1.9 kWh/m ²	1.3 to 1.5 kWh/m ²	1.67 to 1.88 kWh/m ²	1.75 to 1.99 kWh/m ²	1.35 to 1.55 kWh/m ²
Average wind speed at 10m	4.9 m/s	5.5 m/s	2.8 m/s	4.8 m/s	2.9 m/s	2.7 m/s

Table 06.01 – Geographical and meteorological information of selected Omani locations (Gastli and Charabi 2010; Anagreh and Bataineh 2011).

6.2.6 Data Results

According to the input data collected from the experiments and produced by the model using the experimental data assigned in the control panel, the outputs measure some targets including productivity, efficiency, temperature, and salinity ratios. Figure 06.04 shows the variation in real-time operating conditions data that have been assigned in this work. The operating conditions include variations in solar irradiation, [W/m^2], ambient temperature, [$^{\circ}\text{C}$], average wind speed [m/s], inlet air [$^{\circ}\text{C}$], recirculating brackish water temperatures [$^{\circ}\text{C}$] and RH [%] over the course of a solar year. Any variations in these operating conditions will inevitably affect system performance and productivity.

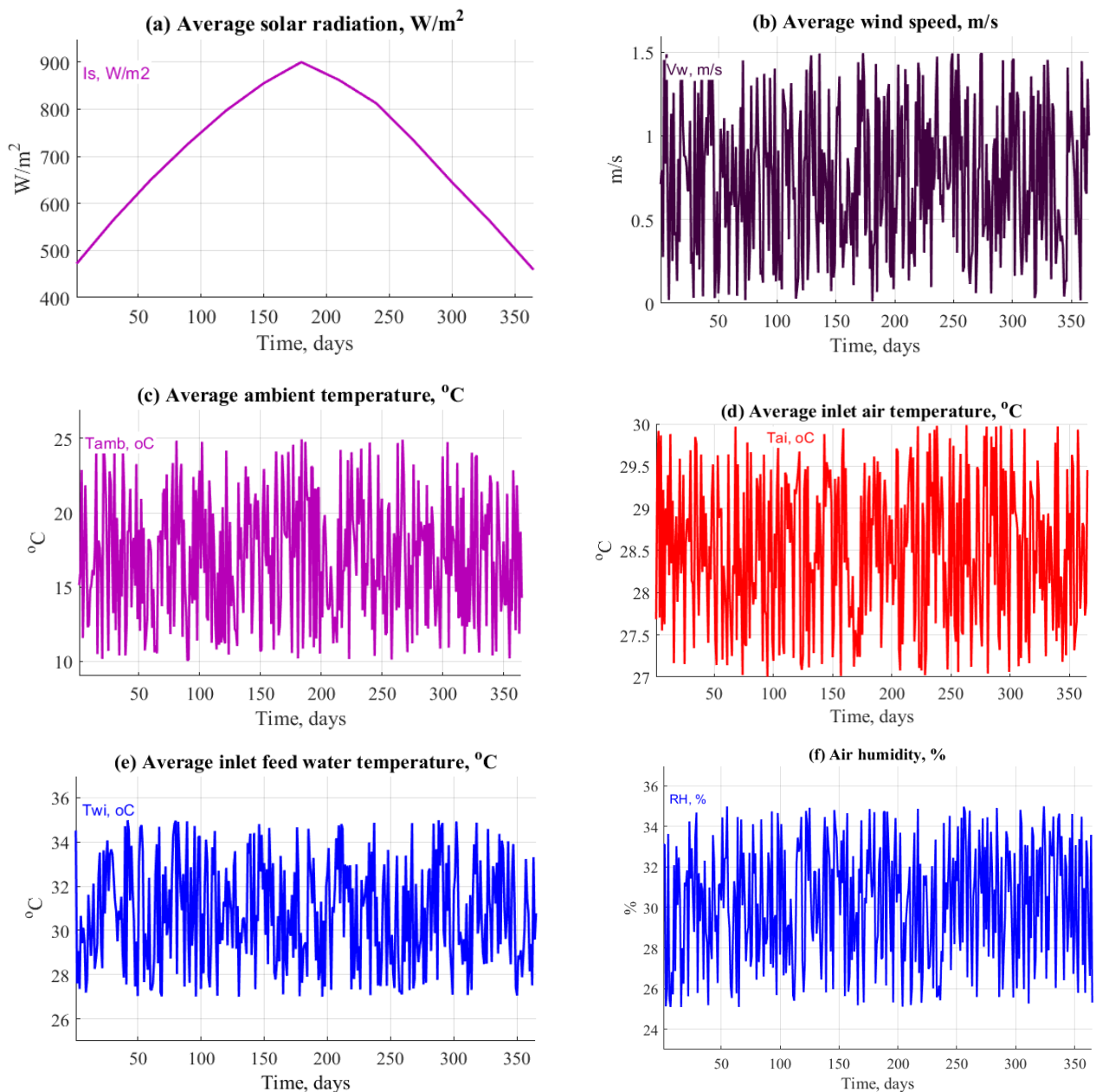


Figure 06.04 – SWD and SWI – Average operating conditions during a solar year.

For the 1st configuration (SWI with soil membrane), Figure 06.05 shows the performance data of the FPC (air and water) and the SWI used as a dehumidifier unit for the plantation and desalination processes. Figure 06.05-a, b shows the fin efficiency and flow factor of the FPC.

The fin efficiency of the water FPC is notably higher than for the air type. However, the flow factor is found to be in the range of 0.8 to 0.85 for water and air, respectively. The thermal efficiency (Figure 06.05-c) was in the range of 60 to 70%, increasing appreciably during summer (days 180 to 280). Outlet FPC water and air temperatures (Figure 06.05-d) are also higher in summertime (days 180 to 280). Increasing the air and water temperature of the feed would be most helpful in improving the system's productivity. As predicted, the thermal power output through the water type FPC is much greater than that for the air FPC (Figure 06.05-e). The overall heat loss was found to be in the range of 5 to 6.5~7W/m² °C, as shown in Figure 06.05-f.

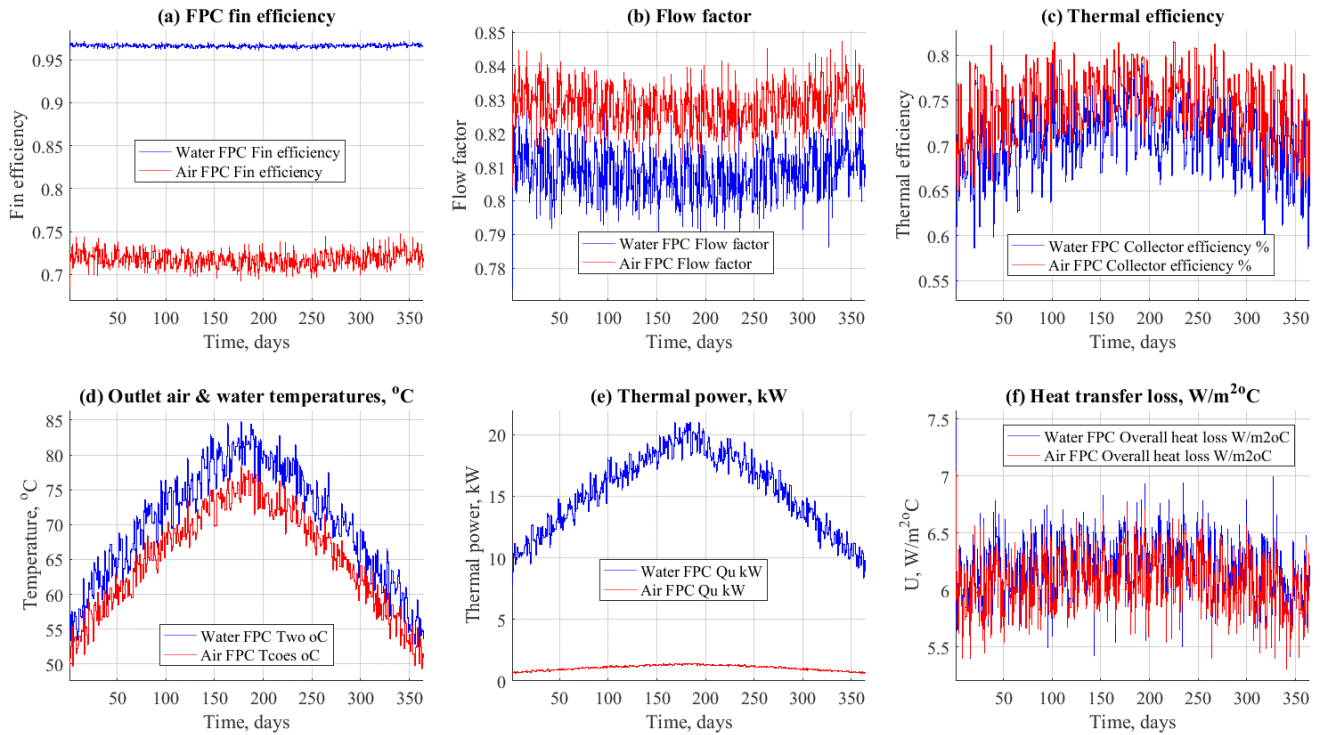


Figure 06.05 – Air & water FPC performance results over the course of a solar year (365 days).

For the 1st configuration (SWI with soil membrane), Figure 06.06 shows the data results over one solar year (365 days) pertaining to RH, effectiveness, RR, productivity, vapour flow rate, and blowdown temperature. As expected, the dry air humidity (Figures 06.06-a) was found to reach a minimum during the spring and summer (days 80 to 300) due to the increase in heat gain by the FPC. The dehumidifier's effectiveness was high (Figures 06.06-b) at around 90%. The RR (Figures 06.06-c) fell into the range of 8 to 16%, as expected, although this will increase in summertime owing to the increase in the vapour flow rate generated (Figures 06.06-e) and the productivity (Figures 06.06-d). The brine blowdown temperature (Figure 06.06-f) was found not to exceed 32°C.

Total SWI productivity over the course of a solar year varied from 20 to 40 kg/day as an accumulative daily sum, increasing with the rise in daily solar irradiation.

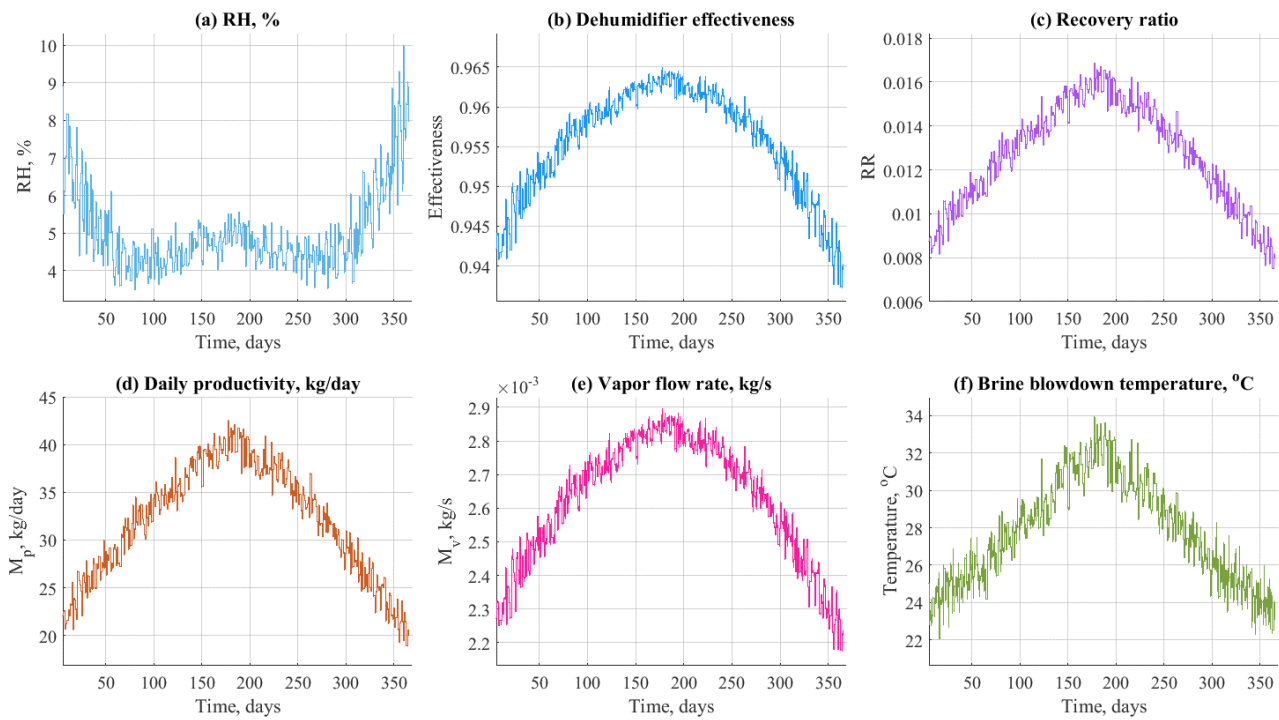


Figure 06.06 – SWI data for a full solar year for RH, effectiveness, RR, productivity, vapour flow rate and blowdown temperature.

For the 2nd configuration SWD (with plastic cover), Figure 06.07 shows the data obtained for a solar year. The RR (Figure 06.07-a) varied between 8 and 16.5%, showing a slight increase as compared to the 1st configuration. The deviation between vapour and distillate product flow rates (Figure 06.07-b) reflects losses from the system even with the cover (with a deviation of around 50%). The variation in air blowdown after condensation (Figure 06.07-c) shows that the temperature range of the final dried air exiting the system was in the range of 25 to 26°C, while the variation in the brine and vapour temperatures (Figure 06.07-d) showed a range of 55 to 80 °C across a complete solar year. Increasing the inlet feed water and air temperatures would be expected to have a massive effect on the brine and vapour temperatures, as expected. In fact, increasing the incidence of solar radiation would increase the temperature towards the range of 50 to 80°C.

The 2nd configuration exhibits a little higher productivity than the 1st configuration (Figure 06.07-f), presenting daily productivity in the range of 20 to 42 kg/day with the expectation of a substantial increase in the summertime.

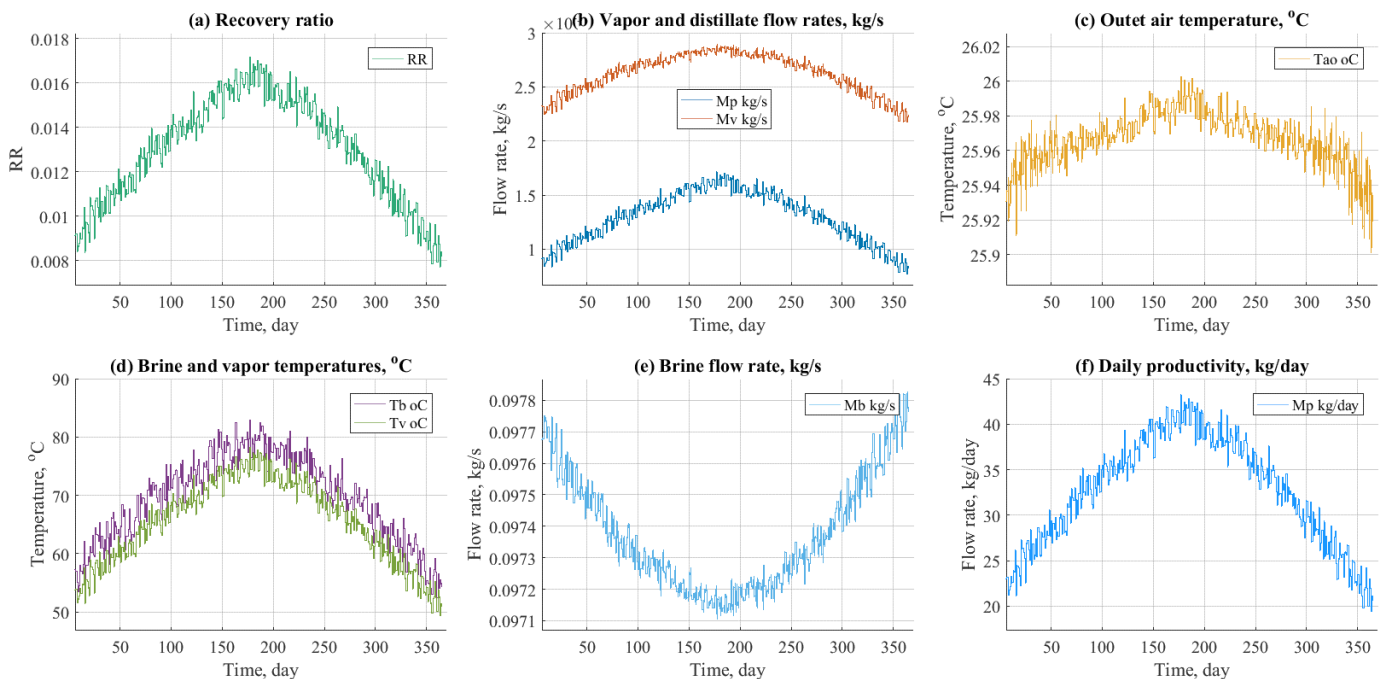


Figure 06.07 – SWD data for an entire solar year pertaining to RH, effectiveness, RR, productivity, vapour flow rate and blowdown temperature.

Figure 06.08 shows the effects of air mass flow rate on such process parameters as dry air temperature, daily average productivity, and brine blowdown temperature for both SWI and SWD. Increasing the air flow rate would reduce the dry air temperature (from 100°C to 65°C). However, it would also increase the productivity for both configurations. The covered SWD configuration shows a slight increase in productivity as compared to the membrane SWI configuration (Figure 06.08-c). A value of 0.0351 kg/s (approx. 155 m³/h) for the air flow rate would probably induce a substantial increase in terms of system productivity.

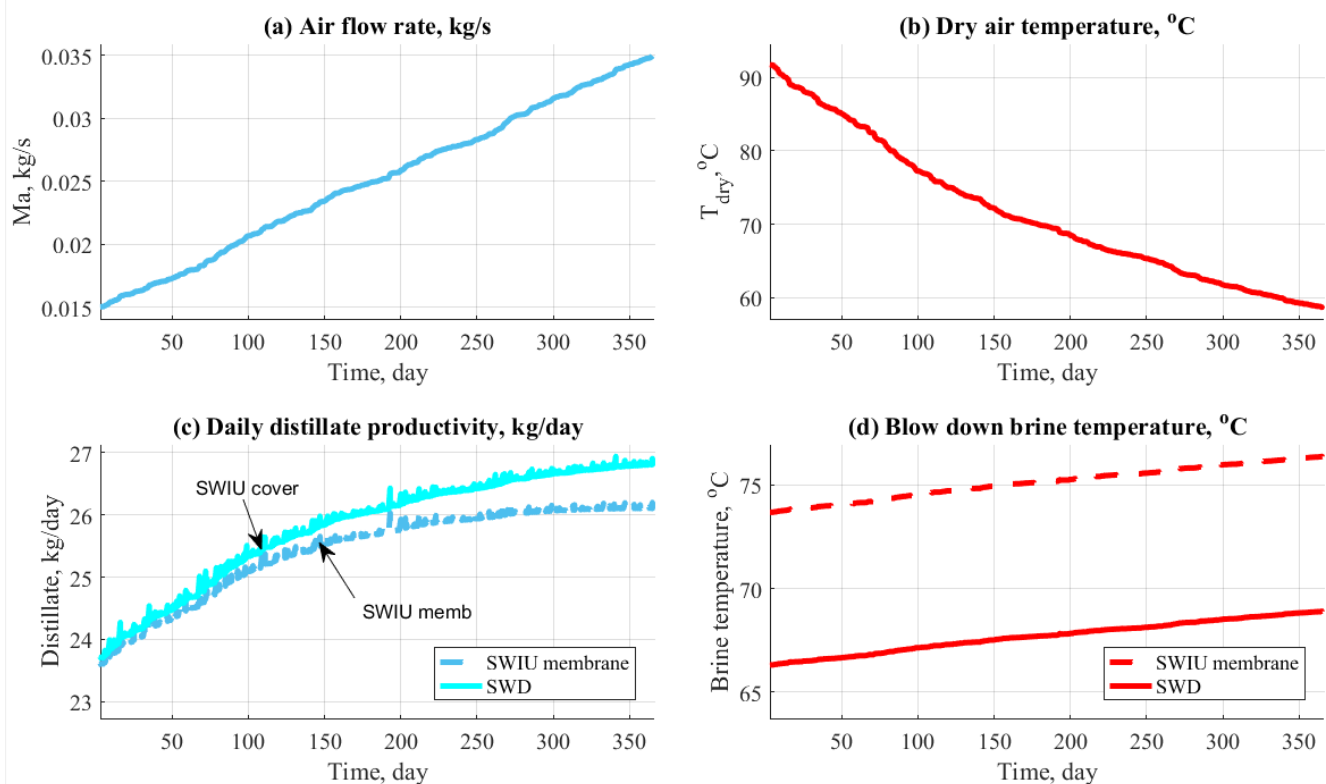


Figure 06.08 – Effect of feed air temperature on process parameters for SWI and SWD.

Figure 06.09 shows that increasing the water flow rate would decrease productivity because it would affect the inlet hot water temperature to the rig. SWI has a slight increase in daily average productivity compared to SWD (Figure 06.09-c). A value below 0.03 kg/s (108 L/h) for the water flow rate would be remarkable and essential for the increase of system productivity.

The massive effect on productivity would be happened based on an increase of inlet air and water temperatures for both types.

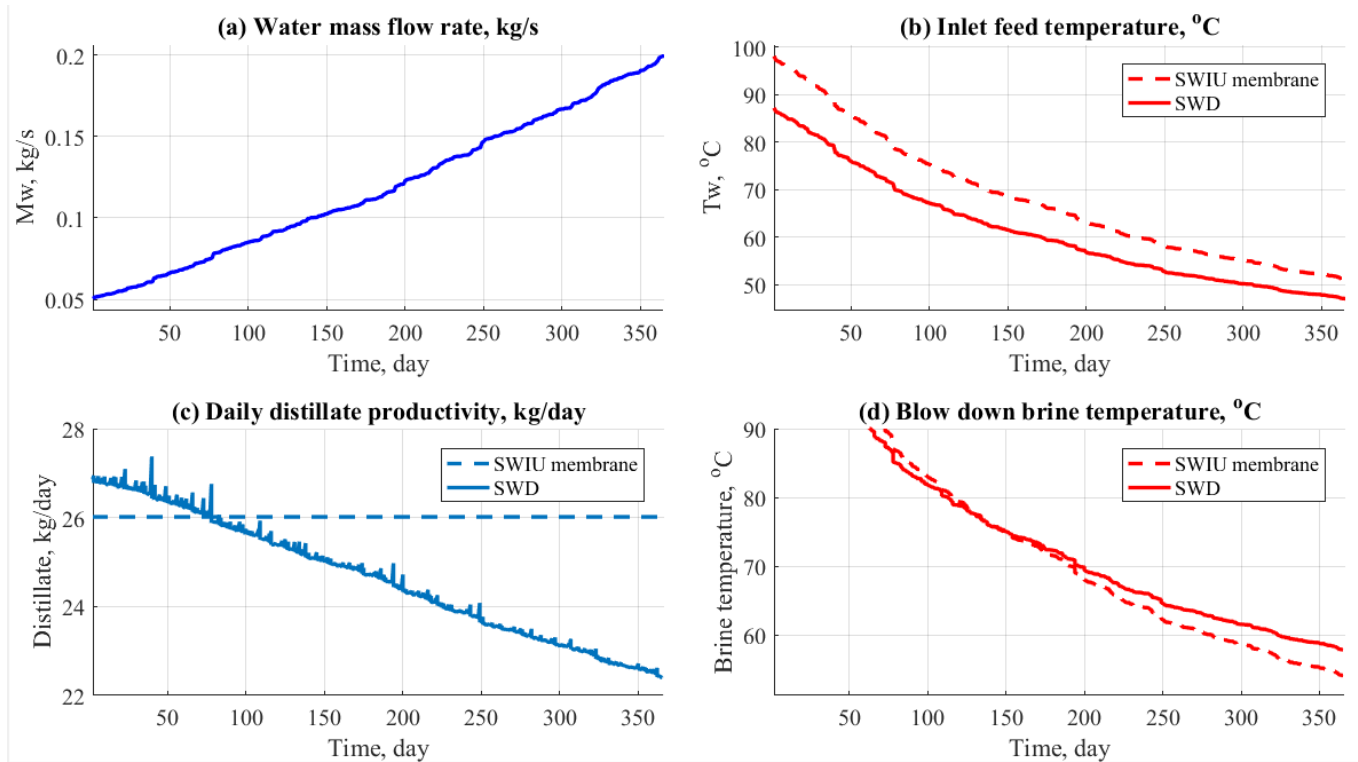


Figure 06.09 – Effect of feed water flow rate on process parameters for SWI and SWD.

Figure 06.10 shows the effect of feedwater and soil temperatures on system productivity for both SWI and SWD configurations. Increasing feedwater temperature would increase system productivity under some circumstances (Figure 06.10-a), although increasing soil temperature would decrease the total system productivity in the SWI (Figure 06.10-b). As expected, lowering the soil temperature is essential for the condensation process to occur and increase productivity.

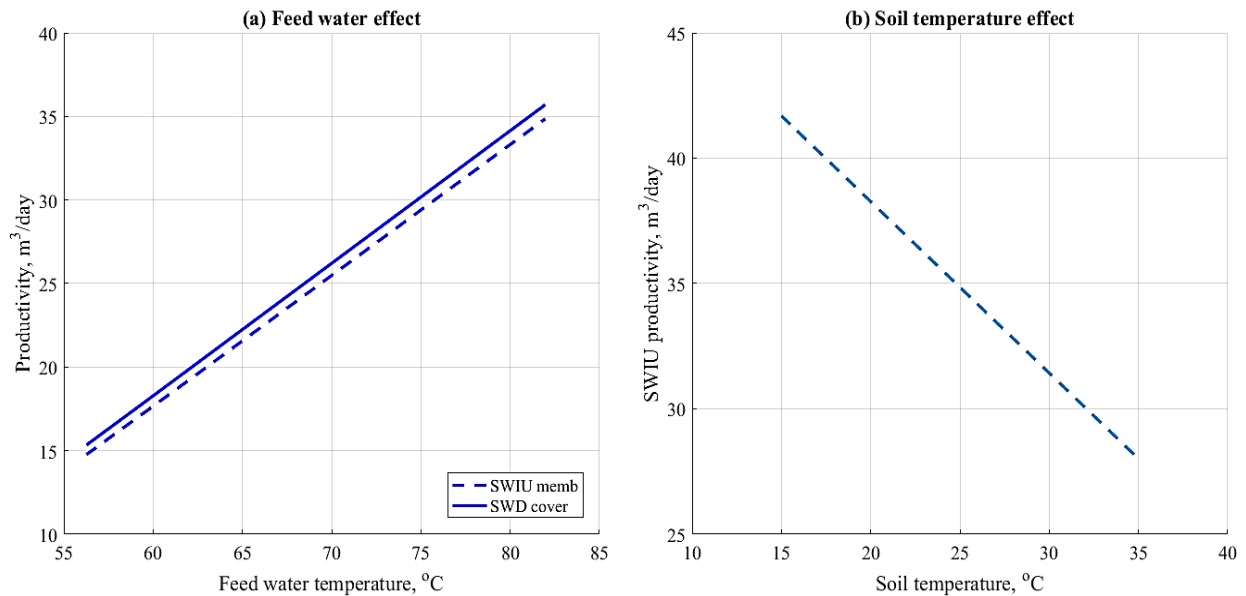


Figure 06.10 – SWI and SWD - Temperature effects on system productivity for both configurations relating to feed and soil.

Figure 06.11 shows that increasing solar radiation would affect productivity. Summer months have the highest daily productivity, as increasing solar irradiation would increase the air and water temperatures for both configurations.

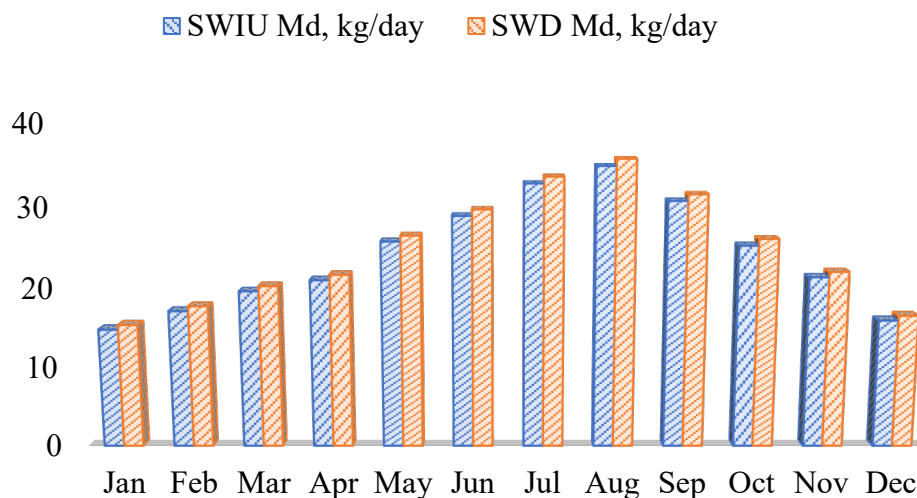


Figure 06.11– Productivity of SWD and SWI for 1 year period.

6.3 Comparison between Experimental Results and Modelling

The modelling results revealed that the system's daily productivity, based on the model's assumptions, was in the range of 15 to 35 kg/day for both configurations and that this productivity increased with solar radiation throughout the day. The constructed model was run based on the experimental data over a specific period to compare the modelling and experimental results. SWD was used rather than SWI irrigation, as the daily productivity was directly measured rather than being calculated in terms of soil water retention. The productivity of the SWD system as tested and measured during our main experimental trial during the period from April to May was 27 litres/day (10.8 l/m²/day) and, over this specific period, the input data modelled and reported below ranged from 21 to 23.5 kg/day.

SWD Model input data:

Evaporation surface area: 2.5 m²

Air flow rate (M_a): approx. 0.025- 0.030 kg/s

Air temperature (T_a): 50° C

Recirculated brackish water flow rate (M_w): 1.5 m³/h

Recirculated brackish water temperature (T_w): 42-58°C with 50 °C average

Dry air humidity (RH): 80 %

The results of the modelling showed productivity ranging from 23.53 kg/day to 26.70 kg/day for the same period (Table 06.02) and confirmed to be in line with the experimental results, but there may be needed further investigations and more experimental data to predict the real convergence of the results.

T _w [°C]	M _w [m ³ /h]	T _a [°C]	M _a [kg/s]	Dry air RH, [%]	Product, [kg/day]	
					Modelled	Experimental
50	1.5	50	0.015	80	16.27	
50	1.5	50	0.020	80	20.09	
50	1.5	50	0.025	80	23.53	21,00
50	1.5	50	0.030	80	26.70	23,50
50	1.5	50	0.035	80	29.65	
50	1.5	50	0.035	70	38.18	
50	1.5	50	0.035	60	43.30	
50	1.5	50	0.035	50	46.57	
50	1.5	50	0.035	40	48.69	

Table 06.02– Productivity modelling results based on solar radiation from April-May in Oman using experimental procedures.

The difficulties in collecting precise data in the field experiments and the low amount of data collected during the experiment itself made the validation between theory (model) and experimental data very difficult giving more a qualitative indication of the tendency of the productivity than a real quantitative convergence.

A comparison with other prior modelled or experimented technologies was also quite difficult owing to variations in input parameters, although the main sources for this work were the studies on condensation irrigation by Lindblom (2003, 2006), Lindblom and Nordell (2003, 2006, 2007) and Okati et al. (2016, 2018, 2019).

The model developed for SWD was run according to the previously modelled system for drinking water production with a similar incoming air temperature, RH and other parameters at the dehumidification stage. The results reported in Figure 06.03 were as found.

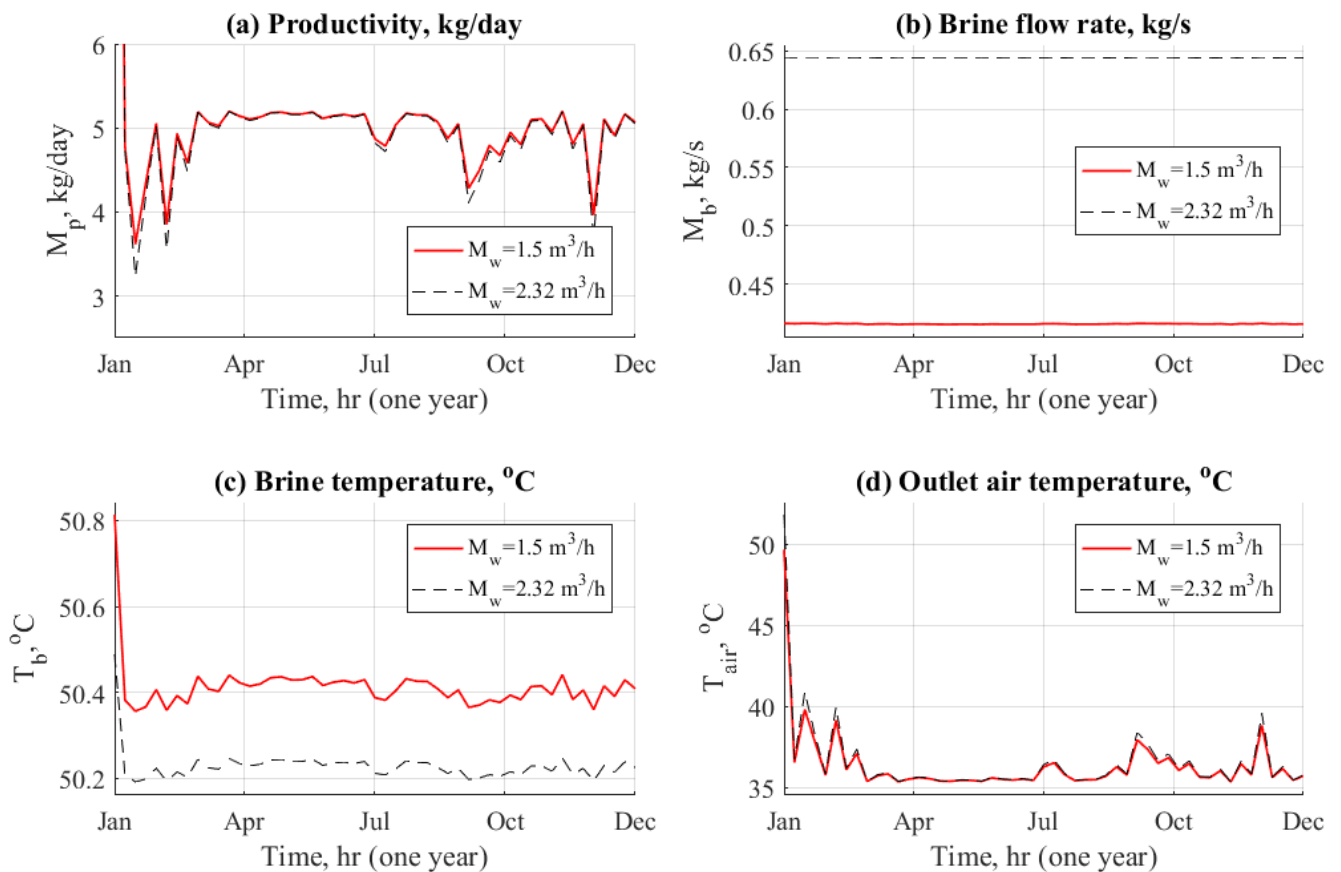


Figure 06.12– Modelling results for SWD for given parameters derived from the experiments of Lindblom (2003), Lindblom and Nordell (2007), and Okati et al. (2019).

The results obtained, as presented for the SWD model, had a productivity of 5 kg/day for a condensation surface of 2.5 m² (equivalent to 2 l/m²/day) or, for the same condensation surface using a 0.2 m diameter pipe, of 1.30 l/m/day.

The modelled productivity of SWD appears to be lower than that of Lindblom and Nordell (2007) who estimated a yield of 2.30 l/m/day and Okati et al. (2019) who reported 2.43 l/m/day, although their initial assumptions were inappropriate for real-world experiments using cheap solar technologies for air and water heating.

One of the primary advantages of SWD and SWI is that productivity remains constant despite the rig's length, while for condensation irrigation, the productivity is reduced drastically for longer pipes. One of the main objectives of this work was to develop a novel, sustainable and affordable SWD technique that could be coupled with irrigation and implemented in arid regions, one which is suitable for small-scale applications, easy to build with local products, and can be managed by unskilled workers. Production efficiency is always an important objective where water treatment is concerned but, in this work, system costs and simplicity are preferred and implemented wherever possible, leaving aside comparable, more efficient and costlier higher-tech solutions.

A detailed cost investigation is performed in Chapter 7 to show that both the experimental results and modelling have demonstrated the feasibility of SWD and SWI in remote, arid regions. They constitute a low-cost technique for producing irrigation water of very low salinity that can be used directly or else combined with drip irrigation.

6.4 Conclusions

The performance modelling technique used for the proposed SWI and SWD systems showed that traditional models are too complex to accurately detail the specific design parameters (including power, module efficiency, flow rates, soil, air and water physical properties, energy & exergy streams, design limits, etc). Even if the results are in agreement with the experiment, experimental unit construction is necessary to understand the real-world performance of such complex systems and understand their practical applicability in arid regions.

The results from the model were in reasonable agreement with the experimental productivity over the months tested. The modelling results revealed that daily system productivity would be in the range of 15 to 35 l/day over the course of an entire year for both configurations, with any variations arising explained by the increases in day length and increased solar radiation, which of course tend to increase system productivity. The model introduced showed many advantages as compared to those presented within the literature, including easy model construction; a broad range of power coverage; ready compatibility with other technologies such as desalination processes; and the fact that only one parameter needs to be assigned (i.e. the power load) to solve the model outputs. However, despite all these improvements, the model proved to be insufficiently accurate to predict the precise output for each of the various input parameters and thus should be adapted and improved.

7. Cost Estimation and Economic Analyses

7.1 Introduction to Cost Analyses

The cost of water is normally the most important metric for a desalination system, whether used for drinking water or irrigation. It is often measured in terms of dollars per cubic metre. The cost varies according to the technology used and the scale of the system, as large-scale desalination plants using either membrane or thermal processes are cheaper than even the most competitive small-scale systems. This cost efficiency is achieved using highly energy-efficient multi-stage systems and associated economies of scale (Karangianis et al. 2008). In the remote regions of arid countries, where there is a pressing need for small production plants with a fresh-water output below 100 m³/day, the cost of water is important though not the primary consideration. Most existing solutions for cheap water desalination are, in fact, unsuitable for small-scale applications as they generally require high capital costs for infrastructure, such as power and plumbing, as well as skilled employees for implementation and management of their daily operation. SWI and SWD offer the opportunity of investigating whether such low capital, sustainable, and novel seawater desalination techniques can be coupled with irrigation and implemented in arid regions. The target of reducing capital cost has been achieved and successfully demonstrated both in the experimental unit and in the proposed system scale-up.

In this section, a cost analysis of the proposed desalination systems is performed. The costs of the various components used and proposed are calculated in OR (Omani Rial) and USD (the currency exchange rate in 2016 was 1 RO= 2.59 USD) and are based on the Omani electricity market prices in 2016. The capital cost (CAPEX) and operational costs (OPEX) of the experimental unit and an optimised version are proposed and compared together with alternative desalination systems. Specifically, RO is the most appealing technology even if it is not designed for small-scale applications. However, when coupled with renewable energy, it may present an attractive solution in terms of reducing environmental impact due to lower conventional energy consumption and lower gas emissions (Karagiannis et al. 2008) despite a higher energy cost (Antonyan, 2019).

7.2 Cost Estimation and Economic Analyses

The current techniques of SWI and SWD under investigation have demonstrated low capital costs. Cost estimation and economic analyses have also been made for SWD as, for SWI, the fresh-water produced is not collected but rather directly transferred to the soil and we would need to estimate an equivalent amount of fresh-water produced considering the equivalent water necessary to irrigate soil via drip irrigation after deducting losses due to evaporation and transportation rates.

The estimated capital cost of the SWD experimental unit for an equivalent of a cubic metre of clean water was about 0.16 RO/m³ (or 0.41 \$/m³). This figure takes into account the cost of equipment and materials for the unit over its 10-year lifetime in addition to the solar heating equipment (Table 07.01).

<i>Item</i>	<i>Exp. SWD System</i>	<i>Remarks</i>
CAPEX	0.16 OR/m ³ (0.41 \$ /m ³)	583 OR/m ³ (1510 \$ /m ³) total system capital investment and amortisation over a period of 10 years.
OPEX	8.4 OR/m ³ (21.75 \$ /m ³)	Electrical power (420 kWh/m ³) at a tariff of 0.02 OR/kWh (0.052 \$/kWh).
Total Production costs	8.56 OR/m ³ (22.16 \$ /m ³)	High cost for the SWD due to the high energy cost for electrical heating and air blowing/pumping.

Table 07.01 - Estimated Cost of the current experimental SWD unit per equivalent cubic metre of fresh-water produced (Muscat's Electricity Distribution Comp. 2018)

The breakdown of the cost of the investment was about 40% for materials and 60% for equipment and instruments. The CAPEX of the system was low because the SWD technique only required low-cost plastic materials to construct the ducts and the frames, cheap low-pressure pumps to circulate the water, low-cost air blower and low-cost solar thermal techniques for heating purposes (as outlined in Table 07.02). The operational costs of the experimental unit were initially high. It was calculated and reported as 420 kWh/m³ as electrical resistances were used to provide the additional water heating required and these were very energy-intensive. The consumption by the electrical resistances accounted for over 90% of the system's energy requirement.

<i>Item</i>	<i>Description</i>	<i>Cost (RO)</i>	<i>%</i>	<i>Remarks</i>
Materials	PVC materials for piping, frames, and unit cover	350 RO (906,5 \$)	60	Low cost, new or used plastic materials (mainly PVC)
Equipment	Pumps, valves, air blower and solar heating unit	233.0 RO (603,5 \$)	40	Low-pressure feeding pump + low-pressure air blower + low-cost solar thermal heaters.

Table 07.02 - Breakdown of the estimated CAPEX cost for the SWD experimental unit per equivalent cubic metre of fresh-water produced.

The high OPEX and, consequently, the total water production cost of the experimental unit, before the implementation of the solar thermal heaters, was calculated to be 8.56 OR/m³ (22.16 \$/m³). In practice, the power cost could have been further reduced, as the heating unit did not need to be operated continuously, especially after optimising the design parameters and operating conditions. Power consumption and its relative costs could have been further reduced by using a PV system for driving the air blower, while the water circulation pumps and industrial blower of the experimental unit could have been replaced with a low power consumption one.

The projected costs of the SWD technique for a large-scale commercial unit able to produce 100 m³/day were also considered, based on the experimental unit data and scaling up, using the advantages of economy of scale and the recommended improvements to the technique including system optimisation. In the scaled-up process presented (Table 07.03), the heating was expected to be provided only by the sun using low-cost solar heating techniques, which are accounted for in the capital costs, while the construction materials used were still sourced from locally available low-cost plastic components. Moreover, the system was considered without the use of high-pressure pumps or expensive instrumentation. The electrical energy requirements, solely for pumping the feed water and powering the air blower, were estimated to be about 18-20 kWh to produce the equivalent of a cubic metre of clean water. These estimated energy consumption figures were about three times higher than the ideal values calculated via Bernoulli of 6-7 kWh (without considering highly efficient pumps and air blowers). Additional energy reduction could have been achieved by implementing the power supply with solar PV. Staff and maintenance costs were not included in the estimates for the full-scale SWD system, as they were expected to be small and account for less than 5% of the operating costs. This is because no specialist staff are required and there is only minimal maintenance due to the low level of complexity of the system.

<i>Item</i>	<i>SWD System</i>	<i>Remarks</i>
CAPEX	0.07 OR/m ³ . (0.18 \$ /m ³)	250 OR/m ³ over 10 years (647 \$ /m ³)
OPEX	0.40 OR/ m ³ . (1.04 \$ /m ³)	20 kWh/m ³ electrical power to drive pumps and blower required at a power tariff of 0.02 OR/kWh.
Production cost [OR/m³]	0.47 OR/ m ³ . (1.22 \$ /m ³)	Cost for the SWD is low if solar energy is used to provide heat.

Table 07.03 - Projected costs of the SWD technique for a scaled-up version with a production capacity of 50 m³/day.

According to the aforementioned considerations, the projected total cost for the commercial (or near-market) application of the seawater distillation technique for a unit with a capacity below 100 m³/day, for an equivalent of a cubic metre of clean water, was about 0.47 OR/m³ (1.22 \$/m³) with a very low CAPEX amortisation, representing only 15% of the total water cost.

A scaled-up SWD system appeared to be very competitive as compared with other desalination technologies of low production capacity, especially given that RO is currently the most efficient technology and one that can be easily powered by renewable energy (Antonyan, 2019). RES have low energy productivity (Shahzad et al., 2017) and they are not able to supply the appropriate energy demand for medium and large-scale desalination plants. Moreover, they are unable to deal with the large-scale energy demands of thermal desalination processes.

Membrane methods require around 5 times less energy than thermal methods (Antonyan, 2019). Consequently, it is economically more beneficial to combine RES with membrane technologies rather than with thermal ones.

RO technology only requires electrical energy for efficient feed water pumping, dosing/filter pumps, and permeate water pump, and high-pressure pumps consume about 80% of the total electrical energy requirement (Farooque et al. 2008). These can readily be driven by solar and wind energy. Normally, for small production plants, solar energy is preferred (Cipollina et al., 2014), although the need to run the process continuously requires the use of such energy-storing devices as batteries, thereby increasing the total system capital costs (Mohamed et al., 2006).

The average energy consumption for seawater RO is given by Antonyan (2019), spanning a wide range from 2.4 to 17.9 kWh/m³, with an average energy consumption of 5.5 kWh/m³. This value is highly dependent on the capacity of the desalination plant, as smaller installations, remote locations, and inexperience in design and operation may increase the energy footprint. Small-scale RO systems, rated below 80 m³/day, are unable to use an efficient energy recovery system (Kadaj et al. 2018), thereby increasing their energy demand drastically.

Focusing on RO plants with a production capacity below 100 m³/day (Table 07.04), an average energy demand of 9.5 kWh/m³ (Cipollina et al. 2014; Abdelkareem et al. 2017; Albloushi et al. 2019; Ali et al. 2017) and a capital cost for a PV-RO system of 3,085 OR/m³ (9,855 \$/m³) (Antonyan 2019) can be considered, giving a total water production cost for a PV-RO system of 0.89 OR/m³ (2.30 \$/m³) (Table 07.05).

Desalination method	RO	RO	RO	RO
Capacity [m ³ /day]	20	<24	<50	<100
Electrical energy [kW h/m ³]	7 to 5	7.7 to 3.8	24 to 17.9	15
Thermal energy [MJ/ m ³]	none	none	none	none
Total average electricity [kWh/m m ³]	6	5,8	10,2	15
RES source	PV	PV	PV	PV
<i>Reference</i>	Cipollina et al. (2014)	Abdelkareem et al. (2017)	Albloushi et al. (2019)	Ali et al. (2017)
Average Electricity needed [kWh/ m ³]	9,25			

Table 07.04 - Summary of desalination technologies powered by solar energy with a production capacity below 100 m³/day.

In Table 07.05, the projected cost of the SWD technique for scaled-up commercial units is compared with a similarly sized PV-RO. It shows that SWD is highly competitive in terms of CAPEX and in line with OPEX and that the production of water using SWD and, consequently SWI, is a sustainable and effective solution that should be implemented in arid regions.

Item	SWD System	Remarks	PV-RO Systems	Remarks
CAPEX	0.07 OR/m ³ (0.18 \$ /m ³)	250 OR/m ³ over 10 years (647 \$ /m ³)	0.52 OR/m ³ (1.35 \$ /m ³)	3,805 OR/m ³ (9,855 \$/m ³) over 20 years
OPEX	0.40 OR/m ³ (1.04 \$ /m ³)	20 kWh/m ³ electrical power required at a power tariff of 0.02 OR/kWh.	0.37 OR/m ³ (0.96 \$ /m ³)	Electrical energy for RO process is about 50% of the OPEX and the rest 50% for chemicals, staff & maintenance.
Production cost OR/m ³	0.47 OR/m ³ (1.22 \$ /m ³)	Cost of SWD is low if solar energy is used to provide heat.	0.89 OR/m ³ (2.30 \$ /m ³)	Bigger RO plants may have a much lower production cost. These values are valid for smaller sized ones.

Table 07.05 - Projected costs of the SWD technique large-scale units as compared with PV-RO.

RO systems are, in fact, more complex and need a higher level of capital cost and expensive three-phase type power units to drive their high-pressure pumps, while the SWD technique only requires a normal single-phase power supply. RO also requires the use of chemicals for water pre-treatment and skilled staff for maintenance and these have a major impact on the operational costs, contributing more than 50% of total cost (Figure 07.01) (Shazhad et al. 2017).

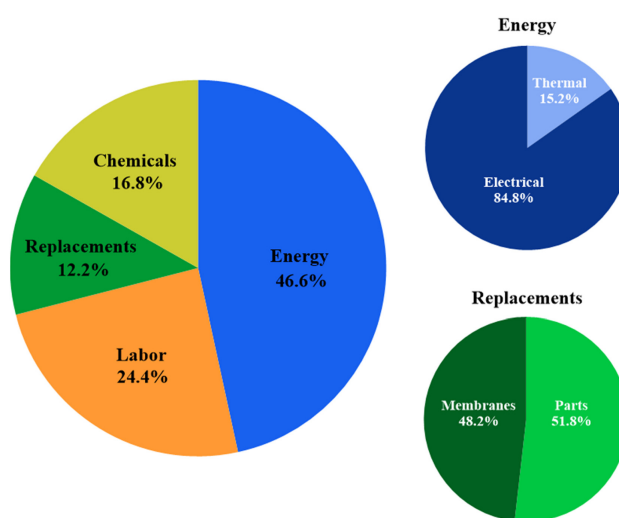


Figure 07.01 - Operational costs of an RO system (Shazhad et al. 2017).

SWI and SWD have successfully demonstrated that (1) they can be easily implemented in remote areas of arid regions; (2) they are efficient and able to reduce capital costs; and (3) they can benefit from further R&D before being taken to the market. Their low energy footprint and production cost

place them favourably as compared to new solar MD and solar ME dehumidification approaches (Figure 07.02).

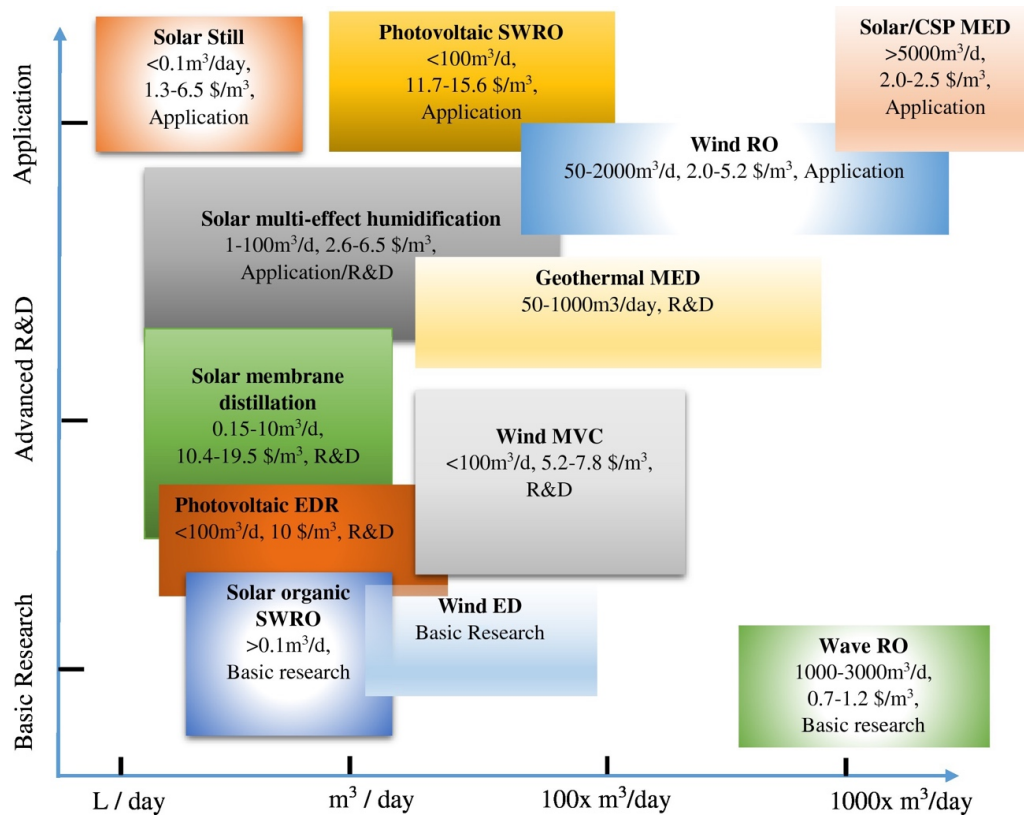


Figure 07.02 - Renewable energy operated desalination technologies status: Capacity, production cost and technology trend (Shahzad et al. 2017).

8. Conclusions and Recommendations for Future Work

8.1 Conclusions and Novelties

The use of seawater for agricultural purposes is limited and has only been investigated over the past few decades due to rising water production costs. Normally the strategy is to preserve water using smart irrigation and infrastructure modernisation.

Countries with the greatest experience are Spain, Israel and the Middle East, where many studies have investigated traditional desalination technologies (RO, MED, MSF) coupled with irrigation and the use of solar greenhouses. The use of humidification-dehumidification and subsurface irrigation has also been explored.

The basic idea before starting the project surrounded coupling irrigation with a SP in combination with a MD system. A patent for such an arrangement had been filed by Surrey University in 2008 (A. O. Sharif, Separation Method, European Patent No. EP2089142). The investigations of the present project indicate that the use of such a SP built and operated in Oman for heat generation was impractical as the following outcomes were observed:

- Operation of a SP in Oman and other GCC countries proved difficult because of dust and cleaning problems. Addressing this problem could make the SP technique a more economical option.
- Sand particles (mostly clay particles) adhered to the SP cover and blocked the sunlight.
- SP technology presents a low-cost option for heat generation but is of low efficiency and there are difficulties in constructing and maintaining such devices.
- The use of an FPC/PV/AGMD would afford remarkable productivity as compared to SP/PV/AGMD (from modelling).
- The SP cover would reduce the productivity by 3% using an AGMD AQ24 and by 4% with an AQ7 type.
- A greater SP depth would increase thermal energy and membrane productivity.

Additionally, the reduction in the costs of other emerging and competitive solar heating systems such as HPs, Flat Plate Collectors and Concentrated Solar Cells makes the SP less competitive.

However, the project has resulted in innovative new designs for the SWI and SWD techniques. Their novelty surrounds the enhanced water evaporation rate using an aeration process and an innovative condensation process of introducing water vapour either inside or outside the soil. The new SWI

technique mimics the natural water cycle of evaporation and condensation, albeit in a small enclosed system. It provides a suitable and alternative irrigation technique by producing water of low salinity from seawater (or any other impure water source) without having to resort to traditional expensive industrial desalination methods using membranes or distillation. Similarly, the modified SWD technique provides a low-cost distillation system. The field trials have demonstrated that both the SWI and the SWD techniques are cheaper options in terms of their capital cost, as compared with conventional membrane and thermal distillation methods for smaller units, for a fresh-water production of below 100 m³/day.

The electrical energy requirements of the SWD and SWI techniques to drive the feed pump and the air blower are around 20 kWh per cubic metre of clean water, twice the equivalent electrical energy requirement of a PV-RO system. However, no high-pressure pumps, high chemical consumption or skilled operators are required. It should be noted that the 20 kWh/m² required is a high estimated specific energy consumption, a trade-off between energy and capital costs, and a better efficiency could be achieved with more efficient equipment and materials, although this would incur higher construction and staff costs. This project has also confirmed that the proposed techniques can be constructed locally without the need for expensive equipment or specialist skills, and that the SWD technique can be scaled up without incurring challenging engineering issues. However, in scaling SWI, controlling the water temperature and limiting heat transfer to the soil may be detrimental to crop sowing and growth. The project has also bridged the gap between modelling at a laboratory scale and a real-world field trial in a harsh environment.

8.2 Analysing the Commercial Viability of Large Commercial Units

The SWD technique, as experimented with and modelled in this project, had a limited production capacity of about 27 litres per day. This was based on a designed evaporation surface area of only 2.5 m², an operating temperature range of 42 to 58°C (average of 50°C), an air flow rate of 65 m³/h, and on the operating conditions as reported in the experimental data. Together these gave a baseline production rate of about 10.8 l/m²/day. This unit could then be scaled up to achieve greater productivity, as:

1. Increasing the operating temperature to 85°C would multiply the evaporation rate by more than 8-fold (Figure 08.01). Assuming only a 5-fold increase, a rate of 10.8 l/m²/day could be improved to around 54.0 l/m²/day;

2. Additionally, a 5-fold increase in the air flow rate to 350 m³/h (as increasing the air flow rate will require only a small amount of energy due to the low density of air as compared with water) would have a linear effect in increasing the evaporation rate if the air temperature can be kept constant, although the rate would increase non-linearly if the air temperature also increased;
3. Further, improving the cooling effect would enhance the condensation process.

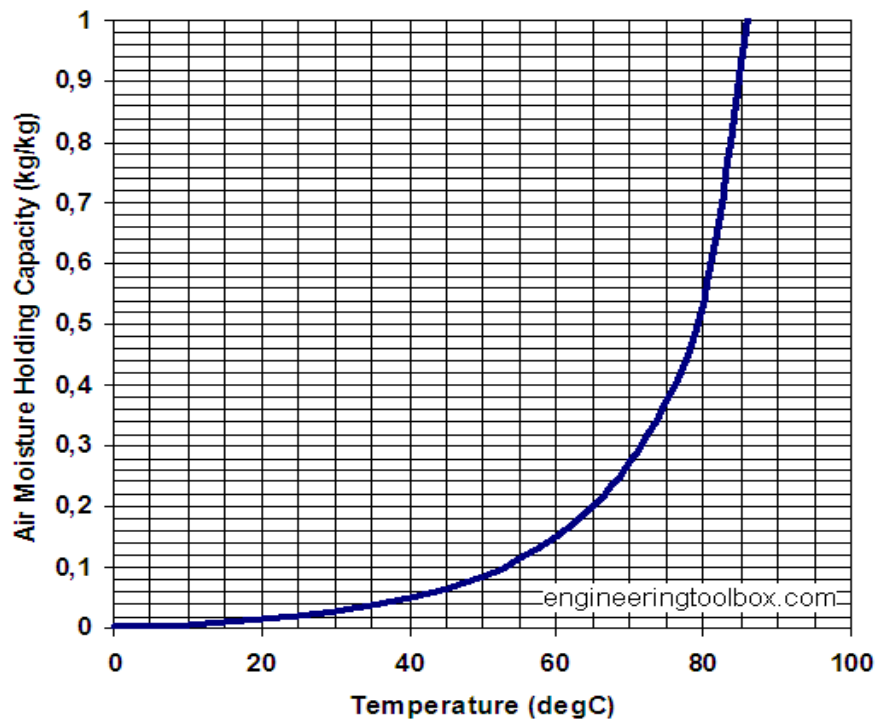


Figure 08.01 - Moisture content of saturated air relative to temperature (Engineeringtoolbox.com)

Combining the effects of increasing both the air flow rate to about 350 m³/h and the air temperature to about 85°C, in addition to improving the cooling effect, would further increase the evaporation rate by around 3-fold to about 160 l/m²/day. Scaling up the current distillation unit to one with a larger area of 200 m² would theoretically increase productivity to 32,000 l/day (32 m³/day). Additionally, the distilled water of low salinity produced could be mixed with a small proportion of salty water (circa. 10-15%) to further increase the volume of suitable irrigation water.

The estimated capital cost for such a large-scale commercial SWD system to produce about 32 m³/day of clean water for trees and date palm irrigation would be about 8,750 RO (22,662.5 \$) with a lifespan of around ten years, making it a viable solution for farming or landscape applications. The amount of

water produced would be sufficient to irrigate some 225 mature date palm trees, estimating a daily water requirement of 140 l/day for a mature date palm in Oman.

8.3 Recommendations for Future Works

Various steps and measures have been recommended to increase the performance of the techniques and reduce the cost of the water produced (OR/m³ or \$/m³). Both techniques can be taken to the next step of field demonstration via the following recommended steps:

I. For the SWI technique:

- Increasing the supply seawater temperature (ideally 60-90°C).
- Increasing the air flow rate to increase the aeration process (i.e. >350 m³/hr).
- Decreasing the air temperature to enhance cooling of the soil (the difference between air temperature and feed water temperature should be >10 °C).
- Enhancing vapour distribution through the soil using more porous soils.
- Increasing condensation by enhancing soil cooling using water and/or air-cooling techniques. (e.g., apply opposite cooling flow in the soil to decrease soil temperature and thereby increase the condensation of fresh-water according to temperature differences).
- Enhancing soil moisture content by increasing soil water-absorbing using clay and highly absorbent polymers.

II. For the SWD technique:

- Increase the evaporation surface area of the tent by increasing its width.
- Increase the condensation surface area.
- Enhancing evaporation by increasing both feed seawater and air temperatures as well air flow rate.
- Enhancing condensation by increasing the temperature difference between the inside and the outside of the tent by using outside cooling, including shading, air cooling and water cooling.
- Enhancing condensation by increasing the pressure inside the condensation chamber by using corrosion-resistant materials such high density plastics that can tolerate temperatures of up to 85°C.

- Having separate evaporation and condensation chambers in which more effective cooling techniques can be used to enhance the condensation.
- Enhancing evaporation by creating a vacuum in the evaporation chamber.

The trials have indicated that both SWI and SWD techniques are best suited for a controlled environment such as a greenhouse. The next step for the SWI techniques should be carried out in a large greenhouse in which all of the preceding recommendations are considered.

Further, to maximise the use of the greenhouse, the SWI technique could be applied in multiple layers as a form of vertical farming which will allow maximum use of the available greenhouse area.

Similarly, the SWD technique could be deployed in a large greenhouse where the evaporation area will be increased substantially and where the operating conditions of temperatures and air flow rates could be easily controlled.

It can be concluded, at this stage, that both techniques can produce water of low salinity at low capital cost and reasonable energy cost, especially where solar energy is available for both heating and electrical production. They can be scaled up and commercialised for a small production unit with the indicated recommendations.

References

- Abdelkareem, M.A., Assad, M.E.H., Sayed, E.T. and Soudan, B., 2018. Recent progress in the use of renewable energy sources to power water desalination plants. *Desalination*, 435, pp.97-113.
- Abdel-Salam, M.S., Hilal, M.M., El-Dib, A.F. and Abdel Monem, M., 1993. Experimental study of humidification-dehumidification desalination system. *Energy sources*, 15(3), pp.475-490.
- Abdullah, A.S., Younes, M.M., Omara, Z.M., Essa, F.A., 2020. New design of trays solar still with enhanced evaporation methods e comprehensive study. *Sol. Energy* 203, 164 e174.
- Agha, K.R., 2009. The thermal characteristics and economic analysis of a solar pond coupled low temperature multi-stage desalination plant. *Solar energy*, 83(4), pp.501-510.
- Ahmed, M., Arakel, A., Hoey, D., Thumarukudy, M.R., Goosen, M.F., Al-Haddabi, M. and Al-Belushi, A., 2003. Feasibility of salt production from inland RO desalination plant reject brine: a case study. *Desalination*, 158(1-3), pp.109-117.
- Albloushi, A., Giwa, A., Mukherjee, D., Calabro, V., Cassano, A., Chakraborty, S. and Hasan, S.W., 2019. Renewable energy-powered membrane systems for water desalination. In *Current Trends and Future Developments on (Bio-) Membranes* (pp. 153-177). Elsevier.
- Ali, A., Tufa, R.A., Macedonio, F., Curcio, E. and Drioli, E., 2018. Membrane technology in renewable-energy-driven desalination. *Renewable and Sustainable Energy Reviews*, 81, pp.1-21.
- Almanza, R. and Castaneda, R., 1993. What type of clays can be used as liners for NaCl solar ponds? *Solar energy*, 51(4), pp.293-297.
- Almanza, R. and Lozano, M.C., 1990. Mechanical and thermal tests of a bentonite clay for use as a liner for solar ponds. *Solar energy*, 45(4), pp.241-245.
- Almanza, R., Martínez, A. and Segura, G., 1989. Study of a kaolinite clay as a liner for solar ponds. *Solar energy*, 42(5), pp.395-403.
- Alenezi, I., 2012. Salinity gradient solar ponds: Theoretical modelling and integration with desalination. University of Surrey (United Kingdom).
- Ali, H.M., 1987. An experimental study on a modified design compact shallow solar pond. *International journal of energy research*, 11(4), pp.613-616.
- Al-Enezi, G., Ettouney, G., Fawzy, N., 2006. Low temperature humidification dehumidification desalination process. *Energy Convers. Manage*, 47, pp. 470-484.
- Al-Hallaj, S., Farid, M.M., Tamimi, A.R., 1998. Solar desalination with a humidification–dehumidification cycle: performance of the unit. *Desalination* 120, 273–280.
- Al-Homoud, A. A., Al-Marafie, A., Al-Kandari, A., Abou-Seido, E., 1989. Performance results of preliminary operation of Kuwait solar pond, *International Journal of Ambient Energy*, 10.1080/01430750.1989.9675142, 10, 4, (207-212).
- Al-Karaghoul, A., Renne, D., Kazmerski, L. L., 2009. Solar and wind opportunities for water desalination in the Arab regions - *Renewable and Sustainable Energy Reviews* 13 2397–2407.

- Al-Marafie, A.M.R., Al-Homoud, A.A., Al-Kandari, A. and Abou-Seido, E., 1991. Performance of 1700 m² solar pond operation in arid zone. *International Journal of Energy Research*, 15(7), pp.535-548.557-564, March 23-26, Cairo, Egypt.
- Amara, M.B., Houcine, I., Guizani, A. and Mâalej, M., 2004. Experimental study of a multiple-effect humidification solar desalination technique. *Desalination*, 170(3), pp.209-221.
- Amer, A. M., 1986. A salt gradient solar pond at Alexandria. *ASRE'86*, Vol. 1(48), pp. 557-564, March 23-26, Cairo, Egypt.
- Anagreh, Y., Bataineh, A., 2011. Renewable energy potential assessment in Jordan, *Renew. Sustain. Energy Rev.*, vol. 15, no. 5, pp. 2232–2239, 2011, doi: 10.1016/j.rser.2011.02.010.
- Andrews, J. and Akbarzadeh, A., 2005. Enhancing the thermal efficiency of solar ponds by extracting heat from the gradient layer. *Solar Energy*, 78(6), pp.704-716.
- Angeli, C., Leonardi, E. and Maciocco, L., 2006. A computational study of salt diffusion and heat extraction in solar pond plants. *Solar Energy*, 80(11), pp.1498-1508.
- Antonyan, M., 2019. Energy footprint of water desalination (Master's thesis, University of Twente).
- Aramesh, M., Kasaeian, A., Pourfayaz, F. and Wen, D., 2017. Energy analysis and shadow modeling of a rectangular type salt gradient solar pond. *Solar Energy*, 146, pp.161-171.
- Aramesh, M., Pourfayaz, F. and Kasaeian, A., 2017. Numerical investigation of the nanofluid effects on the heat extraction process of solar ponds in the transient step. *Solar Energy*, 157, pp.869-879.
- ASHRAE Handbook of Fundamentals, American Society of Heating Refrigeration and Air Conditioning Engineers, Inc., PP.27: 1-27:42, 1985.
- Assari, M.R., Tabrizi, H.B., Nejad, A.K. and Parvar, M., 2015. Experimental investigation of heat absorption of different solar pond shapes covered with glazing plastic. *Solar energy*, 122, pp.569-578.
- Assouad, Y., Lavan, Z., 1988. Solar desalination with latent heat recovery, *J. Solar Energy Eng.*, 110, 14–16.
- Assouline, S., Narkis, K. and Or, D., 2010. Evaporation from partially covered water surfaces. *Water resources research*, 46(10).
- Assouline, S., Narkis, K. and Or, D., 2011. Evaporation suppression from water reservoirs: Efficiency considerations of partial covers. *Water Resources Research*, 47(7).
- Atiz, A., Bozkurt, I., Karakilcik, M. and Dincer, I., 2014. Investigation of turbidity effect on exergetic performance of solar ponds. *Energy conversion and management*, 87, pp.351-358.
- Azzam Reda A. I., 1980. Agricultural polymers polyacrylamide preparation, application and prospects in soil conditioning, *Communications in Soil Science and Plant Analysis*, 11:8, 767-834.
- Ben-Amara, M., Houcine, I., Guizani, A., Mfialej, M., 2004. Experimental study of a multiple-effect humidification solar desalination technique. *Desalination* 170, 209–221.
- Bernad, F., Casas, S., Gibert, O., Akbarzadeh, A., Cortina, J.L. and Valderrama, C., 2013. Salinity gradient solar pond: Validation and simulation model. *Solar energy*, 98, pp.366-374.
- Berkani, M., Sissaoui, H., Abdelli, A., Kermiche, M. and Barker-Read, G., 2015. Comparison of three solar ponds with different salts through bi-dimensional modeling. *Solar Energy*, 116, pp.56-68.

- Betts, R.A., Alfieri, L., Bradshaw, C., Caesar, J., Feyen, L., Friedlingstein, P., Gohar, L., Koutroulis, A., Lewis, K., Morfopoulos, C. and Papadimitriou, L., 2018. Changes in climate extremes, fresh-water availability and vulnerability to food insecurity projected at 1.5 C and 2 C global warming with a higher-resolution global climate model. *Philosophical Transactions of the Royal Society A: Mathematical, Physical and Engineering Sciences*, 376(2119), p.20160452.
- Bezir, N.C., Dönmez, O., Kayali, R. and Özek, N., 2008. Numerical and experimental analysis of a salt gradient solar pond performance with or without reflective covered surface. *Applied Energy*, 85(11), pp.1102-1112.
- Bezir, N.C., Dönmez, O., Kayali, R. and Özek, N., 2008. Numerical and experimental analysis of a salt gradient solar pond performance with or without reflective covered surface. *Applied Energy*, 85(11), pp.1102-1112.
- Boubakri, A., Guermazi, N., Elleuch, K. and Ayedi, H.F., 2010. Study of UV-aging of thermoplastic polyurethane material. *Materials Science and Engineering: A*, 527(7-8), pp.1649-1654.
- Bouranis, D. L., Theodoropoulos, A. G., Drossopoulos, J. B., 1995. Designing synthetic polymers as soil conditioners. *Commun. Soil Sci. Pl. Anal.* 26: 1455–1480.
- Bourouni, K., Chaibi M., Tadrist L., 2001. Water desalination by humidification and dehumidification of air: state of the art, *Desalination*, 137 (2001) 167–176.
- Bowman, D. C., Evens, R. Y., Paul J. L., 1990. Fertilizer salts reduce hydration of polyacrylamide gels and affect physical properties of gel-amended container media. *J. Am. Soc. Hort. Sci.* 115: 382–386.
- Bozkurt, I., Atiz, A., Karakilcik, M. and Dincer, I., 2014. An investigation of the effect of transparent covers on the performance of cylindrical solar ponds. *International journal of green energy*, 11(4), pp.404-416.
- Bozkurt, I., Deniz, S., Karakilcik, M. and Dincer, I., 2015. Performance assessment of a magnesium chloride saturated solar pond. *Renewable Energy*, 78, pp.35-41.
- Bozkurt, I., Mantar, S. and Karakilcik, M., 2015. A new performance model to determine energy storage efficiencies of a solar pond. *Heat and Mass Transfer*, 51(1), pp.39-48.
- Brady, N.C. and Weil, R.R., 1999. Soil organic matter. The nature and properties of soils. Prentice Hall, Upper Saddle River, New Jersey, pp.446-490.
- Bryant, H.C. and Colbeck, I., 1977. A solar pond for London?. *Solar Energy*, 19(3), pp.321-322.
- Burston, I., 2002. Conservation of water from open storages by minimising evaporation (Doctoral dissertation, RMIT University).
- Camp, C., 1998. Subsurface drip irrigation: a review. *Transactions of the ASAE* 41(5), 1353–1367.
- Caruso, G., Naviglio, A., Principi, P. and Ruffini, E., 2001. High-energy efficiency desalination project using a full titanium desalination unit and a solar pond as the heat supply. *Desalination*, 136(1-3), pp.199-212.
- Cengel, Y.A., Boles, M.A. and Kanoglu, M., 2011. Thermodynamics: an engineering approach (Vol. 5, p. 445). New York: McGraw-hill.
- Chafik, E., 2002. A new seawater desalination process using solar energy. *Desalination* 153, 25–37.
- Chafik, E., 2003. A new type of seawater desalination plants using solar energy. *Desalination* 156, 333–348.

- Chaibi, M., 2000. An overview of solar desalination for domestic and agriculture water needs in remote arid areas, *Desalination*, 127 (2000) 119–133.
- Chaibi, M., 2003. Greenhouse systems with integrated water desalination for arid areas based on solar energy, Doctoral thesis, Swedish University of Agricultural Sciences, Alnarp, 2003.
- Chaibi, M., Jilar, T., 2004. System design, operation and performance of roof-integrated desalination in greenhouses, *Solar Energy*, Volume 76, Issue 5, 2004, Pages 545-561, ISSN 0038-092X, <https://doi.org/10.1016/j.solener.2003.12.008>.
- Chaibi, M., 2011. Greenhouse with Integrated Solar Desalination for Arid Regions, Lambert Academic Publishing.
- Chiasson, A.D., Spitler, J.D., Rees, S.J. and Smith, M.D., 2000. A model for simulating the performance of a shallow pond as a supplemental heat rejecter with closed-loop ground-source heat pump systems. *Ashrae transactions*, 106, p.107.
- Choudhary, M.I., 1995. (King Saud University, Riyadh, Saudi Arabia.); Shalaby, A.A.; Al-Omran, A.M.; Water holding capacity and evaporation of calcareous soils as affected by four synthetic polymers. *Communications in Soil Science and Plant Analysis* Volume 26, 1995 - Issue 13-14.
- Chung, T., Zhang, S., Wang, K. Y., Su, J., Ling, M., 2012. Forward osmosis processes: Yesterday, today and tomorrow -*Desalination*, Volume 287, 15 February 2012, Pages 78–81.
- Cipollina, A., Tzen, E., Subiela, V., Papapetrou, M., Koschikowski, J., Schwantes, R., Wieghaus, M. and Zaragoza, G., 2015. Renewable energy desalination: performance analysis and operating data of existing RES desalination plants. *Desalination and Water Treatment*, 55(11), pp.3120-3140.
- Dai Y.J., Zhang H.F., 2000. Experimental investigation of a solar desalination unit with humidification and dehumidification. *Desalination*, 130, pp. 169-175.
- Davies, P. and Paton, C., 2004. The Seawater Greenhouse in the United Arab Emirates: thermal modelling and evaluation of design options, *Desalination*, in press.
- De Boodt, M., 1975. Use of soil conditioners around the world. In *Soil Conditioners*. (B Stewart, M. Stelly, R. C. Dinauer and J. M. Padrutt, ed.), pp. 1–12. Special Publ. Series, Madison, SSSA Soil Science Society of America Inc.
- De Varennes, A., Balsinhas, A. and Carqueja M. J., 1997. Effects of two polyacrylate polymers on the hydrophysical and chemical properties of a sandy soil, and on plant growth and water economy, *Revista de Ciencias Agrárias*, vol. 20, no. 4, pp. 13– 27, 1997.
- Dehghan, A.A., Movahedi, A. and Mazidi, M., 2013. Experimental investigation of energy and exergy performance of square and circular solar ponds. *Solar energy*, 97, pp.273-284.
- Dhliwayo, D. K. C., 1993. The effect of a superabsorbent on soil water retention of two soils and on the growth, development, and yield of winter wheat (*Triticum aestivum* L., cv. Pote), *Zimbabwe Journal of Agricultural Research*, vol. 31, no. 1, pp. 53–64, 1993.
- Dickinson, W. C., Clark, A. F. and Iantuono, 1976. A. Shallow solar ponds for industrial process heat: the ERDA--SOHIO project. United States: N. p., Web.
- Dickinson, W. C., and Cheremisinoff, P. N., 1980. *Solar Energy Technology Handbook*, Marcel Dekker, New York, (1980) 374.

- Duffie, J.A. and Beckman, W.A., 2013. Solar engineering of thermal processes. John Wiley & Sons.
- Elashmawy, M., 2017. An experimental investigation of a parabolic concentrator solar tracking system integrated with a tubular solar still. *Desalination* 411, 1 e 8. <https://doi.org/10.1016/j.desal.2017.02.003>.
- Elsayed, M.M., Taha, I.S. and Sabbagh, J.A., 1994. Design of solar thermal systems. Jeddah, Saudi Arabia: Scientific Publishing Center, King Abdulaziz University.
- El-Agouz, S.A., Abugderah, M., 2008. Experimental analysis of humidification process by air passing through seawater. *Energy Convers. Manage.*, 49 pp. 3698-3703.
- El-Agouz, S.A., 2010. A new process of desalination by air passing through seawater based on humidification-dehumidification process. *Energy* 35, pp- 5108-5114.
- El-Amir, S., Helalia, A. M., Wahdan A., and Shawky, M. E., 1991. Effect of two polymers on corn (*Zea mays* L.) growth and water economy in sandy soils, *Soil Technology*, vol. 4, no. 2, pp. 177–181, 1991.
- El-Hady, O. A., Shaaban, S. M., and Wanas, S. A., 2006. Hydrophilic polymers for improving the conditioning effect of manures and organic composts. I. Production and water and fertilizers use efficiency for tomato grown in sandy soil, *Egyptian Journal of Soil Science*, vol. 46, no. 1, pp. 79–90, 2006.
- El-Kady, M., El-Shibini, F., 2001. Desalination in Egypt and the future application in supplementary irrigation, *Desalination*, Volume 136, Issues 1–3, 2001, Pages 63-72, ISSN 0011-9164, [https://doi.org/10.1016/S0011-9164\(01\)00166-7](https://doi.org/10.1016/S0011-9164(01)00166-7).
- El-Sebaei, A.A., 2005. Thermal performance of a triple-basin solar still. *Desalination*, 174: 23-37.
- El-Sebaei, A.A., Ramadan, M.R.I., Aboul-Enein, S., Khallaf, A.M., 2011. History of the solar ponds: A review study - *Renewable and Sustainable Energy Reviews*, Volume 15, Issue 6, August 2011, Pages 3319–3325.
- Entezar, A., Wang, R.Z., Zhao, S., Mahdini, E., Wang, J.Y., Tu, Y.D., Hu, D.F., 2019. Sustainable agriculture for water-stressed regions by air-water-energy management - *Energy* 181 (2019) 1121e1128.
- Ettouney, H., 2005. Design and analysis of humidification dehumidification desalination process *Desalination*, 183, pp. 341-352.
- Farahbod, F., Mowla, D., Jafari, Nasr M.R., Soltanieh M., 2013. Experimental study of a solar desalination pond as second stage in proposed zero discharge desalination process - - *Solar energy* 97,138.
- Fath, H., 1998. Solar distillation: a promising alternative for water provision with free energy, a simple technology and a clean environment, *Desalination*, 116 (1998) 45–56.
- Fath, H., and Ghazy, A., 2002. Solar desalination using humidification–dehumidification technology, *Desalination*, 142 (2002) 119–133.
- FAO, 2008. Workshop on “Irrigation of Date Palm and Associated Crops” -In collaboration with Faculty of Agriculture, Damascus University - Damascus, Syrian Arab Republic, 27-30 May 2007 - Food and Agriculture Organization of the United Nations, Regional Office for the Near East Cairo.
- FAO, 2012. Crop Production - Statistics Division, Food and Agriculture Organization, Rome, Italy
- Faqeha, H., Bawahab, M., Vet, Q.L., Faghih, A., Date, A. and Akbarzadah, A., 2019. An experimental study to establish a salt gradient solar pond (SGSP). *Energy Procedia*, 160, pp.239-245.

- Farid, M., Al-Hajaj, S., 1996. Solar desalination with a humidification–dehumidification cycle. *Desalination* 106, 427–429.
- Farid, M., Parekh, S., Selman, J.R., Al-Hallaj, S., 2002. Solar desalination with a humidification dehumidification cycle: mathematical modeling of the unit. *Desalination*, 151 (2002), pp. 153-164..
- Farooque, A.M., Jamaluddin, A.T.M., Al-Reweli, A.R., Jalaluddin, P.A.M., Al-Marwani, S.M., Al-Mobayed, A.A. and Qasim, A.H., 2008. Parametric analyses of energy consumption and losses in SWCC SWRO plants utilizing energy recovery devices. *Desalination*, 219(1-3), pp.137-159.
- Fath, H.E.S., El-Helaby, S.O., Soliman, A.M., 2004. Solar desalination using humidification–dehumidification processes. Part II. An experimental investigation. *Energy Convers. Manage.* 45, 1263–1277.
- Fisher, U., Weinberg, J., and Doron, B., 1988. Integration of solar pond with water desalination. *Renewable energy systems and Desalination*, 2(3), pp.110-118.
- Folchitto, S., 1991. Seawater as salt and water source for Solar Ponds, *Solar Energy*, Volume 46, Issue 6, 1991, Pages 343-351, ISSN 0038-092X, [https://doi.org/10.1016/0038-092X\(91\)90049-3](https://doi.org/10.1016/0038-092X(91)90049-3).
- Franzluebbers, A. J., 2002. Water infiltration and soil structure related to organic matter and its stratification with depth. *Soil and Tillage Research* 66, 197–205.
- Ganesh, S. and Arumugam, S., 2016. Performance study of a laboratory model shallow solar pond with and without single transparent glass cover for solar thermal energy conversion applications. *Ecotoxicology and environmental safety*, 134, pp.462-466.
- Ganguly, S., Date, A. and Akbarzadeh, A., 2017. Heat recovery from ground below the solar pond. *Solar Energy*, 155, pp.1254-1260.
- Garg, H.P., Adhikari, R.S. and Kumar, R., 2003. Experimental design and computer simulation of multi-effect humidification (MEH)-dehumidification solar distillation. *Desalination*, 153(1-3), pp.81-86.
- Garzia-Rodriguez, L., 2002. Seawater desalination driven by renewable energies: a review, *Desalination*, 143, 103–113.
- Gastli, A., and Charabi, Y., 2010. Solar electricity prospects in Oman using GIS-based solar radiation maps, *Renew. Sustain. Energy Rev.*, vol. 14, no. 2, pp. 790–797, 2010, doi: 10.1016/j.rser.2009.08.018.
- Garg, H.P., Bandyopadhyay, P., Rani, U., Hrishikesan, D.S., 1982. Shallow solar pond: State-Of-The-Art - *Energy Convers Mgmt.*, 22, pp. 117–131.
- Garg, H.P., 1987. *Advances in solar energy technology*, vol. ID Reidel Publishing Company, Dordrecht, Holland.
- Garmana, M.A. and Muntasserb, M.A., 2008. Sizing and thermal study of salinity gradient solar ponds connecting with the MED desalination unit. *Desalination*, 222(1-3), pp.689-695.
- Gasulla, N., Yaakob, Y., Leblanc, J., Akbarzadeh, A. and Cortina, J.L., 2011. Brine clarity maintenance in salinity-gradient solar ponds. *Solar Energy*, 85(11), pp.2894-2902.
- Geesing, D., Schmidhalter, U., 2004. Influence of sodium polyacrylate on the water-holding capacity of three different soils and effects on growth of wheat. *Soil Use and Management*, 20, 207-209.
- Ghani, F., Fernandez, E.F., Almonacid, F. and O'Donovan, T.S., 2017. The numerical computation of lumped parameter values using the multi-dimensional Newton-Raphson method for the characterisation of a multi-junction CPV module using the five-parameter approach. *Solar Energy*, 149, pp.302-313.

- Ghars Ali M., Parre E., Debez A., Bordenave M., Richard L., Leport L., Bouchereau A., Savouré A., Abdelly C., 2008. Comparative salt tolerance analysis between *Arabidopsis thaliana* and *Thellungiella halophila*, with special emphasis on K⁺/Na⁺ selectivity and proline accumulation, *Journal of Plant Physiology*, Volume 165, Issue 6, 2008, Pages 588-599, ISSN 0176-1617, <https://doi.org/10.1016/j.jplph.2007.05.014>.
- Ghazal, M.T., Atikol, U., Egelioglu, F., 2014. An experimental study of a solar humidifier for HDD systems, *Energy Convers. Manage*, 82, pp. 250-258.
- Gleick, P.H., 1993. *Water in crisis* (Vol. 100). New York: Oxford University Press.
- Glückstern, P., 1991. Potential uses of renewable energy for water desalination. European seminar on new technologies for use of renewable energy sources in water desalination, Athens.
- Gong, H., Chen, K., 2012. The regulatory role of silicon on water relations, photosynthetic gas exchange, and carboxylation activities of wheat leaves in field drought conditions. *Acta Physiologiae Plantarum* 34, 1589–1594.
- González, D., Amigo, J., Lorente, S., Bejan, A. and Suárez, F., 2016. Constructal design of salt-gradient solar pond fields. *International Journal of Energy Research*, 40(10), pp.1428-1446.
- Goutham, K.A.R.A.K.A.V.A.L.A.S.A. and Krishna, C.S., 2013. Solar pond technology. *Int. J. Eng. Res. Gen. Sci*, 1(2), pp.12-22.
- Göhlman, A., 1987. Heating of Frozen ground. Master Thesis 1987:030 CIV Luleå University of Technology, Sweden..
- Graeter, F., Duerrbeck, M., and Rheinlaender, J., 2001. Multi-effect still for hybrid solar/fossil desalination of sea and brackish water, *Desalination*, 138, 111–119.
- Gustafsson, A-M, Lindblom, J., 2001. Underground condensation of humid air: a solar driven system for irrigation and drinking-water production. Master Thesis 2001:140 CIV Luleå University of Technology, Sweden.
- Haddad, O., Al-Nimer, M., and Maqableh A., 2000. Enhanced solar still performance using a radiative cooling system, *Renewable Energy*, 21, 459–469.
- Harrington, J.F. and Kozlowski, T.T., 1972. Seed storage and longevity. *Seed biology*, 3, pp.145-245.
- Hassairi, M., Safi, M.J. and Chibani, S., 2001. Natural brine solar pond: an experimental study. *Solar Energy*, 70(1), pp.45-50.
- Hatfield, J. L., Prueger, J. H., 2015. Temperature extremes: Effect on plant growth and development, *Weather and Climate Extremes*, Volume 10, Part A, Pages 4-10, ISSN 2212-0947, <https://doi.org/10.1016/j.wace.2015.08.001>. (<https://www.sciencedirect.com/science/article/pii/S2212094715300116>).
- Hausherr, B., Ruess, K., 1993. Sea water desalination and irrigation with moist air, Ingenieurbüro Ruess und Hausherr, Switzerland.
- Hitsov, I., De Sitter, K., Dotremont, C., Cauwenberg, P. and Nopens, I., 2017. Full-scale validated Air Gap Membrane Distillation (AGMD) model without calibration parameters. *Journal of membrane science*, 533, pp.309-320.

- Hoffman, D., 1992. The application of solar energy for large-scale seawater desalination. *Desalination*, 89(2), pp.115-183.
- Hongsheng, L., Dan, W. and MaoZhao, X., 2020, March. Experimental Study on the Thermal Performance of a Porous Medium Solar Pond. In 2020 4th International Conference on Green Energy and Applications (ICGEA) (pp. 106-110). IEEE.
- Hottel, H.C., 1976. A simple model for estimating the transmittance of direct solar radiation through clear atmospheres. *Solar energy*, 18(2), pp.129-134.
- Hottel, H.C., Whillier, A., 1958. Evaluation of flat plate collector performance. *Trans. Conf. on the use of Solar Energy*, 2 part 1, p. 74.
- Hottel, H.C. and Woetz, B.B., 1942. *Transaction of the American Society of Mechanical Engineering*, 64p. 91.
- Howari, F.M., Sadooni, F.N. and Goodell, P.C., 2008. Assessment of water bodies of United Arab Emirates coastal Sabkhas as potential sites for natural salinity gradient solar ponds. *Journal of Energy Engineering*, 134(4), pp.111-120.
- Hull, J.R., 1980. Membrane stratified solar pond - *Solar Energy*, 25, p. 317.
- Hull, J.R., 1985. Solar pond ground heat loss to a moving water table. *Solar Energy*, 35(3), pp.211-217.
- Hull, J.R., 1986. Solar ponds using ammonium salts. *Solar Energy*, 36(6), pp.551-558.
- Hull, J.R., Bushnell, D.L., Sempsrote, D.G. and Pena, A., 1989. Ammonium sulfate solar pond: observations from small-scale experiments. *Solar energy*, 43(1), pp.57-64.
- Husain, M., Patil, P.S., Patil, S.R. and Samdarshi, S.K., 2004. Combined effect of bottom reflectivity and water turbidity on steady state thermal efficiency of salt gradient solar pond. *Energy conversion and management*, 45(1), pp.73-81.
- Iler, R. K., 2001. *Surface and colloid science*. Vol. 6 311 (Wiley, New York, 1973) - Matichenkov, V. & Bocharnikova, E. In *Studies in Plant Science* Vol. 8 eds G. H. Snyder L.E. Datnoff & G. H. Korndörfer) 209–219 (Elsevier, 2001).
- Iqbal, M., 2012. *An introduction to solar radiation*. Elsevier.
- IRENA, 2013. *Water Desalination Using Renewable Energy*, Mirei Isaka (misaka@irena.org) http://iea-etsap.org/E-TechDS/PDF/I12IR_Desalin_MI_Jan2013_final_GSOK.pdf accessed 24.09.12. (2013.01.007 IP).
- Jaefarzadeh, M.R., 2004. Thermal behavior of a small salinity-gradient solar pond with wall shading effect. *Solar Energy*, 77(3), pp.281-290.
- Jaefarzadeh, M.R., 2006. Heat extraction from a salinity-gradient solar pond using in pond heat exchanger. *Applied Thermal Engineering*, 26(16), pp.1858-1865.
- Jayaprakash, R., Perumal, K., Arunkumar, T., Kumar, S. and Kojima, T., 2011. Effect of Carboxy Methyl Cellulose Gel on Thermal Energy storage of Ground Shallow Solar Pond. *Journal of Chemical Engineering of Japan*, pp.1106140215-1106140215.
- Johnson, A., Mu, L., Park, Y.H., Valles, D.J., Wang, H., Xu, P., Kota, K., Kuravi, S., 2019. A thermal model for predicting the performance of a solar still with Fresnel lens. *Water* 11, 1860. <https://doi.org/10.3390/w11091860>.

- Johnson, M. S., and Leah, R. T., 1990. Effects of superabsorbent polyacrylamide on efficacy of water use by crop seedlings. *J. Sci. Fd Agric.* 52: 431–434.
- Jubran, B.A., El-Baz, A.R., Hamdan, M.A. and Badran, A.A., 1996. Experimental investigation of local clays and clay schemes as liners for solar ponds. *International journal of energy research*, 20(7), pp.637-642.
- Kabeel, A.E., Hamed Mofreh, H., Omara, Z.M., Sharshir, S.W., 2014. Experimental study of a humidification-dehumidification solar technique by natural and forced air circulation, *Energy*, Volume 68, Pages 218-228, ISSN 0360-5442, <https://doi.org/10.1016/j.energy.2014.02.094>.
- Kabeel, A.E., Khairat Dawood, M.M., Ramzy, K., Nabil, T., Elnaghi, B., Elkassar, A., 2019. Enhancement of single solar still integrated with solar dishes: an experimental approach. *Energy Convers. Manag.* 196, 165e174. <https://doi.org/10.1016/j.enconman.2019.05.112>.
- Kadaj, E. and Bosleman, R., 2018. Energy recovery devices in membrane desalination processes. In *Renewable energy powered desalination handbook* (pp. 415-444). Butterworth-Heinemann.
- Kalogirou, S.A., 2005. Seawater desalination using renewable energy sources. *Progress in energy and combustion science*, 31(3), pp.242-281.
- Karagiannis, I.C. and Soldatos, P.G., 2008. Water desalination cost literature: review and assessment. *Desalination*, 223(1-3), pp.448-456.
- Karakilcik, M., Dincer, I. and Rosen, M.A., 2006. Performance investigation of a solar pond. *Applied Thermal Engineering*, 26(7), pp.727-735.
- Karakilcik, M., Kıymac, K. and Dincer, I., 2006. Experimental and theoretical temperature distributions in a solar pond. *International Journal of Heat and Mass Transfer*, 49(5-6), pp.825-835.
- Karim, C., Slim, Z., Kais, C., Jomâa, S.M. and Akbarzadeh, A., 2010. Experimental study of the salt gradient solar pond stability. *Solar Energy*, 84(1), pp.24-31.
- Karunamurthy, K., Murugumohankumar, K. and Suresh, S., 2012. Use of CuO nano-material for the improvement of thermal conductivity and performance of low temperature energy storage system of solar pond. *Digest Journal of Nanomaterials and Biostructures*, 7(4), pp.1833-1841.
- Katekar, V. P., Deshmukh, S. S., 2021. Techno-economic review of solar distillation systems: A closer look at the recent developments for commercialization, *Journal of Cleaner Production*, Volume 294, 2021, 126289, ISSN 0959-6526.
- Kaushik, N.D., Bansal, P.K., Sodha, M.S., 1980. Partitioned solar pond collector/storage system - *Applied Energy* - Volume 7, Issues 1–3, November 1980, Pages 169-190.
- Kaviti, A.K., Yadav, A., Shukla, A., 2016. Inclined solar still designs: a review, *Renew. Sustain. Energy Rev.*, 54, pp. 429-451.
- Khalil, A., El-Agouz, S.A., El-Samadony, Y.A.F., Abdo A., 2015. Solar water desalination using an air bubble column humidifier. *Desalination*, 372, pp. 7-16.
- Khalilian, M., 2017. Assessment of the overall energy and exergy efficiencies of the salinity gradient solar pond with shading effect. *Solar Energy*, 158, pp.311-320.
- Klein, S.A., 1975. Calculation of flat-plate collector loss coefficients. *Solar energy*, 17, p.79.

- Klingler, A.L. and Teichtmann, L., 2017. Impacts of a forecast-based operation strategy for grid-connected PV storage systems on profitability and the energy system. *Solar Energy*, 158, pp.861-868.
- Kudish, A.I. and Wolf, D., 1978. A compact shallow solar pond hot water heater. *Solar Energy*, 21(4), pp.317-322.
- Kumar, A., and Kishore, V.V.N., 1999. Construction and operational experience of a 6000 m² solar pond at Kutch, India. *Solar energy*, 65(4), pp.237-249.
- Kurt, H., Halici, F. and Binark, A.K., 2000. Solar pond conception—experimental and theoretical studies. *Energy conversion and management*, 41(9), pp.939-951.
- Kurt, H. and Ozkaymak, M., 2006. Performance evaluation of a small-scale sodium carbonate salt gradient solar pond. *International journal of energy research*, 30(11), pp.905-914.
- Kurt, H., Ozkaymak, M. and Binark, A.K., 2006. Experimental and numerical analysis of sodium-carbonate salt gradient solar-pond performance under simulated solar-radiation. *Applied energy*, 83(4), pp.324-342.
- Kuylensstierna, J., Björklund, G., and Najlis P., 2009. Sustainable water future with global implications: everyone's responsibility, in *Natural resources forum*, Vol. 21, Wiley Online Library, pp. 181–190.
- Kyathsandra, J.M., 1988. Performance of a solar pond coupled multi-stage flash desalination system. The University of Texas at El Paso.
- Lashin A., Soliman *H. A., 1996. The use of air flow through water for water evaporation - *Assistant Professor, Associate Professor, Department of Mechanical Engineering, Shoubra Faculty of Engineering, Zagazig University, EGYPT. Proceedings of the Fifth International Conference on Energy and Environment, Cairo, Egypt.
- Leblanc, J. and Andrews, J., 2007, October. Solar-Powered Desalination: A Modelling and Experimental Study. In *AIP Conference Proceedings* (Vol. 941, No. 1, pp. 249-263). American Institute of Physics.
- Leblanc, J., Akbarzadeh, A., Andrews, J., Lu, H. and Golding, P., 2011. Heat extraction methods from salinity-gradient solar ponds and introduction of a novel system of heat extraction for improved efficiency. *Solar Energy*, 85(12), pp.3103-3142.
- Li, N., Yin, F., Sun, W., Zhang, C. and Shi, Y., 2010. Turbidity study of solar ponds utilizing seawater as salt source. *Solar Energy*, 84(2), pp.289-295.
- Lin, E.I.H., 1982. A saltless Solar Pond – Proceedings of the International Solar Energy Society, p. 225.
- Lindblom, J., Nordell, B., 2003. Condensation Irrigation - a system for desalination and irrigation, Proceedings of the International Conference on Energy and Environment (ICEE_03), 14-15 October 2003. Brack, Libya. Published in *Energy and Life* 20:61-66 (Paper I of Lindblom Licentiate Thesis of 2006).
- Lindblom, J., Nordell, B., 2006a. Water Production by Underground Condensation of Humid Air, Desalination 189:248-260 (Paper II of Lindblom Licentiate Thesis of 2006) (Paper I of Lindblom doctoral Thesis of 2012).
- Lindblom, J., Nordell, B., 2006b. Condensation Irrigation - a system for desalination and irrigation, submitted to *Transport in Porous Media* (Paper III of Lindblom Licentiate Thesis of 2006).
- Lindblom, J., Nordell, B., 2007. Underground production of Humid air for drinking water production and subsurface irrigation. *Desalination* 2007; 203:417–434 (Paper II of Lindblom doctoral Thesis of 2012).

- Lindblom, J., Nordell, B., 2011. Experimental study of underground irrigation by condensation of humid air in perforated pipes. Technical report. Division of Architecture and Water, Department of Civil, Environmental and Natural resources engineering, Luleå University of Technology. ISBN 978-91- 7439-513-6 (Paper V of Lindblom doctoral Thesis of 2012).
- Liu, H., Jiang, L., Wu, D. and Sun, W., 2015. Experiment and simulation study of a trapezoidal salt gradient solar pond. *Solar Energy*, 122, pp.1225-1234.
- Lu, H., Swift, A.H., Hein Jr, H.D. and Walton, J.C., 2004. Advancements in salinity gradient solar pond technology based on sixteen years of operational experience. *J. Sol. Energy Eng.*, 126(2), pp.759-767.
- Lu, H., Walton, J.C. and Swift, A.H., 2001. Desalination coupled with salinity-gradient solar ponds. *Desalination*, 136(1-3), pp.13-23.
- Lu, H., Walton, J.C. and Hein, H., 2002. Thermal desalination using MEMS and salinity-gradient solar pond technology. NASA STI/Recon Technical Report N, 3, p.00498.
- Malik, N., Date, A., Leblanc, J., Akbarzadeh, A. and Meehan, B., 2011. Monitoring and maintaining the water clarity of salinity gradient solar ponds. *Solar energy*, 85(11), pp.2987-2996.
- Malik, M., Tiwari, G., Kumar, A., and Sodha, M., 1996. *Solar Distillation: A Practical Study of a Wide Range of Stills and their Optimum Design Construction and Performance*, Pergamon Press, 1996.
- Managecraft, 2001. Results of analysis of coconut husk fibre or Coco-Peat. Managecraft (GH) Ltd., Box 207, Takoradi, Ghana.
- Manchanda, H. and Kumar, M., 2015. A comprehensive decade review and analysis on designs and performance parameters of passive solar still. *Renewables: Wind, Water, and Solar*, 2(1), pp.1-24.
- Manges, H., 1966, February. Evaporation suppression by chemical and mechanical treatments. In *Proceedings of the Oklahoma Academy of Science* (pp. 251-254).
- Mathioulakis, E., Belessiotis, V., Delyannis, E., 2007. Desalination by using alternative energy: Review and state-of-the-art - Desalination, Volume 203, Issues 1–3, 5 February 2007, Pages 346–365.
- Mesa, A. A., Gromez, C. M., Azpitarte R.U., 1997. Energy saving and desalination of water. - *Desalination* 1997; 108:43e50.
- Mink, G., Aboabbous, M. and Karmazsin E., 1998. Design parameters, performance testing and analysis of a double-glazed, air-blown solar still with heat recycling, *Solar Energy*, 62, 309–317.
- Mohamed, E.S., Papadakis, G., Mathioulakis, E. and Belessiotis, V., 2006. An experimental comparative study of the technical and economic performance of a small reverse osmosis desalination system equipped with an hydraulic energy recovery unit. *Desalination*, 194(1-3), pp.239-250.
- Modi, K.V., Nayi, K.H., Sharma, S.S., 2020. Influence of water mass on the performance of spherical basin solar still integrated with parabolic reflector. *Ground. Sustain. Dev.* 10, 100299.
- Molineaux, B., Lachal, B. and Guisan, O., 1994. Thermal analysis of five outdoor swimming pools heated by unglazed solar collectors. *Solar Energy*, 53(1), pp.21-26.
- Monjezi, A.A. and Campbell, A.N., 2016. A comprehensive transient model for the prediction of the temperature distribution in a solar pond under Mediterranean conditions. *Solar energy*, 135, pp.297-307.
- Mulder, G., Six, D., Claessens, B., Broes, T., Omar, N. and Van Mierlo, J., 2013. The dimensioning of PV-battery systems depending on the incentive and selling price conditions. *Applied energy*, 111, pp.1126-1135.

- Murthy, G.R. and Pandey, K.P., 2002. Scope of fertiliser solar ponds in Indian agriculture. *Energy*, 27(2), pp.117-126.
- Murthy, G.R. and Pandey, K.P., 2003. Comparative performance evaluation of fertiliser solar pond under simulated conditions. *Renewable energy*, 28(3), pp.455-466.
- Müller-Holst, H., Engelhardt, M., Herve, M., and Scholkopf W., 1998. Solar thermal seawater desalination systems for decentralized use, *Renewable Energy*, 14, 311–318.
- Müller-Holst, H., Engelhardt, M. and Scholkopf, W., 1999. Small-scale thermal seawater desalination simulation and optimization of system design, *Desalination*, 122, 255–262.
- Nafey, A.S., Fath, H.E.S., El-Helaby, S.O., Soliman, A.M., 2004. Solar desalination using humidification–dehumidification processes. Part II. An experimental investigation. *Energy Convers. Manage.* 45, 1263–1277.
- Naim, M., Mervat, A. and El-Kawi Abd, 2003. Non-conventional solar stills. Part 1: Non-conventional solar stills with charcoal particles as absorber medium, *Desalination*, 153, 55–64.
- Nakoa, K., Rahaoui, K., Date, A. and Akbarzadeh, A., 2015. An experimental review on coupling of solar pond with membrane distillation. *Solar Energy*, 119, pp.319-331.
- Newell, T.A., Cowie, R.G., Upper, J.M., Smith, M.K. and Cler, G.L., 1990. Construction and operation activities at the University of Illinois salt gradient solar pond. *Solar Energy*, 45(4), pp.231-239.
- Nie, Z., Bu, L., Zheng, M. and Huang, W., 2011. Experimental study of natural brine solar ponds in Tibet. *Solar Energy*, 85(7), pp.1537-1542.
- Nordell, B., 1987. Dimensionering av klimatsystem vid Hietalas vaxthus i Overtornea. LuTU, Avdelningen for Vattenteknik. Lulea. Intern rapport nr 1987:06..
- Okati, V., Behzadmehr, A., Farsad S., 2016. Analysis of a solar desalinator (humidification–dehumidification cycle) including a compound system consisting of a solar humidifier and subsurface condenser using DoE - *Desalination* 397 (2016) 9–21.
- Okati, V., Farsad, S., Behzadmehr A., 2018. Numerical analysis of an integrated desalination unit using humidification- dehumidification and subsurface condensation processes, *Desalination*, Volume 433, 1 May 2018, Pages 172-185.
- Okati, V., Ebrahimi-Moghadam, A., Behzadmehr, A., Farzaneh-Gord, M., 2019. Proposal and assessment of a novel hybrid system for water desalination using solar and geothermal energy sources, *Desalination*, Volume 467, Pages 229-244, ISSN 0011-9164, <https://doi.org/10.1016/j.desal.2019.06.011>.
- Ortabasi, U., Dyksterhuis, F.H. and Kaushika, F.H., 1983. Honeycomb stabilized saltless solar pond. *Sol. Energy*; (United Kingdom), 31(2).
- Oueslati, A., Megriche, A., Hannachi, A., Elmaaoui, M., 2017. Performance study of humidification–dehumidification system operating on the principle of an airlift pump with tunable height, *Process Safety and Environmental Protection*, Volume 111, 2017, Pages 65-74, ISSN 0957-5820, <https://doi.org/10.1016/j.psep.2017.05.018>.
- Ouchi, S., Nishikawa, A., and Fujita, F., 1989. Soil-improving effect of a super-water-absorbent polymer. I. Total volume, three-phase distribution, and available water of super-water-absorbent polymer mixed soils. *Jap. J. Soil Sci. Pl. Nutr.* 60: 15–21.

- Parekh, S., Farid, M. M., Selman, R.R., Al-Hallaj, S., 2003. Solar desalination with humidification–dehumidification technique - a comprehensive technical review. *Desalination* 2003; 160:167–86.
- Pawar, S.H. and Chapgaon, A.N., 1995. Fertilizer solar ponds as a clean source of energy: some observations from small scale experiments. *Solar Energy*, 55(6), pp.537-542.
- Pei, Z.F., Ming, D.F., Liu, D., Wan, G.L., Geng, X.X., Gong, H.J. and Zhou, W.J., 2010. Silicon improves the tolerance to water-deficit stress induced by polyethylene glycol in wheat (*Triticum aestivum* L.) seedlings. *Journal of Plant Growth Regulation*, 29(1), pp.106-115.
- Punyasena, M.A., Amarasekara, C.D., Jayakody, J.R.P., Perera, P.A.A. and Ehamparam, P., 2003. An investigation of rain and wind effects on thermal stability of large-area saltpan solar ponds. *Solar Energy*, 74(6), pp.447-451.
- Qiblawey, H. M. *, Banat, F., 2006. Solar thermal desalination technologies, Department of Chemical Engineering, Jordan Univ.of Science and Technology, P.O. Box 3030, 22110 Irbid, Jordan email: hazim@just.edu.jo Received 19 December 2006; accepted 3 January 2007 (2013.01.003).
- Qingchun, G., Mingming, L., Tai-Shung, C., 2013. Draw solutions for forward osmosis processes: Developments, challenges, and prospects for the future - *Journal of Membrane Science*, Volume 442, 1 September 2013, Pages 225–237.
- Rabl, A. and Nielsen, C. E., 1975. Solar Ponds for Space Heating" *Solar Energy* 17, 1-12.
- Radhwan, M., 2005. Transient performance of a stepped solar still with built-in latent heat thermal energy storage, *Desalination*, Volume 171, Issue 1, 2005, Pages 61-76, ISSN 0011-9164.
- RAECO - Rural Area Electricity Company. 2017. ‘Rural Area Electricity Company (RAECO)’. Sultanate of Oman. Annual Report 2017.”.
- Raman, P. and Kishore, V.V.N., 1990. An alternate lining scheme for solar ponds—Results of a liner test rig. *Solar energy*, 45(4), pp.193-199.
- Rheinlaender, J. and Graeter, F., 2001. Technologies for desalination of typically 10 m³ of water per day, *Desalination*, 139, 393–397, Rural Area Electricity Company (2017) - ‘Rural Area Electricity Company (RAECO)’. Sultanate of Oman. Annual Report 2017.”
- Robbins, M.C., Lu, H. and Swift Jr, A.H.P., 1995. Investigation of the suitability of a geosynthetic clay liner system for the El Paso solar pond (No. CONF-950725-). American Solar Energy Society, Boulder, CO (United States).
- Ruskowitz, J.A., Suárez, F., Tyler, S.W. and Childress, A.E., 2014. Evaporation suppression and solar energy collection in a salt-gradient solar pond. *Solar energy*, 99, pp.36-46.
- Rutkowska, M., Krasowska, K., Heimowska, A., Steinka, I. and Janik, H., 2002. Degradation of polyurethanes in sea water. *Polymer Degradation and Stability*, 76(2), pp.233-239.
- Sabrah, R. E. A., Ghoneim, M. F., Abd El-Magid, H. M., and Rabie R. K., 1993. Characteristics and productivity of a sandy soil as influenced by soil conditioners in Saudi Arabia, *Journal of Arid Environments*, vol. 24, no. 3, pp. 297–303, 1993.
- Saleh, A., Qudeiri, J.A. and Al-Nimr, M.A., 2011. Performance investigation of a salt gradient solar pond coupled with desalination facility near the Dead Sea. *Energy*, 36(2), pp.922-931.

- Sayer, A.H., Al-Hussaini, H. and Campbell, A.N., 2016. New theoretical modelling of heat transfer in solar ponds. *Solar Energy*, 125, pp.207-218.
- Sayer, A.H., Al-Hussaini, H. and Campbell, A.N., 2017. An analytical estimation of salt concentration in the upper and lower convective zones of a salinity gradient solar pond with either a pond with vertical walls or trapezoidal cross section. *Solar Energy*, 158, pp.207-217.
- Sayer, A.H., Al-Hussaini, H. and Campbell, A.N., 2018. New comprehensive investigation on the feasibility of the gel solar pond, and a comparison with the salinity gradient solar pond. *Applied Thermal Engineering*, 130, pp.672-683.
- Saxena, A.K., Sugandhi, S. and Husain, M., 2009. Significant depth of ground water table for thermal performance of salt gradient solar pond. *Renewable Energy*, 34(3), pp.790-793.
- Seifert, B., Kroiss, A., Spinnler, M., Sattelmayer, T., 2013. About the history of humidification dehumidification desalination systems. The International Desalination Association World Congress on Desalination and Water Reuse, Tianjin, China. REF: IDAWC/TIAN13-375.
- Schaller, J., Cramer, A., Carminati, A., 2020. Biogenic amorphous silica as main driver for plant available water in soils. *Sci Rep* 10, 2424 - <https://doi.org/10.1038/s41598-020-59437-x> Metrics.
- Schaller, J., Sven, F., Rohn L., Gilfedder, B. S., 2020. Amorphous Silica Controls Water Storage Capacity and Phosphorus Mobility in Soils - *Frontiers in Environmental* 00094 DOI=10.3389/fenvs.2020.00094 ISSN=2296-665X.
- Schwarzer, K., Eugenia, M., Faber, C. and Muller, C., 2001. Solar thermal desalination system with heat recovery, *Desalination*, 137 (2001) 23–29.
- Sethi, A.K., Dwivedi, V.K., 2013. Exergy analysis of double slope active solar still under forced circulation mode. *Desalination Water Treat.* 51, 7394 e 7400. <https://doi.org/10.1080/19443994.2013.777945>.
- Shaffer, L.H., 1978. Viscosity stabilized solar pond - *Proc. Int. Solar Energy Society Congress*, New Delhi (1978), pp. 1171–1175.
- Shahu, V.T. and Thombre, S.B., 2019. Air gap membrane distillation: A review. *Journal of Renewable and Sustainable Energy*, 11(4), p.045901.
- Shahzad, M.W., Burhan, M., Ang, L. and Ng, K.C., 2017. Energy-water-environment nexus underpinning future desalination sustainability. *Desalination*, 413, pp.52-64.
- Sharif, A.O., Sanduk, M., Taleb, H.M., 2010. The date palm and its role in reducing soil salinity and global warming - *Acta Horti.*, 882 (2010), pp. 59-64.
- Sharma, R. K., and Verma, H. D., 1996. Effect of irrigation scheduling and other agronomic manipulations on yield and water economy in sugarcane, *Indian Journal of Agronomy*, vol. 41, no. 1, pp. 122–126, 1996.
- Shi, Y., Yin, F., Shi, L., Wence, S., Li, N. and Liu, H., 2011. Effects of porous media on thermal and salt diffusion of solar pond. *Applied energy*, 88(7), pp.2445-2453.
- Silva, C., González, D. and Suárez, F., 2017. An experimental and numerical study of evaporation reduction in a salt-gradient solar pond using floating discs. *Solar energy*, 142, pp.204-214.
- Silva, G. and Almanza, R., 2009. Use of clays as liners in solar ponds. *Solar Energy*, 83(6), pp.905-919.

- Sodha M., Kumar A., Tiwari G. and Tyagi R. (1981) - Simple multiple wick solar still: analysis and performance, *Solar Energy*, 26 (1981) 127–131.
- Sogukpinar, H., Karakilcik, M., Bozkurt, I. and Cag, S., 2016, October. Numerical evaluation of the performance increase for a solar pond with glazed and unglazed. In 2016 IEEE International Conference on Power and Renewable Energy (ICPRE) (pp. 598-601). IEEE.
- Solimana, A.M., Al-Falahic, A., Eldeanb, M.A.S., Elmnifid, M., Hassane, M., Younisf, B., Mabroukb, A. and Fathh, H.E., 2020. A new system design of using solar dish-hydro combined with reverse osmosis for sewage water treatment: case study Al-Marj, Libya. *Desalination and Water Treatment*, 193, pp.189-211.
- Srithar, K., Rajaseenivasan, T., 2017. Performance analysis on a solar bubble column humidification dehumidification desalination system. *Process Safety and Environmental Protection*. Volume 105, Pages 41-50, ISSN 0957-5820, <https://doi.org/10.1016/j.psep.2016.10.002>.
- Szacsvay, T., Hofer-Noser, P. and Posnansky, M., 1999. Technical and economic aspects of small-scale solar-pond-powered seawater desalination systems. *Desalination*, 122(2-3), pp.185-193.
- Tabor, H., 1958. Radiation, convection, and conduction of coefficients in solar collectors. *Bull. Res. Counc. Isr.*, 6 Sect C, p. 155.
- Tabor, H., 1966. Solar Ponds, *Science Journal* (1966) 66-71.
- Tabor, H. and Matz, R., 1965. Solar Pond Project, *Solar Energy* 9 (1965) 177-182.
- Taga, M., Matsumoto, T., Ochi, T., 1990. Studies on membrane viscosity stabilized solar pond - *Solar Energy*, 45 (6), pp. 315–324.
- Tanaka, T., Yamashita, A. and Watanabe, K., 1981. *Proc. International Solar Energy Congress, Brighton, England, Vol. 2, 1981, p. 1087.*
- Tleimat, M. W., 1980. Freezing methods. In: Spiegler KS, Laird ADK, editors. *Principles of desalination. Part B*. 2nd ed. New York: Academic Press; 1980. p. 359–400.
- Tsilingiris, P.T., 2007. The influence of binary mixture thermophysical properties in the analysis of heat and mass transfer processes in solar distillation systems. *Solar Energy*, 81(12), pp.1482-1491.
- Tundee, S., Terdtoon, P., Sakulchangsatjatai, P., Singh, R. and Akbarzadeh, A., 2010. Heat extraction from salinity-gradient solar ponds using heat pipe heat exchangers. *Solar Energy*, 84(9), pp.1706-1716.
- UNEP, U.D., FAO, 2012. *SIDS-Focused Green Economy: An Analysis of Challenges and Opportunities*. Nairobi: United Nations Environment Programme. Available online at: http://www.unep.org/pdf/Green_Economy_in_SIDS.pdf (Accessed July, 16, 2015).
- Valderrama, C., Gibert, O., Arcal, J., Solano, P., Akbarzadeh, A., Larrotcha, E. and Cortina, J.L., 2011. Solar energy storage by salinity gradient solar pond: Pilot plant construction and gradient control. *Desalination*, 279(1-3), pp.445-450.
- Vitner, A., Reisfeld, R. and Sarig, S., 1984. Self-generation of a laboratory scale saturated solar pond. *Sol. Energy; (United Kingdom)*, 32(5).
- Walton, J., Lu, H., Turner, C., Solis, S. and Hein, H., 2004. Solar and waste heat desalination by membrane distillation. *Desalination and water purification research and development program report*, (81), p.20.

- Wang, Y.T. and Gregg, L.L., 1990. Hydrophilic polymers—their response to soil amendments and effect on properties of a soilless potting mix, *Journal of the American Society for Horticultural Science*, vol. 115, no. 6, pp. 943–948, 1990.
- Wang, J. and Seyed-Yagoobi, J., 1995. Effect of water turbidity on thermal performance of a salt-gradient solar pond. *Solar energy*, 54(5), pp.301-308.
- Wang, H., Wu, Q., Mei, Y., Zhang, L. and Pang, S., 2018. A study on exergetic performance of using porous media in the salt gradient solar pond. *Applied Thermal Engineering*, 136, pp.301-308.
- Wang, H., Yu, X., Shen, F. and Zhang, L., 2015. A Laboratory experimental study on effect of porous medium on salt diffusion of salt gradient solar pond. *Solar energy*, 122, pp.630-639.
- Wang, H., Zou, J., Cortina, J.L. and Kizito, J., 2014. Experimental and theoretical study on temperature distribution of adding coal cinder to bottom of salt gradient solar pond. *Solar energy*, 110, pp.756-767.
- World Health Organization, 2008. Water (No. WHO/HSE/PHE/AMR/08.01. 01). World Health Organization.
- Widegren, M., 1986. Condensation irrigation, a desalination-irrigation system. WREL LuTH. Graduate Thesis 1986:002 E.
- Whillier, A., 1953. Solar energy collection and its utilization for house heating (Doctoral dissertation, Massachusetts Institute of Technology).
- Xie, M., Ge, S. and Sun, W., 2006. Numerical simulation of double-diffusive dynamical model of a solar pond considering the effect of turbidity and wind. *Journal of Thermal Science*, 15(2), pp.168-174.
- Yaakob, Y., Date, A. and Akbarzadeh, A., 2011, June. Heat extraction from gradient layer using external heat exchangers to enhance the overall efficiency of solar ponds. In 2011 IEEE Conference on Clean Energy and Technology (CET) (pp. 23-28). IEEE.
- Yaakob, Y., Ul-Saufie, A.Z., Idrus, F. and Ibrahim, D., 2016, October. The development of thermosiphon heat exchanger for solar ponds heat extraction. In AIP Conference Proceedings (Vol. 1774, No. 1, p. 060003). AIP Publishing LLC.
- Yadav, Y.P. and Yadav, S.K., 2004. Parametric studies on the transient performance of a high-temperature solar distillation system. *Desalination*, 170(3), pp.251-262.
- Yangyuoru, M. *, Boateng, E. Adiku, S.G.K., Acquah, D., Adjadeh, T. A. and Mawunya, F., 2006. Effects of Natural and Synthetic Soil Conditioners on Soil Moisture Retention and Maize Yield - - College of Agriculture & Consumer Sciences, Agricultural Research Centre, Kpong, University of Ghana, Legon-Accra, Ghana - West Africa Journal of Applied Ecology (WAJAE) –ISSN: 0855-4307 Volume 9 (Jan – Jun 2006) - www.wajae.org..
- Yau, M.K. and Rogers, R.R., 1996. A short course in cloud physics. Elsevier.
- Yeung, M.R., Yuen, P.K., Dunn, A. and Cornish, L.S., 1992. Performance of a solar-powered air conditioning system in Hong Kong. *Solar energy*, 48(5), pp.309-319.
- Zangrando, F., 1980. A simple method to establish salt gradient solar ponds. *Solar Energy*, 25(5), pp.467-470.
- Zaragoza, G., Ruiz-Aguirre, A. and Guillén-Burrieza, E., 2014. Efficiency in the use of solar thermal energy of small membrane desalination systems for decentralized water production. *Applied Energy*, 130, pp.491-499.

Zhang, Z.M. and Wang, Y.F., 1990. A study on the thermal storage of the ground beneath solar ponds by computer simulation. *Solar Energy*, 44(5), pp.243-248.

Zhao, S., Zou, L., Chuyang, T. Y., Mulcahy D., 2012. Recent developments in forward osmosis: Opportunities and challenges - *Journal of Membrane Science*, Volume 396, 1 April 2012, Pages 1–21.

Ziapour, B.M., Shokrnia, M. and Naseri, M., 2016. Comparatively study between single-phase and two-phase modes of energy extraction in a salinity-gradient solar pond power plant. *Energy*, 111, pp.126-136.

Ziapour, B.M. and Shokrnia, M., 2017. Exergoeconomic analysis of the salinity-gradient solar pond power plants using two-phase closed thermosyphon: A comparative study. *Applied Thermal Engineering*, 115, pp.123-133.

Zuo, G., Wang, R., 2013. Novel membrane surface modification to enhance anti-oil fouling property for membrane distillation application, *Journal of Membrane Science*, Volume 447, 15 November 2013, Pages 26–35 <http://dx.doi.org/10.1016/j.memsci.2013.06.053>.

Permissions table

Figure/ Table No.	Name of work	Source of work	Copyright holder and contact	permission requested on	I have permissi on yes /no	Permission note
Figure 01.10	Diagram of typical MSF unit	Al-Karaghoul et al. (2019)	Copyright © 2009 Published by Elsevier Ltd.	04.02.2022	yes	License nr 5242071093711
Figure 01.11	Diagram of typical MED unit	Al-Karaghoul et al. (2019)	Copyright © 2009 Published by Elsevier Ltd.	04.02.2022	yes	License nr 5242071093711
Figure 01.12	Diagram of typical VC unit	Al-Karaghoul et al. (2019)	Copyright © 2009 Published by Elsevier Ltd.	04.02.2022	yes	License nr 5242071093711
Figure 01.13	Diagram of RO desalination	Al-Karaghoul et al. (2019)	Copyright © 2009 Published by Elsevier Ltd.	04.02.2022	yes	License nr 5242071093711
Figure 01.14	Spiral-Wound (SW) membranes	Al-Karaghoul et al. (2019)	Copyright © 2009 Published by Elsevier Ltd.	04.02.2022	yes	License nr 5242071093711
Figure 01.15	Hollow-Fibre (HF) membranes	Al-Karaghoul et al. (2019)	Copyright © 2009 Published by Elsevier Ltd.	04.02.2022	yes	License nr 5242071093711
Figure 01.16	Ion Exchange Electro Dialysis unit ED part.1	Al-Karaghoul et al. (2019)	Copyright © 2009 Published by Elsevier Ltd.	04.02.2022	yes	License nr 5242071093711
Figure 01.17	Ion Exchange Electro Dialysis unit ED part.2	Al-Karaghoul et al. (2019)	Copyright © 2009 Published by Elsevier Ltd.	04.02.2022	yes	License nr 5242071093711
Figure 01.18	Schematic representations of the osmosis phenomena in reverse and forward osmosis	Zhao et al. (2012)	Copyright © 2012 Published by Elsevier B.V.	04.02.2022	yes	License nr 5242080644679
Figure 01.19	Schematic representation of Forward Osmosis process	Zhao et al. (2012)	Copyright © 2012 Published by Elsevier B.V.	04.02.2022	yes	License nr 5242080644679
Figure 01.20	Schematic representation of Membrane Distillation	Zuo et al. (2013)	Copyright © 2013 Published by Elsevier B.V.	04.02.2022	yes	License nr 5242081480109
Figure 01.23	Greenhouse with integrated solar still on the roof	Chaibi (2004)	Copyright © 2004 Published by Elsevier Ltd.	06.02.2022	yes	License nr 5243160441183
Figure 01.24	Stepped solar still connected to a greenhouse for heating and humidifying air	Radhwan (2005)	Copyright © 2005 Published by Elsevier B.V.	04.02.2022	yes	License nr 5242090333948

Figure 01.25	Schematic of triple basin solar still	El-Sebaï (2005)	Copyright © 2005 Published by Elsevier B.V.	04.02.2022	yes	License nr 5242090603161
Figure 02.06	Autoflesh desalination system powered by an SGSP	Szacsvey et al. (1999)	Copyright © 1999 Published by Elsevier B.V.	05.02.2022	yes	License nr 5242361053378
Figure 02.07	MED desalination unit coupled with an SGSP and evaporation pond	Garmana and Munstasser (2008)	Copyright © 2006 Published by Elsevier B.V.	05.02.2022	yes	License nr 5242370584350
Figure 03.02	Configuration of the SGSP and the heat fluxes used to develop the mathematical model	González et al. (2014)	Copyright © 2016 Published by John Wiley & Sons, Ltd.	05.02.2022	yes	License nr 5242380701485
Figure 03.03	Energy balance between layers zone of SGSP	Bernard et al. (2013)	Copyright © 2013 Published by Elsevier Ltd.	05.02.2022	yes	License nr 5242381146179
Figure 04.07	Design of horizontal diffuser	Valderrama et al. (2011)	Copyright © 2011 Published by Elsevier B.V.	05.02.2022	yes	License nr 5242381398103
Figure 05.02	Outline of the CI system. Ambient air is warmed and humidified by solar thermal energy and led into buried pipes, where it is cooled and dehumidified	Lindblom J. and Nordell B. (2006)	Copyright © 2006 Published by Elsevier B.V.	04.02.2022	yes	License nr 5242110080763
Figure 05.04	Section of buried drainage pipes. The pipe diameter D, depth d and spacing cc are indicated	Lindblom and Nordell (2007)	Copyright © 2007 Published by Elsevier B.V.	06.04.2022	yes	License nr 5243250359153
Figure 05.05	Condensation rate for the system per pipe and unit length during the first 90 days.	Lindblom and Nordell (2006)	Copyright © 2006 Published by Elsevier B.V.	04.02.2022	yes	License nr 5242110080763
Figure 05.06	Accumulated water production along the first 50 m of a drainage pipe in a system with different spacing	Lindblom and Nordell (2006)	Copyright © 2006 Published by Elsevier B.V.	04.02.2022	yes	License nr 5242110080763
Figure 05.07	Humidification-Dehumidification system	Okati et al.(2019)	Copyright © 2019 Published by Elsevier B.V.	04.02.2022	yes	License nr 5242091099847
Figure 05.08	Effect of solar collector's outlet air temperature on the mass flow rate of the produced fresh-water	Okati et al.(2019)	Copyright © 2019 Published by Elsevier B.V.	04.02.2022	yes	License nr 5242091099847
Figure 05.09	Effect of solar collector's outlet water temperature on the mass flow rate of the produced fresh-water	Okati et al.(2019)	Copyright © 2019 Published by Elsevier B.V.	04.02.2022	yes	License nr 5242091099847
Figure 05.10	The effect of the water or air temperatures on vapour content difference	El-Agouz et al. (2008)	Copyright © 2008	04.02.2022	yes	License nr 5242100805979

	at different headwater ΔH and air velocities		Published by Elsevier Ltd.			
Figure 05.11	The effect of the water or air temperatures on the humidification efficiency at different headwater ΔH and air velocities	El-Agouz et al. (2008)	Copyright © 2008 Published by Elsevier Ltd.	04.02.2022	yes	License nr 5242100805979
Figure 05.12	The effect of the temperatures of seawater on productivity at different air flow rates	El-Agouz (2010)	Copyright © 2010 Published by Elsevier Ltd	04.02.2022	yes	License nr 5242100365620
Figure 05.13	Schematic view of bubble column humidifier with (a) direct air supply (b) preheated air supply	Srithar et al. (2017)	Copyright ©2016 Institution of Chemical Engineers. Published by Elsevier B.V. All rights reserved.	04.02.2022	yes	License nr 5242101168772
Figure 07.01	Operational Costs of an RO system	Shazhad et al. (2017)	Copyright © 2017 Published by Elsevier B.V.	05.02.2022	yes	License nr 5242391137310
Figure 07.01	Renewable energy operated desalination technologies status: Capacity, production cost and technology trend	Shazhad et al. (2017)	Copyright © 2017 Published by Elsevier B.V.	05.02.2022	yes	License nr 5242391137310

Appendix I - Abbreviations and Symbols

AGMD - Air Gap Membrane Distillation
CAPEX – Capital Expenditure
CF - Concentration Factor
COR - Concentration level of rejected brine (mg/l)
CPL - Cost Per Litre
CS1 - Circulation Rate of 1^o first effect/stage (l/min)
DS - Draw Solution
DI - Diffuse Irradiance
ECP - External Concentration Polarisation
ED - Electro Dialysis
FPC - Flat Plate Collector
FO - Forward Osmosis
FR - Flash Range (°C),
GH - Green House
GHI - Global Radiation Irradiance
GOR - Gain ratio
HEX - Heat exchanger unit
HF - Hollow Fibres
HD - Humidification-Dehumidification
HSSP - Honeycomb Stabilised Solar Pond
ICP - Internal Concentration Polarisation
IE - Ion Exchange process
IGH – Inside the Greenhouse
LCOW - Levelized Cost Of Water
LCZ - Lower convective zone
LT-MED Low Temperature Multi-Effect Distillation
NF - Nano Filtration
M - Molarity
MEA - Middle East and Africa
MED - Multi-Effect Distillation
MEMS - Multi-Effect, Multi-Stage flash distillation
MD - Membrane Distillation

MF - Microfiltration
 MoAF - Ministry of Agriculture and Fisheries of Oman
 MSF - Multi-Stage Flash
 MSSP - Membrane Stratified Solar Pond
 MVC - Mechanical Vapour Compression
 N - Number of solute Moles
 NCZ - Non-Convective Zone
 OA - Osmotic Agent
 OGH – Outside the Greenhouse
 OPEX – Operating Expenses
 ORC - Organic Rankine Cycle
 PD - production rate
 PSP - Partitioned Solar Pond
 PR - performance ratio
 RES - Renewable Energy Sources
 RH - Relative Humidity
 RO - Reverse Osmosis or SWRO – Sea Water Reverse Osmosis
 SAP - Sodium Polyacrylate
 SC - Solar Concentrator
 SDI - Subsurface Drip Irrigation
 SGSP - Salinity Gradient Solar Pond
 SPC - Specific Power Consumption
 SSP - Shallow Solar Pond
 STSP - Saturated SP
 SW - Spiral-Wound
 SWD - Seawater Distillation
 SWI - Seawater Irrigation
 TDS - Total Dissolved Salts
 TFC - Thin Film Composite
 TVC - Thermal Vapour Compression
 UCZ - Upper convection zone
 UF - Ultra Filtration
 VC - Vapour Compression
 VSSP - Viscosity Stabilised Solar Pond

WHC - Water Holding Capacity

WRC - Water Retention Curve

WRR - Water Recovery Ratio

Appendix II – Nomenclature

Section 3.3.2 - Solar Pond model

A_p : Solar Pond area in $[m^2]$

C_p : heat capacity $[J/kg\ ^\circ C]$

D_{sp} : Solar Pond depth $[m]$

h_{ca} : convective heat transfer between the cover and ambient $[W/m^2\ K]$

H_o : hourly global radiation $[MJ/m^2/day]$

I_b : radiation beam $[W/m^2]$

I_d : diffuse radiation $[W/m^2]$

I_g : global radiation $[W/m^2]$

I_{rw} : flux reflected from the water surface, $[W/m^2]$

I_{sdsp} : solar flux at various depth, $[W/m^2]$

I_{sw} : flux entering the water $[W/m^2]$

k_w : water thermal conductivity $[W/m\ ^\circ C]$

L_p : length of the Solar Pond $[m]$

M : mass of water $[kg]$

$q_{conv.sup}$: heat loss by top convection $[W]$

q_{evap} : heat loss by evaporation $[W]$

q_{ground} : heat loss to the ground $[W]$

q_{in} : heat transfer entering the pond $[W]$

q_{out} : heat transfer exiting the pond $[W]$

q_{solar} : heat received by the solar radiation $[W]$

q_{wall} : heat loss through the walls $[W]$

Q_{load} : pond load $[kW]$

Q_u : the useful heat $[kW]$

t : operating time $[s]$

T : hourly water temperature $[^\circ C]$

T_{amb} : ambient temperature $[^\circ C]$

T_p : pond temperature $[^\circ C]$

T_{pm} : mean pond temperature $[^\circ C]$

$T_{p_{new}}$: new pond temperature $[^\circ C]$

UL : Total losses [$\text{W/m}^2 \text{ } ^\circ\text{C}$]
 V : volume of the pond [m^3]
 V_w : wind speed [m/s]
 W_p : width of the Solar Pond [m]

greek

θ_t : incidence angle [deg]
 θ_r : angle of reflection [deg]
 ρ : brine density of NaCl [kg/m^3]
 τ_a : transmission coefficient of solar radiation [-]

Section 3.3.3 - AGMD model

A_{memb} : membrane area in [m^2]
 C_f : concentration factor [-]
 C_w : overall mass transfer coefficient [$\text{kg/m}^2 \text{ s Pa}$]
 D_{memb} : membrane thickness in [m]
 GOR : gain ratio [$\text{kg/m}^2 \text{ h}$]
 H_{fg} : latent heat of vaporization in [kJ/kg]
 J_p : permeate flux [$\text{kg/ m}^2 \text{ h}$]
 k_g : gas thermal conductivity [$\text{kW/m } ^\circ\text{C}$]
 k_{memb} : thermal conductivity of the membrane [$\text{kW/m } ^\circ\text{C}$]
 K_m : mass transfer coefficient [$\text{kJ/m s } ^\circ\text{C}$]
 LEP : liquid entry pressure [kPa]
 M_b : brine loss in [kg/h]
 M_f : feed mass flow rate [kg/h]
 M_p : permeate flow rate [kg/h]
 MW_w : molecular weight of the water in [kg/mol]
 NOP : number of pores [-]
 P_m : mean vapour partial pressure [kPa]
 PD_{va} : water-air diffusion coefficient and the average pressure [$\text{Pa/m}^2 \text{ s}$]
 $Q_{conduction}$: energy transfer through conduction [kW]
 Q_{memb} : energy transfer through the membrane [kW]

$Q_{vaporization}$: energy transfer through vaporization [kW]

r_{memb} : membrane pore in [m]

$R_{constant}$: specific gas constant in [$kJ/kmol$]

S_b : brine loss salinity [kg/kg]

S_f : feed salinity ratio [kg/kg]

S_p : product salinity ratio [kg/kg]

SPC : specific power consumption [kWh/m^3]

SR : salt rejection [-]

T_{ci} : temperature of the cold side of condensation section [$^{\circ}C$]

T_{hi} : temperature of the hot feed side [$^{\circ}C$]

T_m : mean temperature [$^{\circ}C$]

W_{pump} : pump power [kW]

WRR : water recovery ratio [-]

greek

δ : relative viscosity [-]

ε : membrane porosity [-]

η_{memb} : membrane thermal efficiency [-]

η_{pump} : pump efficiency [-]

γ_w : water surface tension [kN/m]

ρ_w : water density [kg/m^3]

τ : membrane tortuosity [-]

Section 6.2.1 - Flat plate solar collector (air & water)

A_c : collector area in $[m^2]$

A_p : collector perimeter area $[m]$

C_{pa} : air specific heat capacity in function of temperature $[J/kg\ ^\circ C]$

F : efficiency factor $[-]$

FF : flow factor $[-]$

FR : heat removal factor $[-]$

h_b : coefficient heat transfer by convection between the insulated bottom surface and ambient $[W/m^2 K]$

h_e : coefficient heat transfer by convection between the edges of the FPC and the ambient $[W/m^2 K]$

h_w : heat transfer coefficient for air $[W/m^2 K]$

I_s : incident solar radiation in function of time $[W/m^2]$

NG : number of the glass cover $[-]$

M_f : mass flow rate of the fluid (either air or water) $[kg/s]$

$Q_{th,a}$: amount of thermal useful load absorbed by the gas (air or water vapour) $[kW]$

Q_u : useful energy $[kW]$

T_{amb} : ambient temperature $[^\circ C]$

T_{ci} : inlet air/water temperature through the FPC $[^\circ C]$

T_{co} : outlet air/water temperature through the FPC $[^\circ C]$

T_{fm} , The mean fluid temperature $[^\circ C]$

T_{mp} : is mean plate temperature $[^\circ C]$

T_{mpn} : new mean plate temperature $[^\circ C]$

T_p : plate temperature $[^\circ C]$

U_b : heat losses from the bottom $[W/m^2\ ^\circ C]$

U_e : edge losses $[W/m^2\ ^\circ C]$

U_L : FPC's overall heat loss coefficient $[W/m^2\ ^\circ C]$

U_T : total losses $[W/m^2\ ^\circ C]$

V_w : wind speed $[m/s]$

greek

β : tilt angle [deg]

δ : thickness of the insulation below the collector plate [m]

ε_g : glass emissivity [-]

ε_p : plate emissivity [-]

k : thermal conduction coefficient of the insulation below the collector plate [W/m K]

η : thermal efficiency of the FPC [-]

σ : Stephan Boltzmann constant [W/m² K⁴]

$\tau\alpha$: transmittance absorptance of the unit [-]

6.2.2 – SWI with membrane model and 6.2.3 SWD without

A_c : still cover area [m²]

A_p : soil Plate area [m²]

C_{pa} air specific heat capacity in function of temperature [J/kg °C]

C_{pw} : water specific heat capacity in function of temperature and salinity ratio [J/kg °C]

h_c : coefficient for heat conduction [W/m² °C]

k : thermal conduction coefficient [W/m °C]:

L : length of the membrane plate [m]

L_c : length of the still cover [m]

\dot{m} : mass flow rate of different (air, vapour, brine, water) [kg/s]

\dot{m}_{ai} : inlet air flow rate [kg/s]

\dot{m}_b : brine flow rate [kg/s]

\dot{m}_v : vapour mass flow rate [kg/s]

\dot{m}_{vi} : inlet vapour mass flow rate [kg/s]

\dot{m}_{vo} : outlet vapour mass flow rate [kg/s]

\dot{m}_{wi} : mass flow rate of inlet water [kg/s]

NTU : number of transfer unit [-]

Q_{mem} : membrane thermal power [kW]

RR: recovery ratio [-]

S_b : brine salinity ratio [g/kg]

S_f : feed salinity ratio [g/kg]

T_{ai} : inlet air temperature from the air heater unit [$^{\circ}\text{C}$]

T_{ao} : outlet air temperature from unit [$^{\circ}\text{C}$]

T_b : brine outlet temperature [$^{\circ}\text{C}$]

T_v : vapour temperature [$^{\circ}\text{C}$]

T_{wi} : inlet water feed temperature from the water heating unit [$^{\circ}\text{C}$]

TA_C : cover tilt angle [deg]

U : overall heat coefficient [$\text{W}/\text{m}^2\text{ }^{\circ}\text{C}$]

W : width of the membrane plate [m]

W_C : width of the still cover [m]

X_p : membrane plate thickness, [m]

greek

ε_{dh} : dehumidifier effectiveness [-]

ω_{ai} : inlet specific humidity of air [%]

ω_{ao} : outlet specific humidity of the air [%]

Appendix III - Mathematical Models (Matlab)

Section 3.3.2.2 - Solar radiation model

Solar radiation model is an effective tool to specify the solar energy over the location of operation at each period of the year, day, hour, minute.

The declination angle throughout the year is defined as:

$$d = 23.45 \sin \left[\frac{360}{365} (284 + n) \right]$$

Where n is the day of the year. The value of n for any day of the month d can be determined easily with the aid of the Table 03.02.

Month	n for the Day of the Month, D	Month	n for the Day of the Month, D
January	D	July	$181 + D$
February	$31 + D$	August	$212 + D$
March	$59 + D$	September	$243 + D$
April	$90 + D$	October	$273 + D$
May	$120 + D$	November	$304 + D$
June	$151 + D$	December	$334 + D$

Table 03.02 – Day of the year determination

The hour angle h is calculated from the following expression:

$$h = 15(LST - 12)$$

Where LST = Local Solar Time [hr].

The following equations are presented to calculate these angles:

$$\cos \theta_H = \cos l \cos h \cos d + \sin l \sin d$$

$$\text{Since } \beta = 90 - \theta_H,$$

$$\sin \beta = \cos l \cos h \cos d + \sin l \sin d$$

The relation gives the sun's azimuth, Φ :

$$\cos \phi = \frac{1}{\cos \beta} (\cos d \sin l \cos h - \sin d \cos l)$$

A summary of the sign convention is:

l : north latitudes are positive, south latitudes are negative.

d : the declination is positive when the sun's rays are north of the equator, i.e., for the summer period in the northern hemisphere, March 22 to September 22 approximately, and negative when the sun's rays are south of the equator.

h : the hour angle is negative before solar noon and positive after solar noon.

Φ : the sun's azimuth angle is negative east of south and positive west of south.

The solar models for the estimation of the total insolation on horizontal surfaces are the following:

ASHREA model:

$$Itl = (G_{bn} \times \cos(z)) + G_d$$

$$G_{bn} = A \exp(-B / \cos(z))$$

$$G_d = C \times G_{bn}$$

$$\cos(z) = \sin\phi \sin(d) + \cos\phi \cos(d) \cos(h)$$

Where, A is the apparent solar irradiance at air mass zero, B is the atmosphere extinction coefficient, and C is the diffuse radiation factor and z is the zenith angle. The following table shows the coefficients for average clear day solar radiation calculations.

	<i>A</i>		<i>B</i>	<i>C</i>	<i>Declination, deg</i>	<i>Equation of Time, hr</i>
	$\frac{\text{Btu}}{\text{hr} \cdot \text{ft}^2}$	$\frac{W}{\text{m}^2}$	<i>Dimensionless Ratios</i>			
January	390	1230	0.142	0.058	−20.0	−0.19
February	385	1215	0.144	0.060	−10.8	−0.23
March	376	1186	0.156	0.071	0.0	−0.13
April	360	1136	0.180	0.097	11.6	0.02
May	350	1104	0.196	0.121	20.0	0.06
June	345	1088	0.205	0.134	23.45	−0.02
July	344	1085	0.207	0.136	20.6	−0.10
August	351	1107	0.201	0.122	12.3	−0.04
September	365	1151	0.177	0.092	0	0.13
October	378	1192	0.160	0.073	−10.5	0.26
November	387	1221	0.149	0.063	−19.8	0.23
December	391	1233	0.142	0.057	−23.45	0.03

Table 03.03 – Coefficients for average clear day solar radiation

HOTTEL model:

Unlike ASHREA model, which gives an estimate for both direct and diffuse radiation, the present model can estimate the direct irradiation only. The direct beam irradiation on horizontal surface is given as following:

$$G = G_o(a_0 + a_1 e^{-k/\cos(z)})$$

Where;

$$G_o = 1353 \times (1 + 0.033 \cos(\frac{360n}{365})) \cos(z)$$

For tropical climate type:

$$a_0 = 0.4237 - 0.00821(6-A)^2$$

$$a_1 = 0.5055 + 0.00595(6.5-A)^2$$

$$k = 0.2711 + 0.01858(2.5-A)^2$$

Where A is the sea level parameter.

The model code for the solar radiation is presented as follows:

```
function [Iext,Tsun,EoT,ST,tsr,tss,Td,h,Alfa,Zhz,Tht,Azu,wss,delta]= SRAs(CT,n,Lst,Lloc,fai,Beta)
% LST = Local Solar Time [hr]
% CT = Clock Time [hr]
% Lstd = Standard Meridian for the local time zone [degrees west]
% Lloc = Longitude of actual location [degrees east]
% EoT = Equation of Time [hr]
% (DT = Daylight Savings Time correction: where.
% DT = 0 if not on Daylight Savings Time,
% otherwise, DT is equal to the number of hours that the time is advanced
% for Daylight Savings Time, usually 1hr)
% solar declination angle:
delta=23.45.*sin((n+284).*(360*pi)/(180*365));
%% solar standard time:
% equation of time:
B=fresh-watern-81) * 360)/365;
% EoT=229.2.*(0.000075+(0.001868.*cos(B.*pi./180))-(0.032077.*sin(B.*pi./180))-
(0.014615.*cos(2.*B.*pi./180))-(0.04089.*sin(2.*B.*pi./180)));
EoT=(9.87.*sin(2.*B.*pi./180))-(7.53.*cos(B.*pi./180))-(1.5.*sin(B.*pi./180));
% EoT=(0.165*sin(2*B*pi/180))-(0.126*cos(B*pi/180))-(0.025*sin(B*pi/180));
% DT=0;
% ST=CT-((1/15)*(Lst-Lloc))+EoT-DT;
ST=CT+(EoT/60)-(4.*(Lst-Lloc)/60);
% ST=CT+(4*(Lst-Lloc))+EoT;
% the hour angle is h:
h=15*(ST-12);
% the number of hours of day time:
Td=(2*180/(15.*pi)).*(acos(-tan(fai.*pi/180).*tan(delta.*pi./180)));
% %hour angle at sun set:
wss=0.5*Td*15;
% the solar sun rise and solar sun set:
tsr=12-0.5*Td;
tss=12+0.5*Td;
%%Solar Angles:
% solar altitude angle:
xx=sin(delta.*pi/180).*sin(fai.*pi/180)+cos(delta.*pi/180).*cos(fai.*pi/180).*cos(h.*pi/180);
Alfa=asin(xx).*(180/pi);
% solar zenith angle:
zz=sin(fai.*pi/180).*sin(delta.*pi/180)+cos(fai.*pi/180).*cos(delta.*pi/180).*cos(h.*pi/180);
Zhz=acos(zz).*(180/pi);
% solar incidence angle:
% lnda=180;
% ff=sin(delta.*pi/180)*sin((fai.*pi/180)-(Beta.*pi/180))+cos(Beta.*pi/180)*cos((fai.*pi/180)-
(Beta.*pi/180))*cos(h.*pi/180);
ff=cos(delta.*pi/180).*cos((fai.*pi/180)-
(Beta.*pi/180)).*cos(h.*pi/180)+sin(delta.*pi/180).*sin((fai.*pi/180)-(Beta.*pi/180));
Tht=acos(ff).*(180/pi);
%for solar azimuth angle:
azz=(cos(delta.*pi/180).*sin(h.*pi/180))./cos(Alfa.*pi/180);
% azz=(sin(h*pi/180))./((sin(fai*pi/180).*cos(h*pi/180))-
((cos(fai*pi/180)).*(tan(delta*pi/180))));
Azu=asin(azz).*(180/pi);
% Azu=atan(azz).*(180/pi);
% Azu=acos(azz)*(180/pi);
%the extraterrestrial radiation:
Isc=1353;
Iext=Isc.*(1+(0.033.*cos((360.*n.*pi)/(365*180))).*(cos(Zhz.*(pi./180))));
% %sun temperature:
% Mean sun earth distance:
Lse=1.5*10^11;
```

```

segma=5.67*10^-8;
%sun diameter:
Rs=(1.39*10^9)/2;
Tsun=((Iext.*(4*pi.*(Lse.^2))./(segma.*(4*pi.*(Rs.^2))).^0.25;
function [Ho,Igr,Hmon]= SRMcalcs(Iext,ST,STD,Td,wss,fai,delta,Slvl)
%% calculations for daily solar radiation:
Ho=(10^-
6).*((24*3600/pi).*(Iext.*((pi.*wss./180).*(sin(fai.*pi/180)).*(sin(delta.*pi/180)))+(cos(fai.*pi/1
80)).*(cos(delta.*pi/180)).*(sin(wss.*pi/180))));
%%THE HOURLY GLOBAL RADIATION RECEIVED BY A HORIZONTAL SURFACE:
Igr=Ho.*(pi./(2.*Td)).*(cos((pi/180).*(180.*(ST-12))./Td));
%%%%%%%%%%%%%%%%%%%%%%%%%%%%%%%%%%%%%%%%%%%%%%%%%%%%%%%%%%%%%%%%%%%%%%%%
%CALCULATIONS FOR MONTHLY AVERAGE OF DAILY TOTAL RADIATION ON ORIZONTAL SURFACES:
aa=-0.309+(0.539.*(cos(fai.*pi./180)))-(0.0693.*Slvl)+(0.290.*(STD./Td));
bb=1.527-(1.027.*(cos(fai.*pi./180)))+(0.0926.*Slvl)-(0.359.*(STD./Td));
Hmon=Ho.*(aa+(bb.*(STD./Td)));
function [Gbn,Gd,Gash]= ASHREA(Zhz,AA,BB,CC)
%%Solar Radiation Models:
%%%%%%%%%%%%%%%%%%%%%%%%%%%%%%%%%%%%%%%%%%%%%%%%%%%%%%%%%%%%%%%%%%%%%%%%

%1: ASHREA MODEL:
Gbn=AA.*(exp(-BB./(cos(Zhz.*pi/180))));
Gd=CC.*Gbn;
Gash=(Gbn.*cos(Zhz.*pi/180))+Gd;
% Gash=(AA.*(exp(-BB./(cos(Zhz.*pi/180)))).*(cos(Zhz.*pi/180)+CC);
function Ghott = HOTTEL(Iext,Zhz,Slvl)
%HOTTEL MODEL:
aoo=0.4237-(0.00812.*(6-Slvl).^2);
a11=0.5055+(0.00595.*(6.5-Slvl).^2);
kk=0.2711+(0.01858.*(2.5-Slvl).^2);
%For tropical climate:
ao=0.95.*aoo;
a1=0.98.*a11;
k=1.02.*kk;
Ghott=Iext.*(ao+(a1.*exp(-k./(cos(Zhz.*pi/180))));
%%%%%%%%%%%%%%%%%%%%%%%%%%%%%%%%%%%%%%%%%%%%%%%%%%%%%%%%%%%%%%%%%%%%%%%%

```

Section 3.3.2.3 - SP model

The model code for the SP with cover is presented as follows:

```
function [Isw, Isdsp, tawa, Tpes, Qload, Ap]=
SPonddes(OH, CS, DS, Dsp, Wp, Lp, dc, kc, Ho, Ig, Ib, Id, Tht, Tamb, Tp, Vw)
%% Pond area, m2:
Ap=Lp.*Wp;
%% Mean pond temp, oC:
Tpm=(Tp+Tamb)./2;
%% Angle of reflection, deg:
Thr=(asin(sin(Tht.*(pi./180))./(1.33))).*(180./pi);
%% The caculation parameters for the transmission and reflection table:
raw1=((sin((Thr-Tht).*(pi./180)).^2)./(sin((Thr+Tht).*(pi./180)).^2));
raw2=((tan((Thr-Tht).*(pi./180)).^2)./(tan((Thr+Tht).*(pi./180)).^2));
raw=(raw1+raw2)./2;
tawr=1-raw;
%% Flux reflected from the water surface, W/m2:
Irw=(Ib.*raw)+(Id.*raw);
%% Thermal diffusivity of water, m2/s:
% alfaw=fkw(Tpm)./(fraww(Tpm).*fcpw(Tpm));
%% Kinematic viscosity of water, Pa.s.m3/kg:
% vis=fmeuw(Tpm)./fraww(Tpm);
%% Rayleigh number:
% Ra=(9.81.*(1./(Tpm+273)).*(Tp-Tamb).*(Lp.^3))./(vis.*alfaw);
%%Convective heat transfer between the cover and ambient:
if Vw<5
    hca=2.8+(3.*Vw);
else
    hca=5.7+(2.8.*Vw);
end
%% Flux entring the water, W/m2:
Isw=Ig-Irw;
%% The transmission of the solar pond based on absorption (1: Nielsen, 2: Bryant & Colbek):
if DS==1
    tawa=(0.237.*exp(-0.023.*Dsp))+(0.193.*exp(-0.45.*Dsp))+(0.167.*exp(-3.*Dsp))+(0.179.*exp(-
35.*Dsp));
else
    tawa=0.36-(0.08.*log(Dsp./(cos(Thr.*pi./180))));
end
%% Solar flux at various depth, W/m2:
Isdsp=(Ib.*tawr.*tawa)+(Id.*tawr.*tawa);
%% Solar pond energy calculation steps, W:
%%The pond calculation parameter:
A1=0.237;A2=0.193;A3=0.167;A4=0.179;
K1=0.023;K2=0.45;K3=3;K4=35;
K11=K1./(cos(Thr.*pi./180).*(1));
K22=K2./(cos(Thr.*pi./180).*(1));
K33=K3./(cos(Thr.*pi./180).*(1));
K44=K4./(cos(Thr.*pi./180).*(1));
x1=(A1./K11).*(1-exp(-1.*(Dsp.*K11)));
x2=(A2./K22).*(1-exp(-1.*(Dsp.*K22)));
x3=(A3./K33).*(1-exp(-1.*(Dsp.*K33)));
x4=(A4./K44).*(1-exp(-1.*(Dsp.*K44)));
Xp=(tawr.*((Ho.*1e6)./(24.*3600))./fkw(Tpm)).*(x1+x2+x3+x4);
% Ap=(1000.*Dsp.*Qload)./(fkw(Tpm).*(Xp-(Tp-Tamb)));
% Qload=(Ap.*(fkw(Tpm).*(Xp-(Tp-Tamb))))./(1000.*Dsp);
%% Total losses, W/m2oC:
if CS==1
    Ulc=1./((Dsp./(1.*fkw(Tpm)))+(dc./kc)+(1./hca));
    Tpes=Tamb+(Isdsp./Ulc)-(((Isdsp./Ulc)+Tamb-Tp).*(exp((-
1.*Ulc.*OH)./(fraww(Tpm).*Dsp.*fcpw(Tpm)))));
    Qload=(Ap.*(fkw(Tpm).*(Xp-(Tpes-Tamb))))./(1000.*Dsp);
    % U=Ulc;
else
    Ul=1./((Dsp./(1.*fkw(Tpm)))+(0)+(1./hca));
    Tpes=Tamb+(Isdsp./Ul)-(((Isdsp./Ul)+Tamb-Tp).*(exp((-
1.*Ul.*OH)./(fraww(Tpm).*Dsp.*fcpw(Tpm)))));
    Qload=(Ap.*(fkw(Tpm).*(Xp-(Tpes-Tamb))))./(1000.*Dsp);
    % U=Ul;
end
%%Thermophysical properties:
%%%%%%%%%%%%%%%%%%%%%%%%%%%%%%%%%%%%%%%%%%%%%%%%%%%%%%%%%%%%%%%%%%%%%%%%
%Water specific heat capacity, J/kg oC:
function Cpw=fcpw(T)
Cpw=(4162.*exp(-4.187e-05.*T)+17.65.*exp(0.01504.*T))./1;
```

```

%Water density, kg/m3:
function Raww=fraww(T)
Raww=-0.009536.*(T.^1.804)+998.7;
% %Water dynamic viscosity, Pa.s:
% function meuw=fmeuw(T)
% meuw=0.001251.*exp(-0.03479.*T)+0.0004611.*exp(-0.006451.*T);
%Water thermal conductivity, W/moC:
function kw=fkw(T)
kw=(0.4413.*exp(-(T-21.64)./167.4).^2)+0.5526.*exp(-(T-249.3)./204.8).^2)./1;

```

Section 3.3.2.4 - AGMD model

The model code for the AGMD is presented as follows:

```
function
[Eff,Eb,Ep,Imd,HP,SPC,Qmem,Effmem,GOR,Mf,Mb,Sb,SR,CF,WR,Pm,LEP,Km,Jp,Cw,Amem,NOP]=AGMD(Effp,Mp,Tref,Thi,Tci,kp,E,rmemb,theta,Dmemb,Rconst,MWw,Sf,Sp)
%Mean temperature, °C:
Tm=(Thi+Tci)./2;
%The mean pressure, kPa:
Pm=(exp(23.328-(3841./(Tm-45+273))))./1000;
% Water surface tension, kN/m:
Gamaw=(-0.1769.*Tm+76.58).*1e-6;
%membrane tortusity:
Taw=((2-E).^2)./E;
%Latent heat of vaporization, kJ/kg:
Hfg=(1.7535.*Tm)+2024.3;
%Liquid entry pressure, kPa:
LEP=(-2.*Gamaw)./rmemb).*cosd(theta);
Tmean=Tm;
if Tmean>50
%Overall mass transfer coeff, kg/m2.s.Pa:
Cw=((2.*E.*rmemb)./(3.*Taw.*Dmemb)).*sqrt((8.*MWw)./(pi.*Rconst.*(Tm+273)));
else
%Proposed the expression amount of the steam/air, Pa.m2/s:
PDva=1.9851e-5.*(Tm.^2.072);
Cw=(E.*PDva.*MWw)./(Taw.*Dmemb.*Rconst.*(Tm+273).*Pm);
end
%Permeat flux, kg/m2.h:
% DELTA=(Hfg./(Rconst.*(Tm+273).^2)).*Pm;
DELTA=1;
Jp=Cw.*DELTA.*(Thi-Tci);
%Mass transfer coeff, kJ/m2.s.°C:
Km=((Jp.*Hfg)./(Thi-Tci)).*1;
%Membrane area, m2:
Amem=Mp./Jp;
%Feed mass flow rate kg/h: REF "Comparative analysis of full-scale membrane
distillation contactors "
Mf=(21.44.*Mp)+21.7;
%Brine loss, kg/h:
Mb=Mf-Mp;
%Salt rejection:
SR=1-(Sp./Sf);
%Brine loss salinity, kg/kg:
Sb=((Mf.*Sf)-(Mp.*Sp))./Mb;
%The concentration factor:
CF=Mf./(Mf-Mp);
%Water recovery:
WR=100.*(1-(1./CF));
%The energy transfer through the membrane Qmem=Qconduction+Qvapor, kW:
Qv=(Jp.*Hfg.*Amem)./3600;
kg=((0.01383.*exp(0.005486.*Tm)))+(3.344e-17.*exp(0.0986.*Tm)).*1e-3;%kW/moC
kmem=(E.*kg)+((1-E).*kp);
% kmem=kp;
Qc=(kmem./Dmemb).*Amem.*Tm;
Qmem=Qc+Qv;
%The gain ratio as a function of specific feed flow rate, kg/m2h:
GOR=6.467.*exp(-0.03327.*(Mf./Amem))+2.49.*exp(-0.002543.*(Mf./Amem));
% GOR=(Mp.*Hfg)./(Qmem.*3600);
%The thermal efficiency:
Effmem=Qv./Qmem;
%No of pores:
NOP=247.3-198.1.*cos(rmemb.*1.13e+07)+237.2.*sin(rmemb.*1.13e+07)-31.65.*cos(2.*rmemb.*1.13e+07)-69.25.*sin(2.*rmemb.*1.13e+07);
%Power, kW:
% HP=(Mf.*Pm)./(3600.*fraww(Tm,Sf).*Effp);
HP=(Mf.*LEP)./(3600.*fraww(Tm,Sf).*Effp);
%Specific power consumption, kWh/m3:
SPC=(1000.*HP)./Mp;
%%%%%%%%%%%%%%%%%%%%%%%%%%%%%%%%%%%%%%%%%%%%%%%%%%%%%%%%%%%%%%%%%%%%%%%%
%Exergy analysis:
%%%%%%%%%%%%%%%%%%%%%%%%%%%%%%%%%%%%%%%%%%%%%%%%%%%%%%%%%%%%%%%%%%%%%%%%
Ms=58.8;
Mw=18;
%%%%%%%%%%%%%%%%%%%%%%%%%%%%%%%%%%%%%%%%%%%%%%%%%%%%%%%%%%%%%%%%%%%%%%%%
%Brine stream:
```

```

Npureb=(1000-Sb)./Mw;
Nsaltb=Sb./Ms;
Nmb=Npureb+Nsaltb;
Xwb=Npureb./Nmb;
Xsb=Nsaltb./Nmb;
% Mmb=(Xsb*Ms)+(Xwb*Mw);
% echb=-Nmb.*(10^-3).*8.314.*(tsea+273).*((Xwb.*log(Xwb))+(Xsb.*log(Xsb)));
echb=Nmb.*(10^-3).*8.314.*(Tref+273).*((-Xwb.*(log(Xwb)))-(Xsb.*(log(Xwb))));
ephb=(fcp(Tm,Sb).*(Tm-Tref))-(fcp(Tm,Sb).*Tref.*(log((Tm+273)/(Tref+273)))+(Pm./fraww(Tm,Sb));
eb=ephb+echb;
Eb=(Mb./3600).*eb;
%%%%%%%%%%%%%%%%%%%%%%%%%%%%%%%%%%%%%%%%%%%%%%%%%%%%%%%%%%%%%%%%%%%%%%%%
%Feed stream:
Npuref=(1000-Sf)./Mw;
Nsaltf=Sf./Ms;
Nmf=Npuref+Nsaltf;
Xwf=Npuref./Nmf;
Xsf=Nsaltf./Nmf;
% Mmf=(Xsf*Ms)+(Xwf*Mw);
% echf=-Nmf.*(10^-3).*8.314.*(tsea+273).*((Xwf.*log(Xwf))+(Xsf.*log(Xsf)));
echf=Nmf.*(10^-3).*8.314.*(Tref+273).*((-Xwf.*(log(Xwf)))-(Xsf.*(log(Xwf))));
ephf=(fcp(Tm,Sf).*(Thi-Tref))-(fcp(Tm,Sf).*Tref.*(log((Thi+273)/(Tref+273)))+(Pm./fraww(Tm,Sf));
ef=ephf+echf;
Ef=(Mf./3600).*ef;
%%%%%%%%%%%%%%%%%%%%%%%%%%%%%%%%%%%%%%%%%%%%%%%%%%%%%%%%%%%%%%%%%%%%%%%%
%Distillate stream:
Npured=(1000-Sp)./Mw;
Nsaltd=Sp./Ms;
Nmd=Npured+Nsaltd;
Xwd=Npured./Nmd;
Xsd=Nsaltf./Nmd;
% Mmd=(Xsd*Ms)+(Xwd*Mw);
% echd=-Nmd.*(10^-3).*8.314.*(tsea+273).*((Xwd.*log(Xwd))+(Xsd.*log(Xsd)));
echd=Nmd.*(10^-3).*8.314.*(Tref+273).*((-Xwd.*(log(Xwd)))-(Xsd.*(log(Xwd))));
ephd=(fcp(Tm,Sp).*(Tm-Tref))-(fcp(Tm,Sp).*Tref.*(log((Tm+273)/(Tref+273)))+(Pm./fraww(Tm,Sp));
ed=ephd+echd;
Ep=(Mp./3600).*ed;
%%%%%%%%%%%%%%%%%%%%%%%%%%%%%%%%%%%%%%%%%%%%%%%%%%%%%%%%%%%%%%%%%%%%%%%%
%Exergy destruction rate, kW:
Imd=HP+Ef-Eb-Ep;
%water density, kg/m3:
function Raww=fraww(T,S)
Yc=((2*(mean(T))-200)/160;
segma=((2000.*S)-150)./150;
ar0=2.01611+0.115313.*segma+0.000326.*((2*(segma.^2))-1);
ar1=-0.0541+0.001571.*segma+0.000423.*((2*(segma.^2))-1);
ar2=-0.006124+0.00174.*segma+0.000009.*((2*(segma.^2))-1);
ar3=0.000346+0.000087.*segma+0.000053.*((2*(segma.^2))-1);
Raww=(0.5*ar0+ar1.*Yc+ar2.*(2*(Yc.^2)-1)+ar3.*(4.*(Yc.^3)-3*Yc)).*1000;
%Specific heat capacity of seawater kJ/kg°C (T=oC, S=kg/kg)
function Cp=fcp(T,S)
%%the specific heat of water at constant pressure is:
a=4206.8-(6.6197.*S)+(1.2288*(10^-2)*(S).^2);
b=-1.1262+(5.4178*(10^-2).*S)-(2.2719*(10^-4)*(S).^2);
c=1.2026*(10^-2)-(5.3566*(10^-4).*S)+(1.8906*(10^-6)*(S).^2);
d=6.8774*(10^-7)+(1.517*(10^-6).*S)-(4.4268*(10^-9)*(S).^2);
Cp=(a+(b.*T)+(c.*(T.^2))+(d.*(T.^3)))./1000;

```

Section 6.2.1 - FPC_for air heating

```
function
[Volstg, Tp, Tcoes, Tmpes, Qu, Qstg, Qloss, Uttotal, FR, F, Fin, FF, Effcol, Icol, EXfcol, Exin]=FPCair (OH, Ac, Is,
Vw, Tamb, Mf, Tci, Tco, Tmp, Sci, Sco, Rawa, Cpa, NG, Beta, Eg, Ep, Ue, Ub, W, H, thic, k)
%The equivalent diameter, m:
De=(4.*W.*H)/(2.*W);
%Thermal useful load on the FPC, kW:
Qthl=Mf.*Cpa.*(Tco-Tci);
%Overall heat transfer loss W/m2oC:
hw=5.7+3.8.*Vw;
f=(1+0.089.*hw-0.1166.*hw.*Ep).(1+0.07866.*NG);
C=520.*(1-0.000051.*(Beta.^2));
e=0.43.*(1-(100./(Tmp+273)));
SEGMA=5.67.*(10.^-8);
Ul=((NG./((C./(Tmp+273)).*(Tmp-Tamb)/(NG+f)).^e)+(1./hw)).^-
1)+((SEGMA.*(Tmp+273+Tamb+273).*((Tmp+273).^2)+((Tamb+273).^2))./((Ep+0.00591.*NG.*hw).^-
1)+((2.*NG)+f-1+(0.133.*Ep))./Eg-NG));
Uttotal=Ul+Ue+Ub;
%Calculated mean plate temperature, oC:
Tmpes=((Ac.*Is./1000)-Qthl)/(Ac.*Uttotal./1000)+Tamb;
%Plate temperature, oC:
Tp=(0.88.*Is./Uttotal)+Tamb;
%Efficiency factor F:
F=(tanh(Mf.*(W-De)./2))./(Mf.*(W-De)./2));
%Heatremoval factor FR:
FR=((Mf.*Cpa)/(Ac.*(Uttotal./1000)).*(1-exp(-1.*(Ac.*(Uttotal./1000).*F)/(Mf.*Cpa))));
%Fin efficiency Fin:
Fin=(tanh(sqrt((Ul./(k.*thic)).*(W-De)./2)))./(sqrt((Ul./(k.*thic)).*(W-De)./2)));
%The flow factor FF:
FF=FR./F;
%Usefull energy, kW:
Qu=Ac.*FR.*(Is./1000)-((Uttotal./1000).*(Tci-Tamb));
%the mean fluid temperature Tfm:
Tfm=Tci+((Qu)/(Ac.*(Uttotal./1000).*FR)).*(1-FF));
%Calculated outlet collector temp, oC:
Tcoes=(2.*Tfm)-Tci;
%the energy loss in the collector in kW and:
Qloss=Ac.*FF.*(Uttotal./1000).*(Tfm-Tamb);
%Thermal storage, kW:
Qstg=(Is.*Ac./1000)-Qu-Qloss;
%Storage volume, m3:
Volstg=(Qstg.*OH)/(Raw.*Cpa.*(Tcoes-Tci));
%Thermal efficiency:
Effcol=(1000.*Qu)/(Is.*Ac);
%Collector inlet and outlet enthalpies, kJ/kg:
Hci=Cpa.*(Tci+273.5);
Hco=Cpa.*(Tco+273.5);
%Collector Irreversibility:
Icol=((Ac.*Is)/1000).*(1-(Tamb+273)/(6000))+Mf.*((Hci-Hco)-((Tamb+273).*(Sci-Sco)));
Exin=Ac.*(Is./1000).*(1-(Tamb+273)/(6000));
%Exergy efficiency:
EXfcol=1-(Icol/(Ac.*(Is./1000).*(1-(Tamb+273)/(6000))));
%%%%%%%%%%%%%%%%%%%%%%%%%%%%%%%%%%%%%%%%%%%%%%%%%%%%%%%%%%%%%%%%%%%%%%%% Air Prop %%%%%%%%%%%%%%%%%%%%%%%%%%%%%%%%%%%%%%%%%%%%%%%%%%%%%%%%%%%%%%%%%%%%%%%%%
% %Air specific heat capacity, J/kgC:
% function Cpa=fcpa(T)
% Cpa=(1.031+0.0001369.*1.0132+0.0001299.*T).*1;
%
% %Air density, kg/m3:
```

```

% function Rawa=frawa(T)
% Rawa=(273.*1.293)./(273.5+T);
%
% %% Air thermal conductivity, W/moC:
% function ka=fka(T)
% ka=(0.0015215+0.097459.*(T+273.5)-3.3322).*1e-3 ;
%
% %%Air dynamic viscosity, Pa.s:
% function meua=fmeua(T)
% meua=(1.6157+(0.06523.*(T+273.5))-3.0297e-05).*1e-6;

%Air specific entropy at 1bar, kJ/kg°C:
% function Sa=fSa(T)
% Sa=7.289.*exp(0.0001551.*T)-0.511.*exp(-0.004961.*T);

```

Section 6.2.1 – FPC for water heating

```

function
[Volstg,Tp,Tcoes,Tmpes,Qu,Qstg,Qloss,Utotal,FR,F,Fin,FF,Effcol,Icol,EXfcol,Exin]=FPCw(OH,Acolt,Is
,Vw,Tamb,Mf,Tci,Tco,Tmp,Hci,Hco,Sci,Sco,Raww,Cpw,NG,Beta,Eg,Ep,Ue,Ub,W,D,thic,k)

%For Liquid & Sub cooling regions:
%Thermal useful load on the FPC, kW:
Qthl=Mf.*Cpw.*(Tco-Tci);
%Overall heat transfer loss W/m2oC:
hw=5.7+3.8.*Vw;
f=(1+0.089.*hw-0.1166.*hw.*Ep).*(1+0.07866.*NG);
C=520.*(1-0.000051.*(Beta.^2));
e=0.43.*(1-(100./(Tmp+273)));
SEGMA=5.67.*(10.^-8);
U1=((NG./((C./(Tmp+273)).*((Tmp-Tamb)./(NG+f)).^e))+1./hw).^-
1)+((SEGMA.*(Tmp+273+Tamb+273).*((Tmp+273).^2)+((Tamb+273).^2))./((Ep+0.00591.*NG.*hw).^-
1))+((2.*NG)+f-1+(0.133.*Ep))./Eg-NG));
Utotal=U1+Ue+Ub;
%Calculated mean plate temperature, oC:
Tmpes=((Acolt.*Is./1000)-Qthl)./(Acolt.*Utotal./1000))+Tamb;
%Plate temperature, oC:
Tp=(0.88.*Is./Utotal)+Tamb;
%Efficiency factor F:
F=(tanh(Mf.*((W-D)./2)))./(Mf.*((W-D)./2));
%Heatremoval factor FR:
% X=(Utotal.*Acolt.*(Tmp-Tci))./(Qthl.*1000);
% FR=1./(X+1);
FR=((Mf.*Cpw)./(Acolt.*(Utotal./1000))).*(1-exp(-1.*(Acolt.*(Utotal./1000).*F)./(Mf.*Cpw))));
%Fin efficiency Fin:
Fin=(tanh(sqrt((U1./((k.*thic)).*((W-D)./2))))./(sqrt((U1./((k.*thic)).*((W-D)./2))));
%The flow factor FF:
FF=FR./F;
%Usefull energy, kW:
Qu=Acolt.*FR.*((Is./1000)-((Utotal./1000).*(Tci-Tamb)));
%the mean fluid temperature Tfm:
Tfm=Tci+((Qu./((Acolt.*(Utotal./1000).*FR)).*(1-FF)));
%Calculated outlet collector temp, oC:
Tcoes=(2.*Tfm)-Tci;
%the energy loss in the collector in W and:
Qloss=Acolt.*FF.*(Utotal./1000).*(Tfm-Tamb);
%Thermal storage, kW:

```

```

% Qstg=Raww.*Vol.*Cpw.*(Tcoes-Tci)./OH;
Qstg=(Is.*Acolt./1000)-Qu-Qloss;
%Storage volume, m3:
Volstg=(Qstg.*OH)./(Raww.*Cpw.*(Tcoes-Tci));
% Effcol=0.768-(2.9.*((Tco-Tamb)./Is))-(0.0108.*(((Tco-Tamb)./Is).^2).*Is);%FPC
% Effcol=0.78-(3.4.*(((Tco+Tci)./2)-Tamb)./Is));%FPC powersol
Effcol=(1000.*Qu)./(Is.*Acolt);
%Collector Irreversibility:
Icol=((Acolt.*Is)./1000).*(1-(Tamb+273)./(6000)))+(Mf.*((Hci-Hco)-((Tamb+273).*(Sci-Sco))));
Exin=Acolt.*(Is./1000).*(1-((Tamb+273)./(6000)));
%Exergy efficiency:
EXfcol=1-(Icol./Acolt.*(Is./1000).*(1-((Tamb+273)./(6000)))));

```

Section 6.2.2 - SWI

```

function [Edh,Qmem,RR,Mp,Mv,Tao,Tb,Tv,Mb,Sb]=
SWIS(L,W,X,kp,Tsoil,Tfi,Mf,Sf,RHw,Tai,Mai,Wai,Wao)
%#codegen
%% Assuming constant dry bulb temperature, oC:
Tv=Tai;
%% Vapour mass flow rate based on air saturation, kg/s:
Mv=(Wao-Wai).*Mai;
%% Brine flow rate, kg/s:
Mb=Mf-Mv;
%% Brine salinity ratio, g/kg:
Sb=(Sf.*Mf)./(Mb.*1);
%% Brine outlet temperature, oC:
Tb=((Mf.*fcp(Tfi,Sf).*Tfi)+(Mai.*fcpa(Tai).*Tai)-(Mv.*fcpa(Tai).*Tv))./(Mb.*fcp(Tfi,Sb))-
(fbpe(Tfi,Sb/1000));
%% For dehumidification process:
%% Soil Plate area, m2:
Ap=L.*W;
%% For convection, W/m2oC:
Re=Mv./(W.*fmeua(Tv));
Pr=(1000.*fcpa(Tv).*fmeua(Tv))./fka(Tv);
Nu=0.332.*(Re.^0.5).*(Pr.^0.333);
hc=(Nu.*fka(Tv))./L;
%% The overall heat coefficient, W/m2oC:
U=1./((X./kp)+(1./hc));
%% Number of transfer unit:
NTU=(U.*Ap)./(Mai.*fcpa(Tv));
%% Effectiveness:
Edh=1-exp(-NTU);
%% Thermal power on the membrane, kW:
Qmem=(U.*Ap.*(Tv-Tsoil))./1000;
%% Outlet air temperature, oC:
Tao=Tv-Edh.*(Tv-Tsoil);
% Tao=(Qmem./(fcpa(Tv).*Mai))+Tsoil;
%% Inlet & Outlet humidity ratio of the air through the membrane soil:
wais=fwa(Tv,RHw);
waos=fwa(Tao,RHw);
%% The system productivity, kg/s:
Mp=(wais-waos).*Mai;
%% The recovery ratio:

```

```

RR=Mp./Mf;
%%%%%%%%%%%%%%%%%%%%%%%%%%%%%%%%%%%%%%%%%%%%%%%%%%%%%%%%%%%%%%%%%%%%%%%%%%
%% Water thermophysical properties:
%% Specific heat capacity of seawater kJ/kg°C (T=oC, S=kg/kg)
function Cp=fcp(T,S)
%%the specific heat of water at constant pressure is:
a=4206.8-(6.6197.*S)+(1.2288*(10^-2)*(S).^2);
b=-1.1262+(5.4178*(10^-2).*S)-(2.2719*(10^-4)*(S).^2);
c=1.2026*(10^-2)-(5.3566*(10^-4).*S)+(1.8906*(10^-6)*(S).^2);
d=6.8774*(10^-7)+(1.517*(10^-6).*S)-(4.4268*(10^-9)*(S).^2);
Cp=(a+(b.*T)+(c.*(T.^2))+(d.*(T.^3)))./1000;
%%%%%%%%%%%%%%%%%%%%%%%%%%%%%%%%%%%%%%%%%%%%%%%%%%%%%%%%%%%%%%%%%%%%%%%%%% Air Prop %%%%%%%%%%%%%%%%%%%%%%%%%%%%%%%%%%%%%%%%%%%%%%%%%%%%%%%%%%%%%%%%%%%%%%%%%%%
%%Air specific heat capacity, kJ/kg°C:
function Cpa=fcpa(T)
Cpa=(1.031+0.0001369.*1.0132+0.0001299.*T).*1;
%%Humidity ratio of the air, kg/kg w=f(Tdb, RH):
function w=fwa(T,RH)
w=-0.06019+0.001095.*T+0.0008145.*RH;
%%Boiling point elevation BPE:
function BPE=fbpe(T,S)
B=(10^-3).*(6.71+(6.43*(10^-2).*T)+(9.74*(10^-5).*(T.^2)));
C=(10^-5).*(2.38+(9.59*(10^-3).*T)+(9.42*(10^-5).*(T.^2)));
BPE=(B+(C.*(S.*1000))).*(S.*1000);
% %Air density, kg/m3:
%Air thermal conductivity, W/m°C:
function ka=fka(T)
ka=(0.0015215+0.097459.*(T+273.5)-3.3322).*1e-3 ;
%Air dynamic viscosity, Pa.s:
function meua=fmeua(T)
meua=(1.6157+(0.06523.*(T+273.5))-3.0297e-05).*1e-6;

```

Section 6.2.2 - SWD Seawater Distillation

```

function [Edh,Qc,RR,Mp,Mv,Tao,Tb,Tv,Mb,Sb]=
SWIS(TAc,Ws,Lc,Xc,kc,Tc,Tfi,Mf,Sf,RHw,Tai,Mai,Wai,Wao)
%#codegen
%% Assuming constant dry bulb temperature, oC:
Tv=Tai;
%% Vapor mass flow rate based on air saturation, kg/s:
Mv=(Wao-Wai).*Mai;
%% Brine flow rate, kg/s:
Mb=Mf-Mv;
%% Brine salinity ratio, g/kg:
Sb=(Sf.*Mf)./(Mb.*1);
%% Brine outlet temperature, oC:
Tb=((Mf.*fcp(Tfi,Sf).*Tfi)+(Mai.*fcpa(Tai).*Tai)-(Mv.*fcpa(Tai).*Tv))./(Mb.*fcp(Tfi,Sb))-
(fbpe(Tfi,Sb/1000));
%% For dehumidification process:
%% The cover width based on tilt angle and still width:
Wc=2.*(Ws./(2.*cos(TAc.*pi./180)));
%% Cover area, m2:
Ac=Lc.*Wc;
%% For convection, W/m2oC:
Re=Mv./(Wc.*fmeua(Tv));

```

```

Pr=(1000.*fcpa(Tv).*fmeua(Tv))./fka(Tv);
Nu=0.332.*(Re.^0.5).*(Pr.^0.333);
hc=(Nu.*fka(Tv))./Lc;
%% The overall heat coefficient, W/m2oC:
U=1./((Xc./kc)+(1./hc));
%% Number of transfer unit:
NTU=(U.*Ac)./(Mai.*fcpa(Tv));
%% Effectiveness:
Edh=1-exp(-NTU);
%% Thermal power on the cover, kW:
Qc=(U.*Ac.*(Tv-Tc))./1000;
%% Outlet air temperature, oC:
Tao=Tv-Edh.*(Tv-Tc);
%% Inlet & Outlet humidity ratio of the air through the membrane soil:
wais=fwa(Tv,RHw);
waos=fwa(Tao,RHw);
%% The system productivity, kg/s:
Mp=(wais-waos).*Mai;
%% The recovery ratio:
RR=Mp./Mf;
%%%%%%%%%%%%%%%%%%%%%%%%%%%%%%%%%%%%%%%%%%%%%%%%%%%%%%%%%%%%%%%%%%%%%%%%%%
%% Thermophysical properties%%%%%%%%%%%%%%%%%%%%%%%%%%%%%%%%%%%%%%%%%%%%%%%%%%%%%%%%%%%%%%%%%%%%%%%%%%
%% Water thermophysical properties:
%% Specific heat capacity of seawater kJ/kg oC (T=oC, S=kg/kg)
function Cp=fcp(T,S)
%%the specific heat of water at constant pressure is:
a=4206.8-(6.6197.*S)+(1.2288*(10^-2)*(S).^2);
b=-1.1262+(5.4178*(10^-2).*S)-(2.2719*(10^-4)*(S).^2);
c=1.2026*(10^-2)-(5.3566*(10^-4).*S)+(1.8906*(10^-6)*(S).^2);
d=6.8774*(10^-7)+(1.517*(10^-6).*S)-(4.4268*(10^-9)*(S).^2);
Cp=(a+(b.*T)+(c.*(T.^2))+(d.*(T.^3)))./1000;
%%%%%%%%%%%%%%%%%%%%%%%%%%%%%%%%%%%%%%%%%%%%%%%%%%%%%%%%%%%%%%%%%%%%%%%%%% Air Prop %%%%%%%%%%%%%%%%%%%%%%%%%%%%%%%%%%%%%%%%%%%%%%%%%%%%%%%%%%%%%%%%%%%%%%%%%%%
%%Air specific heat capacity, kJ/kg oC:
function Cpa=fcpa(T)
Cpa=(1.031+0.0001369.*1.0132+0.0001299.*T).*1;
%%Humidity ratio of the air, kg/kg w=f(Tdb, RH):
function w=fwa(T,RH)
w=-0.06019+0.001095.*T+0.0008145.*RH;
%%Boiling point elevation BPE:
function BPE=fbpe(T,S)
B=(10^-3).*(6.71+(6.43*(10^-2).*T)+(9.74*(10^-5).*(T.^2)));
C=(10^-5).*(2.38+(9.59*(10^-3).*T)+(9.42*(10^-5).*(T.^2)));
BPE=(B+(C.*(S.*1000))).*(S.*1000);
%%Air thermal conductivity, W/moC:
function ka=fka(T)
ka=(0.0015215+0.097459.*(T+273.5)-3.3322).*1e-3 ;
%%Air dynamic viscosity, Pa.s:
function meua=fmeua(T)
meua=(1.6157+(0.06523.*(T+273.5))-3.0297e-05).*1e-6;

```